Analysis of the Max Network in Drosophila

Dissertation

zur

Erlangung der naturwissenschaftlichen Doktorwürde
(Dr. sc. nat.)

vorgelegt der

Mathematisch-naturwissenschaftlichen Fakultät

der

Universität Zürich

von

Dominik Steiger

von

Waldkirch-Bernhardzell SG

Promotionskomitee

Dr. Peter Gallant (Leitung der Dissertation)
Prof. Dr. Alex Hajnal (Vorsitz)
Prof. Dr. Konrad Basler
Prof. Dr. Robert N. Eisenman
Prof. Dr. Ernst Hafen

Zürich, 2007

For Ines

Table of contents

Acknowledgements

First and foremost, I want to thank Peter Gallant for giving me the opportunity to work under his supervision, and for his excellent support, guidance and advice. In addition, I would like to thank past and present members of the Gallant lab for assistance, discussions and a wonderful working atmosphere: Mirjam Balbi, Paola Bellosta, Anja Egli, Michael Furrer, Chanqing Li, Sonali Mohanty, Nadine Müller, Regina Perez and Daniela Schwinkendorf.

For specific support, I am very grateful to: Michael Spörry, Anni Strässle and Raymond Grunder (sequencing), Peder Zipperlen and Matthias Bodmer (qRTPCR), Christof Hugentobler (injections, eye sections, electron microscopy), Michel Nakano and Urs Ziegler (confocal microscopy), Noemi Arnold, Oriel Carreno, Laura Damerius, Nicole Meier and Sandra Peterhans (group projects in genetics and developmental biology courses). I thank Hugo Stocker and Konrad Basler for providing me fly stocks used in this work. I am especially indebted to Robert Eisenman and Sarah Pierce for providing me the *dm*^{4} *dmnt*^{1} recombinants prior to publication. For discussions and helpful suggestions, I would like to acknowledge the members of the Hafen and Basler groups, Konrad Basler, Ernst Hafen and Hugo Stocker. I thank Christian Lehner for careful reading of the manuscript and for important comments.

I am thankful for the support and patience of my wife, friends and family. Last, not least, I want to express my deep gratitude to my parents, Hedwig and Peter Steiger, who made it possible for me to undergo this endeavor.

Abbreviations

>	FRT (abbreviation in genotype annotations, e.g. *tub>dmyc>GAL4*)
AA	amino acid
AED	[time] after egg deposition
bHLHzip	basic helix-loop-helix leucine zipper
cDNA	complementary DNA
dmax-IR	*dmax* inverted repeat
DNA	deoxyribonucleic acid
dsRNA	double stranded RNA
f, m, v	female(s), male(s), virgin female(s)
FRT	flipase recombination target
GFP	green fluorescent protein
HAT	histone acetyltransferase
HDAC	histone deacetylase
kb	kilo base pairs
L1, L2, L3, P	first, second, third larval stage, pupal stage
lacZ-IR	*lacZ* inverted repeat
OreR	Oregon R (wild type strain)
ORF	open reading frame
PCR	polymerase chain reaction
qRTPCR	quantitative real time RT-PCR
RNA	ribonucleic acid
RNA*i*	RNA interference
RT	reverse transcription
SID	Sin3-interaction domain
UAS	upstream activating sequence
UTR	untranslated region

Zusammenfassung

dmyc, das *Drosophila*-Homolog der *myc*-Proto-Onkogene in Säugetieren, spielt eine wichtige Rolle in der Kontrolle des Wachstums auf zellulärer und organismischer Ebene. Zusammen mit den antagonistisch agierenden Proteinen der Mad/Mnt-Familie (dMnt in *Drosophila*) und dem zentralen Kofaktor Max (dMax in *Drosophila*) bilden die Myc-Proteine ein Transkriptionsfaktor-Netzwerk: das Max-Netzwerk.

Im Gegensatz zu *dmyc*- und *dmnt*-Mutanten sind *dmax*-Mutanten bis jetzt noch nicht studiert worden. In dieser Arbeit präsentieren wir ein RNA*i*-System, mit dem wir *in vivo* die Expression von *dmax* stark erniedrigen können, und wir haben *dmax*-Nullmutanten erzeugt. Diese experimentellen Werkzeuge erlaubten uns, eine detaillierte Analyse der Funktionen von *dmax* durchzuführen, die zeigte, dass *dmax* sowohl im larvalen, als auch im imaginalen Wachstum benötigt wird. Bei Verlust von *dmax*-Funktionen stellten sich Phänotypen ein, die ähnlich derer in *dmyc*-hypomorphen Mutanten waren. Ausserdem konnten wir positive genetische Interaktionen mit *dmyc* und zwei *dmyc*-Kofaktoren (*reptin* und *pontin*) zeigen. Zusammen mit den bereits beschriebenen *dmyc*- und *dmnt*-Nullmutanten erlaubte die Erzeugung von *dmax*-Nullmutanten eine gründliche genetische Analyse des Max-Netzwerks in *Drosophila.* Indem wir Wachstum und Überleben der verschiedenen null-mutanten Kombinationen von *dmyc*, *dmnt* und *dmax* verglichen, konnten wir zeigen, dass *dmnt* einen direkten antagonistischen Effekt auf das *dmyc*-abhängige Wachstum und Überleben hat. Des weiteren entdeckten wir, dass ein wichtiger Teil der Funktionen von *dmyc* nicht von *dmax* abhängt, ein Resultat, das den etablierten Vorstellungen widerspricht.

Wir charakterisierten das Wesen dieser *dmax*-unabhängigen Funkionen *dmycs* in einer ausgedehnten loss-of-function-Analyse, mittels derer wir zeigten, dass diese Funktionen wichtig sind für die RNA-Akkumulation in jungen L1-Larven, für das Wachstum und die Endoreplikation der polyploiden larvalen Gewebe, aber auch für das Wachstum in imaginalen Geweben sowie für die Zell-Kompetition. Ausserdem fanden wir in verschiedenen *dmyc*-Überexpressions-Situationen Evidenz für *dmax*-unabhängige Funktionen von *dmyc*: Wir konnten nachweisen, dass die Überexpression von *dmyc* im *Drosophila*-Auge *dmax*-unabhängige Effekte zeitigte, die in Verbindung zu Apoptose stehen. In *dmax*-null-mutanten Flügel-Imaginalscheiben konnte *dmyc* immer noch Zell-Kompetition induzieren. In *dmax*-null-mutanten Larven fanden wir, dass konditionale Überexpression von *dmyc* zu Häutungs-Defekten führt und die Verpuppung verhindert, indem *dmyc* mit dem Ecdyson-System interferiert - möglicherweise ein Hinweis auf bisher unbekannte Zusammenhänge zwischen *dmyc* und der zeitlichen Regulation der Larvenstadien und der Metamorphose.

Die diesen *dmax*-unabhängigen Funktionen von *dmyc* zugrundeliegenden molekularen Mechanismen harren einer Erklärung. Ein Hinweis auf eine mögliche Erklärung, wie *dmyc* auch ohne *dmax* einen

positiven Einfluss auf das Zell-Wachstum hat, mag in der Entdeckung zu sehen sein, dass die Überexpression von *dmyc* in *dmax*-mutanten Larven die Expression von *5sRNA*, *tRNA(Leu)* und von zwei snoRNAs stimuliert.

Summary

dmyc, the *Drosophila* homolog of the mammalian *myc* proto-oncogenes, plays an important role in the control of cellular and organismal growth. Myc proteins, along with their antagonists of the Mad/Mnt protein family (dMnt in *Drosophila*), have been shown to function in a transcription factor network in which the activity of the network members depends on the binding to the central cofactor Max (dMax in *Drosophila*).

While *dmyc* and *dmnt* mutants have been studied, *dmax* mutants have not been available so far. In this study, we present a conditional gene silencing system that allows to create situations of low *dmax* levels and we report the generation of *dmax* null mutants. Using both these tools, we conducted a detailed functional analysis of *dmax*, showing that *dmax* is required for both the growth of polyploid larval and diploid imaginal cells. Loss of *dmax* produced phenotypes that were reminiscent of *dmyc* hypomorphic phenotypes. Positive genetic interactions with *dmyc* and two cofactors, *reptin* and *pontin* could be shown. Together with the already available null mutants of *dmyc* and *dmnt*, the *dmax* null mutants allowed for a rigorous genetic analysis of the *Drosophila* Max network: By comparing the growth and survival of different null mutant combinations of the Max network members, we could show that *dmnt* directly antagonizes *dmyc*-dependent growth and survival. Furthermore, we discovered that an important part of the functions of *dmyc* do not require *dmax*, in contradiction to the current model of *dmyc* function.

We performed a detailed loss of function analysis of the nature of these *dmax*-independent functions of *dmyc*, showing that these functions are important for the accumulation of total RNA in young L1 larvae, for the growth and endoreplication of the polyploid larval tissues, but also for the growth of imaginal tissues and in cell competition. Moreover, we found several lines of evidence for *dmax*-independent functions in situations where *dmyc* was overexpressed. In the *Drosophila* eye, overexpression of *dmyc* could be shown to have *dmax*-independent effects that are associated with apoptosis. In *dmax* null imaginal wing discs, *dmyc* could still induce cell competition. In *dmax* null larvae, conditional overexpression of *dmyc* interfered with ecdysone signaling, resulting in molting phenotypes and a block of pupariation, pointing to a previously unknown connection between *dmyc* and the regulation of developmental timing.

The molecular mechanisms underlying these *dmax*-independent functions of *dmyc* remain to be elucidated. However, the discovery that overexpression of *dmyc* in *dmax* null larvae resulted in the upregulation of *5sRNA*, *tRNA(Leu)* and of two snoRNAs might at least partially explain how *dmyc* can have a positive influence on growth in the absence of *dmax.*

Introduction

1. The proto-oncogene *myc*

myc is one of the most intensively studied proto-oncogenes. As one of the most frequently activated oncogenes, *myc* is estimated to be mutated in 20% of all human cancers (Nesbit et al., 1999). More than two decades ago, *myc* was found as the transforming principle of avian myelocytomatosis virus, deriving its name from this avian retrovirus (Sheiness et al., 1978). The viral version, termed *v-myc*, was shown to be the retrovirally captured homolog of a mammalian gene, termed *c-myc* (Vennstrom et al., 1982). The discovery that Burkitt's lymphoma is caused by a chromosomal translocation of *c-myc* in B cells has established *myc's* role as a prototypical oncogene (Hollis et al., 1984) that was later found to be involved in many human cancers. Besides *c-myc*, further paralogs are known in humans: *N-myc*, which is frequently found mutated in neuroblastomas and retinoblastomas (Kohl et al., 1983), and *L-myc*, first found in lung carcinomas (Nau et al., 1985). *S-myc* and *B-myc* have also been described, the latter gene only in rodents. These paralogs lack neoplastic potential (Henriksson and Luscher, 1996).

1.1. Biological functions of *myc*

myc genes encode transcription factors that play an important role in growth control, regulating proliferation, cell growth, differentiation and apoptosis (amongst others). Myc expression, both on the transcriptional and post-transcriptional level, is controlled by a wide range of growth factors, cytokines and mitogens (Kelly et al., 1983; Shibuya et al., 1992) and Myc activity links mitogenic signaling and the cell cycle. Myc and Ras have been shown to collaborate in inducing accumulation of active cyclin E/Cdk2 and E2F, thus inducing cell-cycle entry (Leone et al., 1997). Lack of Myc expression prevents quiescent cells from entering the cell cycle upon exposure to mitogenic signals (Roussel et al., 1991; Barone and Courtneidge, 1995). Conversely, overexpression of Myc can drive quiescent cells into the cell cycle and has been shown to promote S-phase entry and shorten G1-phase in cycling cells (Karn et al., 1989). Ectopic expression of c-Myc in the absence of survival factors does not only promote proliferation, but also leads to apoptosis in an, at least partly, Arf-Mdm2-p53-pathway-dependent manner (Askew et al., 1991; Evan et al., 1992; Zindy et al., 1998). Myc expression rapidly decreases during the terminal differentiation of many cell types and it has been shown that Myc overexpression can prevent cells from undergoing terminal differentiation, reviewed in (Henriksson and Luscher, 1996).

The functions of c-Myc and N-Myc are essential for development: *c-myc* null mice die before 10.5 days of gestation (Davis et al., 1993), *N-myc* null mice at 11.5 days of gestation (Sawai et al., 1991; Sawai et al., 1993), while *L-myc* null mice have a wild type phenotype (Hatton et al., 1996).

From the findings above, a picture of Myc as an important regulator of proliferation had emerged. However, more recent studies have shown that Myc has an at least as important role in the regulation of cell growth (defined as the increase in cellular mass). This was compellingly shown in *Drosophila*, where Myc primarily regulates cell size (Johnston et al., 1999), and also in mammalian systems (Iritani and Eisenman, 1999; Schuhmacher et al., 1999). Transcriptome profiling techniques (such as SAGE and microarrays) made it possible to show that the most distinctive target genes downstream of Myc are the genes involved in ribosome biosynthesis and protein biosynthesis, e.g. Boon et al. (2001); Hulf et al. (2005), see also Zeller et al. (2003). Myc does not only regulate RNA polymerase II-transcribed protein-coding genes, it has also been shown that Myc controls the transcription of RNA polymerase III-dependent small RNA genes (Gomez-Roman et al., 2003) in mammals and of RNA polymerase I-dependent ribosomal RNA (Grandori et al., 2005; Grewal et al., 2005) in mammals and in *Drosophila*.

1.2. Molecular function of *myc*

Myc proteins are members of the basic region/helix-loop-helix/leucine zipper (bHLHzip) superfamily of transcriptional regulators and have been shown to function as transcription factors. Myc possesses an N-terminal transactivation domain (Kato et al., 1990) and the C-terminal bHLHzip domain that is required for heterodimerization and DNA binding. Key to understanding Myc's function as a transcription factor was the discovery of its heterodimerization partner, the small bHLHzip protein Max (Blackwood and Eisenman, 1991; Prendergast et al., 1991). Myc/Max heterodimers have been shown to bind to DNA sequences called E-boxes (canonical sequence: CACGTG) (Blackwood and Eisenman, 1991) and variants thereof (Blackwell et al., 1993; Grandori et al., 1996). Heterodimerization of Myc with Max and subsequent binding to E-boxes is required for the transactivation effects of Myc (Amati et al., 1992; Crouch et al., 1993) and has been shown to be required for the cell cycle progression, apoptotic and oncogenic effects of the overexpression of Myc in cell culture systems (Amati et al., 1993a; Amati et al., 1993b). However, overexpression of Myc has been shown to induce apoptosis in PC12 cells (Wert et al., 2001), a cell line that does not express a functional Max transcript (Hopewell and Ziff, 1995).

More recent studies have provided evidence that transactivation by Myc may be mediated by chromatin modifying (histone modification) and chromatin remodeling (nucleosome movement/displacement) systems. The Myc transactivation domain binds to the TRRAP protein, a factor that is part of the SAGA and Tip60 histone acetyltransferase (HAT) complexes and that is also found in a complex containing the Swi/Snf-related p400 protein (Cowling and Cole, 2006). TRRAP function was shown to be required for Myc-mediated transformation (McMahon et al., 1998). Besides HAT-containing complexes, chromatin remodeling systems are likely to be involved in Myc-mediated transactivation, since overexpression of dominant-negative forms of BRG1, a Swi/Snf complex

member, blocks c-Myc-mediated transactivation (Cheng et al., 1999). Furthermore, Myc has been shown to bind to Tip48 and Tip49, two DNA-helicase/ATPases found in the Tip60 HAT complex, but also in chromatin remodeling complexes (Shen et al., 2000; Wood et al., 2000), and homologs of Tip48 and Tip49 (Reptin and Pontin) have been shown to interact genetically with Myc both in *Drosophila* (Bellosta et al., 2005) and in *Xenopus* (Etard et al., 2005).

Myc has also the potential to repress certain target genes, many of which contain TATA-less promoters featuring a specific initiator element (Inr) that is recognized by the activating transcription factor Miz-1. Myc has been shown to bind Miz-1 and is believed to be recruited to the Inr promoters through this interaction (and not by direct binding to the DNA), leading to a repression of the target gene (Wanzel et al., 2003). Miz-1 binds to Myc's bHLHzip domain, but does not preclude binding to Max, because binding occurs on opposite sides of the domain, and indeed it has been shown that the presence of Max is required for Myc-mediated repression (Mao et al., 2003). The exact mechanism of Myc-mediated repression remains unclear, but presumably involves disruption of the binding of p300 to Miz-1 (Staller et al., 2001).

2. *max*

The small protein Max has no transactivation domain of its own, consisting mainly of a bHLHzip domain, and it was shown to be transcriptionally inert in reporter assays (Kato et al., 1992; Min and Taparowsky, 1992). Besides Max's important ability to form heterodimers with Myc, Max has also been shown to form homodimers which bind to the same E-boxes that are recognized by Myc/Max heterodimers (Blackwood and Eisenman, 1991; Prendergast et al., 1991). While it has been reported that Max homodimers repress the transcription of E-box reporters (Kretzner et al., 1992), the biological relevance of this finding is unclear, since DNA binding by Max homodimers is inhibited by constitutive CKII-mediated phosphorylation (Berberich and Cole, 1992) and Max homodimers did not repress Myc-responsive genes *in vivo* (Yin et al., 1998).

CKII-mediated phosphorylation of Max is also relevant in the recently described caspase-mediated degradation of Max during Fas-mediated apoptosis (Krippner-Heidenreich et al., 2001). At present it is not clear whether this degradation process is just a part of the general apoptotic dismantling of a cell, or whether it has a dedicated regulatory purpose that might be important in the context of Myc-induced apoptosis.

Several splice forms of *max* exist in mammals (Blackwood and Eisenman, 1991; Makela et al., 1992; Vastrik et al., 1993; Arsura et al., 1995). The high degree of conservation of the *max* gene structure - the exon-intron boundaries are identical in insect *max* (Gallant, 2006), theoretically allowing the formation of the same splice forms that exist in vertebrates - might imply that alternative splice forms of *max* have biological importance.

Consistent with Max's essential role as a cofactor of Myc, *max* null mice are not viable. *max* null mice die at much earlier stages (4.5 - 7.25 days of gestation) than *c-myc* or *N-myc* null mice (Shen-Li et al., 2000). The longer survival of *c-myc* or *N-myc* null mutants might be due to redundant functions of *c-myc* and *N-myc*.

The only *max* mutant cell line that has been studied so far is the rodent PC12 cell line. In these cells, a mutation in the *max* locus precludes the formation of functional *max* transcript. Overexpression of Myc has been reported to induce apoptosis in PC12 cells, suggesting that at least a part of the role of Myc in apoptosis is dMax-independent.

3. *myc*, *max*, *mad,* and more: the Max network

Max has important functions beyond its role as a cofactor of Myc. The identification of a set of Myc-related bHLHzip proteins that heterodimerize with Max and function as transcriptional repressors has placed Max at the centre of a transcription factor network, called the Max network. Expression cloning and yeast two hybrid assays led to the discovery of the four closely related bHLHzip proteins Mad1, Mxi1, Mad3 and Mad4 (also called MXD1-4) and later of the proteins Mnt (also called Rox) and Mga (Ayer et al., 1993; Zervos et al., 1993; Hurlin et al., 1995; Hurlin et al., 1997b; Hurlin et al., 1999).

Five of these proteins, Mad1, Mxi1, Mad3, Mad4 (also called MXD1-4) and Mnt possess N-terminal SID domains (Sin3-interaction domains) that mediate interaction with Sin3 corepressors and they have been shown to function as transcriptional repressors that can block Myc-dependent cell transformation in cell culture assays (Ayer et al., 1993; Hurlin et al., 1995; Koskinen et al., 1995; Schreiber-Agus et al., 1995; Hurlin et al., 1997a). Transcription assays showed that Mad proteins and Mnt repress the expression of synthetic reporters in an E-box-dependent manner (Ayer et al., 1993; Hurlin et al., 1997a). The Mad proteins, and also Mnt, therefore appear to function as direct antagonists of Myc (Figure I). Consistent with such a model, increased expression of several Mad proteins is associated with cellular differentiation and growth arrest (Ayer and Eisenman, 1993; Chin et al., 1995), and Mxi1 as well as Mnt proteins act as tumor suppressors (reviewed in Hurlin and Huang, 2006). Knock-out mice mutant for *mad1*, *mxi1*, *mad3* and *mnt* have been generated (Foley et al., 1998; Schreiber-Agus et al., 1998; Queva et al., 2001; Hurlin et al., 2003). While *mad1*, *mxi1* and *mad3* mice were viable and displayed rather subtle phenotypes, *mnt* null mice die at or soon after birth.

Recent studies have shown that *mnt* plays a central role in antagonizing Myc function: Cells that are mutant for *mnt* show many of the hallmark aspects of Myc overexpression. Deletion of *mnt* leads to disrupted cell cycle control, transformation and enhanced levels of apoptosis (Hurlin et al., 2003; Nilsson et al., 2004). Conditional deletion of *mnt* in breast epithelial cells, T-cells and B-cells in transgenic mice leads to tumorigenesis (Hurlin et al., 2003; Dezfouli et al., 2006; Hurlin and Huang, 2006; Toyo-oka et al., 2006). Importantly, each of these cell types has been shown to be prone to tumorigenesis by Myc overexpression in transgenic mice (Nesbit et al., 1999). Furthermore, Myc and

Mnt have been shown to regulate a similar set of target genes (Toyo-oka et al., 2006). Taken together, these data indicate that Mnt operates in the same cells and at the same times like Myc, directly antagonizing Myc function.

Less is known about the biological functions of Mga, a large protein that possesses two DNA binding domains: the bHLHzip domain and a T-domain (Hurlin et al., 1999). However, Mga was shown to inhibit Myc-dependent cell transformation (Hurlin et al., 1999) and Mga/Max complexes were identified as part of an E2F6 repression complex (Ogawa et al., 2002), making it possible that also Mga acts as Myc antagonist.

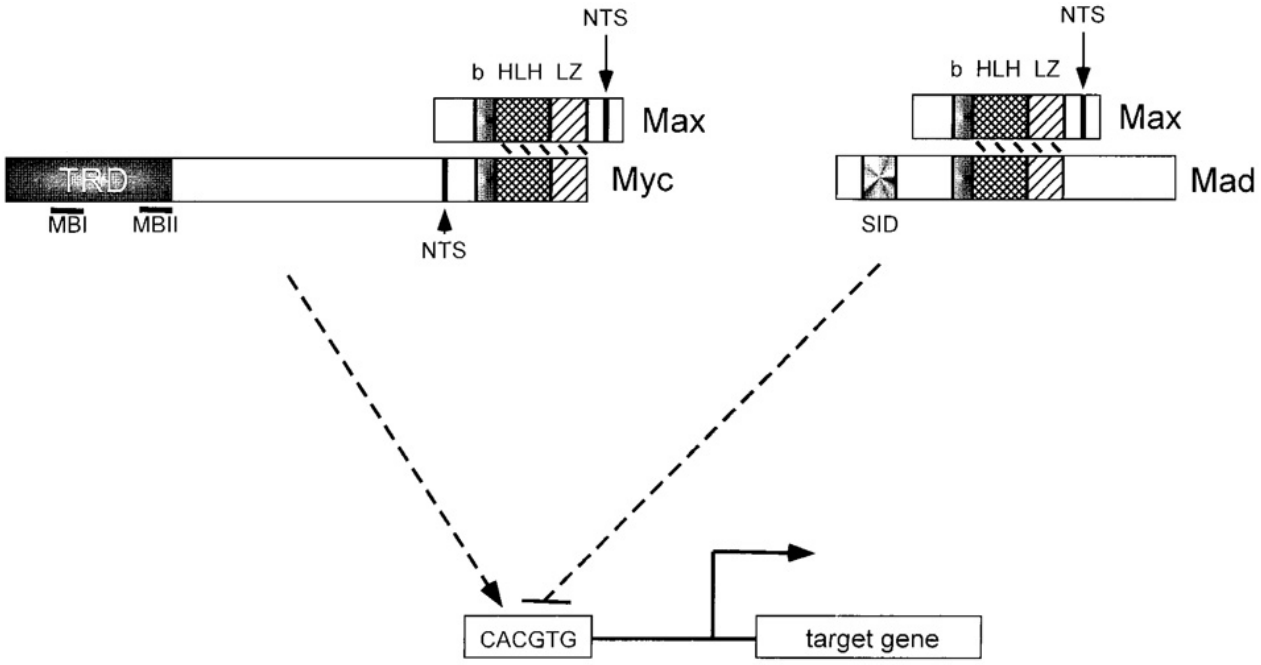

Figure I

The diagram depicts the association of Max with either Myc or Mad/Mnt proteins. The heterodimeric transcription factors are shown to regulate transcription of a hypothetical target gene through the E box element, 5'-CACGTG-3'. The Myc/Max heterodimer binds E-boxes and activates transcription possibly through histone acetylation and direct interaction of the Myc transregulatory domain with the transcriptional machinery. Mad/Max complexes recruit Sin3 corepressors and histone deacetylases to the Sin3-interacting domain (SID) to repress E-box-driven transcription. The Myc, Mad and Max functional domains are shown, with all three proteins containing the basic helix-loop-helix leucine zipper (bHLHZip). NTS is the nuclear targeting signal. TRD is the Myc transactivation domain, containing the Myc box I (MBI) and Myc Box II (MBII) regions. (modified from Dang et al., (1999) Experimental Cell Research 253:63-77)

4. The Max network in *Drosophila*

4.1. *Drosophila* orthologs

The identification of dMyc, the sole Myc ortholog in *Drosophila*, in yeast two-hybrid screens, using human Max protein as bait, has made it possible to study Myc in a genetically tractable animal model (Gallant et al., 1996; Schreiber-Agus et al., 1997). The gene that encodes dMyc turned out to be identical to the *diminutive* gene (*dm*), a gene that had been described based on a mutation (dm^1) in the 1930s (Bridges, 1935). While "*dm*" is the official designation, the synonym "*dmyc*" is widely used in the literature. After its identification, dMyc was then used to identify the *Drosophila* ortholog of Max (dMax). As in vertebrates, dMyc and dMax form heterodimers and these bind to the canonical E-box sequence (Gallant et al., 1996). More recently, dMnt has been described as the sole *Drosophila* ortholog of the vertebrate Mad/Mnt protein family (Loo et al., 2005). Thus, the Max network is conserved in *Drosophila*, but much simpler than in vertebrates, featuring one member of each protein class.

4.2. *dmyc*

The bHLHzip domain of dMyc is highly conserved, and also the domains important for transactivation (MBI, MBII) and the acidic region are conserved, albeit to a lesser degree (Gallant, 2006). dMyc and c-Myc can functionally substitute for each other surprisingly well: dMyc can transform rat embryo fibroblast upon coexpression of oncogenic Ras (Schreiber-Agus et al., 1997), functionally substitutes for c-Myc in transactivation assays (Gallant et al., 1996) and rescues growth defects of mouse embryo fibroblasts derived from *c-myc* conditional knock-outs (Trumpp et al., 2001). Conversely, two c-Myc isoforms (c-Myc2 and MycS) can rescue the otherwise complete lethality of a strong hypomorphic *dmyc* mutant, allowing these flies to develop into fertile adults (Benassayag et al., 2005). Taken together, these findings show a high degree of functional conservation between vertebrate and *Drosophila* Myc.

Loss of dMyc function is associated with growth defects. Mutants hypomorphic for dMyc can reach adulthood, but show a developmental delay, smaller body size, reduced weight and a thin bristle phenotype. The small size of these mutants is due to smaller cell size (Johnston et al., 1999). Strong hypomorphic mutants and null mutants die as larvae (Maines et al., 2004; Pierce et al., 2004). *dmyc* mutant clones show growth defects both in diploid and polyploid (endoreplicating) tissues (Johnston et al., 1999; Maines et al., 2004; Pierce et al., 2004). Conversely, dMyc overexpression leads to bigger diploid cells and to a tremendous increase in the size of endoreplicating cells.

dMyc has an effect on both the cell cycle and on cellular growth (defined as the increase in cell mass over time). While *dmyc* hypomorphic mutant imaginal wing disc cells show a slight accumulation in G1 phase and smaller size, overexpression of dMyc strongly accelerates G1-S transition. However, the

overall duration of the cell cycle cannot be shortened by the overexpression of dMyc, since the observed shorter G1 phases go along with longer S and G2 phases. Since dMyc does not increase the cycling rates of these cells, but increases cellular growth, cell size but not cell number is increased (Johnston et al., 1999).

How does dMyc regulate cellular growth? Several lines of evidence point to an important role of dMyc in the control of protein biosynthesis. Firstly, the developmental delay and thin bristle phenotypes of *dmyc* hypomorphic mutants are reminiscent of the phenotypes of *Minute* mutants. *Minute* genes encode ribosomal proteins - *Minute* mutations result in impaired protein biosynthesis. Secondly, overexpression of dMyc strongly increases nucleolar size, indicating higher rates in the production of ribosomes (Grewal et al., 2005). Thirdly, a large number of dMyc target genes is involved in nucleolar function, rRNA processing and ribosome biosynthesis (Orian et al., 2003; Hulf et al., 2005), and dMyc has been shown to regulate RNA polymerase I-dependent transcription (Grewal et al., 2005).

The role of dMyc in the regulation of protein biosynthesis is probably linked to another phenomenon that can be observed both in the context of *dmyc* and *Minute* mutant situations: cell competition in imaginal disc tissues. When $Minute^{+}$ clones are generated in $Minute^{+}/Minute^{-}$ imaginal wing discs, normally sized wings result, but a large part of the heterozygous tissue is found to be replaced by $Minute^{+}$ tissue, implying the elimination of the $Minute^{+}/Minute^{-}$ cells. Conversely, $Minute^{-}/+$ clones are eliminated from wild type imaginal disc tissue, but survive well when surrounded by tissue that is heterozygous mutant for another *Minute* gene (Simpson and Morata, 1981). This phenomenon was termed cell competition. This process has also been observed in *dmyc* mutant situations. Clones mutant for the weak hypomorphic allele dm^{P0} are eliminated from $dm^{P0}/+$ imaginal wing disc tissue by cell competition (Johnston et al., 1999). Recently, this process has been studied more closely, and it has been shown that in situations, where cells with differing *dmyc* levels are juxtaposed, apoptosis is induced in the cells with lower *dmyc* levels (De La Cova et al., 2004; Moreno and Basler, 2004). Strikingly, cells which moderately overexpress *dmyc* have a competitive advantage over wild type cells. Presently, it is not clear whether cell competition exists in mammalian systems. If it exists, it might play an important role in tumorigenesis.

4.3. *dmnt*

The sole *Drosophila* ortholog of the *mad/mxi/mnt* gene family has been termed *dmnt*, because it is most similar to *mnt* in size and overall organization (Loo et al., 2005). Like its mammalian counterparts, dMnt acts as a transcriptional repressor. dMnt forms heterodimers with dMax, binds to canonical E-box sequences and represses transcription via the Sin3 corepressor and recruitment of HDAC. Three splice variants occur: full length dMnt, dMntΔSID (a form lacking the Sin3-interaction domain) and dMntΔZip (a form lacking the leucine zipper) (Loo et al., 2005).

dmnt mutant flies are fully viable, unlike the *mnt* mutant mice which die at birth. These flies have larger cells than wild type animals and a larger total body weight. Conversely, overexpression of *dmnt* in cell clones in the imaginal wing discs results in a strongly reduced size of the clones (and of the individual mutant cells) (Loo et al., 2005).

4.4. *dmax*

Prior to this study (and the diploma thesis preceding it (Steiger, 2002)), no genetic analysis of *dmax* had been undertaken and no *dmax* mutants had been described. Therefore, not much was known about the biological functions of dMax. Like its mammalian counterpart, dMax is required for the regulation of transcription by the other members of the network, forming positively acting dMyc/dMax heterodimers and repressive dMnt/dMax heterodimers that bind to E-box sequences (Gallant et al., 1996; Loo et al., 2005). In embryos, the 1.2 kb *dmax* transcript is expressed ubiquitously, being less restricted in the expression pattern than *dmyc*, but at lower levels than the *dmyc* transcript, especially in earlier stages (Gallant et al., 1996).

5. Project overview

In mammalian systems, a large amount of knowledge about the molecular and biological functions of the Max network has been accumulated. Yet, a rigorous analysis of the functions of the Max network has proved difficult due to functional redundancy among the network members and due to the complexity and diversity of the network's functions. In *Drosophila*, the Max network is conserved in a greatly simpler form, with one ortholog of *myc*, *mnt* and *max* present. Nevertheless, at least a large part of the fundamental functions of both *myc* and *mnt* are conserved. Taken together with the sophisticated genetic tools available, *Drosophila* is therefore an ideal system for a thorough genetic epistasis analysis. While null mutants for both *dmyc* and *dmnt* have been described (Pierce et al., 2004; Loo et al., 2005), mutants for *dmax* have been lacking so far.

With the *dmax*-RNA*i* system and the *dmax* null mutant presented in this study, a functional analysis of *dmax* and a detailed epistatic analysis of the whole Max network became possible. While the analysis showed that loss of *dmax* recapitulates the loss of *dmyc* to a certain extent, striking differences between the phenotypes of *dmyc* and *dmax* mutants were revealed. A detailed analysis of mutant combinations of the Max network members clearly showed that dMyc has important growth functions that do not require dMax, both in diploid an polyploid tissues. Furthermore, the analysis showed that cell competition is partly *dmax*-independent. Experiments in which *dmyc* was overexpressed both in wild type and *dmax* mutant situations provided further evidence for *dmax*-independent functions of *dmyc*: Overexpression of *dmyc* in the eye resulted in *dmax*-independent growth and apoptosis. Strikingly, ubiquitous overexpression of *dmyc* in *dmax* null larvae revealed a connection to the ecdysone system and to the control of the developmental timing. Finally, *dmyc* was shown to

upregulate the levels of transcription of certain small RNA genes (among them 2 snoRNA genes) in the absence of *dmax*, providing a potential molecular basis for the observed *dmax*-independent growth functions of *dmyc*.

Results

1. *dmax*-RNA*i*

In the first part of this study, a system based on transgenic RNA*i* was used to monitor the consequences of reduced *dmax* levels.

1.1. Tools: *dmax*- and *lacZ*-dsRNA constructs

In the diploma thesis that preceded this work, transgenic flies were created that carry constructs that allow a regulated expression of *dmax* or *lacZ* double stranded RNA (Steiger, 2002). In these flies, *dmax* or *lacZ* mRNA is silenced upon expression of *dmax* or *lacZ* double stranded RNA (dsRNA) by RNA interference (RNA*i*). The transgenes consist of inverted repeats of *dmax* or *lacZ* cDNA that were cloned into the expression cassette of the pUAST P element vector (Figure 1). Expression of the inverted repeat cDNA under the control of the yeast transcriptional activator GAL4 leads to the formation of RNA hairpins that provoke RNA interference. The inverted repeats are directly juxtaposed and only separated by an SfiI restriction site containing 5 nonpalindromic nucleotides that help to prevent recombination events during the cloning process. The 784 bp *dmax* repeats correspond to nucleotides 132-915 of the 1011 bp *dmax* transcript. The *lacZ* repeats have a length of 769 bp and contain nucleotides 1847-2615 of the total 3113 bp *lacZ* cDNA.

The *lacZ*-dsRNA construct has been generated for control purposes: we intended to demonstrate that the chosen type of dsRNA construct is capable of strongly and specifically silencing the target gene. The *lacZ*-dsRNA construct also serves as a control in experiments with the *dmax*-dsRNA construct to exclude general consequences of the overexpression of double stranded RNA.

Figure 2 depicts the *dmax* genomic locus. As indicated, the *dmax* cDNA included in the inverted repeat constructs covers almost the whole *dmax* transcript. Contrary to our intentions, a small part of the repeat also covers the first exon of a neighboring gene *(CG9666)*. This exon has been added to the gene prediction in genome version 3. The prediction is supported by two cDNA clones (clones RE16168 5 and RE39930 5). As we show in this work, *CG9666* is not downregulated by *dmax*-RNA*i* and moreover, *CG9666* is nonessential.

Several independent transgenic fly lines have been generated with both of the constructs and an initial characterization of the fly lines has been performed (Steiger, 2002). In this work, the following naming convention will be used: Fly lines carrying the *dmax* dsRNA construct are called *dmax*-IR (inverted repeat) lines, fly lines carrying the *lacZ* dsRNA construct are correspondingly called *lacZ*-IR lines. Independent transgenic lines are labeled with stock numbers (e.g. *dmax*-IR 2-7).

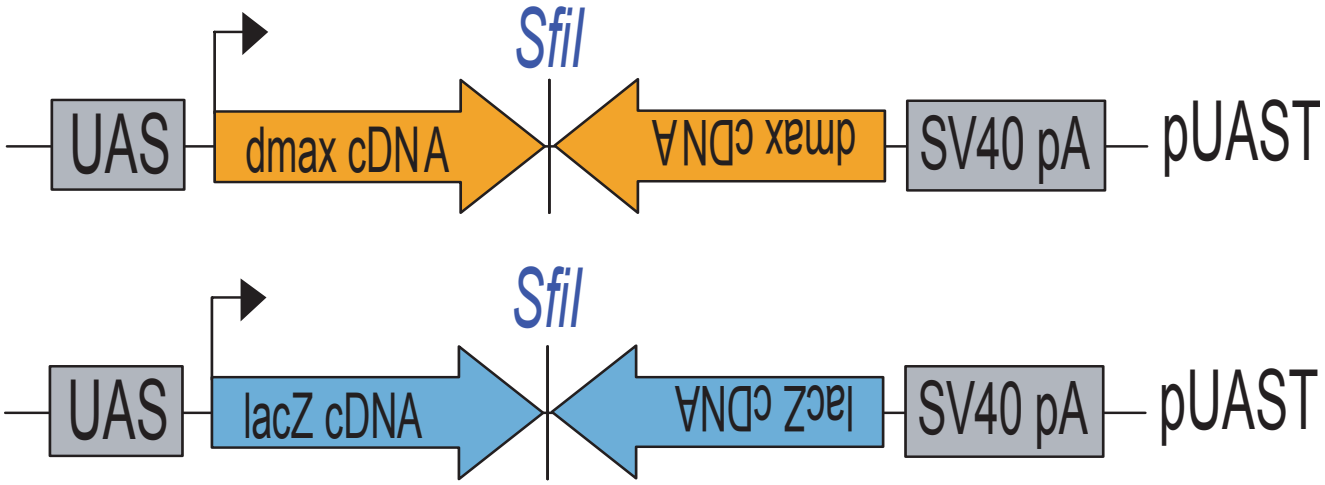

Figure 1
Structure of the *dmax*- and *lacZ*-RNA*i* constructs.

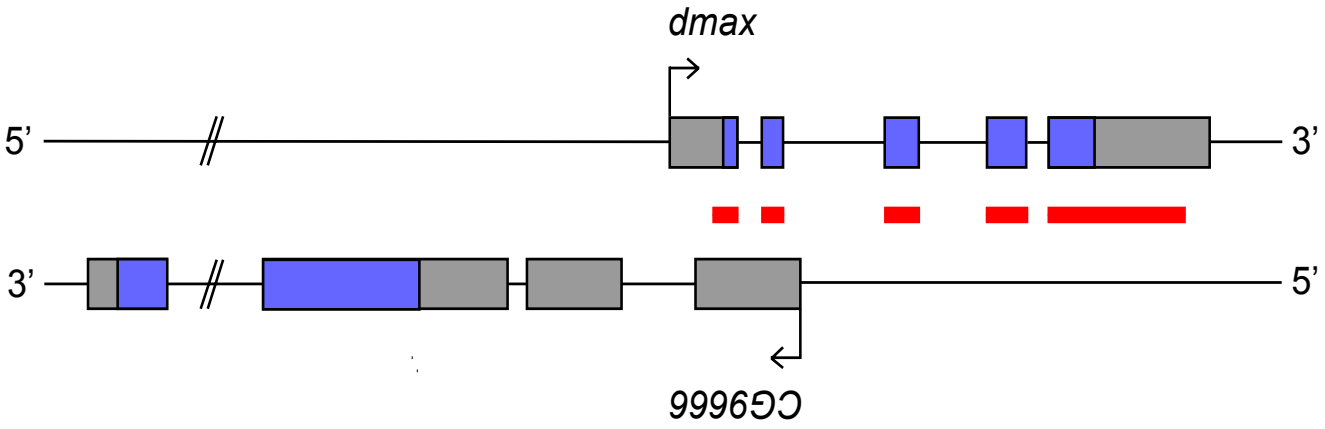

Figure 2
dmax genomic locus. The arrows indicate transcription start sites and the direction of transcription. Grey boxes indicate transcribed DNA, blue boxes indicate open reading frames. Red boxes indicate regions covered by the *dmax* inverted repeats.

1.2. Effects of *dmax*-RNA*i* on viability

1.2.1. *dmax*-RNA*i* causes pupal lethality in a background of reduced *dmax* dosis

In Steiger (2002), an initial characterization of the established *lacZ*-IR and *dmax*-IR lines has been performed. This section gives a brief summary of the performed experiments. Based on the larval and pupal lethal phenotype of strong hypomorphic *dm* mutants like dm^{PG45} or dm^{PL35} (Bourbon et al., 2002), we tested whether we could produce a similar phenotype by overexpressing *dmax* dsRNA with the strong and ubiquitous drivers *actin-GAL4* and *daughterless-GAL4*. Surprisingly, strong ubiquitous overexpression of *dmax* dsRNA did not lead to a noticeable decrease in viability of the flies in most of the experiments. Next, we examined if we would see a stronger effect in flies that carry only one copy of *dmax*. For this purpose, flies were used that are heterozygous for *Df(3L)fz2*, a large deficiency that uncovers the *dmax* locus. Expression of *dmax* dsRNA under control of *actin-GAL4* in this context led to almost complete lethality in 6 out of 10 independent *dmax*-IR lines (0 - 10 % escapers). These lines (*dmax*-IR 2-7, 5-1, 5-2, 6-1, 7-3, 8-1) were chosen for further investigation. The effect is specific for *dmax* RNA*i*, since the presence of *Df(3L)fz2* did not significantly alter the viability of flies in which *lacZ* dsRNA was expressed. The tested *lacZ*-IR lines (*lacZ*-IR 1-1, 3-1, 6-1) have been shown to strongly silence *lacZ* expression (Steiger, 2002).

Df(3L)fz2/+ animals in which *dmax* dsRNA is expressed died as pharate imagines. The morphology of these imagines was normal, except that they frequently showed necrosis of thoracal and postocular air sacs. Less frequently, necrotic lesions of abdominal tissue were observed. The few eclosing escapers had a mostly normal appearance. Infrequently, small necrotic lesions were present. Both uneclosed pharate animals and eclosed escapers had a wild type body size, but thin bristles. Thus, *dmax* is essential for viability and for bristle growth, as is *dmyc*.

1.2.2. *dmax*-RNA*i* causes pupal lethality also in a $dmax^1$ background

The surprisingly strong reduction in viability from complete lack of lethality to almost full lethality in a *Df(3L)fz2/+* background can by explained by the assumption that *dmax* levels in this situation fall short of a critical threshold that is necessary for continuation of development. However, *Df(3L)fz2* is a large deficiency that also uncovers *reptin*, a gene that has been shown to positively interact with *dmyc* (Bellosta et al., 2005). Hence it was possible that the effect seen (even though dependent on RNA*i*) is based on the combined reduction of *dmax* and *reptin* levels. We tested therefore whether the observed strong loss of viability could also be caused by the removal of one copy of *dmax*. Indeed, expression of *dmax* dsRNA with *actin-GAL4* in a $dmax^1$/+ background had the same effect as in a *Df(3L)fz2/+* situation (Figure 3, A-C and D-F), confirming that a strong enough reduction of *dmax* levels alone is sufficient to cause lethality.

1.2.3. The pupal lethality caused by *dmax*-RNA*i* in a *Df(3L)fz2/+* background can be fully rescued by coexpression of a *UAS-dmax* rescue construct

The observed pupal lethality is due to specific silencing of *dmax* and not a consequence of unspecific effects of *dmax*-RNA*i*, since coexpression of a *UAS-dmax* cDNA rescue construct fully restores wild type viability (Figure 3, G-K). This finding also rules out the possibility that the observed effects are due to a reduction of *CG9666* mRNA levels by *dmax*-RNA*i.*

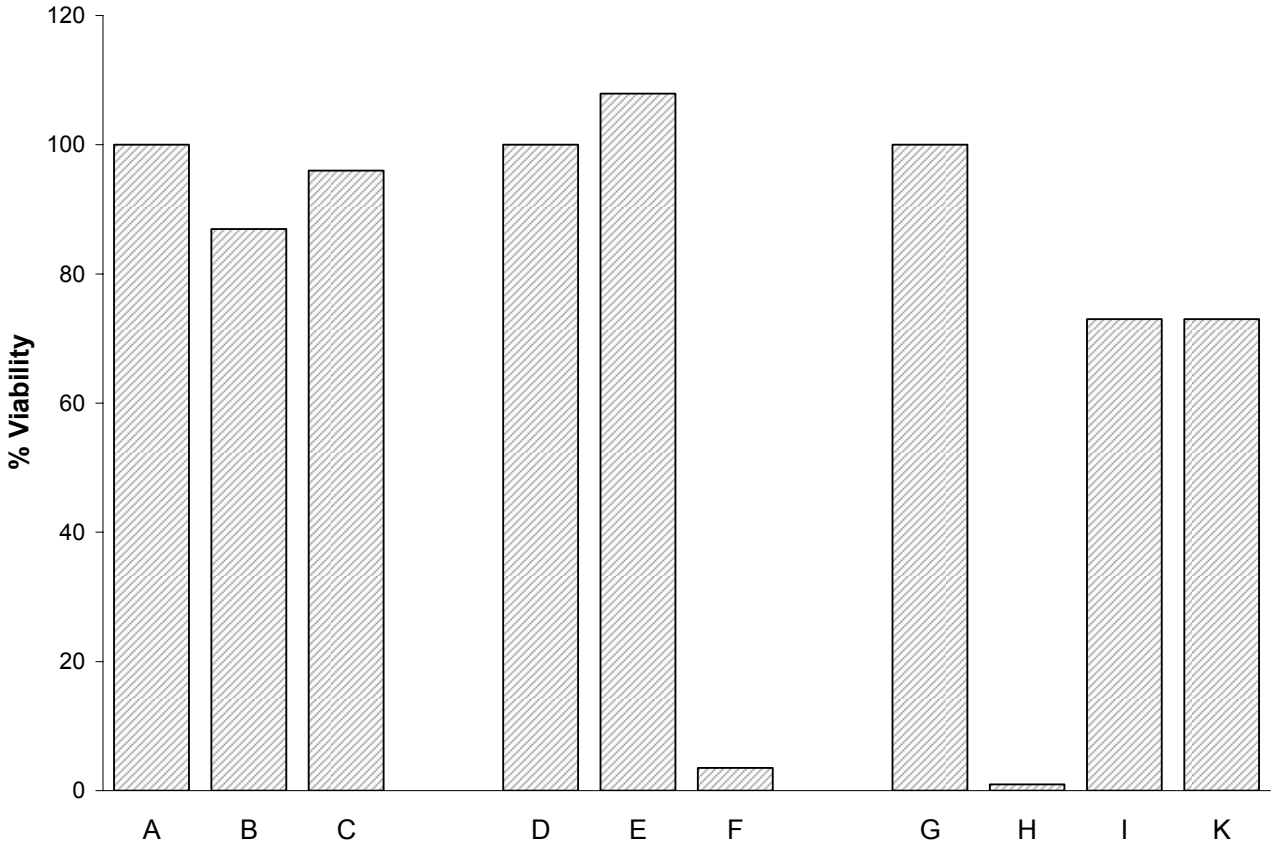

Figure 3
Viability of flies that strongly and ubiquitously express *dmax* dsRNA, in combination with *Df(3L)fz-2* and with a *UAS-dmax* rescue construct. Viability rates of the genotypes B and C are calculated relative to genotype A (the viability of A was set to 100%). Viability rates of the genotypes E and F are calculated relative to genotype D (the viability of D was set to 100%). The viability rate of the genotypes H, I, K is indicated relative to genotype G (the viability of G was set to 100%). For a more detailed explanation of the viability calculations, see Materials and Methods.

Label:	Genotypes:	Eclosed flies:
A	*y w; UAS-dmax-IR(2-7)/CyO, y^+*	199
B	*y w; actin-GAL4/CyO*	173
C	*y w; UAS-dmax-IR(2-7)/actin-GAL4*	191
D	*y w; UAS-dmax-IR(2-7)/CyO, y^+; $dmax^1$/+*	114
E	*y w; actin-GAL4/CyO; $dmax^1$/+*	123
F	*y w; UAS-dmax-IR(2-7)/actin-GAL4; $dmax^1$/+*	4
G	*y w; actin-GAL4/UAS-dmax; UAS-dmax-IR(6-1)/Df(3L)fz2*	100
H	*y w; actin-GAL4/+; UAS-dmax-IR(6-1)/Df(3L)fz2*	1
I	*y w; [UAS-dmax; UAS-dmax-IR(6-1)]/SM5-TM6B*	73
K	*y w; [+; UAS-dmax-IR(6-1)]/SM5-TM6B*	71

1.2.4. Combinations of *dmax* dsRNA constructs cause pupal lethality in a wild type background

Since strong expression of the *dmax* dsRNA constructs led to no reduction of viability in a wild type background (*dmax*-IR 2-7: Figure 3, for the other *dmax*-IR lines see Steiger, 2002), we generated fly lines that carry combinations of *dmax* dsRNA constructs. All combinations that were tested (2-7 + 5-2, 5-2 + 6-1, 5-2 + 7-1 and 2-7 + 5-2 + 6-1) caused almost complete pupal lethality. The effect that was observed was as strong as the effect of expressing single copies of the *dmax* dsRNA constructs in a *Df(3L)fz2*/+ or $dmax^1$/+ background. We concluded that combinations of the *dmax* dsRNA transgenes sufficiently lower *dmax* mRNA levels to cause pupal lethality in a wild type background.

The flies fail to eclose and die as pharate animals. Dissection of such pupal cases revealed normally developed animals with a thin bristle phenotype. Frequently, necrosis of thoracal air sacs, of air sacs in the head and of abdominal trachea was observed (Figure 4). Diffuse patterns of necrosis were observed on the abdomen. It is not clear whether the observed necrosis is an unspecific consequence of the failure of the flies to eclose.

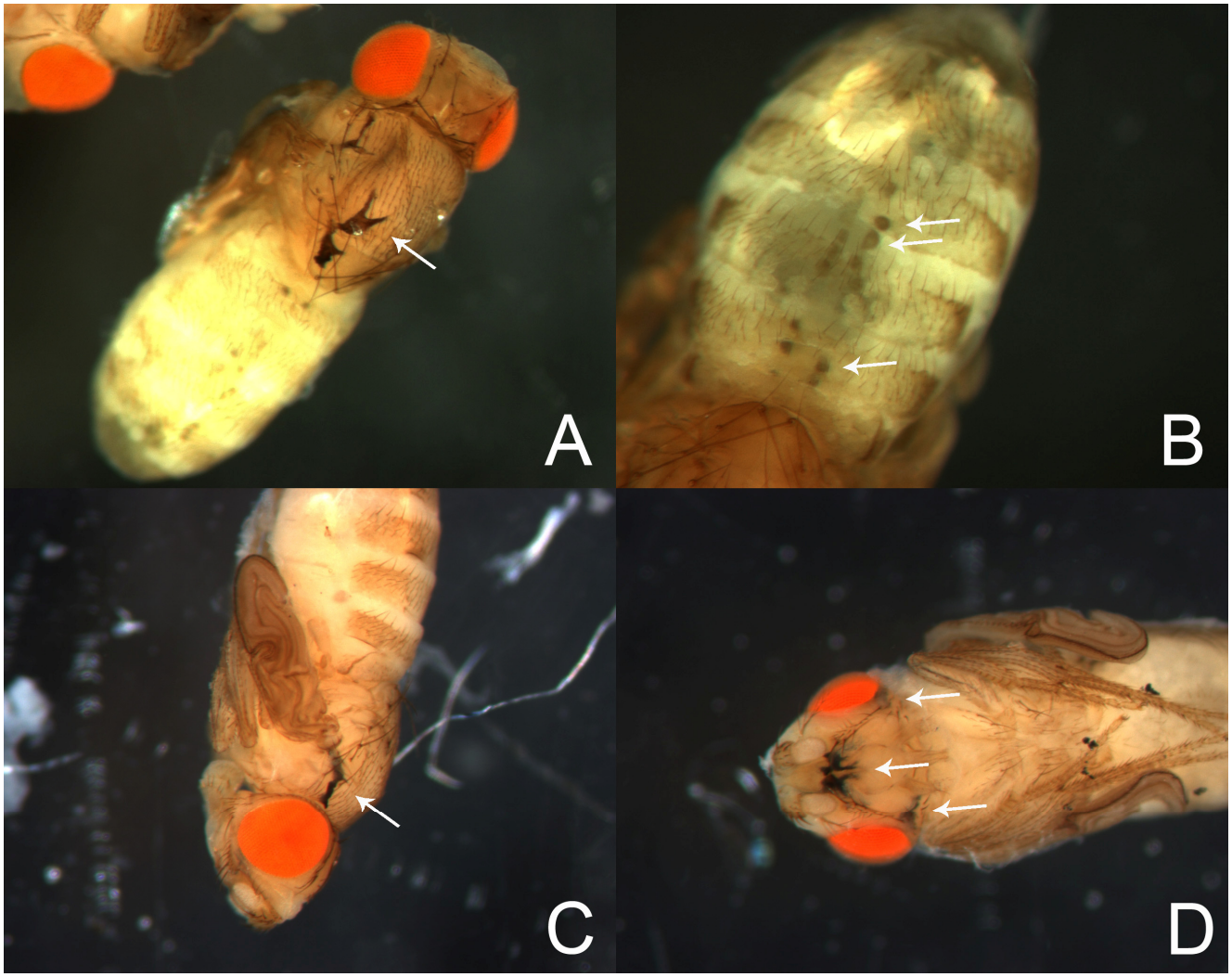

Figure 4

Genotypes:

A	*y w; UAS-dmax-IR(2-7)/+; UAS-dmax-IR(5-2) UAS-dmax-IR (6-1)/da-GAL4*
B	*y w; UAS-dmax-IR(2-7)/+; UAS-dmax-IR(5-2) UAS-dmax-IR (6-1)/da-GAL4*
C	*y w; UAS-dmax-IR(2-7)/actin-GAL4; UAS-dmax-IR(5-2) UAS-dmax-IR (6-1)/+*
D	*y w; UAS-dmax-IR(2-7)/actin-GAL4; UAS-dmax-IR(5-2) UAS-dmax-IR (6-1)/+*

Pharate animals were taken out of their pupal case. The animals have thin bristles. Necrotic spots are visible on the abdomens (A, B [higher magnification], C). Thoracal air sacs and air sacs in the head show widespread necrosis (A, C, D). Arrows indicate necrotic regions.

1.3. *dmax*-RNA*i* strongly decreases *dmax* mRNA levels

Having identified strong *dmax*-IR lines based on the pupal lethality of animals expressing *dmax* dsRNA in a *Df(3L)fz2/+* background, we examined the extent of reduction of *dmax* mRNA levels in flies that express *dmax* dsRNA under control of *actin-GAL4.* For this purpose, we extracted total RNA from wandering larvae that carried the *actin-GAL4* driver and one or three copies of the *dmax* dsRNA transgene. As a control, total RNA was extracted from flies that carried only *actin-GAL4.* Additionally, total RNA was extracted from larvae that carried a P element insertion (*EY02775)* in the second exon of *CG9666* (flies of this genotype were used to create the $dmax^{1}$ null mutant). The total RNAs were retrotranscribed and qRTPCR was performed with primers specific for the *dmax* and *CG9666* 3' UTRs; the amplified sequence did not overlap with the sequence included in the inverted repeat RNA. mRNA levels were calculated relative to reference qRTPCR reactions with primers specific for the *Act42A* or *Rpl32* gene (Figure 5).

The results show that *dmax* mRNA levels in the *dmax*-IR larvae were strongly reduced, even though a full silencing is clearly not achieved. Surprisingly, we could not show that *dmax* mRNA levels are more strongly reduced in the flies carrying three copies of the *dmax*-IR construct. We had expected to find lower mRNA levels in this genotype based on the stronger phenotypes that are created by expressing three copies of the *dmax* dsRNA transgene instead of one copy. Possibly, the additional decrease in *dmax* mRNA levels is too weak to be detected given the experimental errors in qRTPCR experiments, or it affects only a subset of tissues.

dmax RNA levels in the *y w;* $P\{y^{+}\ w^{+}\}CG9666^{EY02775}$ genotype were - if at all - only slightly reduced. The *EY02775* P element insertion is only 400 bp from the start of the *dmax* transcript, but the finding is compatible with the observation that *y w;* $P\{y^{+}\ w^{+}\}CG9666^{EY02775}$ as well as *y w;* $P\{y^{+}\ w^{+}\}CG9666^{EY02775}$*/Df(3L)fz2* flies are fully viable.

According to annotation 3.0 of the *Drosophila* genome, the first exon of *CG9666* overlaps with the first and the second exon of *dmax* and thus with a short region of the *dmax* dsRNA constructs (Figure 2). Nevertheless, *CG9666 levels* seem not to be affected by *dmax*-RNA*i*. This might be due to the shortness of the overlap of the inverted repeat sequence with the *CG9666* transcript or due to the fact that the annotation of *CG9666* in the *Drosophila* genome version three is wrong. *y w;* $P\{y^{+}\ w^{+}\}CG9666^{EY02775}$ flies, which are fully viable, show clearly reduced levels of *CG9666*. The fact that there is substantial expression of *CG9666* in this genotype is still surprising, since the P element is inserted in the second exon of the gene. This might hint to an alternative transcription start site upstream of the *CG9666* ORF, but downstream of the P element insertion.

CG9666 mRNA levels are clearly lower in *y w;* $P\{y^{+}\ w^{+}\}CG9666^{EY02775}$ flies than in flies that express *dmax* dsRNA, but this reduction obviously does not reduce viability (nor does it have any other phenotypic consequences). It is therefore clear that the observed strong pupal lethality caused by *dmax*-RNA*i* is independent of *CG9666.*

Taken together, these findings indicate that *dmax*-RNA*i* specifically decreases *dmax* mRNA levels, thus phenocopying a *dmax* hypomorphic mutant.

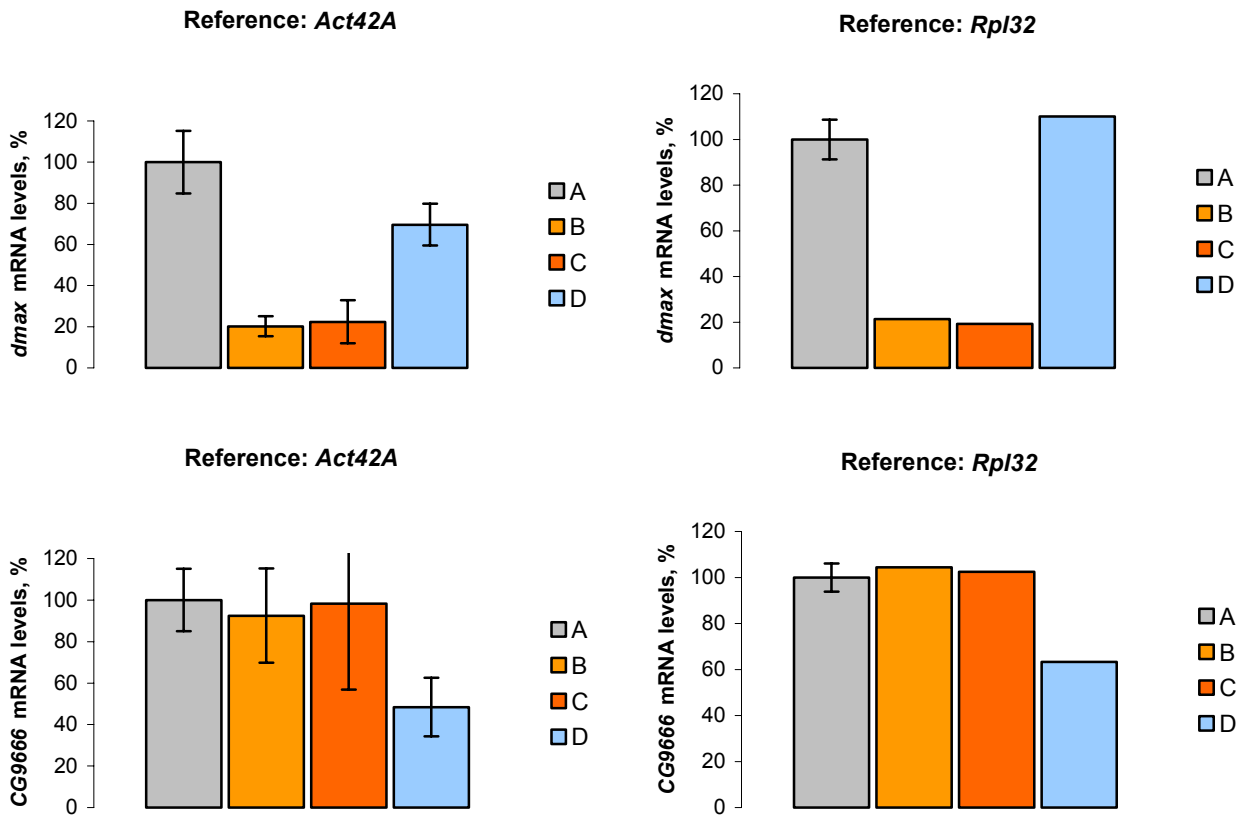

Figure 5
mRNA levels of *dmax* and *CG9666* relative to the reference genes *Act42A* and *RpL32*. Quantitative real time PCR was performed on cDNA from wandering third instar larvae. Values with error bars are based on 2 biological replicates, whereas values without error bars are based on a single RNA sample. The error bars indicate standard deviations.

Genotypes:

A *y w; +/actin-GAL4*

B *y w; UAS-dmax-IR(2-7)/actin-GAL4; TM6B/+*

C *y w; UAS-dmax-IR(2-7)/actin-GAL4; UAS-dmax-IR(5-2) UAS-dmax-IR(6-1)/+*

D *y w; P{y^{+} w^{+}}CG9666^{EY02775}*

1.4. *GAL4* drivers which do not cause mutant phenotypes with the *dmax* dsRNA constructs

The single insertion line *dmax*-IR 2-7 and the recombined line *dmax*-IR 2-7 5-2 6-1 were crossed to the following *GAL4* driver lines: *eyeless-GAL4* (eye and head capsule specific), *pumpless-GAL4* (fat body specific), *engrailed-GAL4* (specific for the posterior compartments), *ELAV-GAL4* (pan-neural) and *forkhead(81.0)-GAL4* (salivary gland specific). At 25° C, expression of *dmax* dsRNA with these drivers did not result in a mutant phenotype. We repeated the experiments at a temperature of 29° C, since GAL4 activity is temperature-dependent and more active at higher temperatures. Experiments above 29° C are not possible, since higher temperatures are not well tolerated by *Drosophila* at extended lengths of time. Also at 29° C, none of the drivers did result in a mutant phenotype.

1.5. *dmax*-RNA*i* reduces body weight

Strong expression of single copies of a *dmax* dsRNA construct that lowers *dmax* mRNA levels to 20% (Figure 5) did generally not lower the viability of the flies, even though there was a certain extent of variability in the survival of male flies whose viability was decreased in some experiments. However, Figure 6 shows that expression of *dmax* dsRNA decreases the weight of females by 19% and of males by 15% relative to the weight of females and males that express *lacZ* dsRNA. The effect is due to the *expression* of the construct, since both transgenes do not reduce body weights in absence of *actin-GAL.* Thus, *dmax* behaves as expected for an essential partner of *dmyc,* since hypomorphic mutants of *dmyc* are smaller than wild type animals (Johnston et al., 1999).

1.6. *dmax*-RNA*i* causes a thin bristle phenotype

One of the hallmarks of *dmyc* hypomorphic mutants is a thin bristle phenotype (macrochaetae that are smaller in relation to overall body size than in wild type animals). This phenotype occurs in mutants that have defects in protein biosynthesis and is typical for *Minute* mutants (Lambertsson, 1998). When *dmax* dsRNA is strongly expressed under control of *actin-GAL4* in a *Df(3L)fz2/+* background, pupal lethality resulted and pharate animals that did not eclose as well as the few escapers showed a thin bristle phenotype. To confirm this phenotype, we expressed *dmax* dsRNA with *scabrous-GAL4* (*sca-GAL4)*, a GAL4 driver that is expressed in bristle progenitor cells. This did not compromise the viability of the flies, but resulted in a thin bristle phenotype. We measured the bristle sizes of the posterior scutellar macrochaetae. In comparison to control flies that expressed *lacZ* dsRNA, the size of the posterior scutellar bristles was reduced by 30% in both males and females that expressed *dmax* dsRNA (Figure 7). One copy of the *dmax* dsRNA construct was sufficient for this decrease; bristle size could not be further reduced in flies that carried three copies of the *dmax* dsRNA construct.

A strong reduction in thoracal bristle size could also be achieved with the driver *decapentaplegic-GAL4* (*dpp-GAL4*). Whereas expression of *dmax* dsRNA with *dpp-GAL4* did not cause a mutant wing

phenotype and did not cause lethality, it reduced the size of the anterior and posterior bristles by more than 50% (Figure 8).

These results show that also in its effect on bristle size, reduction of *dmax* has similar consequences as a reduction of *dmyc* has.

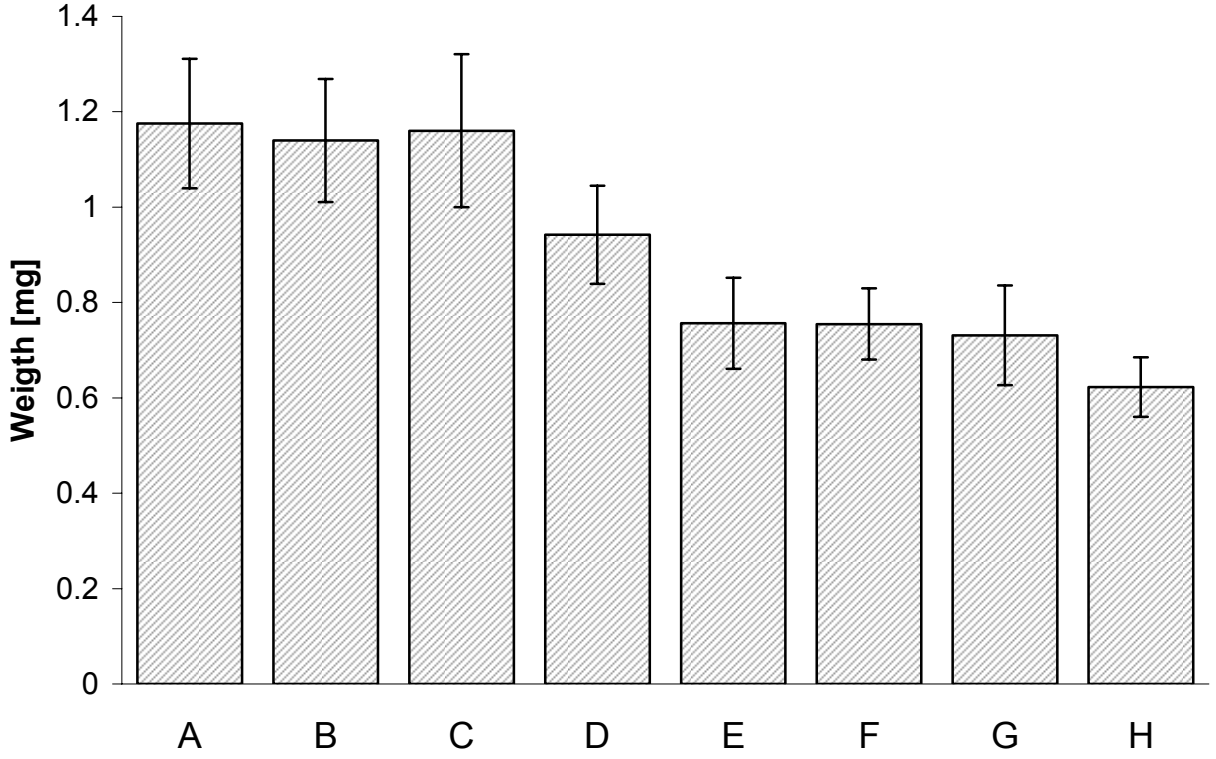

Figure 6
dmax-RNA*i* decreases the body weight of adult females and males, whereas *lacZ*-RNA*i* has no such effect. The error bars indicate standard deviations.

Label:	Genotypes:	Number of measured flies:
Females:		
A	*y w; UAS-lacZ-IR(3-1)/CyO, y*$^{+}$	109
B	*y w; UAS-dmax-IR(2-7)/CyO, y*$^{+}$	90
C	*y w; UAS-lacZ-IR(3-1)/actin-GAL4*	104
D	*y w; UAS-dmax-IR(2-7)/actin-GAL4*	46
Males:		
E	*y w/Y; UAS-lacZ-IR(3-1)/CyO, y*$^{+}$	104
F	*y w/Y; UAS-dmax-IR(2-7)/CyO, y*$^{+}$	108
G	*y w/Y; UAS-lacZ-IR(3-1)/actin-GAL4*	39
H	*y w/Y; UAS-dmax-IR(2-7)/actin-GAL4*	9

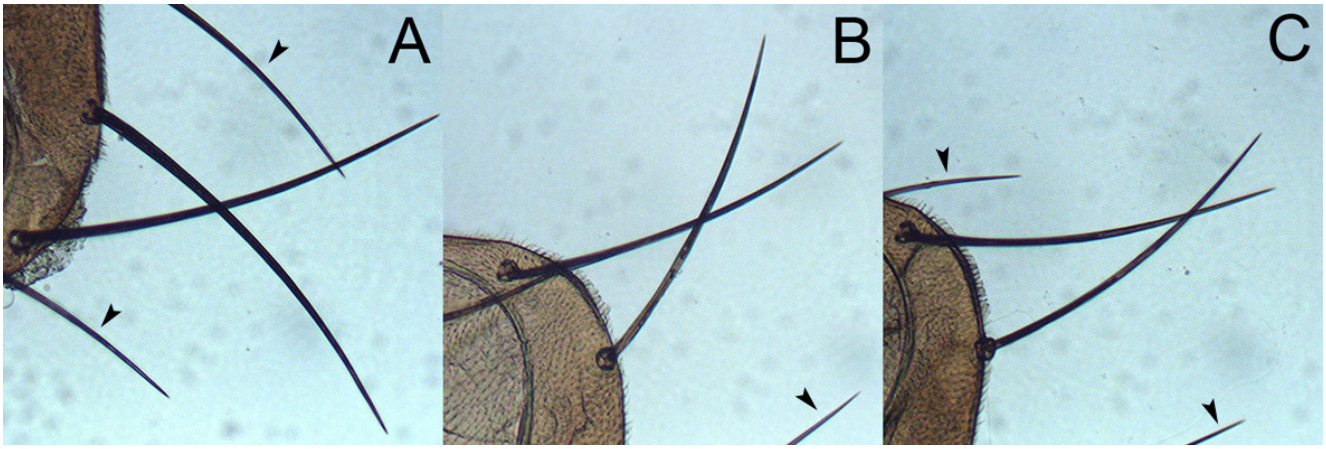

Figure 7
dmax-RNA*i* reduces bristle size. The pictures above show the posterior scutellar bristles (and partly the anterior scutellar bristles (arrowheads)) of flies that express *lacZ* dsRNA (A) and *dmax* dsRNA (B, C) under control of *sca-GAL4*. The chart below depicts the calculated bristle area of the posterior scutellar bristles for females (A, B, C) and males (A', B', C') of the indicated genotypes. For every genotype, the area of both posterior scutellar bristles of 8-10 individual flies was determined. The error bars indicate standard deviations.

Genotypes:

A *y w/w; UAS-lacZ-IR(1-1)/sca-GAL4*
A' *y w/Y; UAS-lacZ-IR(1-1)/sca-GAL4*
B *y w/w; UAS-dmax-IR(2-7)/sca-GAL4*
B' *y w/Y; UAS-dmax-IR(2-7)/sca-GAL4*
C *y w/w; UAS-dmax-IR(2-7)/sca-GAL4; UAS-dmax-IR(5-2) UAS-dmax-IR(6-1)/+*
C' *y w/Y; UAS-dmax-IR(2-7)/sca-GAL4; UAS-dmax-IR(5-2) UAS-dmax-IR(6-1)/+*

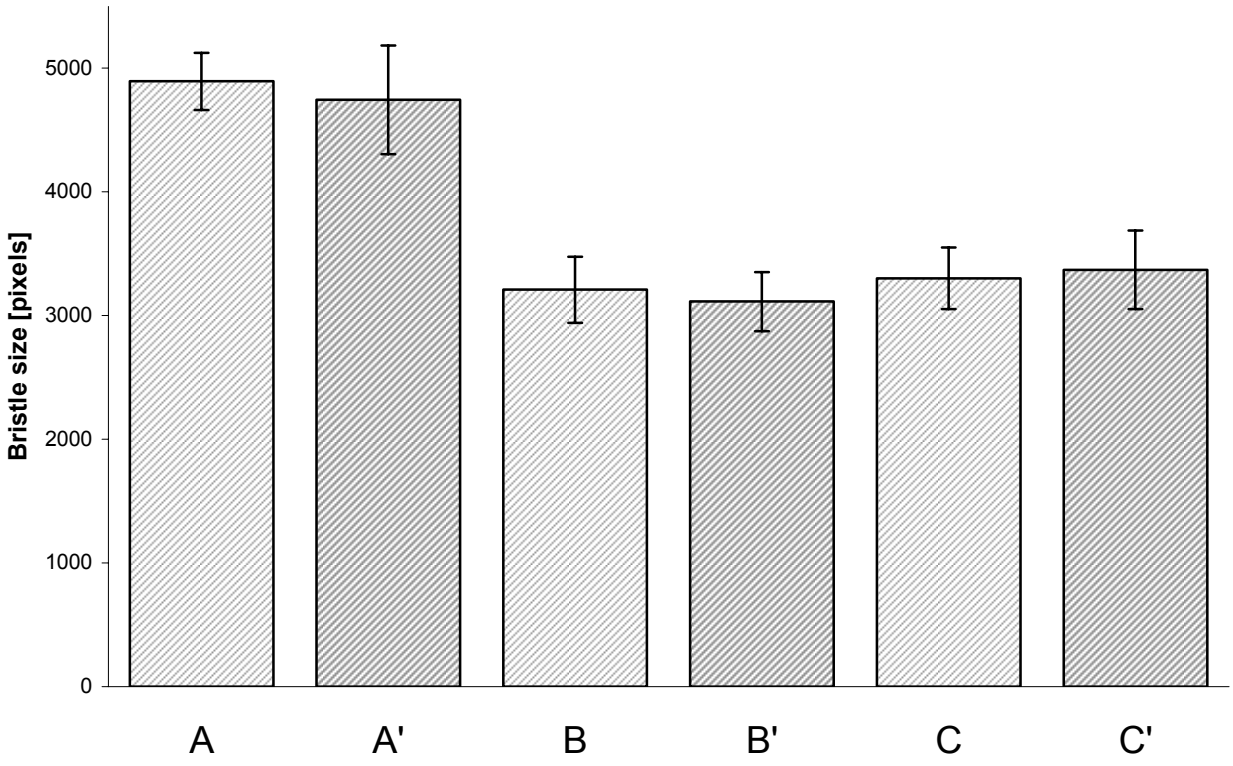

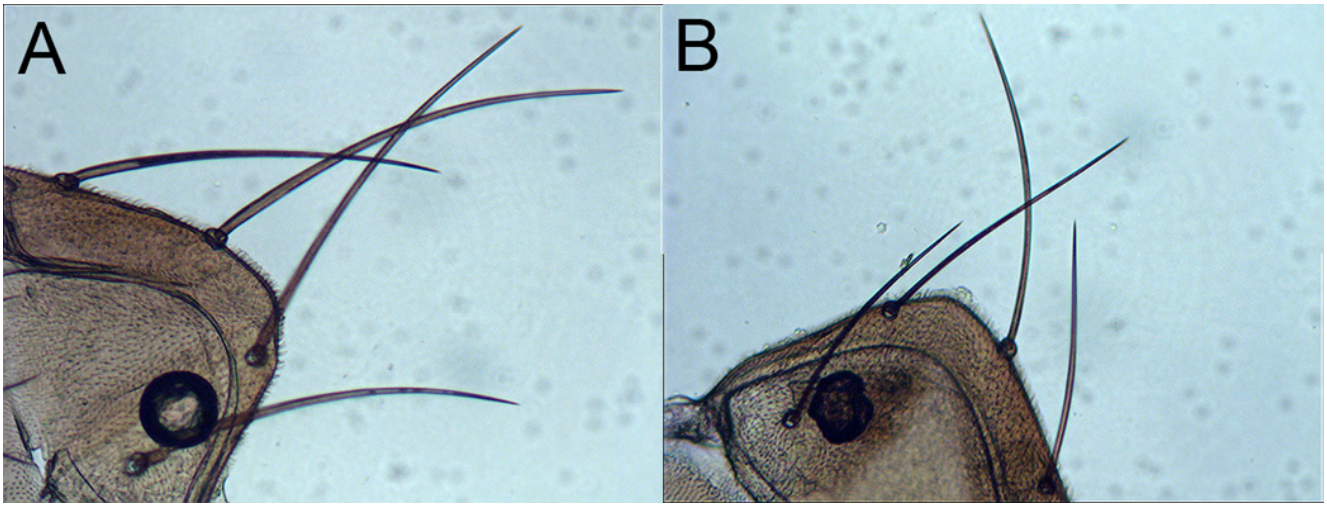

Figure 8
Expression of *dmax* dsRNA under control of *dpp-GAL4* strongly reduces the size of the anterior and posterior scutellar bristles. For every genotype, the area of both anterior and posterior scutellar bristle pairs of 9-11 individual flies was determined. The error bars indicate standard deviations.

Genotypes:

A *y w/Y; UAS-lacZ-IR(1-1)/Sp dpp-GAL4*
B *y w/Y; UAS-dmax-IR(2-7)/Sp dpp-GAL4; UAS-dmax-IR(5-2) UAS-dmax-IR(6-1)/+*

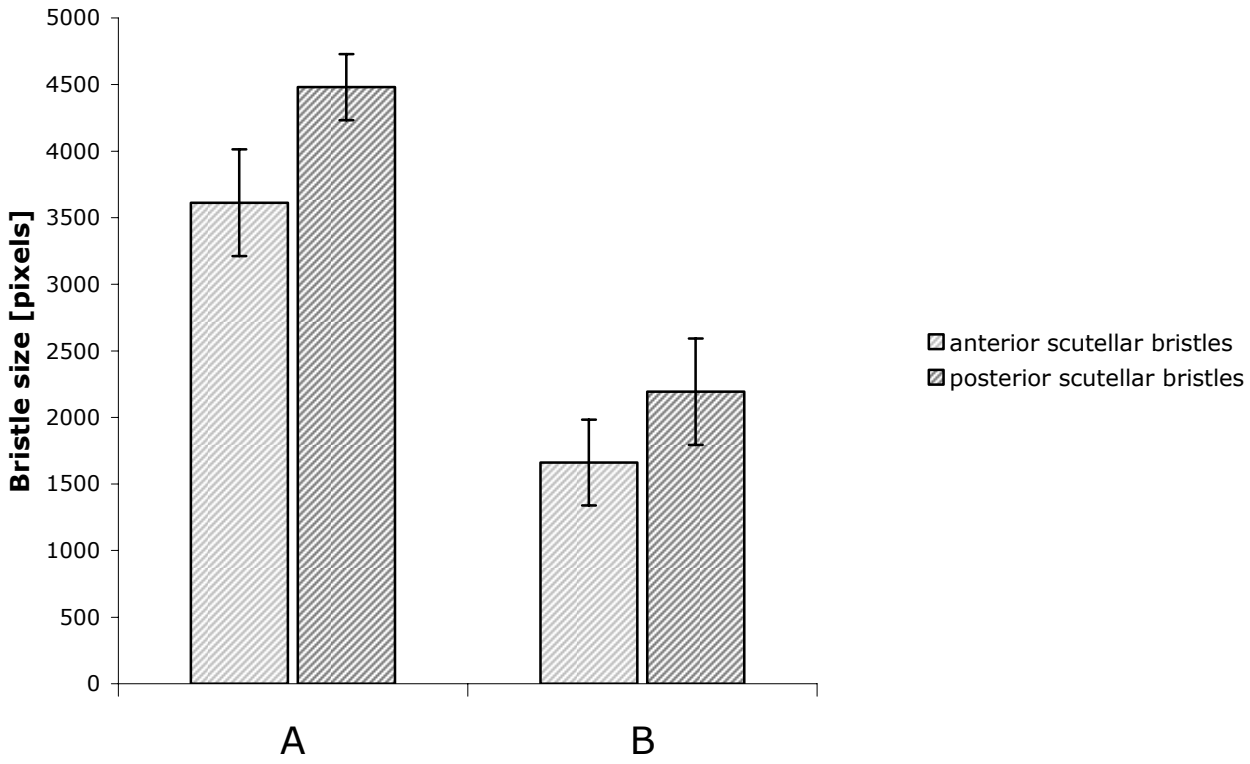

1.7. *dmax*-RNA*i* has a only a weak effect on wing area and wing cell size

Slight discrepancies in the sizes of the dorsal and ventral wing epithelia lead to a bent wing phenotype. The overexpression of a gene with the strong, dorsal compartment specific GAL4 driver *apterous-GAL4* (*ap-GAL4*) therefore is a very sensitive test for growth effects (Montagne et al., 1999). Overexpression of *dmyc* by *ap-GAL4* results in larger cell sizes in the dorsal compartment, causing a prominent bent down phenotype (P. Gallant, unpublished). Therefore, we expected to see a bent up wing phenotype, when *dmax* levels would be reduced. We were surprised to see that the expression of single strong *dmax* dsRNA transgenes did not cause a noticeable bent wing phenotype (*dmax-IR* lines 2-7, 5-2 and 7-3 were tested). We determined the area of the dorsal wing surface and could not find a significant difference to the controls (Figure 9, left chart). Since it was imaginable that a putative reduction in cell size could be compensated by higher cell number and therefore not result in a smaller compartment area, we also determined the dorsal wing cell size. It turned out that there was also no significant difference in dorsal wing cell size (Figure 9, right chart).

Only when we expressed three copies of the *dmax* dsRNA transgenes, a bent up wing phenotype resulted (Figure 10). Since the system is extremely sensitive, this bent up wing phenotype might be caused by an only very slight growth phenotype. However, the effect (bent up wings) is opposite to the effect of *dmyc* overexpression, consistent with dMax's presumed role as a dMyc partner.

Figure 9
Expression of *dmax*-dsRNA with single copy inverted repeat transgenes under control of *ap-GAL4* does not significantly reduce dorsal wing blade surface and dorsal wing cell size. Values are given relative to the A genotype. For every genotype, 6 wings were measured. The error bars indicate standard deviations.

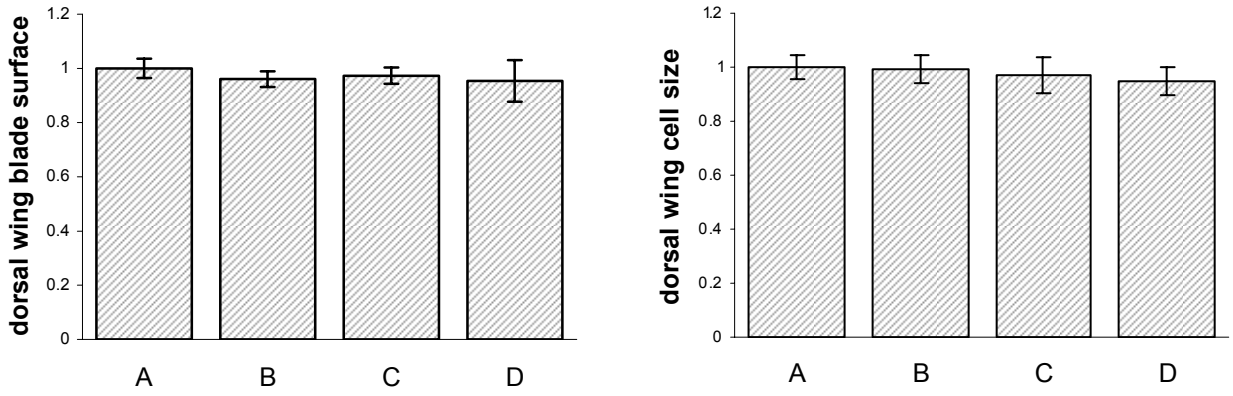

Genotypes:
A *y w/Y; ap-GAL4/+*
B *y w/Y; ap-GAL4/UAS-lacZ-IR(3-1)*
C *y w/Y; ap-GAL4/UAS-dmax-IR(7-3)*
D *y w/Y; ap-GAL4/+; UAS-dmax-IR(5-2)/+*

Figure 10
Expression of three copies of *dmax* dsRNA with *ap-GAL* causes a weak bent up wing phenotype.

Genotypes:
A *y w; ap-GAL4/UAS-lacZ-IR(1-1)*
B *y w; ap-GAL4/UAS-dmax-IR(2-7); UAS-dmax-IR(5-2) UAS-dmax-IR(6-1)/+*

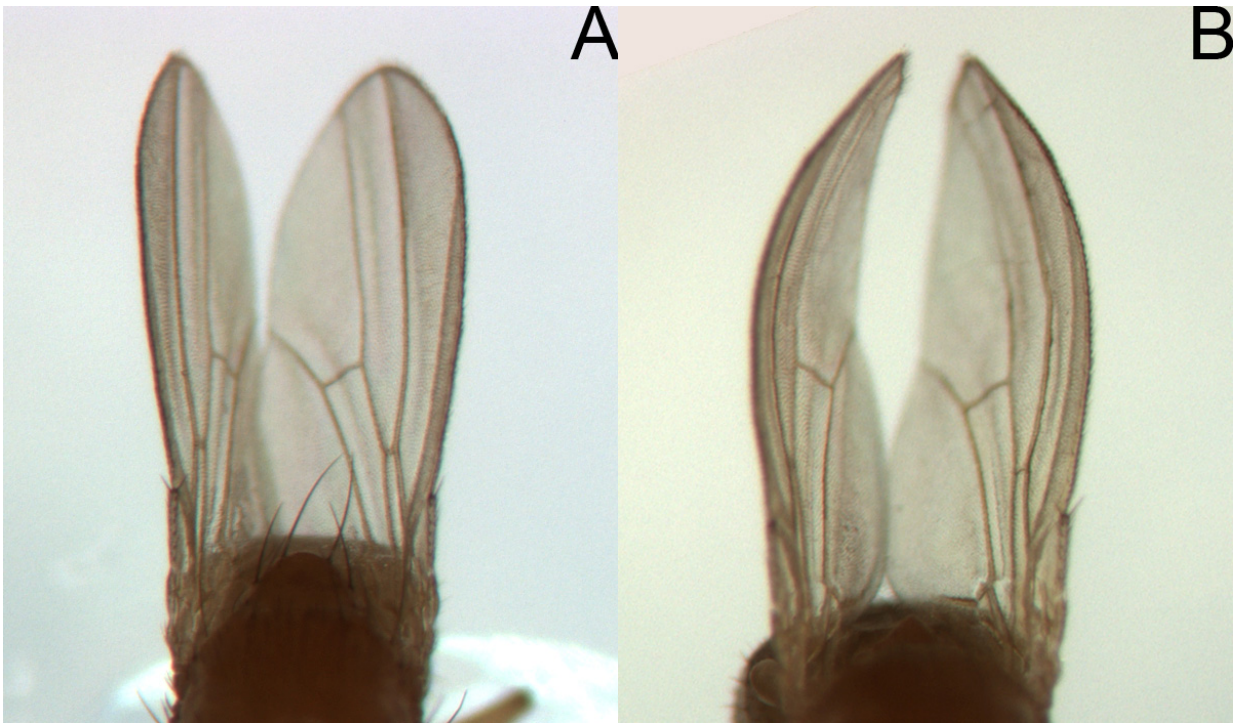

1.8. Genetic interactions

Strong, ubiquitous expression of *dmax* dsRNA with the GAL4 drivers *actin-GAL4* and *daughterless-GAL4* creates a sensitized situation in which small changes in *dmax* levels lead to a remarkable increase in lethality. The viability of flies which express *dmax* dsRNA with *actin-GAL4* or *daughterless-GAL4* was variable from experiment to experiment, ranging from complete viability (Figure 1) to moderately reduced viability, especially in males (Figure 11). However, the combination of two or three *dmax* dsRNA transgenes *invariably* led almost complete pupal lethality, as did the expression of single strong *dmax* dsRNA transgenes in a *Df(3L)fz2/+* background. We concluded that this effect was specific for *dmax*, since it could be rescued by the coexpression of a *UAS-dmax* transgene (Figure 3). We decided to use this sensitive system to study genetic interactions.

1.8.1. *dmax*-RNA*i* interacts with hemizygous dm^{P0}

We tested the effect of reducing *dmax* levels in the hypomorphic *dmyc* mutant dm^{P0}. dm^{P0} flies are viable, but they are smaller than wild type flies, they have a thin bristle phenotype and females are sterile (Johnston et al., 1999). Expression of *dmax* dsRNA under control of the ubiquitous driver *da-GAL4* led to strong pupal lethality in males which are hemizygous for the hypomorphic *dmyc* allele dm^{P0} (Figure 11), whereas it had no effect on females which were heterozygous for the mutant allele. The observed synthetic lethality did not occur in dm^{P0} males that carried a *tub-FRT-dmyc-FRT-GAL4* (*tub>dmyc>GAL4*) transgene. The *tub>dmyc>GAL4* transgene expresses *dmyc* under control of the *tubulin* enhancer and is capable of rescuing *dmyc* null flies to adulthood (Pierce et al., 2004). Notably, dm^{P0} males carrying the rescue construct and expressing *dmax* dsRNA survived better than *y w* males expressing *dmax* dsRNA.

In combination with the demonstrated physical interaction between dMyc and dMax (Gallant et al., 1996) and the similarity of the *dmax* loss of function phenotypes to known *dmyc* loss of function phenotypes, these data strongly argue that dMax is an essential co-factor for dMyc.

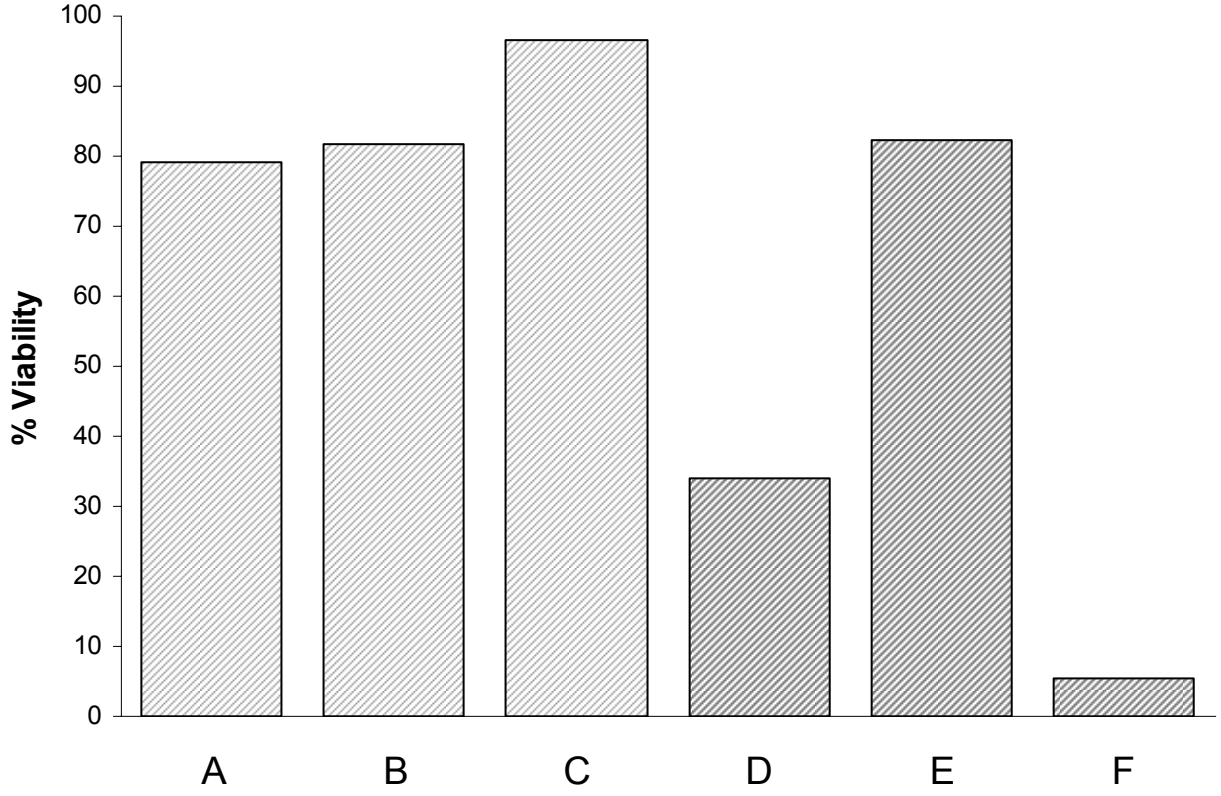

Figure 11
Interaction with dm^{P0}. The chart depicts the viability of the given genotypes. Whereas heterozygosity for the hypomorphic dm^{P0} allele in females had no effect on viability, when *dmax* dsRNA was expressed (A, B, C), homozygosity for dm^{P0} in males led to strong pupal lethality (F). The lethality could be rescued by the presence of a *tub-dmyc* transgene. In this experiment, the expression of *dmax* dsRNA in males led to a decrease in viability already in a *y w* background (D). The indicated viabilities were calculated relative to the offspring numbers of sister genotypes of the same cross (e. g. in A as the ratio of *y w/y w; UAS-dmax-IR(2-7)/+; da-GAL4/+* relative to *y w/y w; CyO/+; da-GAL4/+*). For a more detailed explanation of the viability calculations, see Materials and Methods.

Label:	Genotypes:
A	*y w/y w; UAS-dmax-IR(2-7)/+; da-GAL4/+*
B	dm^{P0} *tub>dmyc[y$^+$]>GAL4/y w; UAS-dmax-IR(2-7)/+; da-GAL4/+*
C	dm^{P0}*/y w; UAS-dmax-IR(2-7)/+; da-GAL4/+*
D	*y w/Y; UAS-dmax-IR(2-7)/+; da-GAL4/+*
E	dm^{P0} *tub>dmyc[y$^+$]>GAL4/Y; UAS-dmax-IR(2-7)/+; da-GAL4/+*
F	dm^{P0}*/Y; UAS-dmax-IR(2-7)/+; da-GAL4/+*

1.8.2. *dmax*-RNA*i* interacts with *reptin* and *pontin*

Since it has been shown that the transcriptional co-activators *Tip48/reptin* and *Tip49/pontin* interact with *dmyc* (Bellosta et al., 2005), we tested whether we would see synthetic lethality with *dmax* RNA*i*. We could indeed show strong dominant interactions with both *reptin* and *pontin*. Both *reptin/+* and *pontin/+* flies are fully viable (Bellosta et al., 2005). Figure 12 shows that expression of *dmax* dsRNA led to a strong reduction of viability in a *reptin/+* background and to complete pupal lethality in a *pontin/+* background. While this data is consistent with Max's role as a cofactor for Myc, the strength of the observed interaction is surprising: The loss of one copy of *pontin* in a *dmax*-RNA*i* situation leads to a stronger reduction in viability than the combination of dm^{P0} and *dmax*-RNA*i*, even though *dmyc* levels in dm^{P0} flies are more strongly reduced than *pontin* levels. Similarly, the loss of *reptin* leads to a strong reduction in viability in the combination with *dmax*-RNA*i*, while it does not affect the viability of dm^{P0} flies (Bellosta et al., 2005).

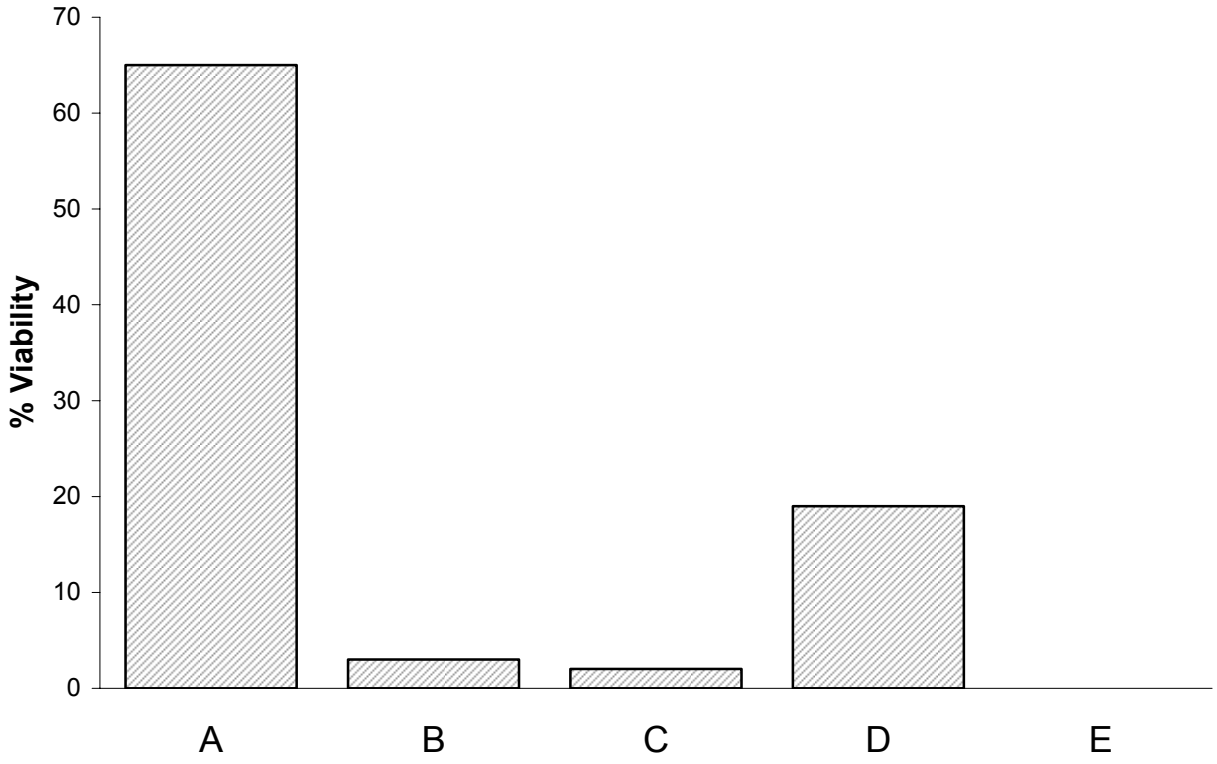

Figure 12
Interaction with *reptin* and *pontin.* In all five genotypes, *dmax* dsRNA was expressed with *actin-GAL4*. Whereas this led to only slightly reduced viability when one copy of the *dmax* dsRNA transgene was expressed (A), expression of three copies led to almost complete pupal lethality (B). One copy of *dmax* dsRNA led to almost complete pupal lethality if expressed in a *Df(3L)fz2/+* background (C). Heterozygosity for *reptin* reduced lethality to less than 20% (D), whereas heterozygosity for *pontin* led to complete pupal lethality. The indicated viabilities were calculated relative to the offspring numbers of sister genotypes of the same cross. For a more detailed explanation of the viability calculations, see Materials and Methods.

Label:	Genotypes:
A	*y w; UAS-dmax-IR(2-7)/actin-GAL4*
B	*y w; UAS-dmax-IR(2-7)/actin-GAL4; UAS-dmax-IR(5-2) UAS-dmax-IR(6-1)/+*
C	*y w; UAS-dmax-IR(2-7)/actin-GAL4; Df(3L)fz2/+*
D	*y w; UAS-dmax-IR(2-7)/actin-GAL4; reptin/+*
E	*y w; UAS-dmax-IR(2-7)/actin-GAL4; pontin/+*

1.9. *dmax*-RNA*i* in the presence of overexpressed *dmyc*

1.9.1. Evidence for *dmax*-independent functions of *dmyc*

Expression of *dmax* dsRNA with the eye-specific GAL4 driver *GMR-GAL4* did not alter ommatidial size and overall eye morphology in a wild type background (Figure 13 A, D and Figure 14 A, D). However, it had a surprising effect on eyes in which *dmyc* was strongly overexpressed. The analysis of this effect has led us to the conclusion that *dmyc* has functions that do not require *dmax.*

Overexpression of one copy of *UAS-dmyc* by *GMR-GAL4* increased ommatidial size by more than 20% but did neither disrupt the regular arrangement of the ommatidia (Figure 14 A, B) nor did it alter eye pigmentation. If a higher dosis of *dmyc* was expressed using three copies of *UAS-dmyc*, ommatidial size was not further increased, but the regular pattern of ommatidia was disrupted, resulting in a rough eye phenotype. Additionally, a pigmentation defect occurred: even though the eye color should be a wild type red (having four *white*$^{+}$-marked transgenes present, one of which - *GMR-GAL4* - causes very dark eyes on its own), the eyes were of an orange color, with interspersed red dots (Figures 13 B, 14 C). When the *dmyc* dosis is further increased by expressing the three transgenes at a higher temperatures than 25° C, the roughness of the eyes (the irregularity of the ommatidial pattern) is also increased and the total eye size is reduced (Figure 13 G, H), presumably due to apoptosis associated with the overexpression of *dmyc* in the eye (L. Montero and P. Gallant, unpublished).

We had expected that a reduction of *dmax* levels in this system would cause a reversion of the observed phenotypes, but instead we found the following: when one copy of *UAS-dmyc* was overexpressed, coexpression of *dmax* dsRNA did cause a partial reversion of ommatidial size (Figure 14 B, E). Strikingly, when *dmax* dsRNA was coexpressed with three copies of *UAS-dmyc*, the ommatidial size was reverted to wild type levels, but roughness was strongly increased and the overall eye shape was changed (the eyes appeared narrower than wild type eyes or eyes in which *dmyc* was overexpressed), giving rise to an eye phenotype that was clearly more remote from wild type eyes than the one of eyes in which three copies of *UAS-dmyc* were overexpressed (Figure 13 B, E, C, F, Figure 14 C, F). *dmax*-RNA*i* did also not suppress the pigmentation defect associated with strong overexpression of *dmyc.* We concluded that there must exist functions of *dmyc* which cause the observed roughness and the pigmentation defect and, importantly, that these functions do not require *dmax*. On the contrary, it seemed possible that these functions become stronger, when *dmax* was removed, since the roughness increased.

Figure 13a
Dissecting microscope pictures, showing the effect of *dmax*-RNA*i* in the presence of overexpressed *dmyc*. Whereas *dmax*-RNA*i* driven by *GMR-GAL4* has no effect on its own (A, D), it strongly modifies a phenotype caused by the overexpression of three copies of *dmyc* (B and C, E and F), reducing ommatidia size, strongly increasing roughness, but not rescuing the pigmentation phenotype associated with the overexpression of three copies of *dmyc*.

Label:	Genotypes:
A	*y w/Y; GMR-GAL4/CyO*
B, C	*y w/Y; GMR-GAL4 UAS-dmyc^{132}/CyO; UAS-dmyc^{13} UAS-dmyc^{42}/+*
D	*y w/Y; GMR-GAL4/UAS-dmax-IR(7-3)*
E, F	*y w/Y; GMR-GAL4 UAS-dmyc^{132}/UAS-dmax-IR(7-3); UAS-dmyc^{13} UAS-dmyc^{42}/+*

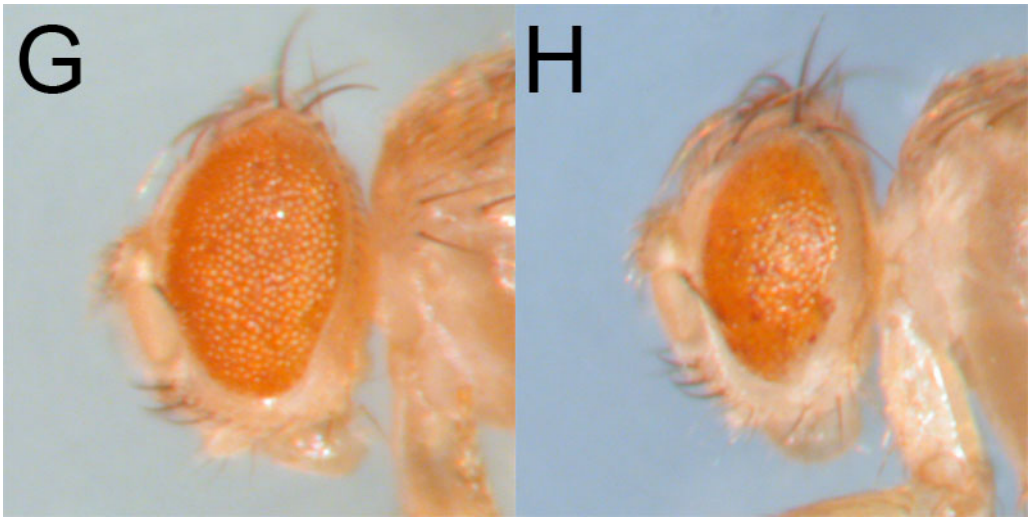

Figure 13b
Further increase of *dmyc* levels by overexpression of three copies of *UAS-dmyc* at a temperature of 29° C does not further increase eye size. Instead, the eye becomes rougher and narrower, while overall eye size is reduced. The resulting eye phenotype is similar to the phenotype produced by co-overexpression of *dmax* dsRNA.

Label:	Genotypes:	
G	*y w/Y; GMR-GAL4 UAS-dmyc^{132}/CyO; UAS-dmyc^{13} UAS-dmyc^{42}/+*	25° C
H	*y w/Y; GMR-GAL4 UAS-dmyc^{132}/CyO; UAS-dmyc^{13} UAS-dmyc^{42}/+*	29° C

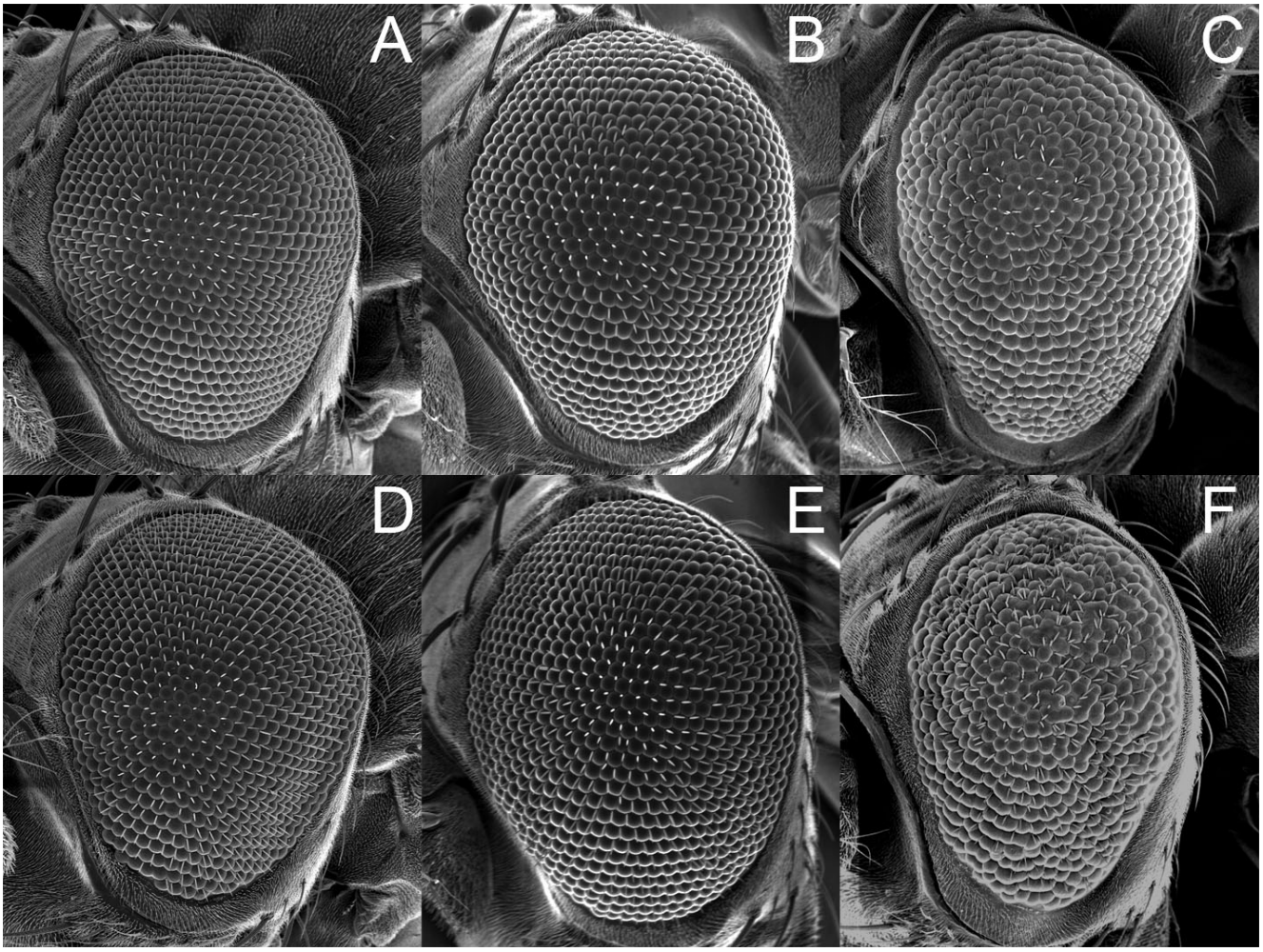

Figure 14a
Silencing of *dmax* has no consequences in a wild type situation (D), partially reduces ommatidia size when one copy of *UAS-dmyc* expressed (E), but strongly decreases ommatidia size and increases roughness, when 3 copies of *UAS-dmyc* are expressed. The pictures are scanning electron micrographs obtained at a magnification of 180-fold.

Label:	Genotypes:
A	*y w/Y; GMR-GAL4*
B	*y w/Y; GMR-GAL4 UAS-dmyc^{132}/CyO, y^{+}*
C	*y w/Y; GMR-GAL4 UAS-dmyc^{132}/+; UAS-dmyc^{13} UAS-dmyc^{42}/+*
D	*y w/Y; GMR-GAL4/UAS-dmax-IR(2-7)*
E	*y w/Y; GMR-GAL4 UAS-dmyc^{132}/UAS-dmax-IR(2-7)*
F	*y w/Y; GMR-GAL4 UAS-dmyc^{132}/UAS-dmax-IR(2-7); UAS-dmyc^{13} UAS-dmyc^{42}/+*

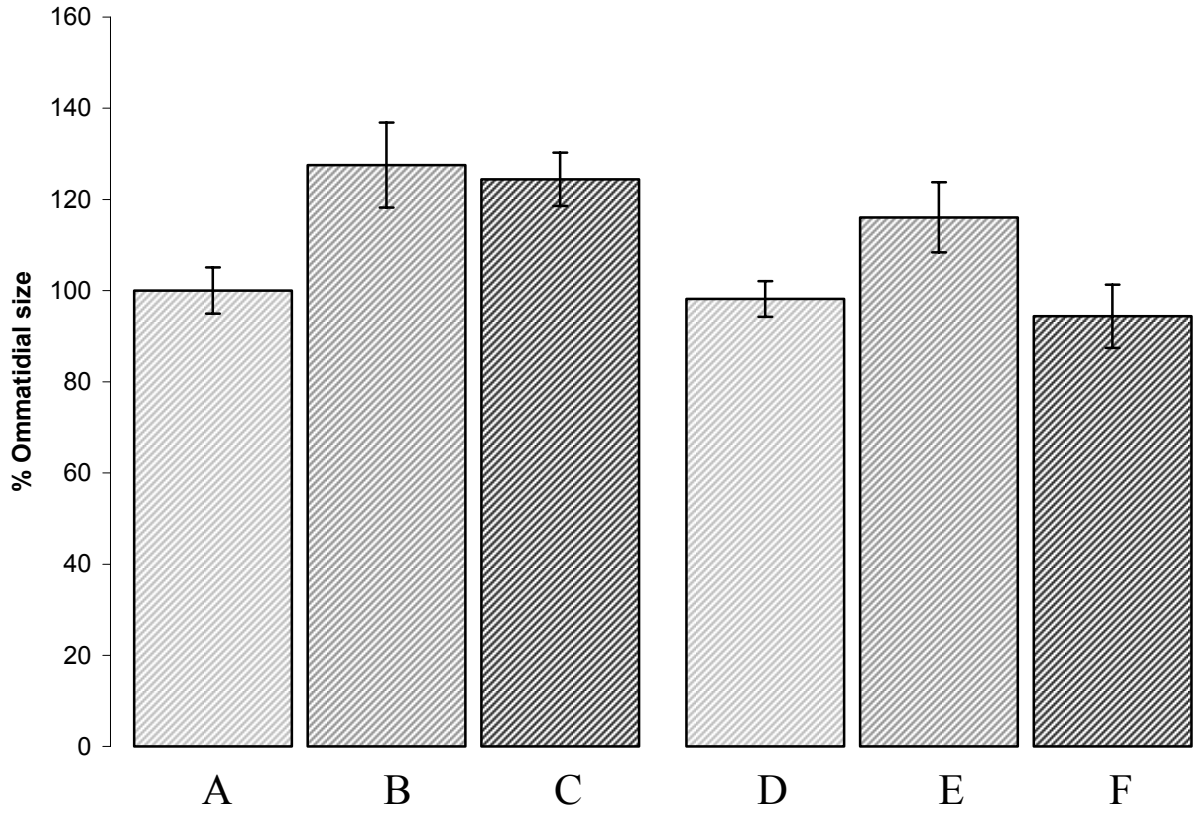

Figure 14b
Ommatidial size (relative to the *y w/Y; GMR-GAL4/+* genotype). The labels correspond to Figure 14a. For every genotype, the size of 20 centrally located ommatidia of 6 individual eyes was determined. The error bars indicate standard deviations.

Label:	Genotypes:
A	*y w/Y; GMR-GAL4*
B	*y w/Y; GMR-GAL4 UAS-dmyc^{132}/CyO, y^{+}*
C	*y w/Y; GMR-GAL4 UAS-dmyc^{132}/+; UAS-dmyc^{13} UAS-dmyc^{42}/+*
D	*y w/Y; GMR-GAL4/UAS-dmax-IR(2-7)*
E	*y w/Y; GMR-GAL4 UAS-dmyc^{132}/UAS-dmax-IR(2-7)*
F	*y w/Y; GMR-GAL4 UAS-dmyc^{132}/UAS-dmax-IR(2-7); UAS-dmyc^{13} UAS-dmyc^{42}/+*

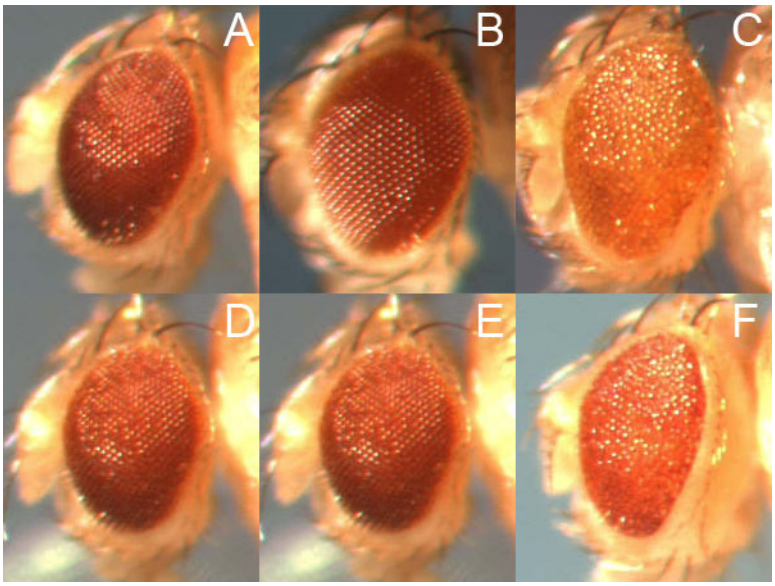

Figure 14c
Strong overexpression of *UAS-dmyc* causes a pigmentation defect that cannot be suppressed by concomitant expression of *dmax* dsRNA. Labels according to Figure 14a.

Label:	Genotypes:
A	*y w/Y; GMR-GAL4*
B	*y w/Y; GMR-GAL4 UAS-dmyc^{132}/CyO, y^{+}*
C	*y w/Y; GMR-GAL4 UAS-dmyc^{132}/+; UAS-dmyc^{13} UAS-dmyc^{42}/+*
D	*y w/Y; GMR-GAL4/UAS-dmax-IR(2-7)*
E	*y w/Y; GMR-GAL4 UAS-dmyc^{132}/UAS-dmax-IR(2-7)*
F	*y w/Y; GMR-GAL4 UAS-dmyc^{132}/UAS-dmax-IR(2-7); UAS-dmyc^{13} UAS-dmyc^{42}/+*

1.9.2. Specificity of the observed interaction

In order to demonstrate that part of the observed interaction of *dmax* dsRNA with overexpressed *dmyc* is not caused by an unspecific titration effect of the *UAS-dmax-IR* transgene on GAL4, we coexpressed a neutral *UAS-GFP* transgene (Figure 15 A-D, A'-D'). Neither did this modify the eye phenotype caused by expression of three copies of *UAS-dmyc*, nor did it weaken or alter the interaction with *dmax*-RNA*i*. Hence there is no evidence for limiting GAL4 levels or for titration effects. Consistently, coexpression of a *lacZ* dsRNA transgene did not modify the phenotype caused by overexpression of three copies of *UAS-dmyc* (data not shown).

Furthermore, we could show that heterozygosity for *Df(3L)fz2* or $dmax^{1}$ had a similar, but slightly weaker effect than *dmax*-RNA*i*: while being neutral in a *GMR-GAL4* background, ommatidial size was reduced, but roughness increased in *GMR-GAL4 3x UAS-dmyc* eyes (Figure 15 E, F, E', F'). The described interaction is therefore a specific consequence of reduced *dmax* levels and not an unspecific consequence of *dmax*-RNA*i*.

1.9.3. Contribution of apoptosis

Because it was known that overexpression of *dmyc* causes apoptosis (L. Montero and P. Gallant, unpublished), we suspected that the roughness and the pigmentation defect which was caused by the overexpression of three copies of *UAS-dmyc* and which could not be suppressed by coexpression of *dmax* dsRNA were due to apoptosis. Therefore, we blocked apoptosis by coexpression of the pan-caspase inhibitor *p35*.

Expression of *UAS-p35* slightly increased the ommatidial size on its own without causing a rough eye phenotype (Figure 16ab A, B). Strikingly, inhibiting apoptosis while three copies of *UAS-dmyc* were expressed led to a strong increase in ommatidial size and to a partial suppression of the rough eye phenotype (Figure 16ab A', B', Figure 16d B). Additionally, the pigmentation defect caused by the strong overexpression of *dmyc* was completely rescued (Figure 16c A', B'). These findings prove that apoptosis caused by the strong overexpression of *dmyc* contributes to the rough eye phenotype and causes the observed pigmentation defect (presumably due to the loss of pigment cells) and they also explain why the expression of three *UAS-dmyc* transgenes does not further increase ommatidial size than the expression of only one *UAS-dmyc* transgene.

Importantly, the strong increase in roughness that was caused by the reduction of *dmax* levels in the *dmyc* overexpression background, could be rescued by the coexpression of *UAS-p35* (Figure 16ab C', D', Figure 16d B', C'). Similarly, the pigmentation defect (Figure 16c C', D') was rescued, resulting in eyes that were overall nearest to wild type eyes. In accordance with these findings, eye sections showed that the overexpression of *dmyc* causes a loss of ommatidial organization and of pigment cells which could not be rescued by *dmax*-RNA*i*, but to a large extent by coexpression of *UAS-p35* (Figure 16e).

Taken together with the data shown in the Figures 13 and 14, these findings provide evidence that part of the effects caused by *dmyc* are caused by functions of *dmyc* which do not require *dmax*. These functions are associated with apoptosis. When *dmax* levels are lowered, *dmax*-dependent growth is reduced, but the consequences of *dmax*-independent functions are exacerbated.

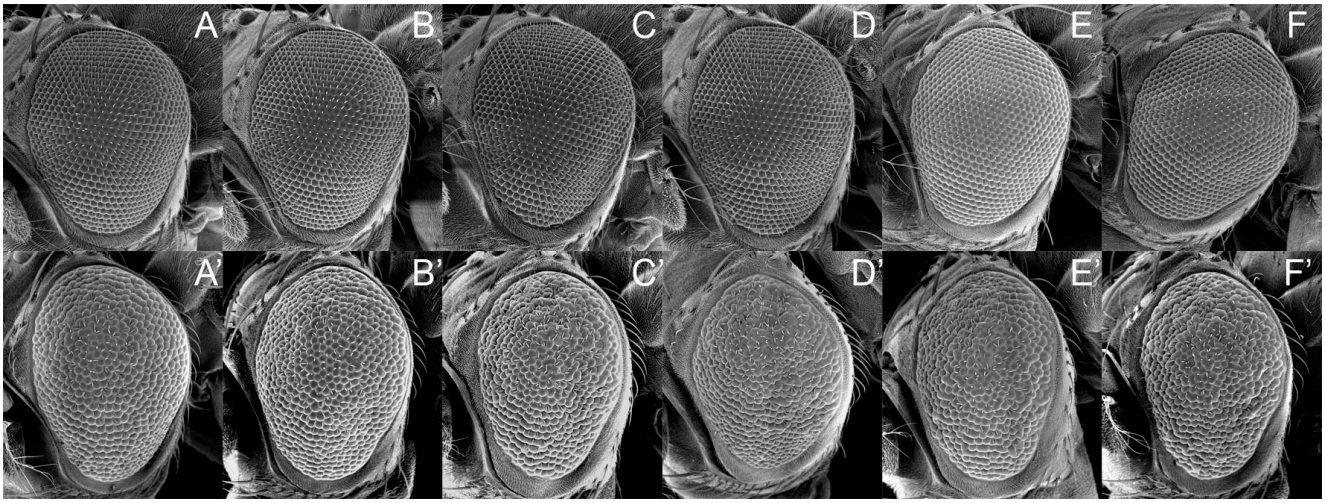

Figure 15a
The effects of the expression of *dmax* dsRNA on the *dmyc* overexpression phenotype (decreased ommatidia size, increased roughness) are specific, since the same changes occur, if *dmyc* is overexpressed in *Df(3L)fz2/+* or $dmax^1$/+ backgrounds. Moreover, titration effects can be excluded, since the co-overexpression of *UAS-GFP* has no influence.

Label:	Genotypes:
A	*y w/Y; GMR-GAL4/+*
B	*y w/Y; GMR-GAL4/+; UAS-GFP/+*
C	*y w/Y; GMR-GAL4/UAS-dmax-IR(2-7)*
D	*y w/Y; GMR-GAL4/UAS-dmax-IR(2-7); UAS-GFP/+*
E	*y w/Y; GMR-GAL4/+;* $dmax^1$*/+*
F	*y w/Y; GMR-GAL4/+; Df(3L)fz2/+*
A'	*y w/Y; GMR-GAL4 UAS-*$dmyc^{132}$*/+; UAS-*$dmyc^{13}$ *UAS-*$dmyc^{42}$*/+*
B'	*y w/Y; GMR-GAL4 UAS-*$dmyc^{132}$*/+; UAS-*$dmyc^{13}$ *UAS-*$dmyc^{42}$*/UAS-GFP*
C'	*y w/Y; GMR-GAL4 UAS-*$dmyc^{132}$*/UAS-dmax-IR(2-7); UAS-*$dmyc^{13}$ *UAS-*$dmyc^{42}$*/+*
D'	*y w/Y; GMR-GAL4 UAS-*$dmyc^{132}$*/UAS-dmax-IR(2-7); UAS-*$dmyc^{13}$ *UAS-*$dmyc^{42}$*/UAS-GFP*
E'	*y w/Y; GMR-GAL4 UAS-*$dmyc^{132}$*/+; UAS-*$dmyc^{13}$ *UAS-*$dmyc^{42}$*/*$dmax^1$
F'	*y w/Y; GMR-GAL4 UAS-*$dmyc^{132}$*/+; UAS-*$dmyc^{13}$ *UAS-*$dmyc^{42}$*/Df(3L)fz2*

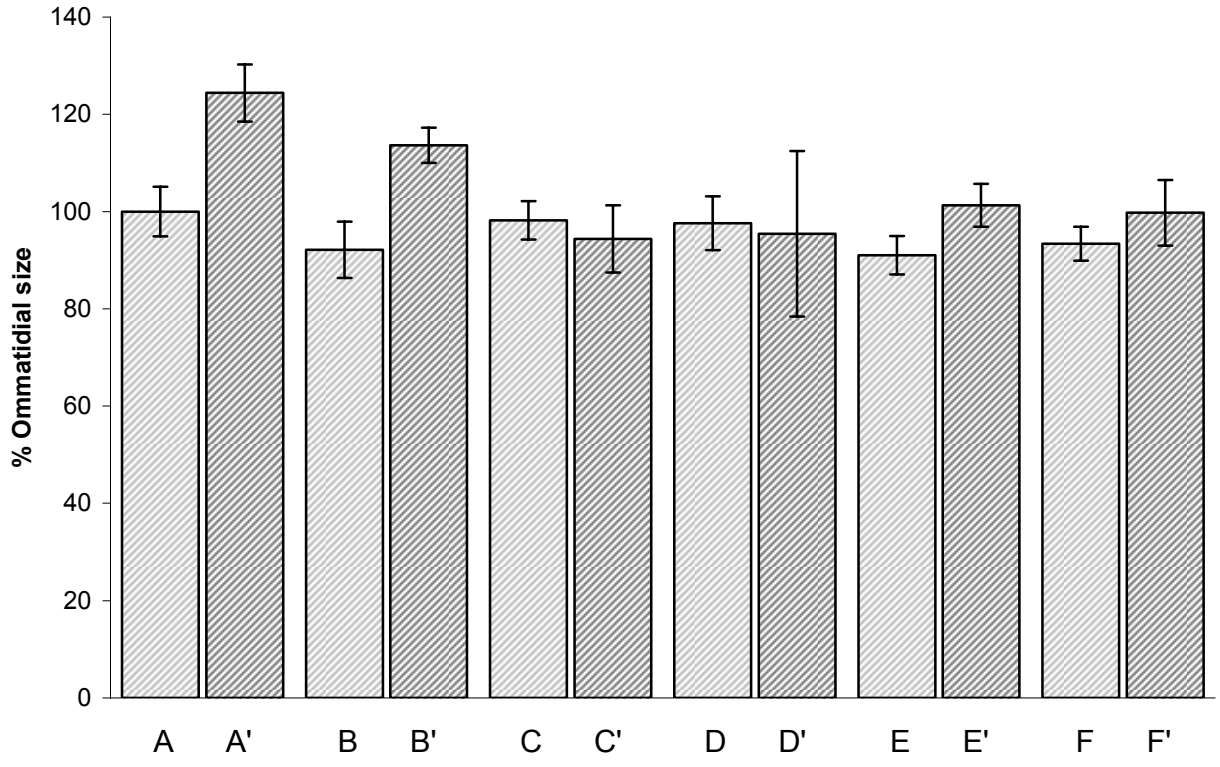

Figure 15b
Ommatidial size (relative to the *y w/Y; GMR-GAL4/+* genotype). The labels correspond to Figure 15a. The genotypes are grouped in pairs: light grey bars belong to genotypes with wild type (endogenous) *dmyc*, dark grey bars belong to the corresponding *dmyc* overexpression genotypes. For every genotype, the size of 20 centrally located ommatidia of 6 individual eyes was determined. The error bars indicate standard deviations.

Label:	Genotypes:
A	*y w/Y; GMR-GAL4/+*
B	*y w/Y; GMR-GAL4/+; UAS-GFP/+*
C	*y w/Y; GMR-GAL4/UAS-dmax-IR(2-7)*
D	*y w/Y; GMR-GAL4/UAS-dmax-IR(2-7); UAS-GFP/+*
E	*y w/Y; GMR-GAL4/+; $dmax^{1}$/+*
F	*y w/Y; GMR-GAL4/+; Df(3L)fz2/+*
A'	*y w/Y; GMR-GAL4 UAS-$dmyc^{132}$/+; UAS-$dmyc^{13}$ UAS-$dmyc^{42}$/+*
B'	*y w/Y; GMR-GAL4 UAS-$dmyc^{132}$/+; UAS-$dmyc^{13}$ UAS-$dmyc^{42}$/UAS-GFP*
C'	*y w/Y; GMR-GAL4 UAS-$dmyc^{132}$/UAS-dmax-IR(2-7); UAS-$dmyc^{13}$ UAS-$dmyc^{42}$/+*
D'	*y w/Y; GMR-GAL4 UAS-$dmyc^{132}$/UAS-dmax-IR(2-7); UAS-$dmyc^{13}$ UAS-$dmyc^{42}$/UAS-GFP*
E'	*y w/Y; GMR-GAL4 UAS-$dmyc^{132}$/+; UAS-$dmyc^{13}$ UAS-$dmyc^{42}$/$dmax^{1}$*
F'	*y w/Y; GMR-GAL4 UAS-$dmyc^{132}$/+; UAS-$dmyc^{13}$ UAS-$dmyc^{42}$/Df(3L)fz2*

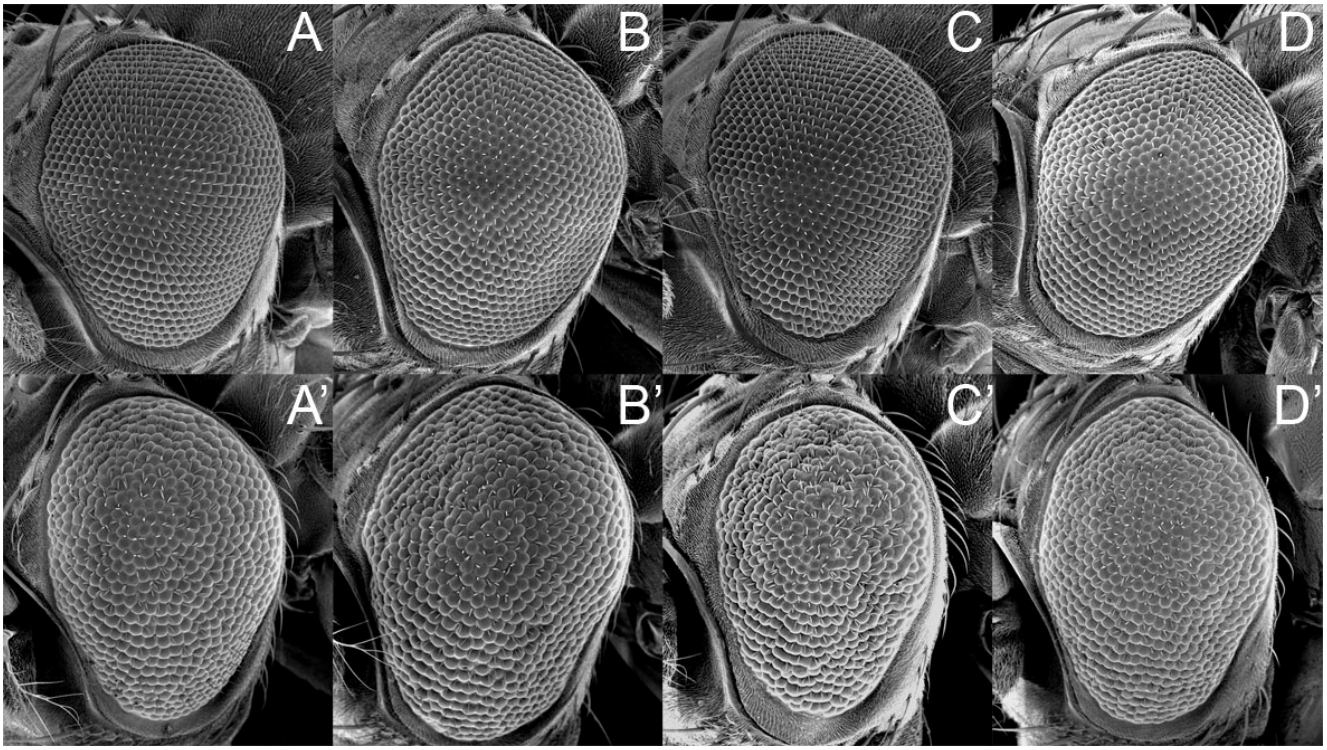

Figure 16a
Overexpression of three copies of *UAS-dmyc* causes apoptosis: suppression of apoptosis by *UAS-p35* further increases ommatidia size (A', B'). Strikingly, the increased roughness by co-overexpression of *dmax* dsRNA is suppressed by *UAS-p35.*

Label:	Genotypes:
A	*y w/Y; GMR-GAL4/+*
B	*y w/Y; GMR-GAL4/+; UAS-p35/+*
C	*y w/Y; GMR-GAL4/UAS-dmax-IR(2-7)*
D	*y w/Y; GMR-GAL4/UAS-dmax-IR(2-7); UAS-p35/+*
A'	*y w/Y; GMR-GAL4 UAS-dmyc^{132}/+; UAS-dmyc^{13} UAS-dmyc^{42}/+*
B'	*y w/Y; GMR-GAL4 UAS-dmyc^{132}/+; UAS-dmyc^{13} UAS-dmyc^{42}/UAS-p35*
C'	*y w/Y; GMR-GAL4 UAS-dmyc^{132}/UAS-dmax-IR(2-7); UAS-dmyc^{13} UAS-dmyc^{42}/+*
D'	*y w/Y; GMR-GAL4 UAS-dmyc^{132}/UAS-dmax-IR(2-7); UAS-dmyc^{13} UAS-dmyc^{42}/UAS-p35*

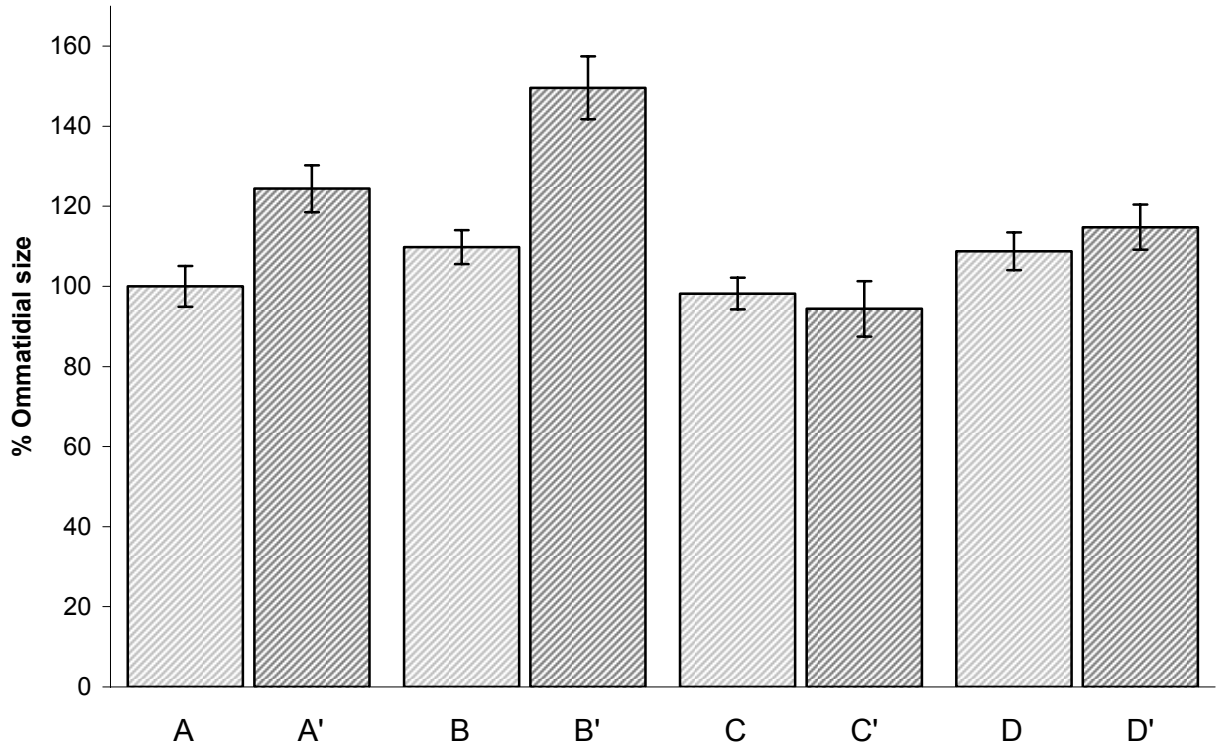

Figure 16b
Ommatidial size (relative to the *y w/Y; GMR-GAL4/+* genotype). The labels correspond to Figure 16a. For every genotype, the size of 20 centrally located ommatidia of 6 individual eyes was determined. The error bars indicate standard deviations.

Label:	Genotypes:
A	*y w/Y; GMR-GAL4/+*
B	*y w/Y; GMR-GAL4/+; UAS-p35/+*
C	*y w/Y; GMR-GAL4/UAS-dmax-IR(2-7)*
D	*y w/Y; GMR-GAL4/UAS-dmax-IR(2-7); UAS-p35/+*
A'	*y w/Y; GMR-GAL4 UAS-dmyc^{132}/+; UAS-dmyc^{13} UAS-dmyc^{42}/+*
B'	*y w/Y; GMR-GAL4 UAS-dmyc^{132}/+; UAS-dmyc^{13} UAS-dmyc^{42}/UAS-p35*
C'	*y w/Y; GMR-GAL4 UAS-dmyc^{132}/UAS-dmax-IR(2-7); UAS-dmyc^{13} UAS-dmyc^{42}/+*
D'	*y w/Y; GMR-GAL4 UAS-dmyc^{132}/UAS-dmax-IR(2-7); UAS-dmyc^{13} UAS-dmyc^{42}/UAS-p35*

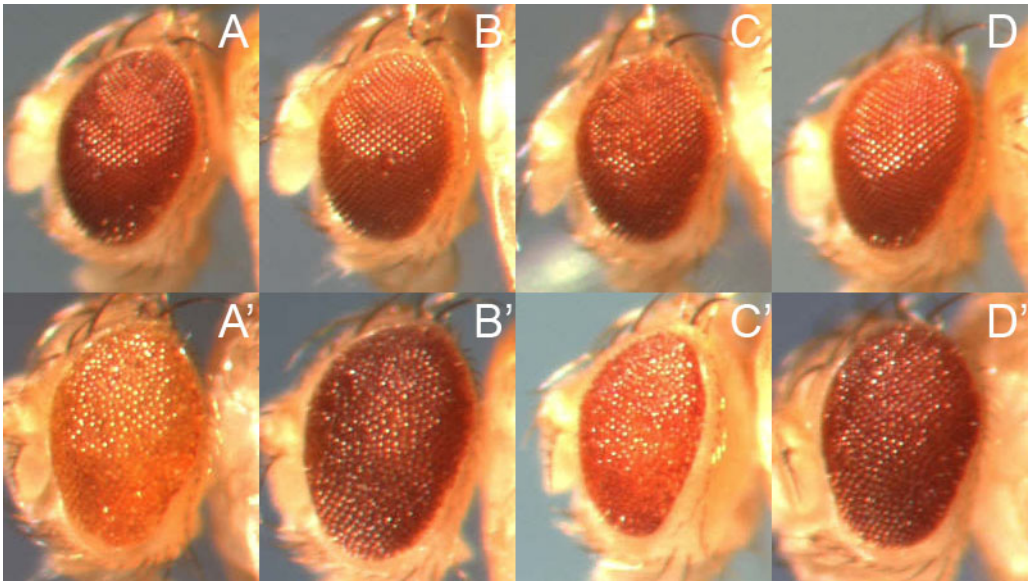

Figure 16c
Overexpression of *UAS-p35* rescues the pigmentation defect which is associated with the overexpression of three copies of *dmyc* and which could not be suppressed by *dmax*-RNA*i*. The labels correspond to Figure 16a.

Label:	Genotypes:
A	*y w/Y; GMR-GAL4/+*
B	*y w/Y; GMR-GAL4/+; UAS-p35/+*
C	*y w/Y; GMR-GAL4/UAS-dmax-IR(2-7)*
D	*y w/Y; GMR-GAL4/UAS-dmax-IR(2-7); UAS-p35/+*
A'	*y w/Y; GMR-GAL4 UAS-dmyc^{132}/+; UAS-dmyc^{13} UAS-dmyc^{42}/+*
B'	*y w/Y; GMR-GAL4 UAS-dmyc^{132}/+; UAS-dmyc^{13} UAS-dmyc^{42}/UAS-p35*
C'	*y w/Y; GMR-GAL4 UAS-dmyc^{132}/UAS-dmax-IR(2-7); UAS-dmyc^{13} UAS-dmyc^{42}/+*
D'	*y w/Y; GMR-GAL4 UAS-dmyc^{132}/UAS-dmax-IR(2-7); UAS-dmyc^{13} UAS-dmyc^{42}/UAS-p35*

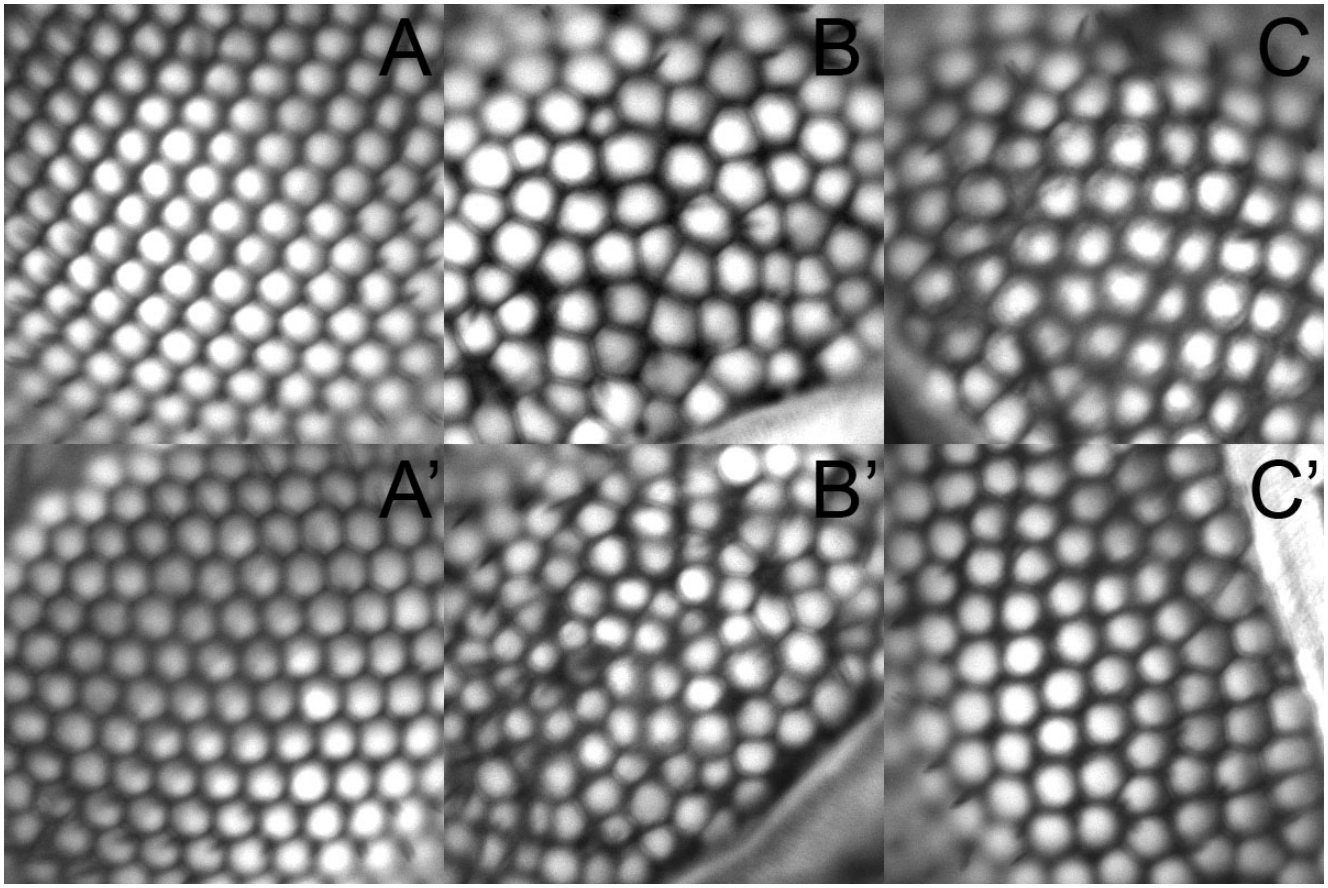

Figure 16d
Rescue of the strong rough eye phenotype resulting of the co-overexpression of *dmax* dsRNA by *UAS-p35*, documented with autofluorescence microscopy.

Label:	Genotypes:
A	*y w/Y; GMR-GAL4/+*
B	*y w/Y; GMR-GAL4 UAS-dmyc^{132}/+; UAS-dmyc^{13} UAS-dmyc^{42}/+*
C	*y w/Y; GMR-GAL4 UAS-dmyc^{132}/+; UAS-dmyc^{13} UAS-dmyc^{42}/UAS-p35*
A'	*y w/Y; GMR-GAL4/UAS-dmax-IR(2-7)*
B'	*y w/Y; GMR-GAL4 UAS-dmyc^{132}/UAS-dmax-IR(2-7); UAS-dmyc^{13} UAS-dmyc^{42}/+*
C'	*y w/Y; GMR-GAL4 UAS-dmyc^{132}/UAS-dmax-IR(2-7); UAS-dmyc^{13} UAS-dmyc^{42}/UAS-p35*

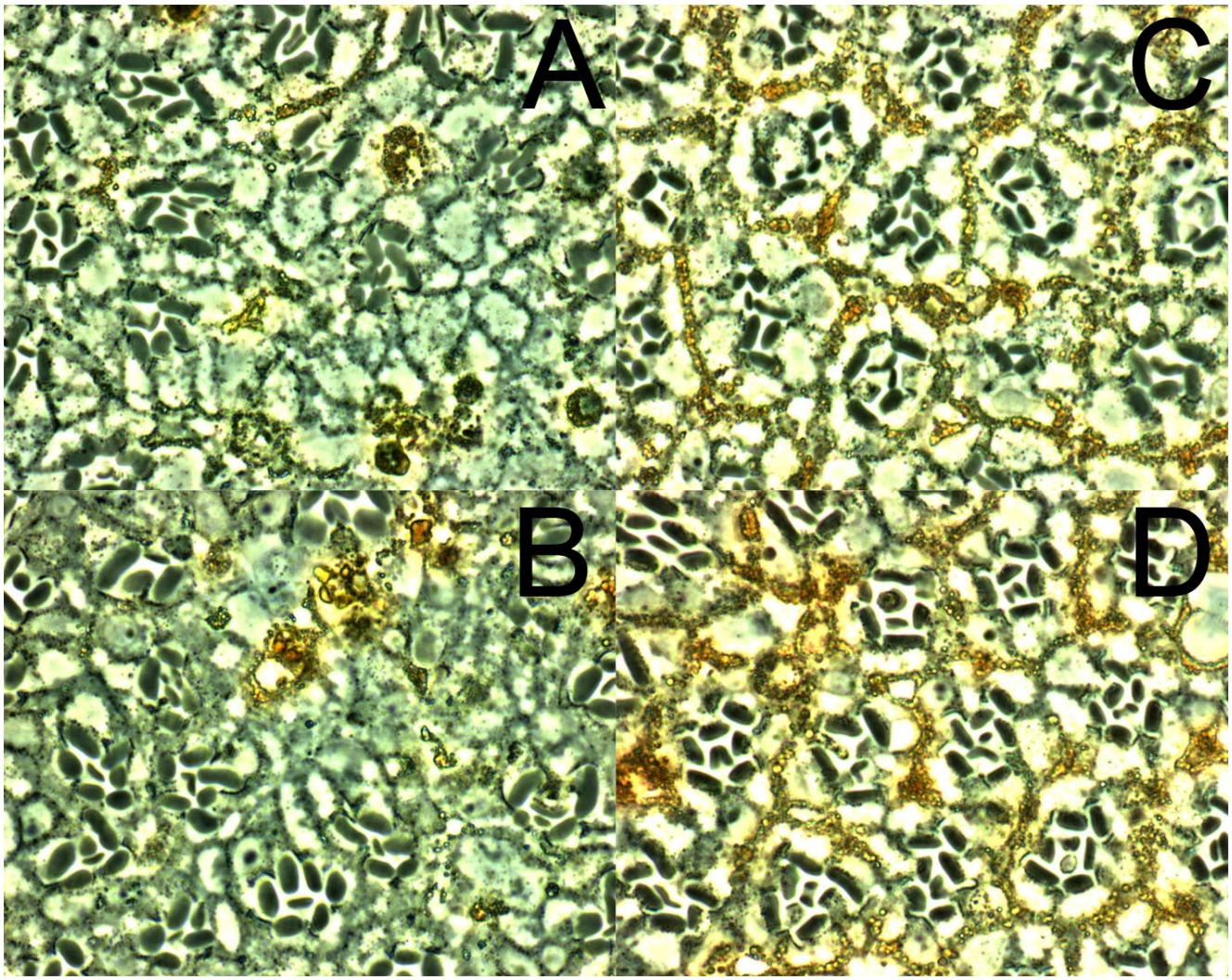

Figure 16e
Sections through adult eyes reveal a rescue of ommatidial structure (especially of pigment cell arrangement) by *UAS-p35.*

Label:	Genotypes:
A	*y w/Y; GMR-GAL4 UAS-dmyc^{132}/+; UAS-dmyc^{13} UAS-dmyc^{42}/+*
B	*y w/Y; GMR-GAL4 UAS-dmyc^{132}/UAS-dmax-IR(2-7); UAS-dmyc^{13} UAS-dmyc^{42}/+*
C	*y w/Y; GMR-GAL4 UAS-dmyc^{132}/+; UAS-dmyc^{13} UAS-dmyc^{42}/UAS-p35*
D	*y w/Y; GMR-GAL4 UAS-dmyc^{132}/UAS-dmax-IR(2-7); UAS-dmyc^{13} UAS-dmyc^{42}/UAS-p35*

1.9.4. Contribution of *dmnt*

So far, our interpretation of the *dmyc* overexpression eye phenotype and the surprising phenotype resulting from downregulation of *dmax* in this context has not taken into consideration a contribution of *dmnt*. One could argue that in a situation of strong overexpression of *dmyc*, loss of dMnt/dMax heterodimers causes the observed rough eye phenotype. We therefore tested the effects of the overexpression of three copies of *UAS-dmyc* and of the coexpression of *dmax* dsRNA in a *dmnt* null background. For this purpose, flies mutant for $dmnt^{1}$, a null mutant, and for $dmnt^{2}$, potentially expressing a form of *dmnt* that lacks the Sin3-interaction domain (SID) interaction domain (Loo et al., 2005), were used. $dmnt^{2}$ behaves like a null mutant (Loo et al., 2005). *dmnt* mutant flies have smooth eyes, but an increased ommatidial size (Figure 17ab A, B, C). When three *UAS-dmyc* transgenes were expressed, the resulting eyes were very similar to the ones resulting from overexpression of *dmyc* in a $dmnt^{+}$ background, showing increased ommatidial size, roughness and a prominent pigmentation defect. Downregulation of *dmax* in this context had the same effect as in a $dmnt^{+}$ background: it decreased the ommatidial size, increased the roughness, but did not rescue the pigmentation defect (Figure 17 D'). We therefore concluded that the effects seen with the overexpression of *dmyc* and the interaction with dmax-RNA*i* are independent of a loss of endogenous *dmnt*.

On the other hand, one could argue that in a situation of strong overexpression of *dmyc,* dMax is sequestered away from dMnt. One could then hypothesize that *dmax*-independent functions of *dmnt* cause the rough eye phenotype. We tested this hypothesis by expressing different *dmnt* transgenes (Figure 18). When a version of *dmnt* was overexpressed that lacks the leucine zipper (*dmnt[dZIP]*) but retains the SID interaction domain (which is essential to dMnt's binding to the SIN3 corepressor and thus for dMnt's function (Loo et al., 2005)), the phenotype of wild type eyes and the one caused by the expression of three copies of *UAS-dmyc* was not changed (Figure 18 A, A', C, C'). We therefore consider it unlikely that the *dmyc* overexpression rough eye phenotype is caused by *dmax*-independent functions of *dmnt*. Conversely, we could phenocopy the effects of *dmax*-RNA*i* by expressing *dmnt[dSID]*, a form of *dmnt* lacking the SID interaction motif but retaining the leucine zipper and therefore retaining it's ability to bind dMax (Figure 18 D, D'). Therefore, the effects described so far clearly are a consequence of the overexpression of *dmyc* and of the availability of dMax to dMyc. If dMax levels are lowered or dMax is titrated away from dMyc, *dmax*- dependent growth functions of *dmyc* are impaired, but not other functions that are associated with apoptosis. Expression of a wild type *dmnt* transgene did not cause a rough eye phenotype on its own, but it reduced the ommatidial size by slightly more than 10%. When it was coexpressed with three copies of *UAS-dmyc*, a very strong rough eye phenotype arose (considerably stronger than the rough eye phenotype seen in context with *dmax*-RNA*i* or *dmnt[dSID]*). This finding may be explained by the combined effect of enhanced dMnt-dMax-mediated repression, loss of *dmax*-dependent functions of *dmyc* and impaired (or unbalanced) *dmax*-independent functions of *dmyc.*

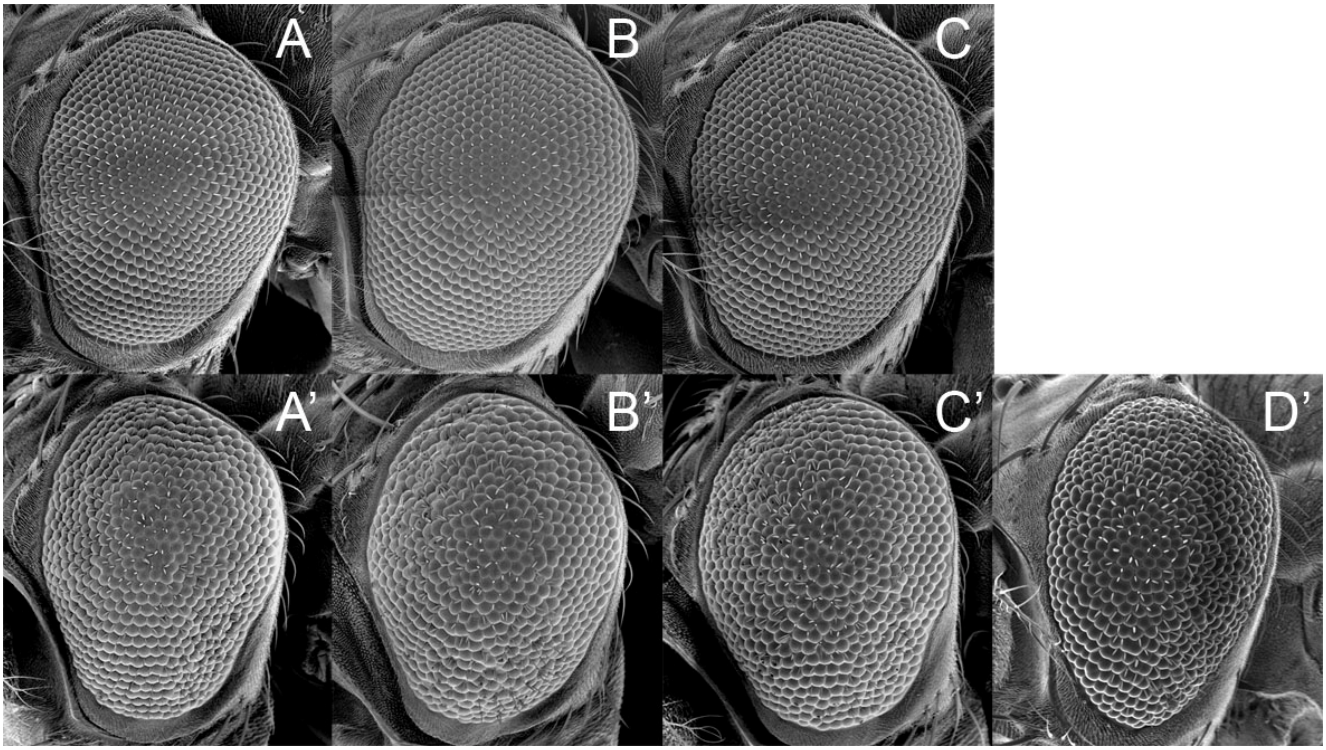

Figure 17a
Removal of *dmnt* does not alter the phenotype associated with strong overexpression of *dmyc.* Also in a *dmnt* null background, expression of *dmax* dsRNA causes increased roughness.

Label:	Genotypes:
A	*w dmnt^{Rev}/Y; GMR-GAL4/+*
B	*w dmnt^{1}/Y; GMR-GAL4/+*
C	*w dmnt^{2}/Y; GMR-GAL4/+*
A'	*w dmnt^{Rev}/Y; GMR-GAL4 UAS-dmyc^{132}/+; UAS-dmyc^{13} UAS-dmyc^{42}/+*
B'	*w dmnt^{1}/Y; GMR-GAL4 UAS-dmyc^{132}/+; UAS-dmyc^{13} UAS-dmyc^{42}/+*
C'	*w dmnt^{2}/Y; GMR-GAL4 UAS-dmyc^{132}/+; UAS-dmyc^{13} UAS-dmyc^{42}/+*
D'	*w dmnt^{1}/Y; GMR-GAL4 UAS-dmyc^{132}/UAS-dmax-IR(2-7); UAS-dmyc^{13} UAS-dmyc^{42}/+*

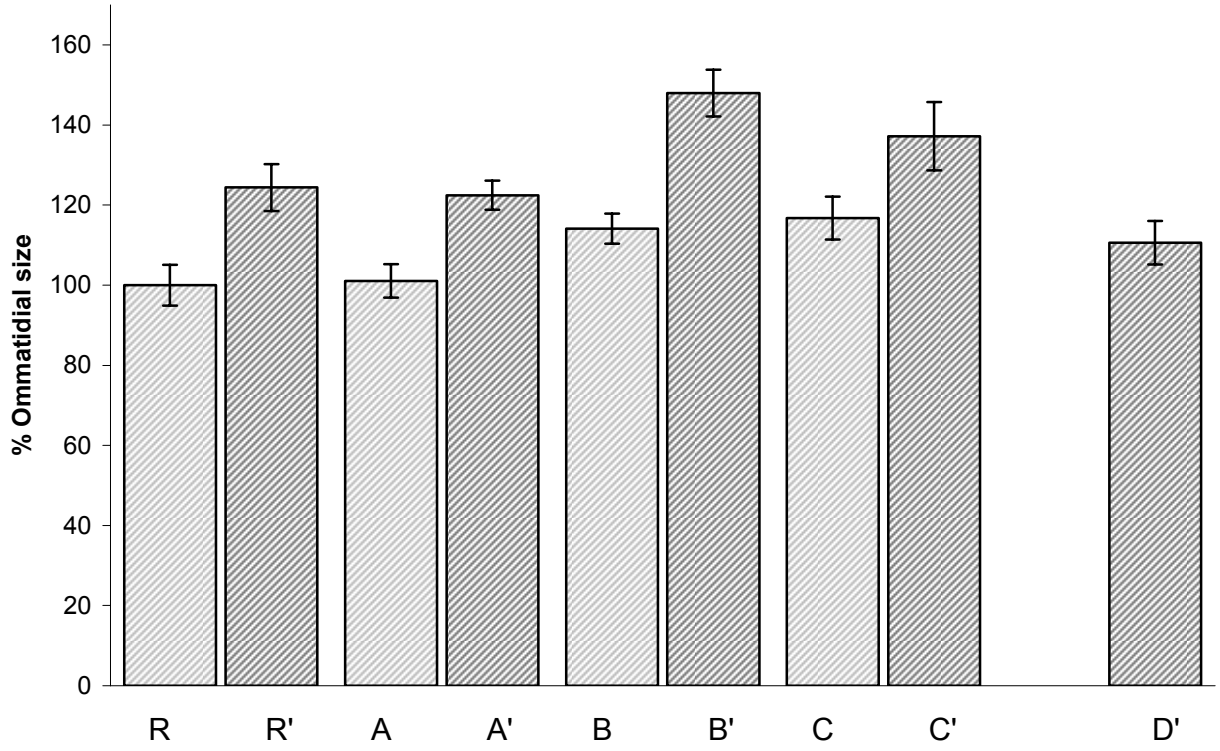

Figure 17b
Ommatidial size (relative to the *y w/Y; GMR-GAL4/+* genotype). The labels correspond to Figure 17a. For every genotype, the size of 20 centrally located ommatidia of 6 individual eyes was determined. The error bars indicate standard deviations.

Label:	Genotypes:
R	*y w/Y; GMR-GAL4/+*
A	*w dmnt^{Rev}/Y; GMR-GAL4/+*
B	*w dmnt^{1}/Y; GMR-GAL4/+*
C	*w dmnt^{2}/Y; GMR-GAL4/+*
R'	*y w /Y; GMR-GAL4 UAS-dmyc^{132}/+; UAS-dmyc^{13} UAS-dmyc^{42}/+*
A'	*w dmnt^{Rev}/Y; GMR-GAL4 UAS-dmyc^{132}/+; UAS-dmyc^{13} UAS-dmyc^{42}/+*
B'	*w dmnt^{1}/Y; GMR-GAL4 UAS-dmyc^{132}/+; UAS-dmyc^{13} UAS-dmyc^{42}/+*
C'	*w dmnt^{2}/Y; GMR-GAL4 UAS-dmyc^{132}/+; UAS-dmyc^{13} UAS-dmyc^{42}/+*
D'	*w dmnt^{1}/Y; GMR-GAL4 UAS-dmyc^{132}/UAS-dmax-IR(2-7); UAS-dmyc^{13} UAS-dmyc^{42}/+*

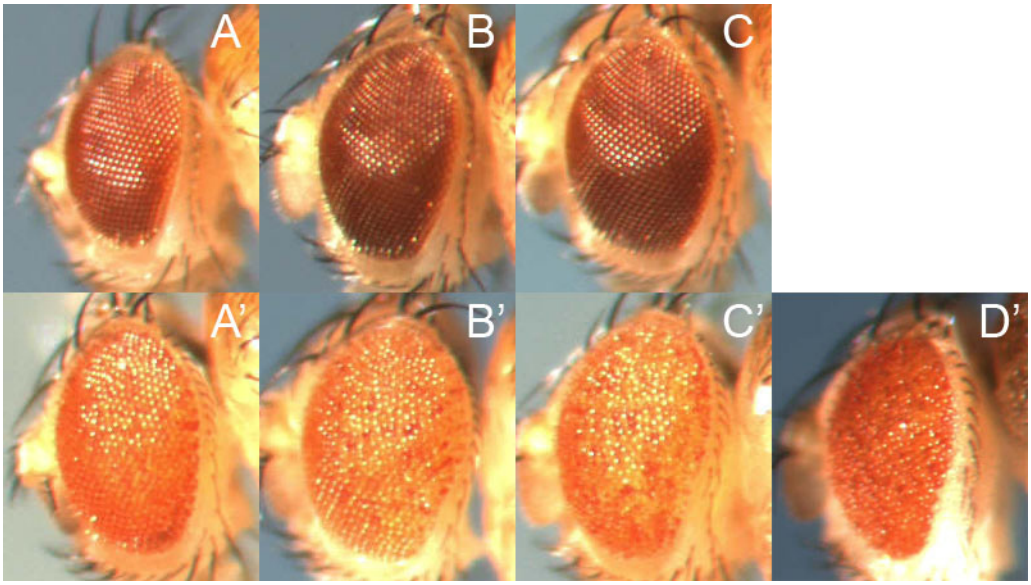

Figure 17c
The pigmentation defect that is caused by the overexpression of three copies of *UAS-dmyc* is also present in absence of *dmnt*, and it cannot be rescued by downregulation of *dmax*.

Label:	Genotypes:
A	*w dmnt^{Rev}/Y; GMR-GAL4/+*
B	*w dmnt^{1}/Y; GMR-GAL4/+*
C	*w dmnt^{2}/Y; GMR-GAL4/+*
A'	*w dmnt^{Rev}/Y; GMR-GAL4 UAS-dmyc^{132}/+; UAS-dmyc^{13} UAS-dmyc^{42}/+*
B'	*w dmnt^{1}/Y; GMR-GAL4 UAS-dmyc^{132}/+; UAS-dmyc^{13} UAS-dmyc^{42}/+*
C'	*w dmnt^{2}/Y; GMR-GAL4 UAS-dmyc^{132}/+; UAS-dmyc^{13} UAS-dmyc^{42}/+*
D'	*w dmnt^{1}/Y; GMR-GAL4 UAS-dmyc^{132}/UAS-dmax-IR(2-7); UAS-dmyc^{13} UAS-dmyc^{42}/+*

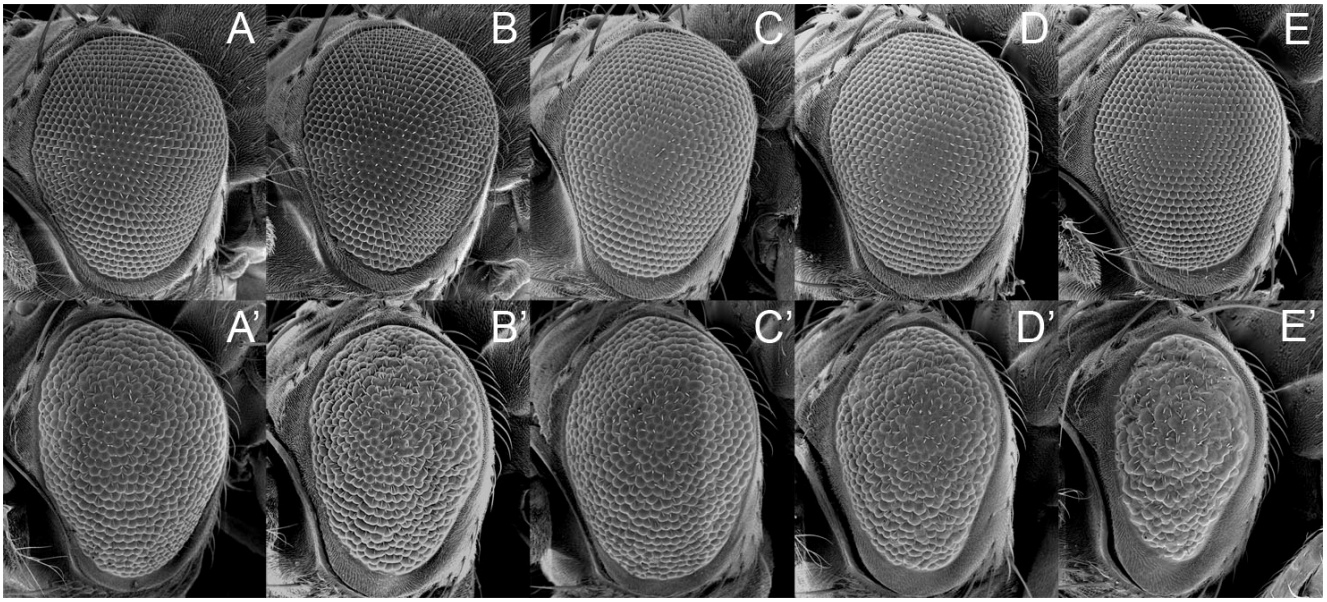

Figure 18a
Titration of *dmax* by overexpression of *UAS-dmnt[dSID]*, but not *UAS-dmnt[dZIP]* has the same effect as overexpression of *dmax* dsRNA.

Label:	Genotypes:
A	*y w/Y; GMR-GAL4/+*
B	*y w/Y; GMR-GAL4/UAS-dmax-IR(2-7)*
C	*y w/Y; GMR-GAL4/+; UAS-dmnt^{BM10-7}[dZIP]/+*
D	*y w/Y; GMR-GAL4/+; UAS-dmnt^{N7-4R}[dSID]/+*
E	*y w/Y; GMR-GAL4/+; UAS-dmnt^{T2-33}[+]/+*
A'	*y w/Y; GMR-GAL4 UAS-dmyc^{132}/+; UAS-dmyc^{13} UAS-dmyc^{42}/+*
B'	*y w/Y; GMR-GAL4 UAS-dmyc^{132}/UAS-dmax-IR(2-7); UAS-dmyc^{13} UAS-dmyc^{42}/+*
C'	*y w/Y; GMR-GAL4 UAS-dmyc^{132}/+; UAS-dmyc^{13} UAS-dmyc^{42}/UAS-dmnt^{BM10-7}[dZIP]*
D'	*y w/Y; GMR-GAL4 UAS-dmyc^{132}/+; UAS-dmyc^{13} UAS-dmyc^{42}/UAS-dmnt^{N7-4R}[dSID]*
E'	*y w/Y; GMR-GAL4 UAS-dmyc^{132}/+; UAS-dmyc^{13} UAS-dmyc^{42}/UAS-dmnt^{T2-33}[+]*

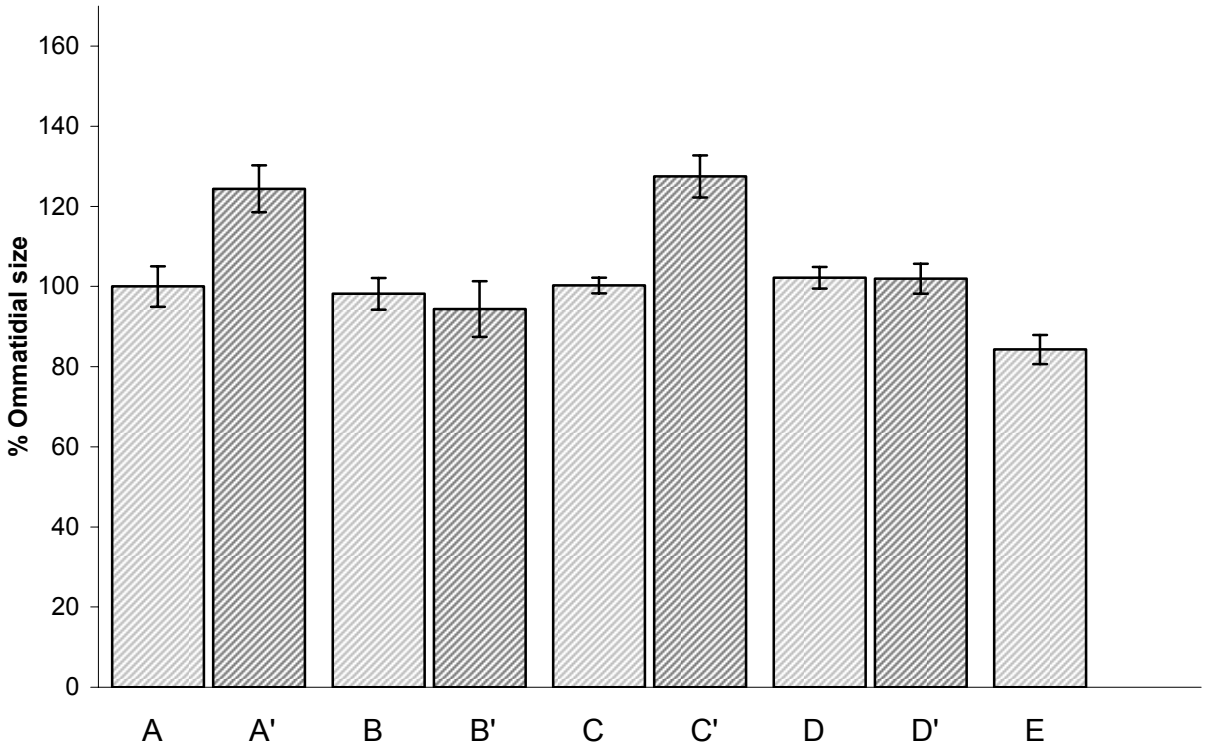

Figure 18b
Ommatidial size (relative to the *y w/Y; GMR-GAL4/+* genotype). The labels correspond to Figure 18a. For every genotype, the size of 20 centrally located ommatidia of 6 individual eyes was determined. The error bars indicate standard deviations.

Label:	Genotypes:
A	*y w/Y; GMR-GAL4/+*
B	*y w/Y; GMR-GAL4/UAS-dmax-IR(2-7)*
C	*y w/Y; GMR-GAL4/+; UAS-dmnt^{BM10-7}[dZIP]/+*
D	*y w/Y; GMR-GAL4/+; UAS-dmnt^{N7-4R}[dSID]/+*
E	*y w/Y; GMR-GAL4/+; UAS-dmnt^{T2-33}[+]/+*
A'	*y w/Y; GMR-GAL4 UAS-dmyc^{132}/+; UAS-dmyc^{13} UAS-dmyc^{42}/+*
B'	*y w/Y; GMR-GAL4 UAS-dmyc^{132}/UAS-dmax-IR(2-7); UAS-dmyc^{13} UAS-dmyc^{42}/+*
C'	*y w/Y; GMR-GAL4 UAS-dmyc^{132}/+; UAS-dmyc^{13} UAS-dmyc^{42}/UAS-dmnt^{BM10-7}[dZIP]*
D'	*y w/Y; GMR-GAL4 UAS-dmyc^{132}/+; UAS-dmyc^{13} UAS-dmyc^{42}/UAS-dmnt^{N7-4R}[dSID]*
E'	*y w/Y; GMR-GAL4 UAS-dmyc^{132}/+; UAS-dmyc^{13} UAS-dmyc^{42}/UAS-dmnt^{T2-33}[+]*

2. *dmax* null mutant

So far we have shown that flies, in which *dmax* levels were reduced by the expression of *dmax* dsRNA, have phenotypes that are in some ways similar to the phenotypes of flies which carry hypomorphic alleles of *dmyc*, such as reduced body weight and thin bristles. These findings met our expectations, since it had been shown previously that Max is an essential cofactor of Myc (Blackwood and Eisenman, 1991; Amati et al., 1992; Blackwood et al., 1992; Amati et al., 1993a; Amati et al., 1993b). However, our surprising finding that dmax-RNA*i* did not suppress the phenotype caused by strong *dmyc* overexpression in the eye but rather increased aspects of the overexpression phenotype has led us to the conclusion that a part of the functions of *dmyc* do not require *dmax*. It was clear that a rigid analysis of the requirement of *dmax* for *dmyc* functions is difficult with RNA*i*, since it was only possible to strongly diminish *dmax* levels, but not to completely abolish *dmax* function. To continue our analysis, we therefore felt that is was crucial to obtain a *dmax* null mutant.

2.1. Generation of a *dmax* null mutant by imprecise excision of a P element

Besides the advantages a GAL4-inducible system provides, one of the main reasons to use an inducible RNA*i* system to study *dmax* was the lack of P elements in the *dmax* locus. When the new P element insertion $P\{y^+\ w^+\}CG9666^{EY02775}$ became available, we decided to use this insertion to generate *dmax* mutants. $y\ w;\ P\{y^+\ w^+\}CG9666^{EY02775}$ is inserted 472 bp upstream of the start of the *dmax* transcript, in the 3' end of the second exon of *CG9666*. We mobilized the P element using the *Δ2-3* P element transposase and collected flies that had lost the w^+ marker, indicating that the P element had been mobilized and lost from the genome. Since we had shown that downregulation of *dmax* transcript levels by *dmax* RNA*i* leads to pupal lethality, we expected to see pupal or earlier lethality with strong hypomorphic *dmax* alleles or with a *dmax* null allele. It was therefore possible to select for imprecise excision events that would cause deletions in the *dmax* locus by directly crossing collected $y^-\ w^-$ flies to flies harboring *Df(3L)fz2* and selecting for lack of viability. For a detailed crossing scheme of the imprecise excision screen, see Material and Methods.

Out of 180 tested $P^{mut[y-\ w-]}$ chromosomes, we identified 5 $P^{mut[y-\ w-]}$ third chromosomes which caused lethality in conjunction with *Df(3L)fz2*. We established stable lines carrying these alleles and subsequently examined these alleles by PCR. To this end, we used a primer annealing to the 3' end of the *dmax* transcript and a second primer annealing directly upstream (relative to *dmax*) of the *EY02775* insertion site. These primers amplify a 2.1 kb fragment on a wild type 3rd chromosome. In the case of imprecise excision events that would cause asymmetrical deletions stretching from the *EY02775* insertion position into *dmax*, we expected to see smaller fragments. In two of the five lines, we could indeed produce smaller fragments. These fragments were then sequenced, revealing two asymmetrical

deletions. The two deletion alleles were termed *dmax*^{1} and *dmax*^{2}. Figure 19 shows the *dmax* locus, the location of the *EY02775* insertion and the *dmax*^{1} and *dmax*^{2} deletions. The exact breakpoints in the two alleles are indicated in Materials and Methods.

In *dmax*^{2}, a 550 bp deletion has been created that deletes most of the first exon of the *dmax* transcript, ending 27 bp upstream of the start of the *dmax* ORF. Flies homozygous for *dmax*^{2} die as pharate imagines. We assumed that *dmax*^{2} represents a strong hypomorphic allele of *dmax*, or possibly a null allele, but we did not further study the allele, since we had generated a molecular null allele with *dmax*^{1}.

The 1.8 kb deletion found in *dmax*^{1} starts precisely at the position where *EY02775* had been inserted, and it stretches into the last exon of *dmax*, deleting the whole *dmax* coding region and therefore being a molecular null allele of *dmax.* We subsequently concentrated on the analysis of *dmax*^{1}.

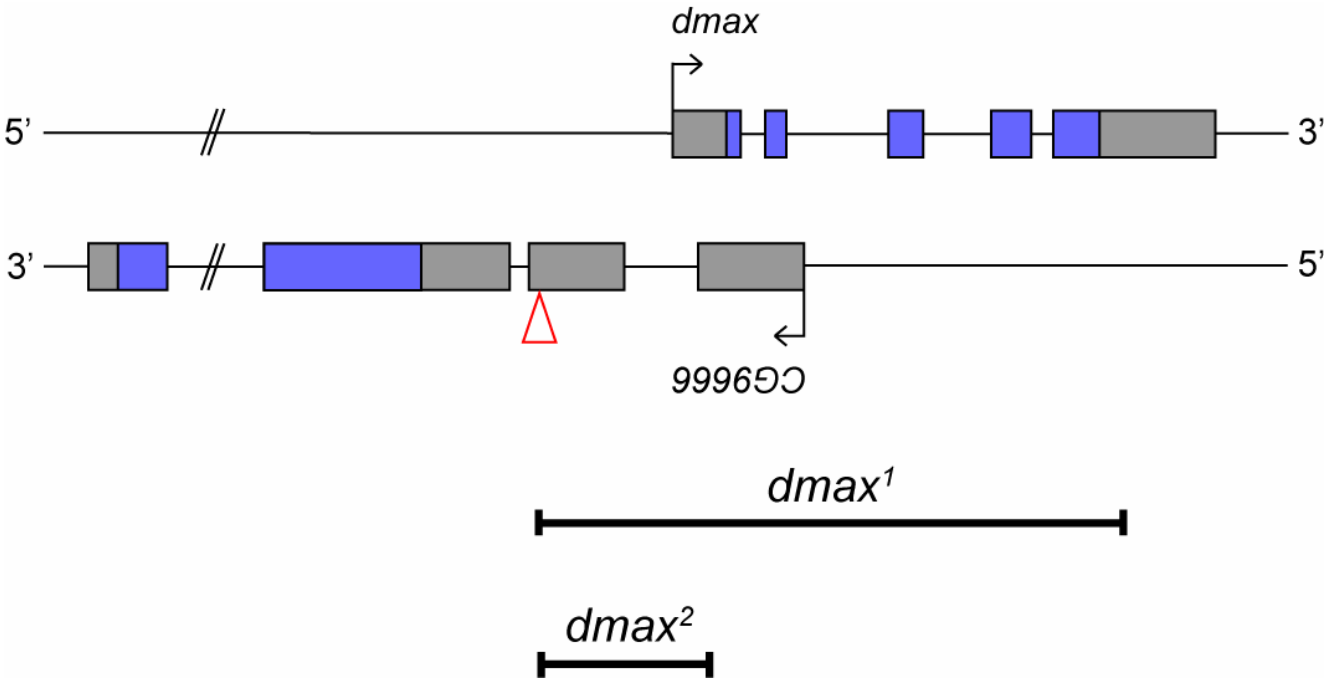

Figure 19
dmax alleles generated in the imprecise excision screen. The diagram shows the *dmax* and the *CG9666* gene. Arrows indicate the start of transcription of *dmax* and *CG9666*. Grey boxes indicate transcribed sequence, blue boxes indicate coding (translated) sequence. The red triangle shows the position of the *EY02775* P element insertion. Indicated are the two deletions generated in the imprecise excision screen, labeled $dmax^1$ and $dmax^2$.

2.2. Characterization of the *dmax*^{1} phenotype

2.2.1. Growth and developmental timing of *dmax*^{1} flies

Based on the selection procedure in the imprecise excision screen, it was clear that flies of a *dmax*^{1}*/Df(3L)fz2* do not reach the adult stage. We therefore expected that *dmax*^{1}*/dmax*^{1} flies would die prior to eclosion. In order to study the phenotype of *dmax*^{1} in larvae or pupae, we constructed stable lines in which the *dmax*^{1} chromosome was put over balancers that were marked by *Tb*, y^{+} or by the constitutive overexpression of GFP. We then used these lines to study the development of flies that were homozygous for *dmax*^{1}.

2.2.2. *dmax*^{1} larvae hatch in normal proportions

The loss of *dmax* did not lead to lethality in the embryonal stage, and *dmax*^{1} larvae hatch in Mendelian proportions, as shown by the following experiment: From a cross of *w; dmax*^{1}*/TM3, Ser GFP* flies *inter se*, we collected L1 larvae that had an age of 24-32 h. From the 106 collected larvae, 76 showed expression of GFP, whereas 30 scored negative for the expression of GFP. Since homozygosity for *TM3, Ser GFP* leads to embryonic lethality, the GFP-positive larvae had the *dmax*^{1}*/TM3, Ser GFP* genotype, whereas the GFP-negative larvae were homozygous for *dmax*^{1}. Based on Mendelian inheritance, the number of homozygous *dmax*^{1} offspring in the *inter se* cross is expected to be half the number of the *dmax*^{1}*/TM3, Ser GFP* offspring, if no lethality occurs. Therefore, the viability of *dmax*^{1} larvae in this cross was high (30 larvae are 78% of the expected 35 larvae).

2.2.3. *dmax*^{1} larvae show impaired growth and a developmental delay

dmax^{1} larvae grow more slowly than wild type control larvae. At 120 h (5 d) after egg deposition (AED), when *dmax*^{1}*/TM3* larvae - which are fully viable and develop normally - had started to pupariate, *dmax*^{1} homozygous larvae were in the L3 stage, but showed a greatly reduced size (Figure 20a). At 192 h (8 d) AED, when wild type controls had undergone metamorphosis, the *dmax*^{1} L3 larvae had reached a size slightly smaller than the one of wild type larvae at 120 h AED (Figure 20b). The smaller size of the whole larvae correlated with the size of larval polyploid tissues: Figure 20c shows fat body and salivary gland cells of *dmax*^{1} larvae (at 120 h and at 192 h AED) compared to *y w* control larvae (at 120 h AED). At 192 h AED, *dmax*^{1} fat body and salivary gland cell nuclei had reached a size slightly smaller than one of *y w* control cells at 120 h AED.

Even though the impaired growth of *dmax*^{1} larvae becomes apparent already in the first larval stage and is clearly visible in the second larval stage, L2-L3 ecdysis is, if at all, only slightly delayed in *dmax*^{1} larvae: We collected *dmax*^{1} larvae that had an age of 54 - 70 h AED. All of these larvae (total number: 25) were in L2. Conversely, in a second collection of *dmax*^{1} larvae of an age of 80 - 94 h AED (total number: 36), all larvae were in the L3 stage. We could therefore define a time window of

70 - 80 h AED for the L2-L3 molt in *dmax*^{1} larvae. Since the L2-L3 molt occurs at 72 h AED in wild type larvae (Ashburner et al., 2005), we concluded that the main developmental delay of *dmax*^{1} larvae occurs in the third larval stage.

The viability of *dmax*^{1} larvae is only slightly lower than the one of wild type controls. Figure 21 shows the percentage of larvae that survived from 48 h AED to 120 h AED (left chart) and from 48 h AED to 192 h AED (right chart). Thus, the strong developmental delay of *dmax*^{1} larvae in L3 is not accompanied by elevated lethality.

2.2.4. *dmax*^{1} L3 larvae have an abnormal mouth hook phenotype

The three larval stages of *Drosophila* can be distinguished by the morphology of the posterior and, more easily, of the anterior spiracles, by the number of teeth of the larval mouth hooks and by the form of the pharyngeal bars (Ashburner et al., 2005). Based on the morphology of the anterior spiracles, the second and the third larval instars of *dmax*^{1} larvae could be clearly distinguished. Figure 22 shows the anterior spiracles of *dmax*^{1} L3 larvae (B) compared to ones of *dmax*^{1}/TM3 heterozygotes (A). *dmax*^{1} L3 anterior spiracles show the hand-shaped form typical of L3 larvae, albeit at a smaller size. However, it proved to be impossible to stage *dmax*^{1} larvae based on the mouth hook teeth number. Whereas *dmax*^{1}/TM3 L3 animals had normal-looking mouth hooks with many teeth (Figure 22 C), all examined *dmax*^{1} L3 mouth hooks were found to have no or only few large teeth (Figure 22 D). The normal number of teeth for L2 wild type larvae is 3, and for L3 wild type larvae is 12 (Ashburner et al., 2005). Additionally, some of the examined mouth hooks of *dmax*^{1} larvae show duplicated mouth hook tips.

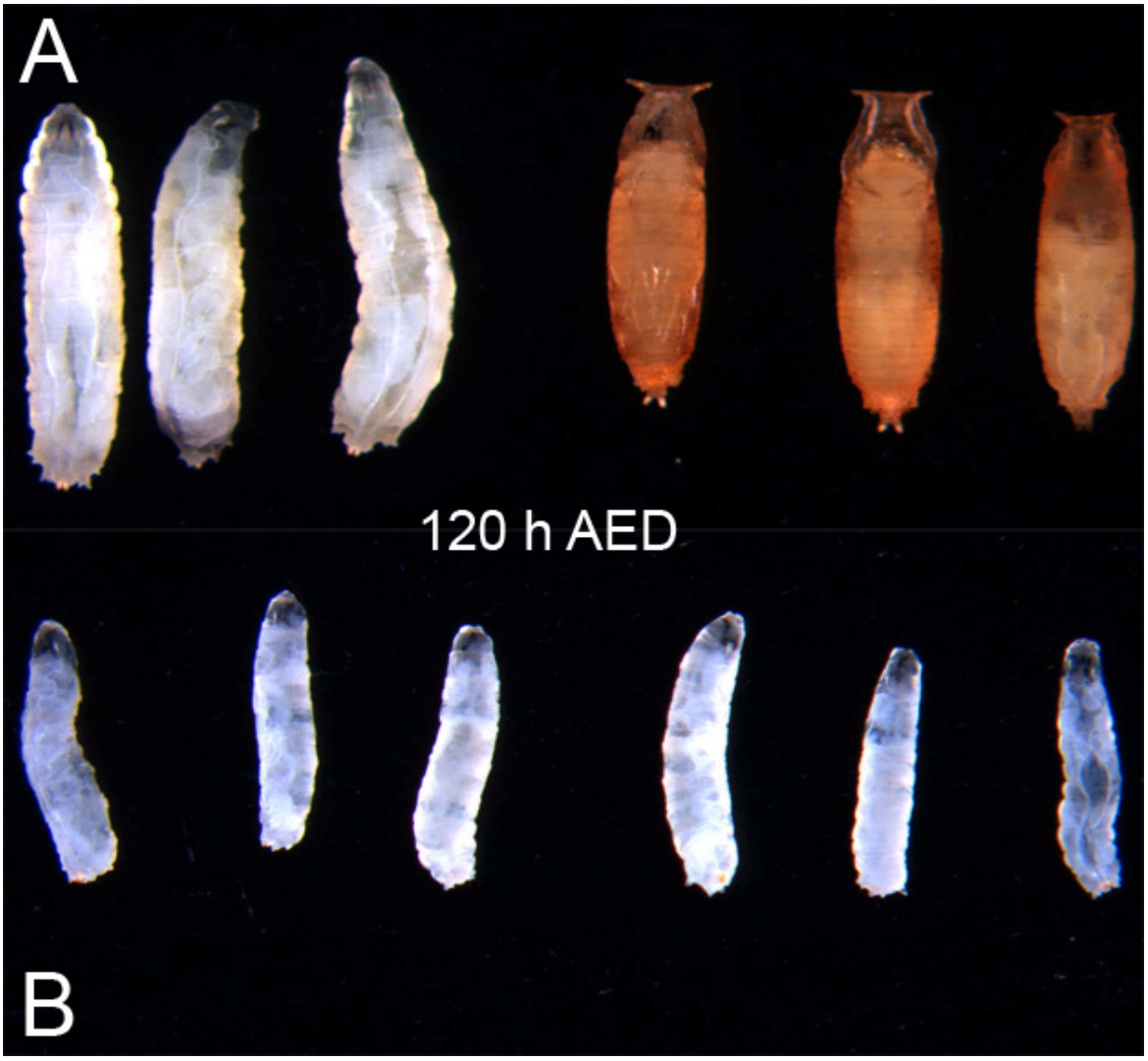

Figure 20a
dmax^{1} larvae grow more slowly than *dmax*^{1}*/TM3, Ser GFP* heterozygotes. At 120 h AED, the heterozygote larvae (A) have reached the end of the third larval stage or already have pupated. At this time point, *dmax*^{1} larvae have all reached L3 stage, but they are much smaller.

Label:	Genotypes:
A	*w; dmax*^{1}*/TM3, Ser GFP*
B	*w; dmax*^{1}

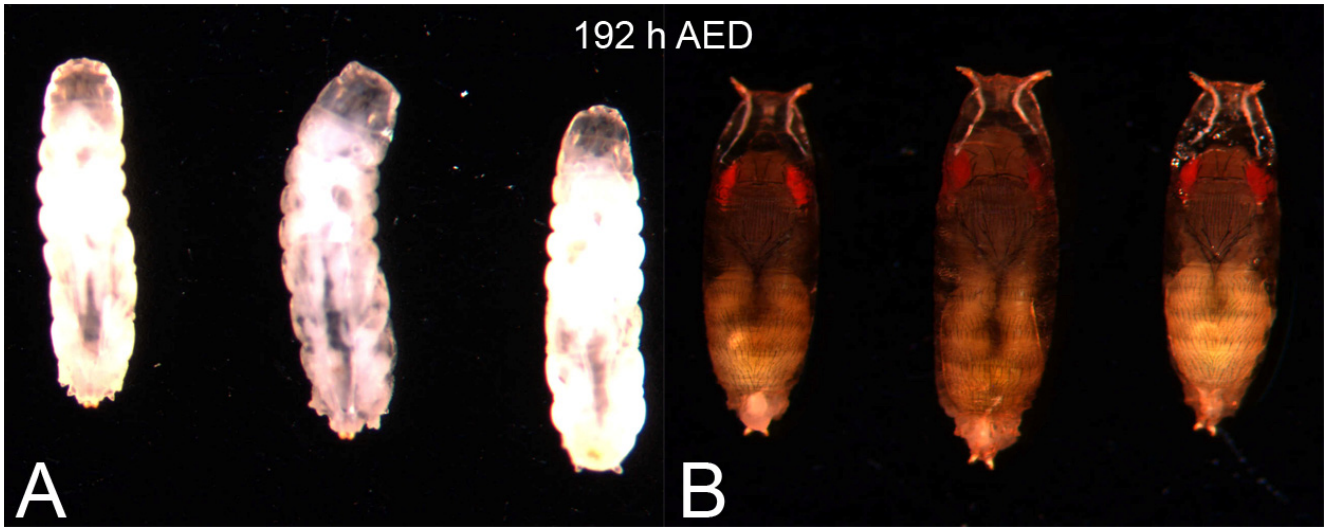

Figure 20b
dmax^{1} animals compared to wild type animals at 192 h AED. At this time point, wild type animals have nearly completed their pupal development. *dmax*^{1} animals are still in the third larval stage, but they have reached a size only slightly smaller than the one of wild type late L3 larvae.

Label:	Genotypes:
A	*w; dmax*^{1}
B	*wt [OreR]*

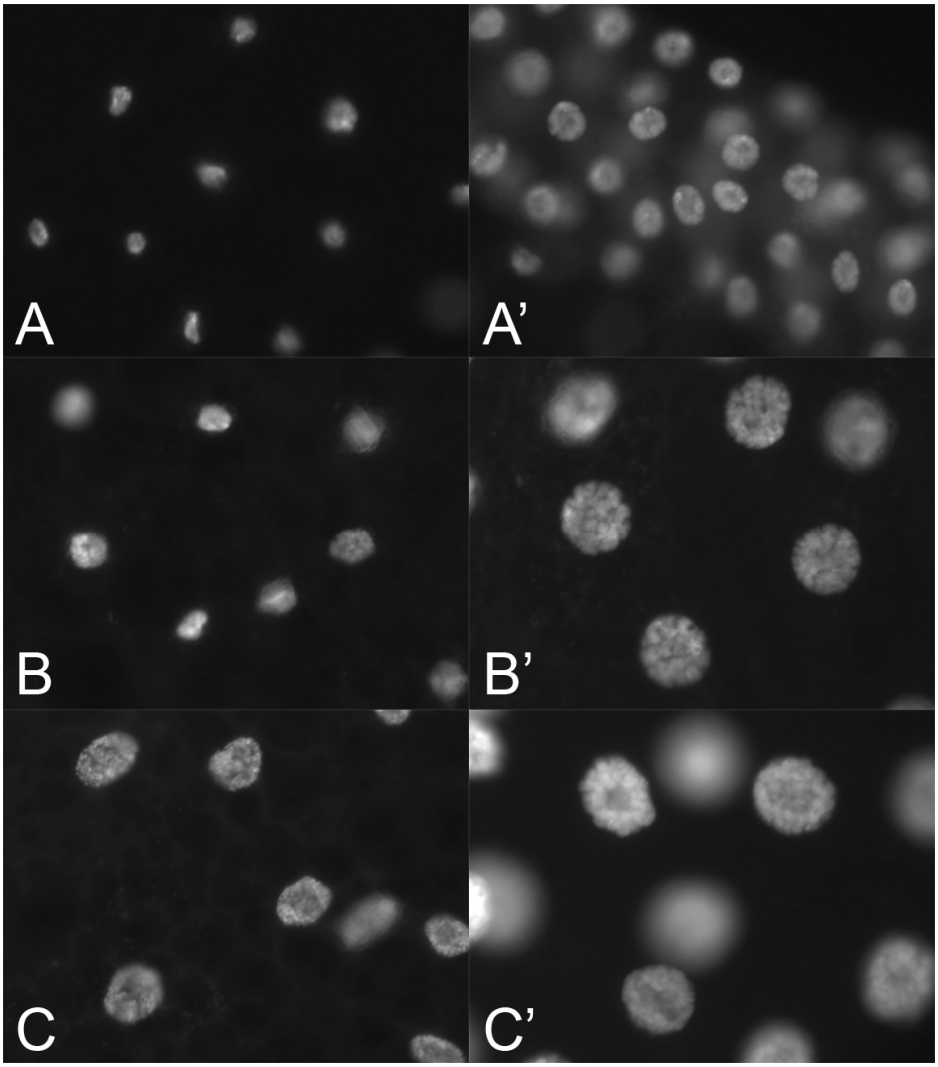

Figure 20c
The sizes of fat body cell nuclei (A, B, C) and salivary gland cell nuclei (A', B', C') of *dmax*^{1} larvae correlate to the observed total larval sizes at the respective times. The pictures show nuclei stained with Hoechst dye and were taken with a 63x objective. Whereas at 5 d AED, *dmax*^{1} fat body and salivary gland cells (A, A') are clearly smaller than *y w* control fat body and salivary gland cells (C, C'), fat body and salivary gland cells reach almost wild type sizes at 8 d AED (B, B')

Label:	Organ:	Time AED:	Genotype
A	fat body cells	120 h AED	*w; dmax*^{1}
A'	salivary gland cells	120 h AED	*w; dmax*^{1}
B	fat body cells	192 h AED	*w; dmax*^{1}
B'	salivary gland cells	192 h AED	*w; dmax*^{1}
C	fat body cells	120 h AED	*y w*
C'	salivary gland cells	120 h AED	*y w*

Figure 21
The viability of *dmax*^{1} animals is only slightly reduced throughout larval development. The graphs shows the survival of control *OreR* and of *w; dmax*^{1} animals from the collection of the larvae (at 48 h AED) until the indicated time points (120 h and 192 h).
Indicated is the average percentage of surviving larvae and the standard deviation. For the 120 h timepoint, 6 experiments with a total number of 209 animals (A) and 131 animals (B) were performed. For the 192 h timepoint, 2 experiments with a total number of 60 animals (A) and 55 animals (B) were performed.

Label:	Genotypes:
A	*wt [OreR]*
B	*w; dmax*^{1}

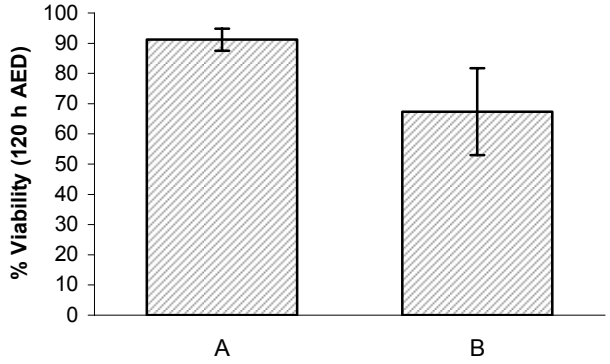

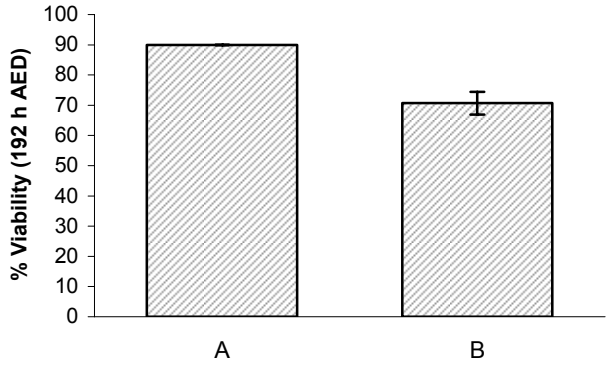

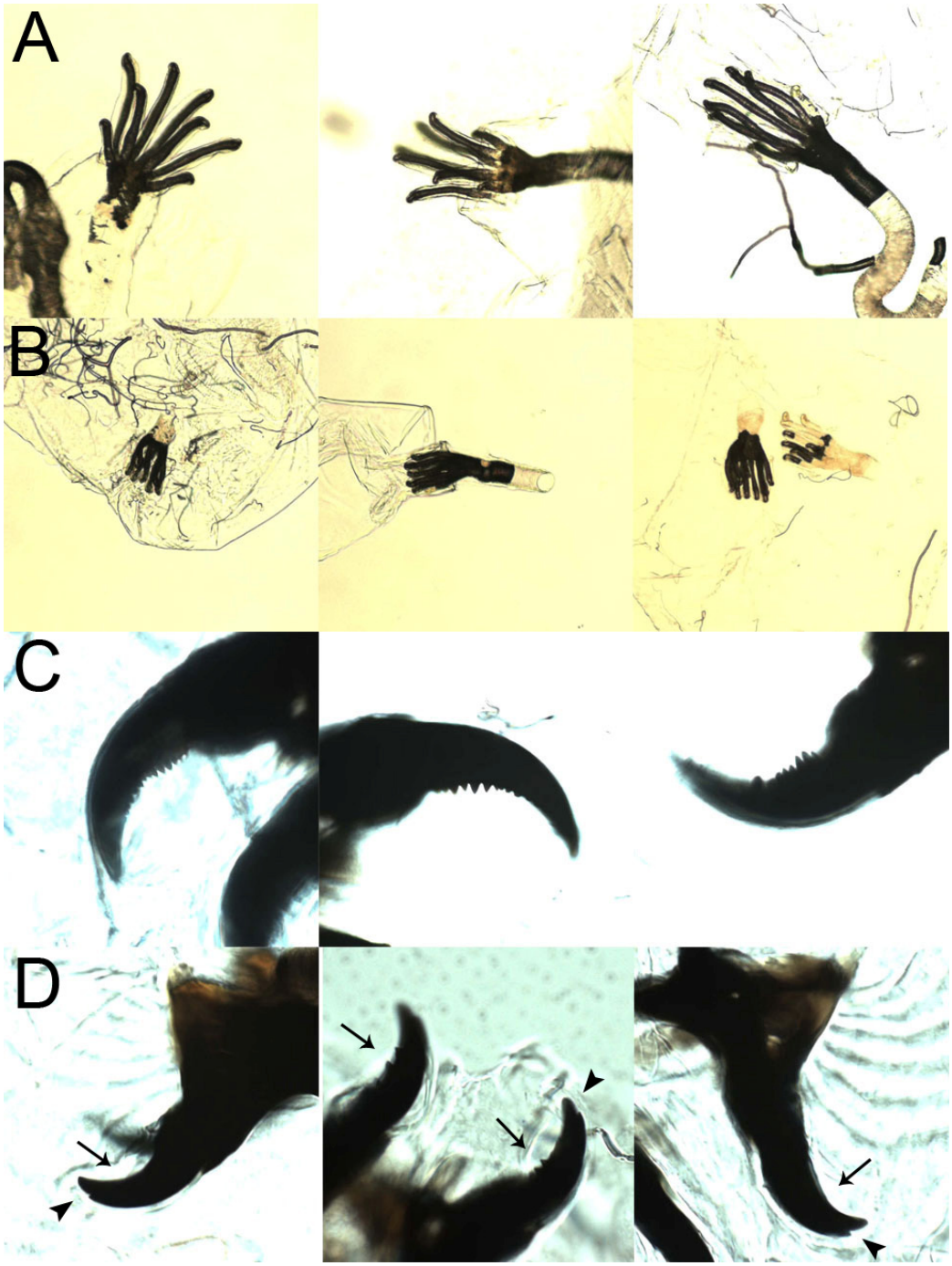

Figure 22
Whereas *dmax*^{1} L3 larvae show anterior spiracles of wild type morphology (albeit of smaller size) (B), their mouth hooks have an aberrant morphology (D): Many mouth hooks have duplicated tips (arrowheads). Some mouth hooks show no teeth, whereas others show a strongly reduced number of teeth (arrows). In comparison, control animals that are heterozygous for *dmax*^{1} show a wild type number of teeth and no mouth hook tip duplications.

Label:	Genotypes:
A, C	*w; dmax*^{1}/TM3, Ser GFP
B, D	*w; dmax*^{1}

2.2.5. *dmax*^{1} larvae pupate and some of them develop into pharate imagines

dmax^{1} larvae undergo pupariation between day 8 and day 9 AED, without having attained wild type size (Figure 23a, 23b). Besides the reduced size, *dmax*^{1} pupae have one feature which distinguishes them from wild type pupae: they rarely ever evert the anterior spiracles. Whereas the majority of the *dmax*^{1} pupae abort metamorphosis and presumably die, a remarkable proportion of the pupae properly undergo metamorphosis and develop into late pupae. Figure 23b shows that more than one third of the *dmax*^{1} pupae developed into pharate adults. The red line in Figure 23b indicates the percentage of *dmax*^{1} pupae that showed darkened macrochaetae and darkened wings (and overall pharate imaginal morphology), markers for late stages of imaginal development. Whereas in wild type pupae these events happen between 72 and 86 h post pupariation, *dmax*^{1} pupae show the changes in pigmentation at 96 h post pupariation and hence are delayed. Even though the resulting *dmax*^{1} pharate imagines show a wild type morphology (Figure 23c) and movement of the legs, they never eclose.

2.2.6. *dmax*^{1} larvae have reduced total RNA levels

We have shown that *dmax*^{1} grow more slowly than wild type control larvae and that they reach the pupal stage with a delay of four days (Figures 20, 23). Figure 24 shows that *dmax*^{1} larvae also have strongly reduced total RNA levels compared to control larvae, both at very early time points of larval development (29-39 h AED, Figure 24a) and at 120 h AED (96 h AED for the control) (Figure 24b). At the later time point, the difference in total RNA in *dmax*^{1} larvae compared to *y w* larvae roughly corresponds to the difference in larval size (Figure 20a). Remarkably, there is as strong a difference in total RNA levels already in L1 larvae, when almost no visible growth has occurred and *dmax*^{1} larvae are very difficult to distinguish from wild type larvae based on total larval size. It has been shown that total RNA levels strongly increase already in the first 24 hours after hatching, along with total DNA content, whereas protein levels do only marginally increase during that time (Church and Robertson, 1966). It is therefore conceivable that mutations that have an impact on the accumulation of DNA and RNA result in markedly decreased RNA levels at time points when total larval size has not strongly increased yet. We furthermore concluded that since the reduction in RNA levels in *dmax*^{1} larvae is as strong in L1 as it is in L3, it is probable that maternally contributed *dmax* mRNA or dMax protein do not play a role in the larval development of *dmax*^{1} animals.

2.2.7. *dmax* mRNA levels in *dmax*^{1} larvae

In order to confirm that *dmax* mRNA is absent in *dmax*^{1} larvae, we extracted RNA from *dmax*^{1} larvae at 120 h AED (and control RNA from *y w* larvae at 96 h AED) and measured *dmax* mRNA levels with qRTPCR. A qRTPCR assay specific for *actin5C* served as a reference. The resulting transcript levels using a *dmax*-specific primer pair were below 4% compared to the *y w* control (Figure 25a). We analyzed the PCR products generated with the *dmax*-specific primers using agarose gel electrophoresis

and could show that on *dmax*^{1} cDNA, the PCR had not resulted in the amplification of the specific *dmax* amplicon, but rather yielded a smear of unspecific bands. Therefore, *dmax*^{1} mRNA levels must be well below the calculated 4% that resulted from the total amount of amplified DNA in the assay. We concluded that *dmax* mRNA levels in 120 h old *dmax*^{1} larvae are below the detection threshold of a qRTPCR assay. Similar results were also obtained with primer pairs specific for *dmyc* and *dmnt* that had been shown to work well in qRTPCR assays, but yielded unspecific amplification products in *dmyc* null and *dmnt* null mutants, respectively (data not shown).

Figure 23a
dmax^{1} larvae (B) reach the pupal stage at day 9 AED, without having attained a wild type body size. At this time point, *y w* control larvae are about to eclose. Some *dmax*^{1} pupae show signs of defective development. However, some of the *dmax*^{1} pupae will continue development and develop into late, pharate adults (see Figure 23b, 23c). *dmax*^{1} pupae almost never show everted anterior spiracles.

Label:	Genotypes:
A	*y w*
B	*y w; dmax*^{1}

Figure 23b
Development of *dmax*^{1} pupae. Depicted are the time courses of puparium formation (blue line) and of the emergence of late, pharate adults (red line). In this experiment, 26 *dmax*^{1} larvae were collected at 120 h AED. All of the *dmax*^{1} larvae pupated within days 8 and 10. More than one third of the pupae continued in development and reached a pharate stage (red line) within days 12 and 13.

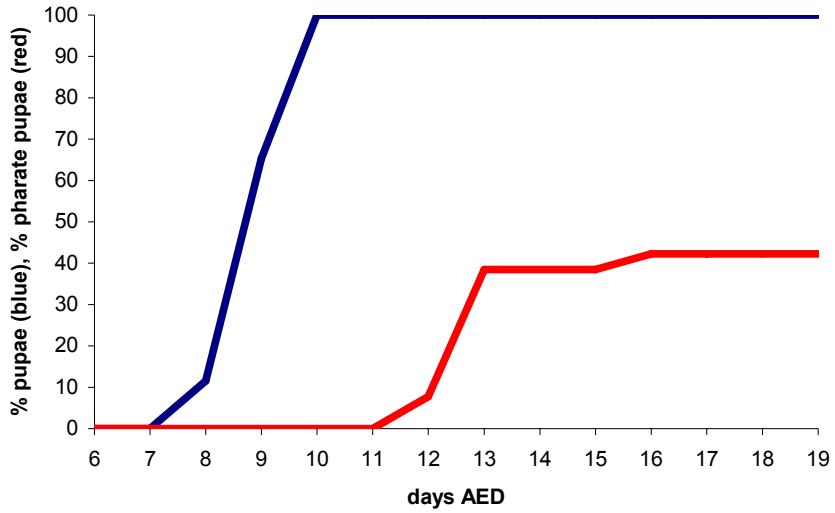

Figure 23c
dmax^{1} pupae develop into perfectly formed pharate imagines. The picture shows imagines that were taken out of their pupal cases. *dmax*^{1} animals are smaller than controls, and they have thin bristles.

Label:	Genotypes:
A	*y w; dmax*^{1}*/TM3, Ser y*$^{+}$
B	*y w; dmax*^{1}

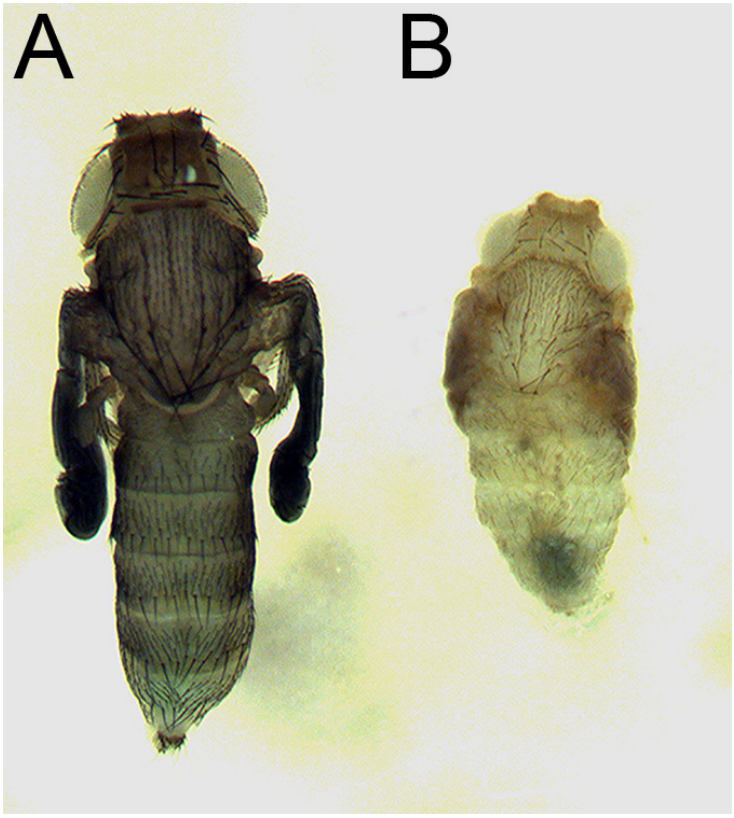

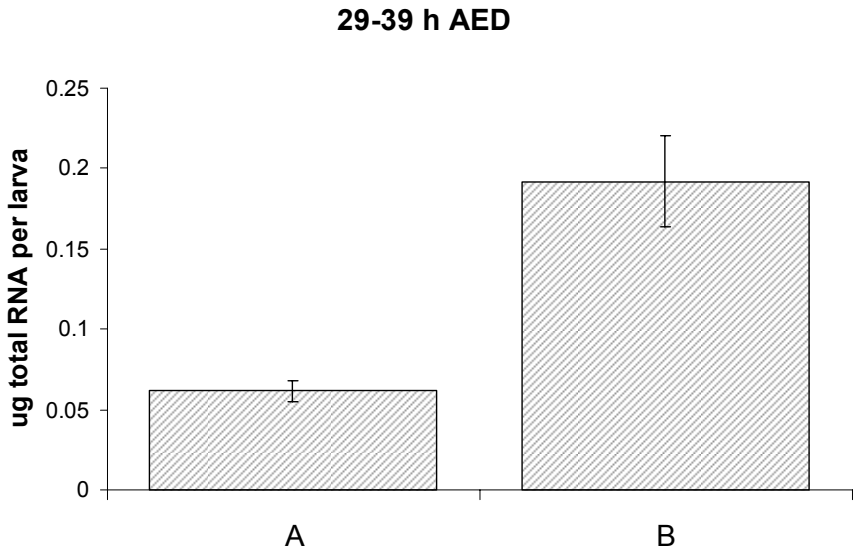

Figure 24a
dmax^{1} L1 larvae show strongly decreased total RNA levels compared to *y w* larvae. Two RNA extractions from 20 larvae were performed per genotype. The chart shows average total RNA amounts per larva and the standard deviation.

Label:	Genotypes:
A	*w; dmax*^{1}
B	*y w*

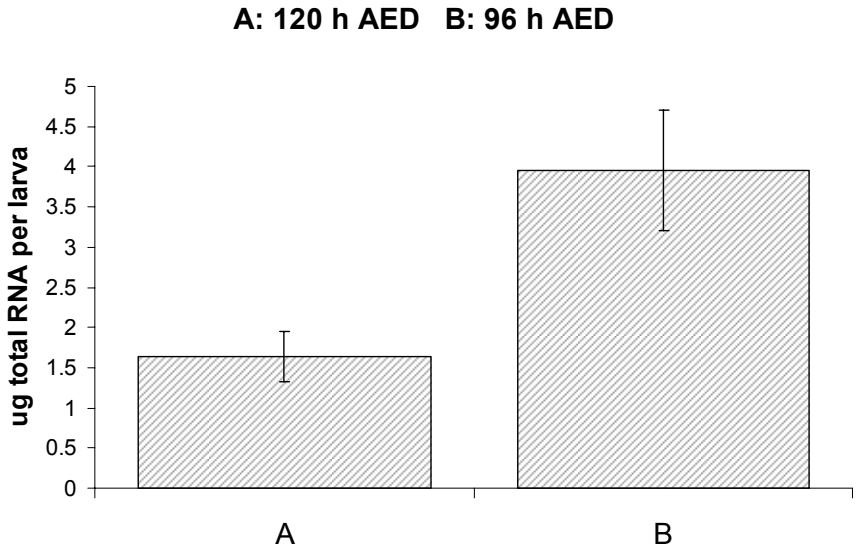

Figure 24b
Total RNA levels of *dmax*^{1} larvae at 120 h AED, compared to the total RNA levels of *y w* larvae at 96 h AED. A shows the average total RNA amount per larva from 5 RNA extractions (20 larvae per extraction) and the standard deviations. B shows the average total RNA amount per larva from 8 RNA extractions (12 larvae per extraction) and the standard deviation.

Label:	Genotypes:
A	*y w/Y, y*$^{+}$*; dmax*^{1}
B	*y w*

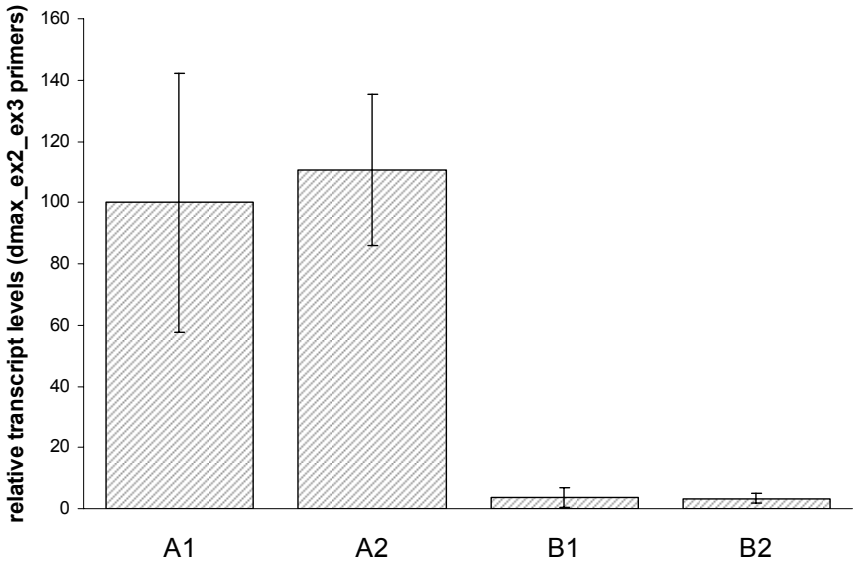

Figure 25a
Relative transcript levels in *y w; dmax*^{1} larvae (120 h AED) (B1, B2) compared to *y w* larvae (96 h AED) (A1, A2), measured in a qRTPCR assay with a *dmax* specific primer pair (dmax_ex2_ex3 primers). The transcript levels were normalized to a *actin5C* reference and the relative transcript level of A1 was arbitrarily set to 100%. Two cDNA preparations originating from two independent RNA extractions were used per genotype (A1, A2, B1, B2), and for each cDNA, 3 PCR reactions were performed. The standard deviations arising from the 3 PCR reactions are shown.

Label:	Genotypes:
A1, A2	*y w*
B1, B2	*y w/Y, y*$^{+}$*; dmax*^{1}

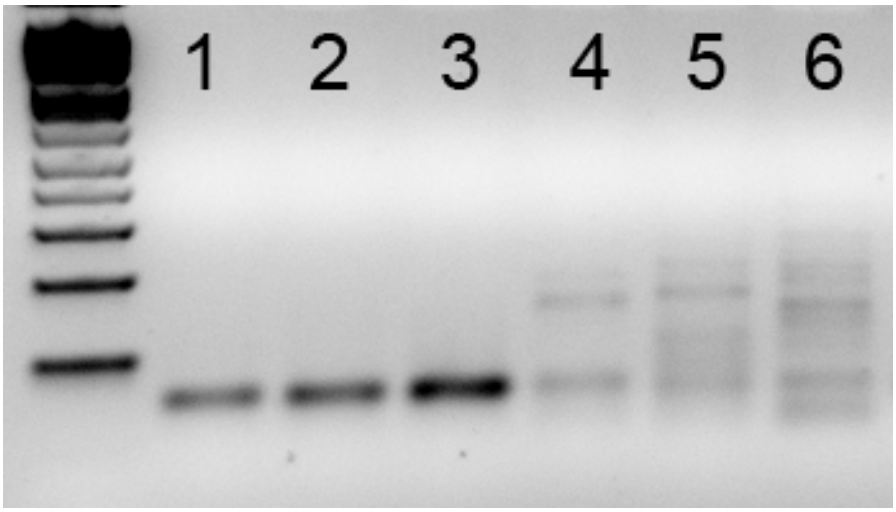

Figure 25b
2% agarose gel, showing the PCR products of the qRTPCR assay with primers specific to *dmax* (dmax_ex2_ex3 primers). Lanes 1, 2, 3 show the PCR product derived from *y w* cDNA (preparation A1 in Figure 25a). Lanes 4, 5, 6 show the PCR products derived from *y w; dmax*^{1} cDNA (preparation B1 in Figure 25a). On *dmax*^{1} cDNA, a smear of weak bands is present. Presumably, this smear is the product of unspecific PCR reactions of the dmax_ex2_ex3 primers which occur in the absence of *dmax* cDNA template.

2.2.8. Rescue of the *dmax*^{1} phenotype

Since the *dmax*^{1} allele consists of a deletion which also deletes the first and most of the second exon of the neighboring gene *CG9666*, it was important to examine to which extent the observed phenotypic effects of the *dmax*^{1} mutation are due to a loss of *dmax* function. Our first attempts to rescue the effects of *dmax*^{1} by expressing *UAS-dmax* transgenes with the strong, ubiquitous GAL4 driver *actin-GAL4* resulted only in a partial rescue: few adult flies eclosed, and they showed a clearly reduced body size and thin bristles (Figure 26). We used two independent *UAS-dmax* transgenes in single copies or in combination without achieving a complete rescue.

A reason for the only partial rescue might be that the expression of *UAS-dmax* by *actin-GAL4* did not fully reflect the expression levels and patterns of endogenous *dmax*. It was further possible that the rescue was not complete because the *UAS-dmax* cDNA construct did not allow the expression of different splice forms of dMax (vertebrate Max exists in different splice forms (Makela et al., 1992), and the architecture of the *max* locus is identical between *Drosophila* and vertebrates (Gallant, 2006)). For these reasons, we decided to clone a genomic *dmax* construct. The genomic region included in the construct is depicted in Figure 27. Relative to *dmax* orientation, the cloned region starts directly 3' of the start of the *CG9666* ORF, comprises the *dmax* transcript, and ends directly 5' of the start of *dmax*'s 3' neighboring gene *CG14084*. Therefore, the genomic rescue constructs includes the *dmax* ORF, but not the ORF of *CG9666.*

We created transgenic fly lines carrying this construct and used an insertion of the construct on the X chromosome (termed *dmax*^{rescue}) in rescue experiments. Figure 28a shows that *dmax*^{rescue} fully rescued the growth and developmental delay phenotype of *dmax*^{1} larvae. In addition, the Figure shows that *dmax*^{1} male and female larvae do not differ in size, a result which will be important for a later experiment. *dmax*^{1} flies carrying one (in males) or two (in females) copies of *dmax*^{rescue} eclosed with normal timing and had a wild type appearance (Figure 28b). Figure 29 lists three test crosses that showed that rescued *dmax*^{1} animals appeared in Mendelian proportions and that rescued *dmax*^{1} females and males are fertile. Stable *y w dmax*^{rescue}*; dmax*^{1} fly lines were established and could be maintained as a stock. Figure 30a shows that rescued *dmax*^{1} larvae which were collected at 48 h AED survived to adulthood as well as *y w* control larvae. Figure 30b shows that the wet weights of rescued *dmax*^{1} females were slightly higher than the ones of *y w* controls, possibly due to expression levels of *dmax*^{rescue} that are higher than the ones of endogenous *dmax.*

Based on these results, we concluded that the *dmax* genomic rescue construct provides a full rescue of the *dmax*^{1} mutant phenotype. Therefore we could exclude that *CG9666* functions play a role in the phenotypes we had described so far.

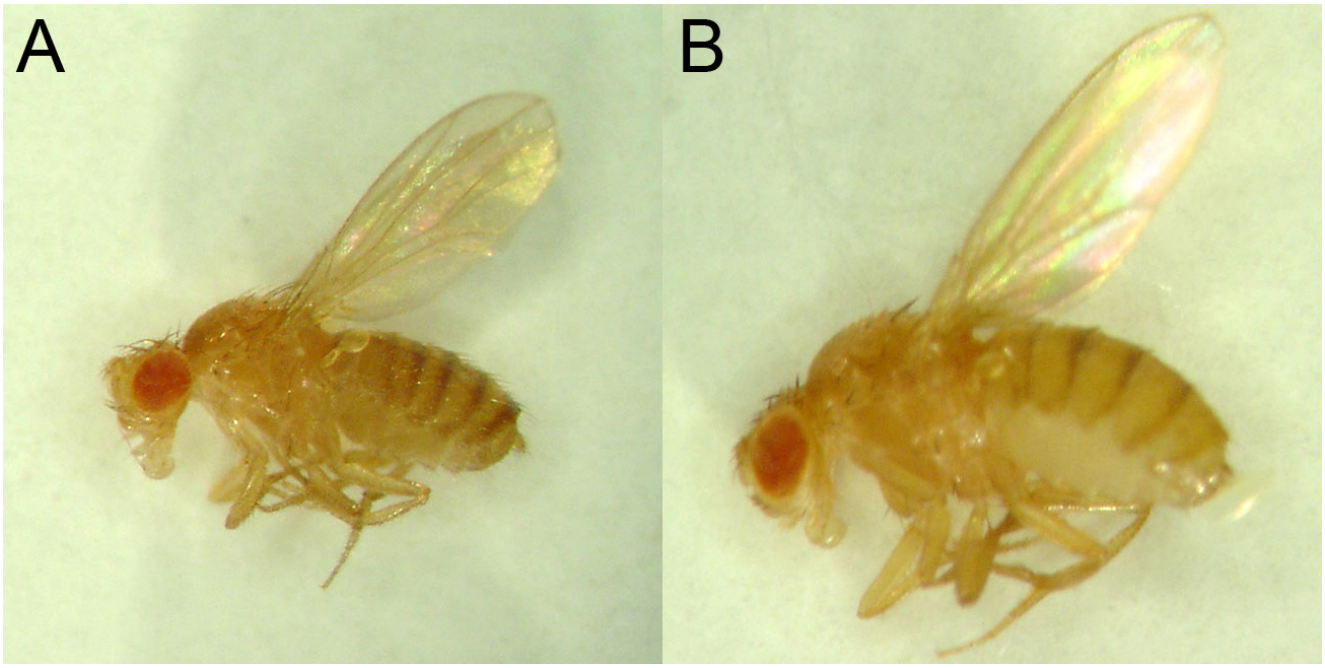

Figure 26
Expression of a *UAS-dmax* transgene under the control of the strong driver *actin-GAL4* does only partially rescue the lethality associated with the loss of *dmax*. The few eclosing flies (A) are clearly smaller than the heterozygous controls (B).

Label:	Genotypes:
A	*y w; UAS-dmax^{16}/actin-GAL4; dmax^{1}*
B	*y w; UAS-dmax^{16}/actin-GAL4; dmax^{1}/MKRS*

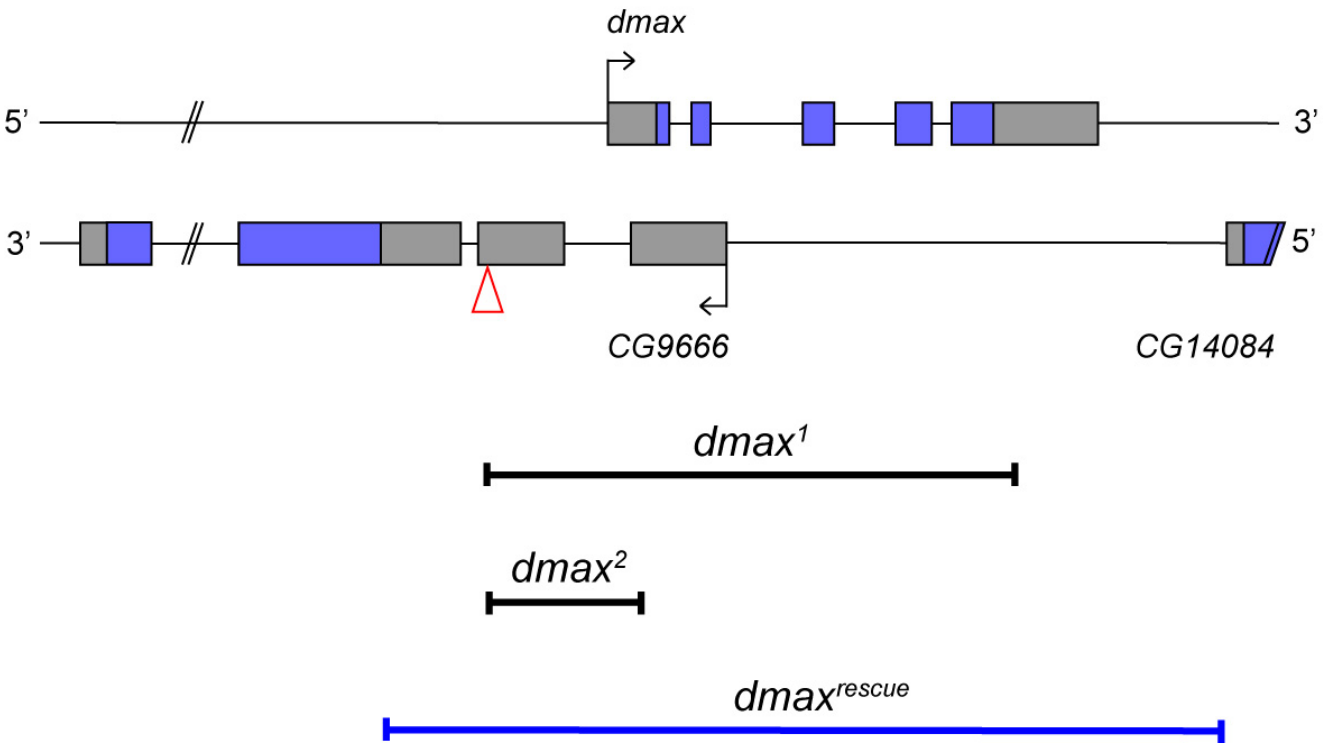

Figure 27
dmax genomic rescue construct. The blue line corresponds to the 2.8 kb fragment that was used to rescue the *dmax*^{1} mutant flies. The cloned sequence starts directly upstream (relative to *CG9666*) of the start of the coding sequence of *CG9666* and ends directly downstream (relative to *CG14084*) of the end of the transcript of *CG14084*, the 3' neighbor of *dmax*. Only the end of *CG14084* is depicted.

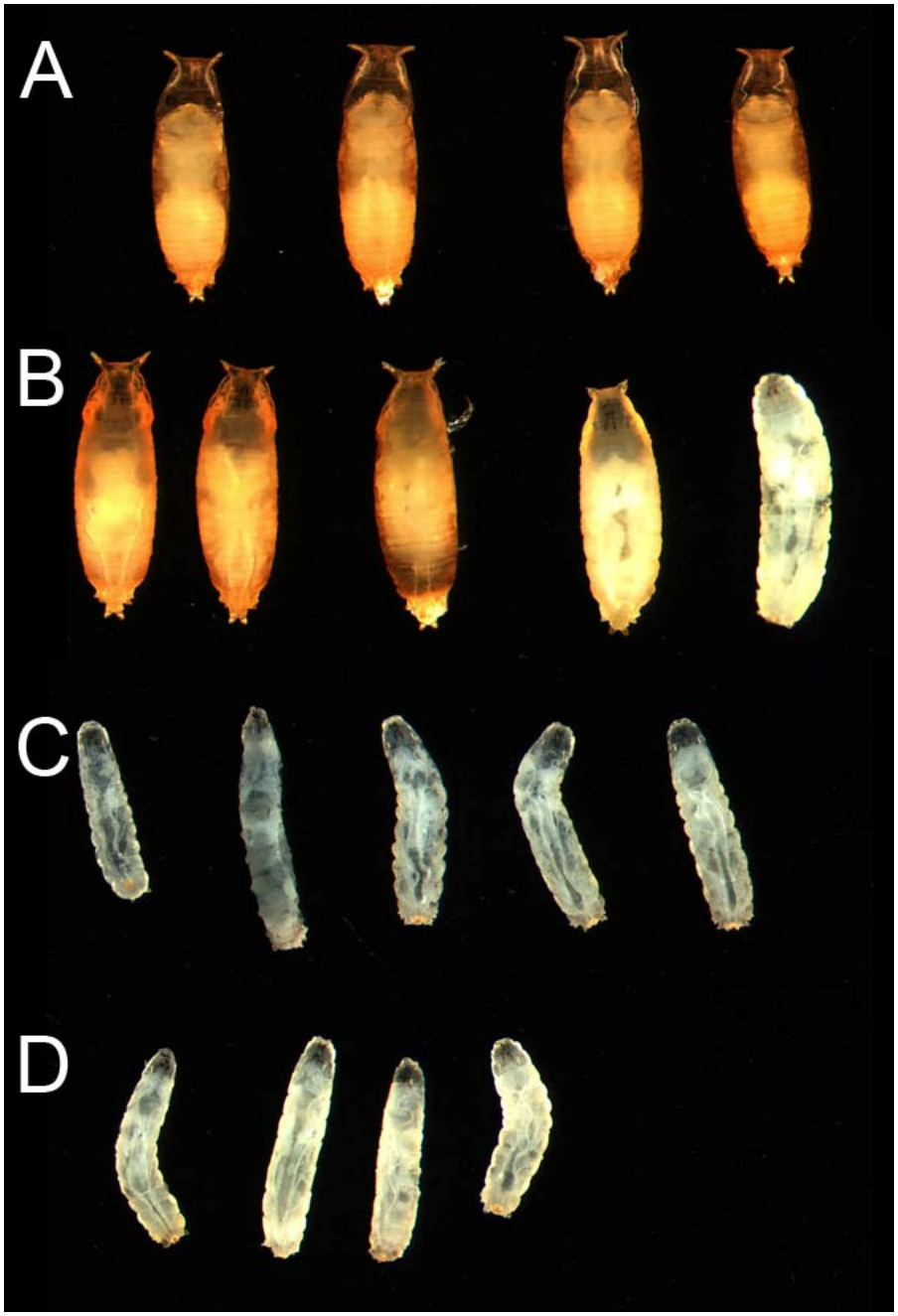

Figure 28a
The presence of one or two copies *dmax*^{rescue} fully rescues the growth and developmental delay phenotype of *dmax*^{1} animals. In addition, the picture shows that male and female *dmax*^{1} do, if at all, only marginally differ in growth. The animals shown in the picture have an age of 120 h.

Label:	Genotypes:
A	*y w dmax*^{rescue}*; dmax*^{1}
B	*y w*
C	♀ *w; dmax*^{1}
D	♂ *w; dmax*^{1}

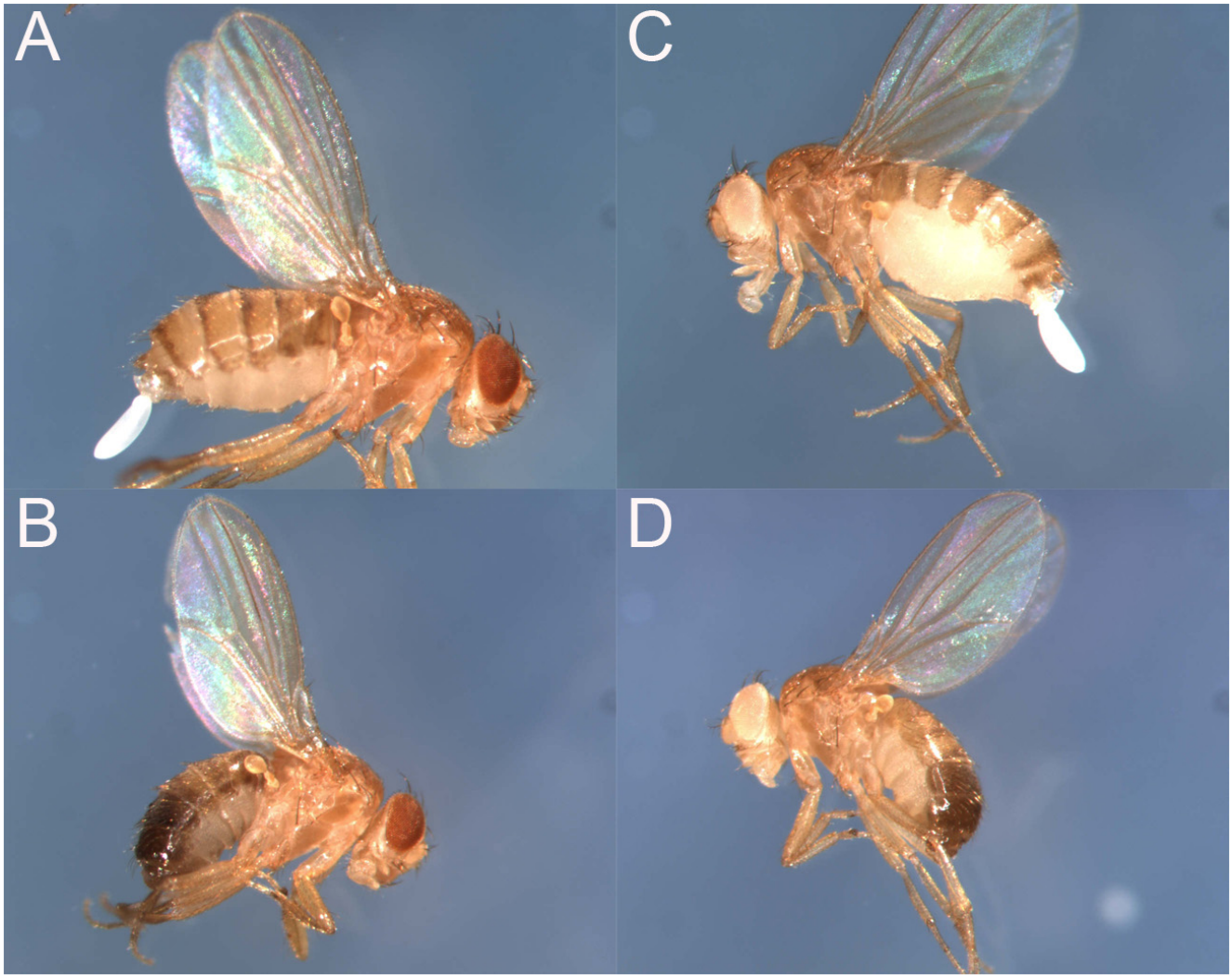

Figure 28b
dmax^{1} flies are rescued to adulthood and full fertility by *dmax*^{rescue}.

Label:	Genotypes:
A	♀ *y w dmax*^{rescue}*; dmax*^{1}
B	♂ *y w dmax*^{rescue}*; dmax*^{1}
C	♀ *y w*
D	♂ *y w*

Figure 29
Crosses documenting the rescue of viability and fertility of *dmax*^{1} animals. Numbers of offspring are indicated. The *dmax*^{1} parents in cross 2 and cross 3 originated from cross 1. For cross 2, two crosses with single virgin females were performed. The numbers of offspring from both crosses are indicated.

Rescue of *dmax*^{1} animals by the presence of one or two copies of *dmax*^{rescue}:

Cross 1: 5 ♂ *y w dmax*^{rescue}*/Y; dmax*^{1}*/MKRS* x 3 ♀ *y w dmax*^{rescue} */FM7; dmax*^{1}*/MKRS*

Offspring			
	♀	*y w dmax*^{rescue}*/y w dmax*^{rescue}*; dmax*^{1}*/dmax*^{1}	22
	♂	*y w dmax*^{rescue}*/Y; dmax*^{1}*/dmax*^{1}	22
	♀	*y w dmax*^{rescue}*/FM7; dmax*^{1}*/dmax*^{1}	16
	♂	*FM7/Y; dmax*^{1}*/dmax*^{1}	0
	♀	*y w dmax*^{rescue}*/y w dmax*^{rescue}*; dmax*^{1}*/MKRS*	42
	♂	*y w dmax*^{rescue}*/Y; dmax*^{1}*/MKRS*	65
	♀	*y w dmax*^{rescue}*/FM7; dmax*^{1}*/MKRS*	23
	♂	*FM7/Y; dmax*^{1}*/MKRS*	17

Rescued females (cross 1 offspring) were homozygous for *dmax*^{1} and they are fertile:

Cross 2: 1 ♀ *y w dmax*^{rescue}*/FM7; dmax*^{1}*/dmax*^{1} x 3 ♂ *y w/Y; dmax0/TM3* (2 crosses)

Offspring:				
	♀	*y w dmax*^{rescue}*/y w; dmax*^{1}*/dmax*^{1}	34	16
	♂	*y w dmax*^{rescue}*/Y; dmax*^{1}*/dmax*^{1}	31	20
	♀	*y w dmax*^{rescue}*/y w; dmax*^{1}*/TM3*	36	12
	♂	*y w dmax*^{rescue}*/Y; dmax*^{1}*/TM3*	18	14
	♀	*y w FM7/y w; dmax*^{1}*/dmax*^{1}	0	0
	♂	*y w FM7/Y; dmax*^{1}*/dmax*^{1}	0	0
	♀	*y w FM7/y w; dmax*^{1}*/TM3*	22	14
	♂	*y w FM7/Y; dmax*^{1}*/TM3*	20	13

Rescued males (cross 1 offspring) were homozygous for *dmax*^{1} and they are fertile:

Cross 3: 2 ♂ *y w dmax*^{rescue}*/Y; dmax*^{1}*/dmax*^{1} x 4 ♀ *w; Df(3L)fz2/TM6C*

Offspring:			
	♂	*w/Y; dmax*^{1}*/Df(3L)fz2*	0
	♂	*w/Y; dmax*^{1}*/TM6C*	56
	♀	*y w dmax*^{rescue}*/w; dmax*^{1}*/Df(3L)fz2*	160
	♀	*y w dmax*^{rescue}*/w; dmax*^{1}*/TM6C*	67

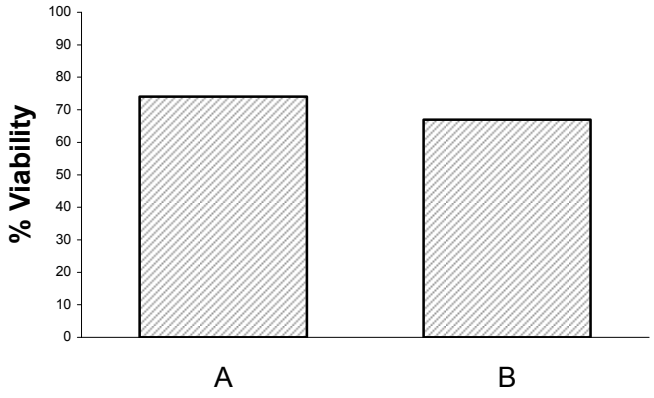

Figure 30a
Survival of *y w dmax*^{rescue}*; dmax*^{1} animals (B) compared to *y w* controls (A). 100 Larvae of each of the respective genotypes were collected at 48 h AED. The chart shows the number of eclosed flies.

Label:	Genotypes:
A	*y w*
B	*y w dmax*^{rescue}*; dmax*^{1}

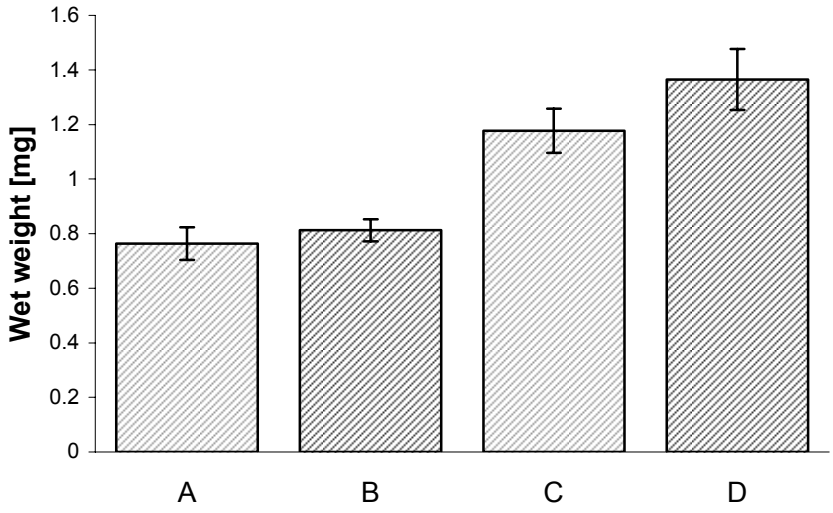

Figure 30b
Wet weight of *y w dmax*^{rescue}*; dmax*^{1} males (B) and females (D) compared to *y w* controls (A, C). The weight of adult flies of an age between 1 and 5 days was determined. The chart shows the average weight and the standard deviation.

Label:	Genotypes:	Number of weighed flies:
A	♂ *y w*	52
B	♂ *y w dmax*^{rescue}*; dmax*^{1}	41
C	♀ *y w*	60
D	♀ *y w dmax*^{rescue}*; dmax*^{1}	38

2.3. Loss of one copy of *dmax* has no effects in wild type flies and only minor effects in dm^{P0} flies

Since we had observed that dm^{P0} males did not survive when *dmax* levels were reduced by *dmax*-RNA*i* (Figure 11), we tested whether the loss of one copy of *dmax* would affect dm^{P0} flies. As a control in these experiments, we used a fly line in which the P element insertion responsible for the dm^{P0} phenotype had been precisely excised: the wild type revertant dm^{P0Rev} line. We examined the survival, the length of development until eclosion and the body weight of hemizygous dm^{P0Rev} (wild type revertant) and dm^{P0} males which were wild type for *dmax* or heterozygous for $dmax^{1}$. Figure 31a shows the length of development until eclosion for the four genotypes. In dm^{P0Rev} males, loss of one copy of *dmax* had no effect on developmental timing. dm^{P0} males showed a developmental delay of 1 day. In this genotype, heterozygosity for *dmax* had a very slight effect: The average eclosion time of dm^{P0} males is delayed by 3.6 h. This extremely small effect is probably only seen due to the large number of flies whose eclosion timing was tracked.

Figure 31b shows that the loss of one copy of *dmax* had no effect on the survival of dm^{P0Rev} or dm^{P0} males. It also shows that dm^{P0} males, even though they are developmentally delayed and clearly smaller than wild type males, survive well.

We examined the wet weight of eclosed flies of all four genotypes (Figure 31c). dm^{P0} males weighed 150 ug less than wild type dm^{P0Rev} males. In both genotypes, heterozygosity for *dmax* had no effect on body weight.

Taken together, these data show that *dmax* is a recessive gene. Furthermore, these data suggest that even in a situation of reduced *dmyc* levels, the loss of one copy of *dmax* is not sufficient to aggravate the growth phenotype caused by reduced *dmyc* levels.

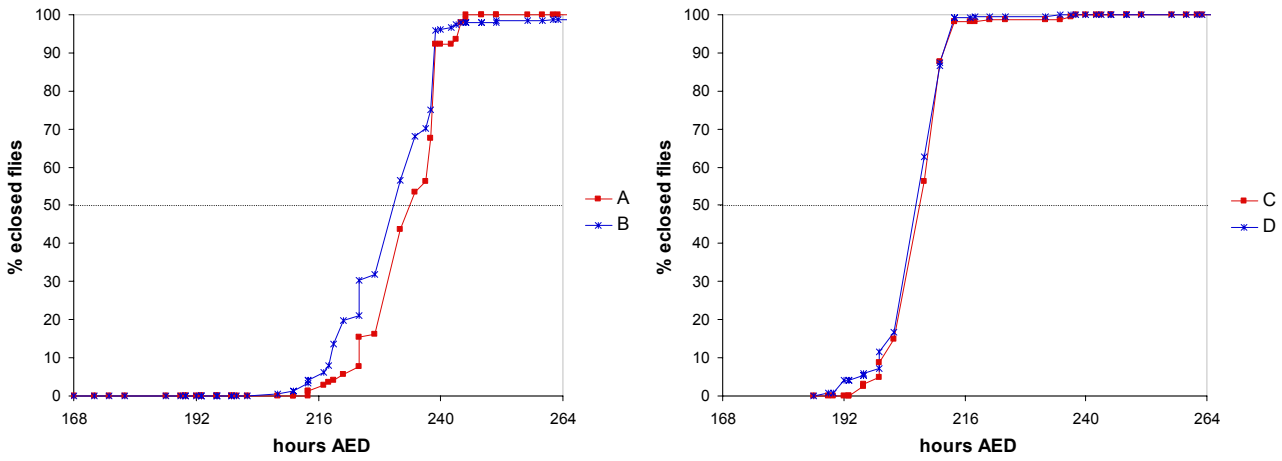

Figure 31a
The loss of one copy of *dmax* in dm^{P0} males leads to a barely detectable developmental delay. The charts show the percentage of eclosed flies at given time points. dm^{P0} animals eclose with a delay of 1 day compared to the dm^{P0Rev} wild type revertants. Number of eclosed flies: A: 142, B: 241, C: 162, D: 223.

Label:	Genotypes:	Median eclosion time [hours/days AED]:
A	*w* dm^{P0}/Y; $dmax^{1}/+$	234.1/9.76
B	*w* dm^{P0}/Y	231.5/9.65
C	*w* dm^{P0Rev}/Y; $dmax^{1}/+$	208.8/8.70
D	*w* dm^{P0Rev}/Y	207.9/8.66

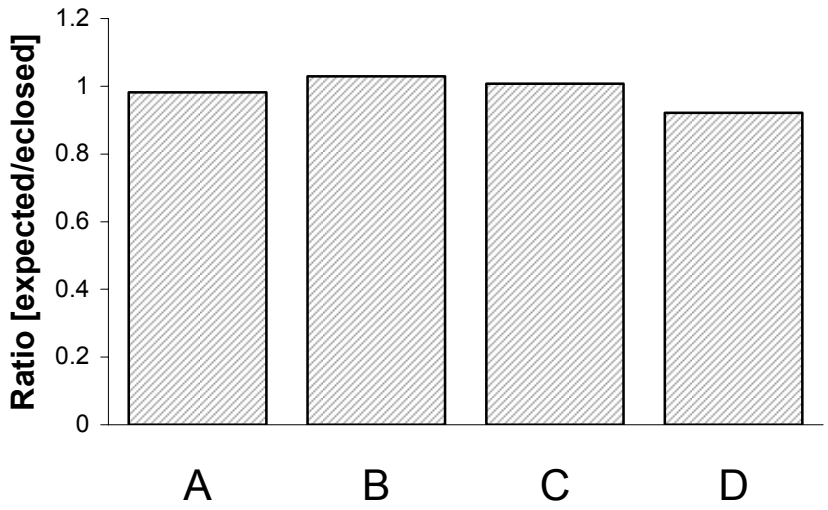

Figure 31b
Survival to adulthood is excellent in all of the tested genotypes: The total number of pupae in the four test crosses was counted. Based on mendelian inheritance, the expected offspring number of the genotypes A - D was calculated and compared to the total number of eclosed flies of the genotypes A-D. The ratio of expected offspring to counted eclosed flies is very close to 1 for all four genotypes. Total number of counted pupae/expected offspring number/counted eclosed flies: A: 1157/145/142, B: 937/234/241, C: 643/161/162, D: 484/242/223. The labels correspond to the genotypes in Figure 31a.

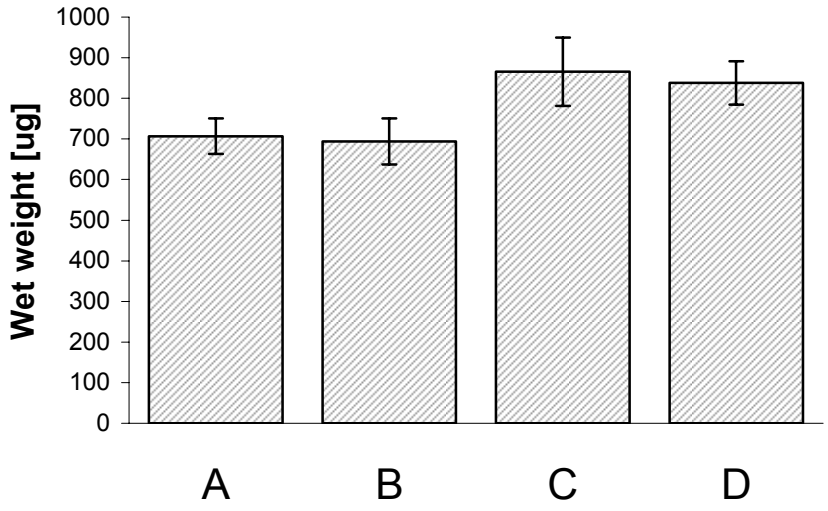

Figure 31c
The loss of one copy of *dmax* does not change the wet weight of dm^{P0} males or of dm^{P0Rev} (wild type revertant) males. For each genotype, 53 flies were weighed. The labels correspond to the genotypes in Figure 31a.

2.4. Comparison of growth and survival in the Max network

There are drastic differences between the *dmyc* and the *dmax* null phenotypes. Figure 32 shows $dmax^{1}$ larvae compared to dm^{A51} larvae at an age of 120 h AED. dm^{A51} is a *dmyc* molecular null allele that was generated by imprecise excision of a P element and that lacks the entire *dmyc* ORF. dm^{A51} animals die as larvae, but they can be rescued to adulthood by expression of a *tub-dmyc* transgene (P. Gallant, unpublished). In contrast to the $dmax^{1}$ larvae that survived well until this time point and do grow, albeit at reduced speed (compare Figures 20, 21), the few dm^{A51} larvae that had survived until 120 h AED displayed an almost complete failure to grow. Due to the fact that *dmyc* null mutants are homozygous lethal and due to *dmyc's* position on the X chromosome, only male dm^{A51} larvae could be collected without employing a rescue construct, whereas the *dmax* larvae were mixed males and females. However, this constitutes no problem for the comparison, since we had shown that $dmax^{1}$ females do not differ in size from $dmax^{1}$ males (Figure 28a).

The difference between the *dmax* null and the *dmyc* null growth phenotypes is highly surprising, if one assumes that all functions of *dmyc* require *dmax*. A *dmax* null mutant should then display as severe growth phenotypes as a *dmyc* null mutant, since *dmyc* would not be functional in the absence of *dmax.* However, if one postulates that dMyc has functions that do not require heterodimerization with dMax, and that these encompass functions that are required in larval growth, the phenotypic differences could be explained.

Since Max is not only required in the heterodimerization with Myc, but also forms heterodimers with Mad/Mnt proteins, an alternative explanation for the observed difference is possible. The mildness of the *dmax* phenotype could be due to the concomitant loss of dMyc/dMax-mediated activating and dMnt/dMax-mediated repressing functions. In the *dmyc* mutant, the formation of repressive dMnt/dMax heterodimers would still be possible (or even be enhanced), giving rise to the more severe growth phenotype. Along these lines, one could postulate the existence of an unknown *dmax*-dependent negative growth regulator besides *dmnt.* As the following experiments show, it was possible to discriminate between these possibilities by examining the effects of different mutant combinations of the Max network components on growth and survival.

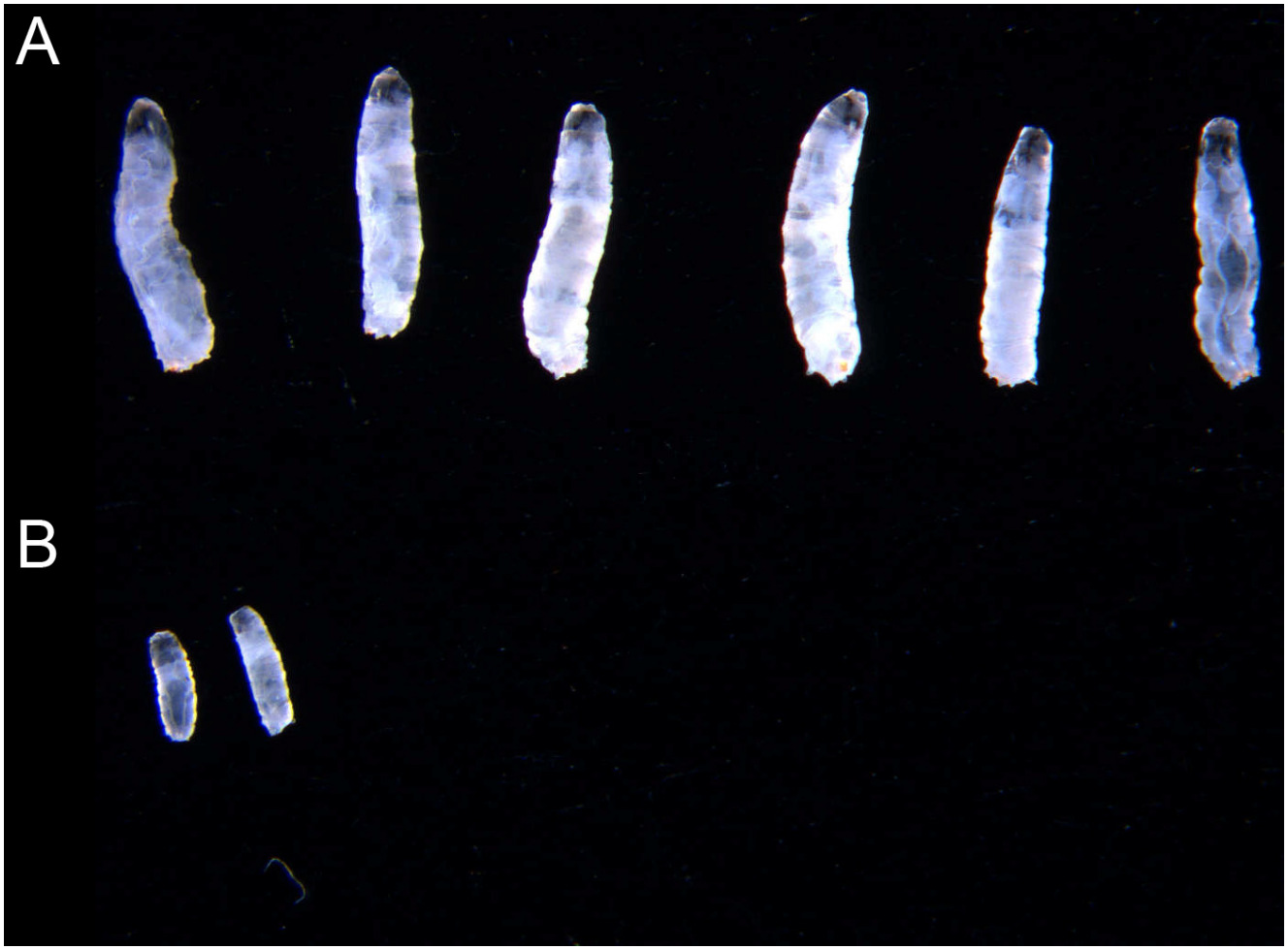

Figure 32
Comparison of *dmax* null larvae and *dmyc* null larvae (5 d AED), revealing a striking difference in the growth phenotype.

Label:	Genotypes:
A	*w; dmax*^{1}
B	*y w dm*^{A51}*/Y*

We included another mutant allele of *dmyc* in our comparisons: dm^2, an allele that had been described to behave genetically as a null allele (Maines et al., 2004), at a time when no molecular null alleles of *dmyc* had been available. The dm^2 mutation is a nonsense mutation that leads to a truncation of the dMyc protein at AA 675, immediately upstream of the leucine zipper motif, but is reported to express normal levels of the truncated protein. Since the leucine zipper motif is necessary for heterodimerization with Max in vertebrates (Blackwood and Eisenman, 1991; Amati et al., 1993a), it is assumed that the mutant form of dMyc which is encoded by the dm^2 allele is not able to bind to dMax anymore. We reasoned that dm^2 should display a less severe phenotype than the molecular null allele dm^{A51}, if it were true that *dmyc* has *dmax*-independent functions (provided that these functions would also not require the leucine zipper). Figure 33 shows a comparison of the survival of $dmax^1$, dm^2 and dm^{A51} larvae from 24 h AED to 48, 72 and 96 h AED. Clearly, dm^2 larvae survived better than dm^{A51} larvae, but much more poorly than $dmax^1$ larvae. The size of dm^2 larvae is also intermediate (Figure 34a). These data suggest that dm^2 is indeed not a null allele, and since the truncated form of dMyc encoded by dm^2 is not able to bind to dMax, the better survival of dm^2 larvae also suggests that there are functions of *dmyc* which are independent of *dmax*. However, the phenotype of dm^2 is clearly not equivalent to $dmax^1$. We next tested indirectly, whether *dmnt* might contribute to the severity of the dm^2 and dm^{A51} phenotypes.

We argued that dm^{A51} $dmax^1$ or dm^2 $dmax^1$ double mutants should display a less severe growth phenotype and should survive better than dm^{A51} or dm^2 single mutants, if it were true that repressive functions of dMnt/dMax heterodimers contributed to the severity of the dm^{A51} and dm^2 phenotypes. As Figure 34 shows, this was indeed the case. By examining the size of the larvae at 120 h AED and their survival at 96 h AED and 120 h AED, we found a rescue both in size and survival for both dm^{A51} $dmax^1$ and dm^2 $dmax^1$ double mutant larvae. The dm^2 $dmax^1$ double mutants were clearly bigger than the dm^{A51} $dmax^1$ double mutants, but still smaller than $dmax^1$ mutants. Taken together, these findings showed that two factors contribute to the striking difference in the growth phenotypes of *dmyc* and *dmax* null mutants: On one hand, there is a contribution of a negative growth regulator that depends on *dmax* (presumably *dmnt*). On the other hand, there must be *dmax*-independent functions of *dmyc*.

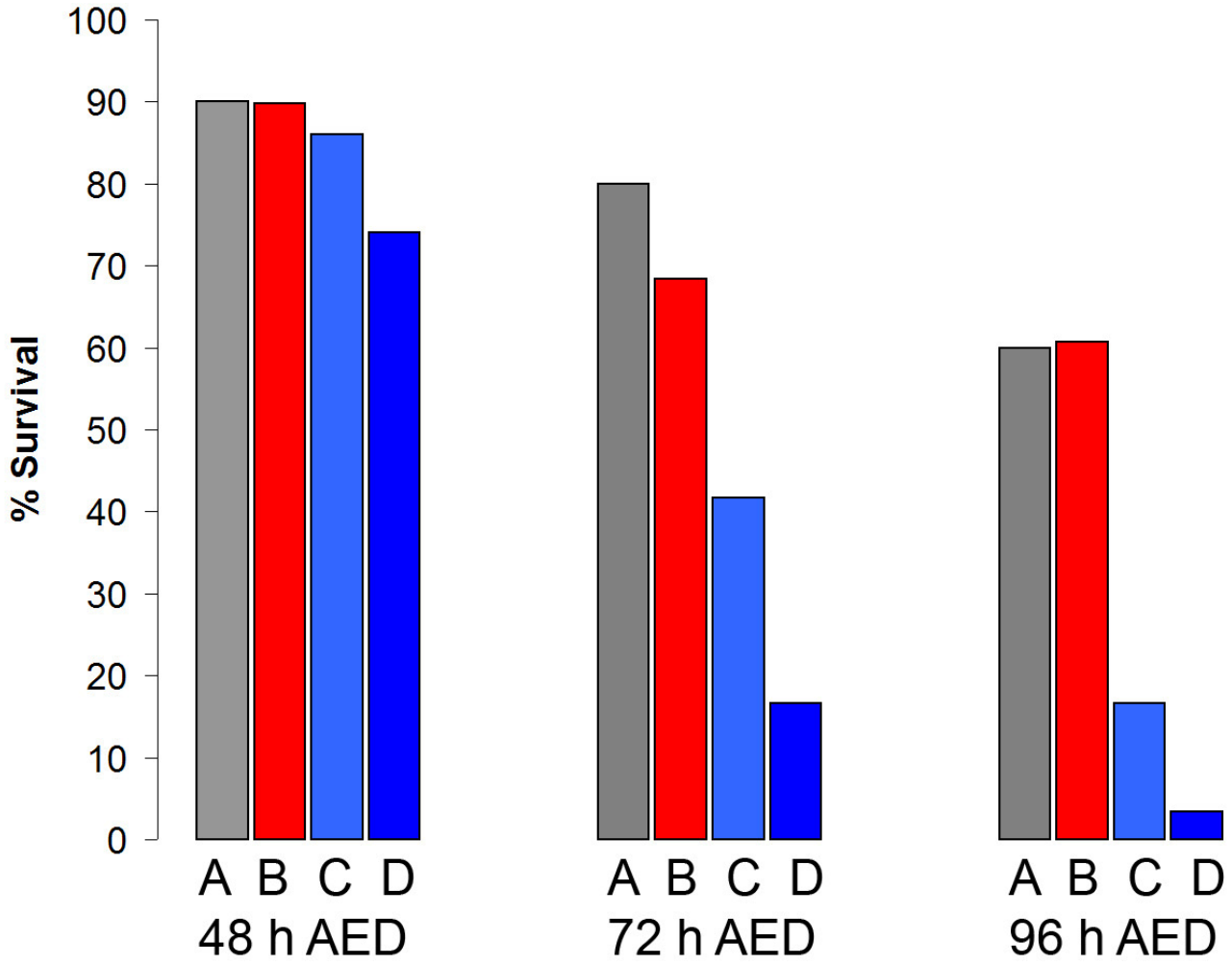

Figure 33
Comparison of the survival of *dmax*^{1} heterozygote larvae (A), *dmax*^{1} larvae (B), *dm*^{2} (C) and *dm*^{A51} (D) larvae at 48 h AED, 72 h AED and 96 h AED. The larvae were collected at 24 h AED. The chart depicts the relative survival of the larvae until the given time points. Number of collected larvae: 48 h AED: 50 each, 72 h AED: 60 each, 96 h AED: 50 (A), 28 (B), 36 (C), 29 (D).

Label:	Genotypes:
A	*w; dmax*^{1}*/TM3, Ser GFP*
B	*w; dmax*^{1}
C	*y w dm*^{2}*/Y*
D	*y w dm*^{A51}*/Y*^{1}

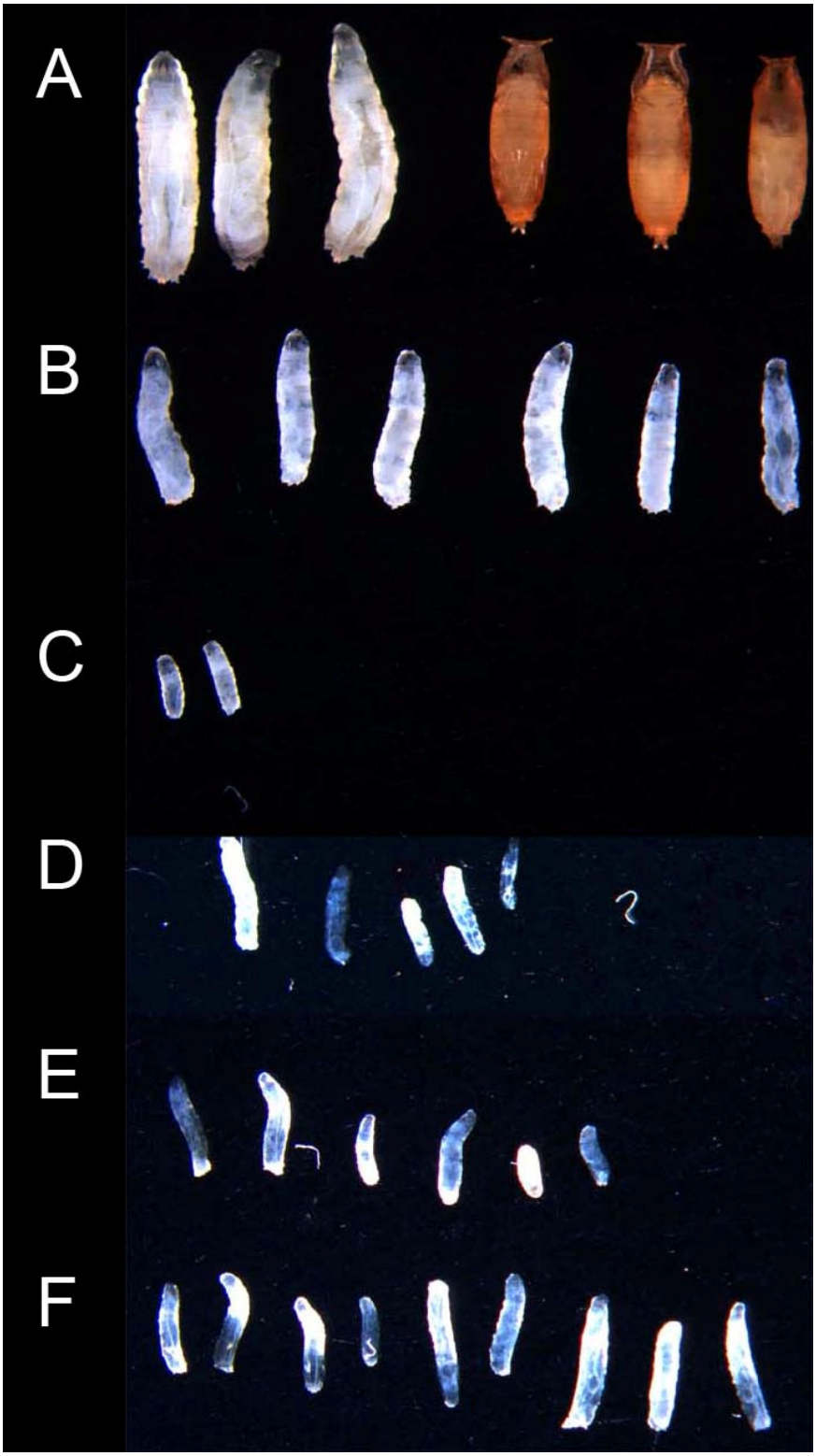

Figure 34a
Loss of *dmax*^{1} in *dm*^{A51} and in *dm*^{2} larvae leads to a partial rescue of the growth phenotype, but the double mutant larvae are still smaller than *dmax*^{1} larvae. The larvae were photographed at 120 h AED.

Label:	Genotypes:	Label:	Genotypes:
A	*w; dmax*^{1}*/TM3, Ser GFP*	D	*y w dm*^{A51}*/Y; dmax*^{1}
B	*w; dmax*^{1}	E	*y w dm*^{2}*/Y*
C	*y w dm*^{A51}*/Y*	F	*y w dm*^{2}*/Y; dmax*^{1}

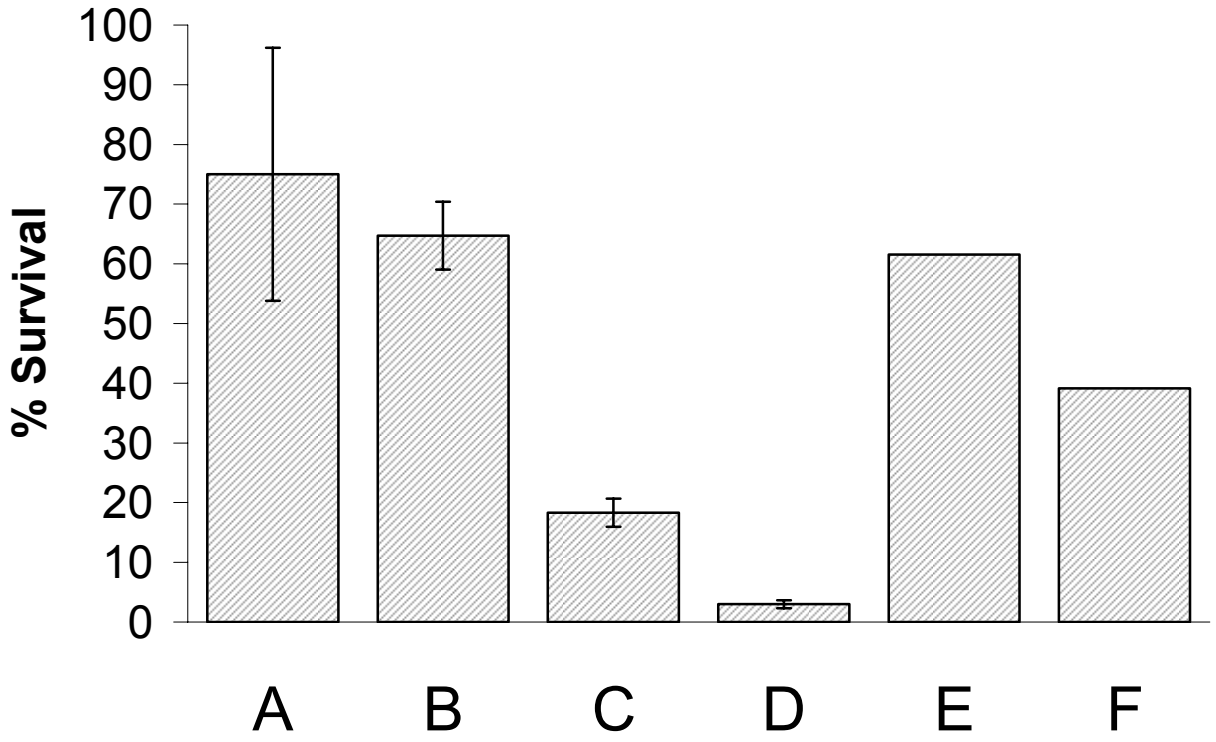

Figure 34b
Survival of the mutant combinations depicted in Figure 34a, at 96 h AED. Larvae of the indicated genotypes were collected at 24 h AED. For the genotypes A - D, two experiments were performed, for E and F, one experiment was performed. The error bars indicate the standard deviations. Total numbers of collected larvae: A: 80, B: 44, C: 76, D: 69, E: 13, F: 23.

Label:	Genotypes:
A	*w; dmax^{1}/TM3, Ser GFP*
B	*w; dmax^{1}*
C	*y w dm^{2}/Y*
D	*y w dm^{A51}/Y*
E	*y w dm^{2}/Y; dmax^{1}*
F	*y w dm^{A51}/Y; dmax^{1}*

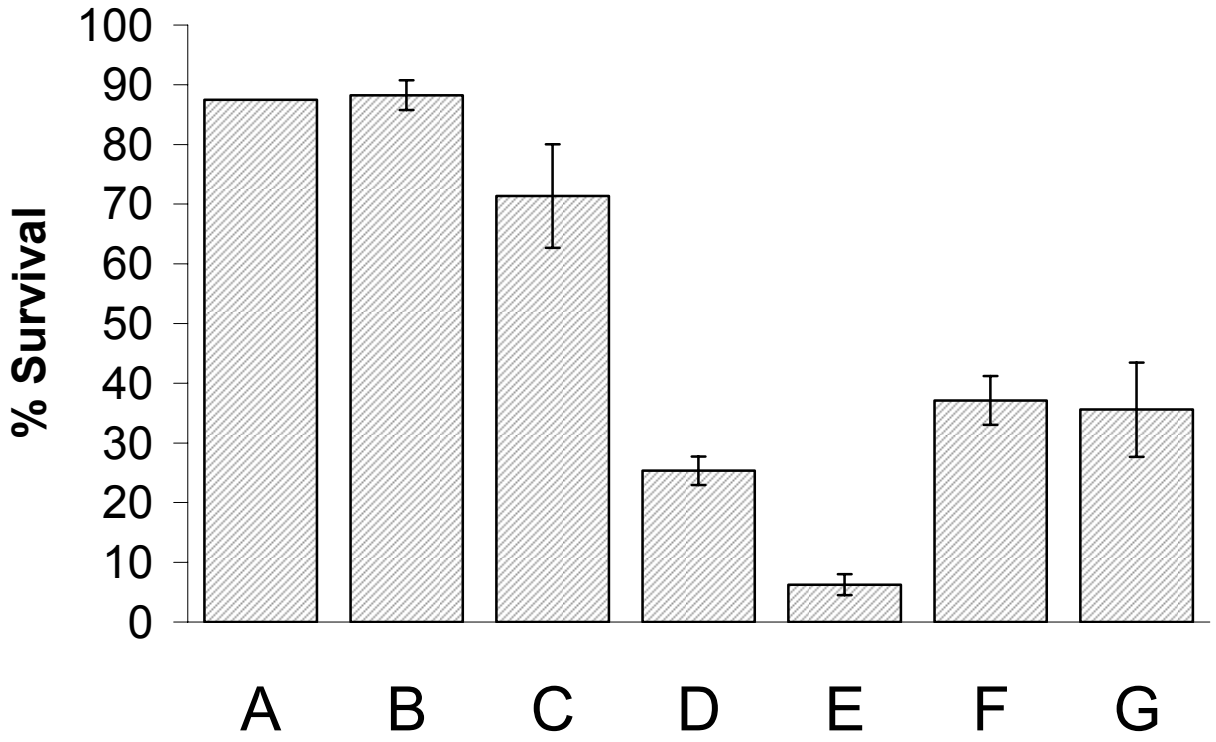

Figure 34c
Survival of the mutant combinations depicted in Figure 34a, at 120 h AED. Larvae of the indicated genotypes were collected at 24 h AED. For the genotypes B - G, error bars indicate the standard deviation of two experiments. For A, only one experiment was performed. Total numbers of collected larvae: A: 40, B: 77, C: 63, D: 75 , E: 80 , F: 68, G: 37.

Label:	Genotypes:
A	*y w*
B	*w; dmax^{1}/TM3, Ser GFP*
C	*w; dmax^{1}*
D	*y w dm^{2}/Y*
E	*y w dm^{A51}/Y*
F	*y w dm^{2}/Y; dmax^{1}*
G	*y w dm^{A51}/Y; dmax^{1}*

In order to confirm and augment these findings, we next made use of the *dmyc* molecular null allele dm^4 (Pierce et al., 2004), the *dmnt* molecular null alleles $dmnt^1$ and $dmnt^2$ (Loo et al., 2005) and of a dm^4 $dmnt^1$ double mutant (unpublished, kindly provided by S. Pierce and R. Eisenman before publication). Using the dm^4 $dmnt^1$ double mutant, it was possible to generate a dm^4 $dmnt^1$ $dmax^1$ triple mutant. We compared the size and the survival of different mutant combinations at 120 h AED, displayed in Figure 35. dm^4 larvae (Figure 35 F) behaved as dm^{A51} larvae, showing a very severe growth phenotype and extremely poor survival. The dm^4 $dmnt^1$ double mutants (Figure 35 C) displayed a clearly milder phenotype, being intermediate between dm^4 and $dmax^1$ larvae (Figure 35 B) both in size and survival. dm^4 $dmax^1$ double mutant larvae (Figure 35 E) and dm^4 $dmnt^1$ $dmax^1$ triple mutant larvae (Figure 35 D) were similar to the dm^4 $dmnt^1$ larvae, albeit both showed slightly smaller sizes and slightly poorer survival. The comparison of the dm^4 and dm^4 $dmnt^1$ mutants proves that *dmnt* is acting as a negative growth regulator, aggravating the effects of a loss of *dmyc*. The clear difference in size and survival between the dm^4 $dmnt^1$ double mutants and the $dmax^1$ mutants again provides evidence for *dmax*-independent functions of *dmyc*, since the dm^4 $dmnt^1$ double mutants should be equivalent to $dmax^1$ mutants if one assumes that all the functions of *dmyc* do require *dmax*. The fact that the dm^4 $dmnt^1$ $dmax^1$ triple mutants do not show better growth and survival compared to the dm^4 $dmnt^1$ double mutant excludes the hypothesis that there is an unknown negative growth regulator besides *dmnt* which requires *dmax* and contributes to the comparative mildness of the $dmax^1$ phenotype. The slightly smaller sizes and poorer survival of the dm^4 $dmax^1$ and dm^4 $dmnt^1$ $dmax^1$ mutants compared to dm^4 $dmnt^1$ might rather be an indication that *dmax* has positive functions independent of *dmyc* and *dmnt.*

At 192 h AED, dm^4 $dmnt^1$ mutant larvae were clearly smaller than $dmax^1$ larvae. Whereas the $dmax^1$ larvae showed no decrease in survival in the period between 120 h and 192 h AED, the survival of the dm^4 $dmnt^1$ larvae dropped from 50% at 120 h AED to 20% at 192 h AED. The fact that the phenotypic differences between the dm^4 $dmnt^1$ and the $dmax^1$ mutant phenotype stays as large at the later time point (regarding size) or even grows larger (regarding survival), taken together with the lack of detectable *dmax* mRNA at 120 h AED, provides strong evidence that the observed differences are not due to maternal contribution of *dmax* mRNA or *dmax* protein, but rather a consequence of the existence of *dmax*-independent functions of *dmyc.*

We also generated $dmnt^1$ $dmax^1$ and $dmnt^2$ $dmax^1$ double mutants and compared their size and survival with dm^4 $dmnt^1$ and $dmax^1$ mutants, at 192 h AED ($dmnt^1$ being a null mutant, whereas $dmnt^2$ does potentially only express the natural *dmnt* splice variant which does not contain the Sin3-interaction domain). Whereas the sizes of the $dmnt^1$ $dmax^1$ and $dmnt^2$ $dmax^1$ double mutants did not differ from $dmax^1$ mutants, the survival of the $dmnt^1$ $dmax^1$ double mutant was moderately reduced, much less so the survival of the $dmnt^2$ $dmax^1$ double mutant (Figure 36). The fact that the loss of *dmnt* has no

impact on the growth of *dmax*^{1} larvae is compatible with a model in which *dmnt* as a negative growth regulator requires *dmax* function.

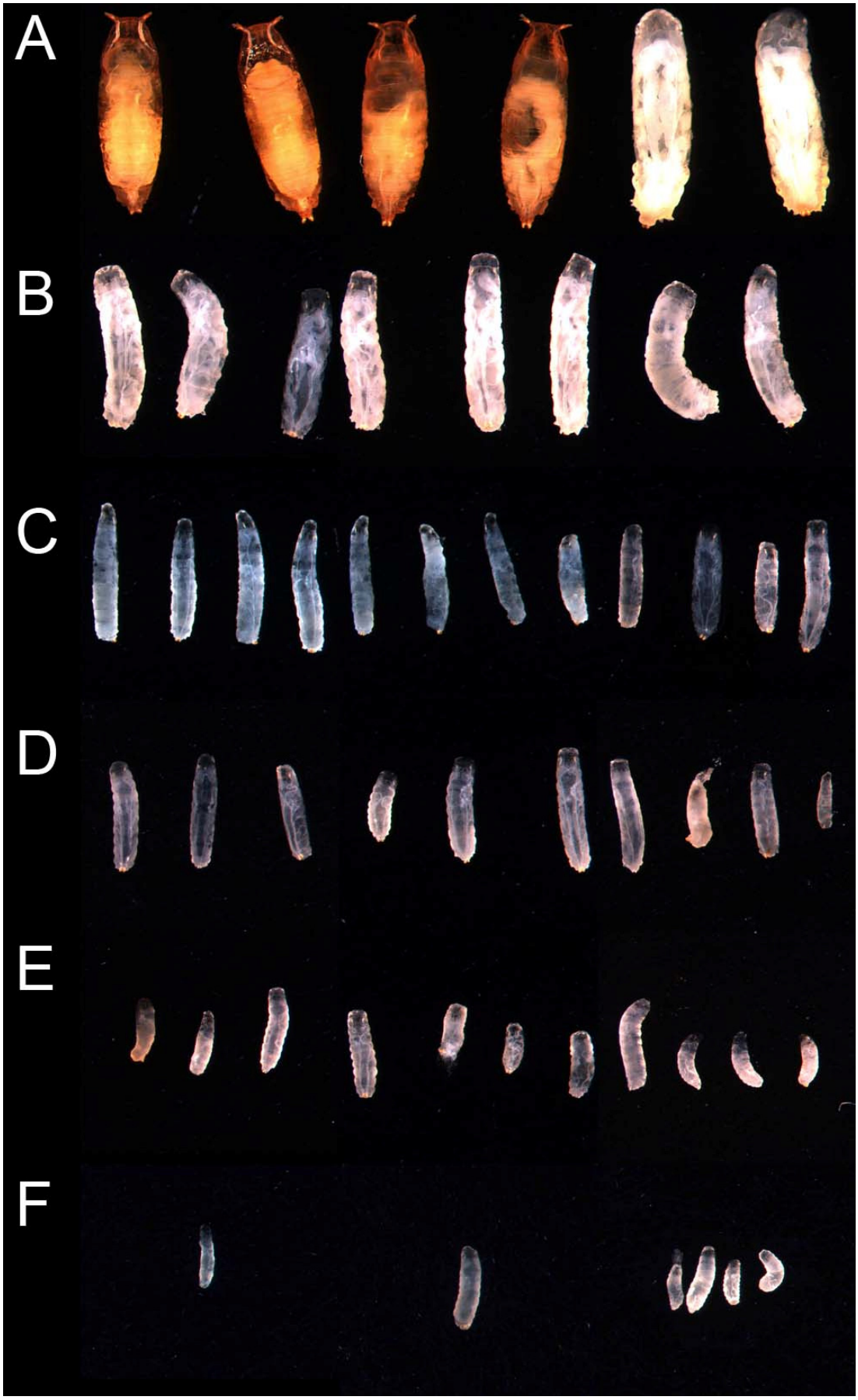

Figure 35a
Comparison of the mutant combinations of the Max network. The larvae were photographed at 120 h AED.

Figure 35a (continued)

Label:	Genotypes:	Label:	Genotypes:
A	*wt [OreR]*	D	*w dm^4 dmnt^1/Y; dmax^1*
B	*w; dmax^1*	E	*w dm^4/Y; dmax^1*
C	*w dm^4 dmnt^1/Y*	F	*w dm^4/Y*

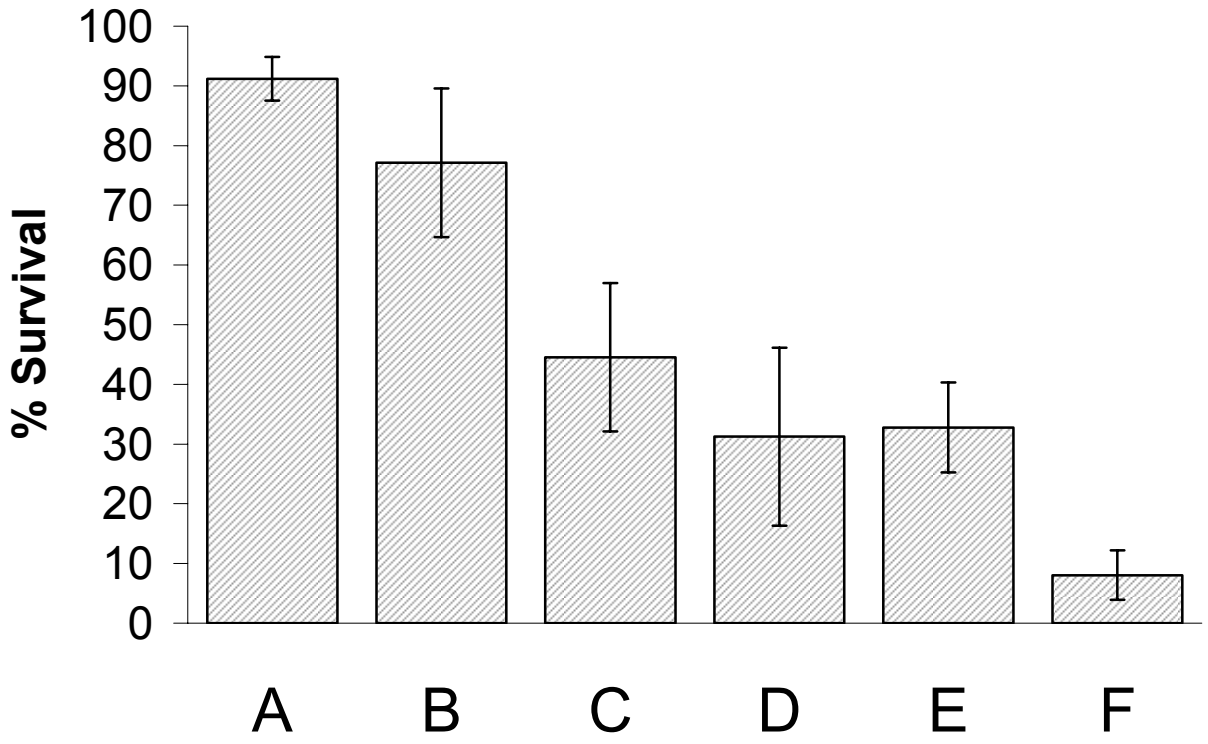

Figure 35b
Survival of the mutant combinations depicted in Figure 35a, at 120 h AED. Larvae of the indicated genotypes were collected at 48 h AED. Error bars indicate standard deviations from independent experiments (A: 6, B: 3, C: 6, D: 3, E: 3, F: 5 experiments). Total number of collected larvae: A: 209, B: 71, C: 236, D: 45, E: 38, F: 147.

Label:	Genotypes:
A	*wt [OreR]*
B	*w; dmax^1*
C	*w dm^4 dmnt^1/Y*
D	*w dm^4 dmnt^1/Y; dmax^1*
E	*w dm^4/Y; dmax^1*
F	*w dm^4/Y*

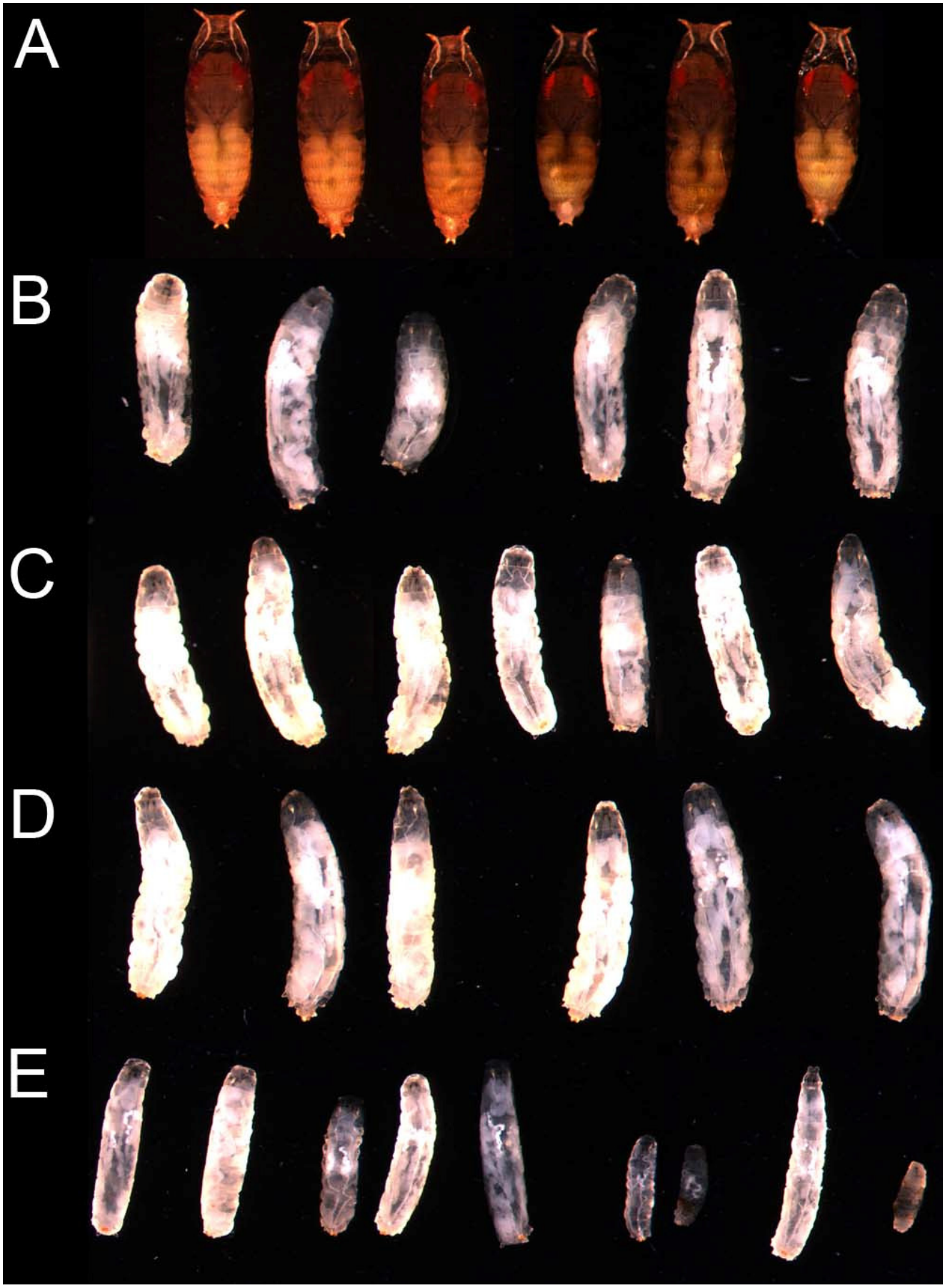

Figure 36a
dmax null larvae do not differ in their growth phenotype from *dmax dmnt* double mutant larvae. The larvae were photographed at 192 h AED.

Figure 36a (continued)

Label:	Genotypes:	Label:	Genotypes:
A	*wt [OreR]*	D	*w dmnt^{2}; dmax^{1}*
B	*w dmnt^{Rev}; dmax^{1}*	E	*w dm^{4} dmnt^{1}/Y; dmax^{1}*
C	*w dmnt^{1}; dmax^{1}*		

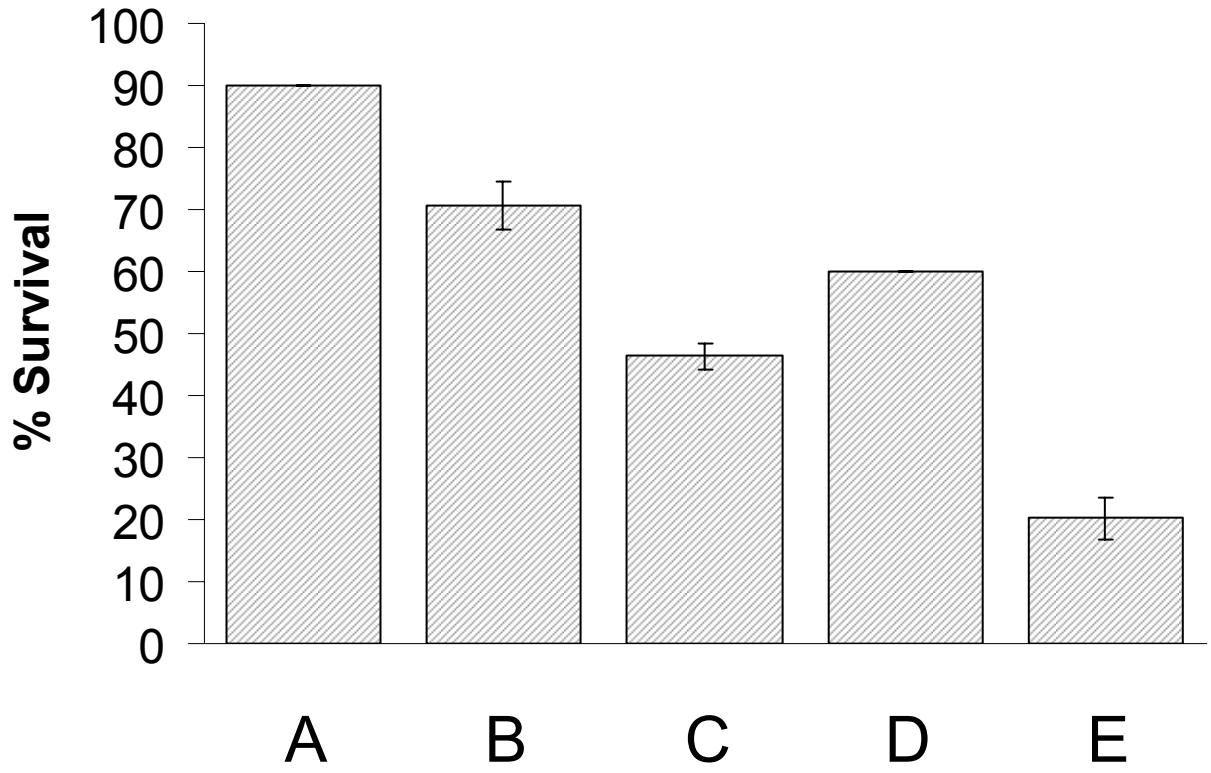

Figure 36b
Survival of the mutant combinations depicted in Figure 36a, at 192 h AED. Larvae of the indicated genotypes were collected at 48 h AED. Error bars indicate standard deviations from two independent experiments. Total number of collected larvae: A: 60, B: 55, C: 52, D: 60, E: 68.

Label:	Genotypes:
A	*wt [OreR]*
B	*w [71NN]; dmax^{1}*
C	*w dmnt^{1}; dmax^{1}*
D	*w dmnt^{2}; dmax^{1}*
E	*w dm^{4} dmnt^{1}/Y; dmax^{1}*

The difference in the severity of the growth phenotypes between *dm*^{4} *dmnt*^{1} larvae and *dmax*^{1} larvae does not only cause different total larval sizes at given time points AED, but is also seen in the sizes of polyploid organs and in total RNA content.

Figure 37a shows larval fat bodies stained with Hoechst dye of *dm*^{4} *dmnt*^{1}, *dmax*^{1} at an age of 120 h or 192 h AED, compared to *y w* control fat bodies at an age of 120 h AED. Whereas at 120 h AED, *dmax*^{1} fat bodies were clearly smaller than *y w* fat bodies, they attained a size only slightly smaller than the one of *y w* control tissue at 192 h AED. *dm*^{4} *dmnt*^{1} fat body tissue was much smaller than *dmax*^{1} tissue at 120 h AED, and it showed much less growth in the period from 120 h AED until 192 h AED, being still smaller at 192 h AED than *dmax*^{1} tissue at 120 h AED. Figure 37b shows fat body nuclei of the described genotypes at a higher magnification. We also examined the size of salivary gland tissue (Figure 37c) with very similar results: Whereas *dmax*^{1} salivary gland cell nuclei reached almost wild type sizes at 192 h AED, *dm*^{4} *dmnt*^{1} salivary gland cell nuclei at 192 h AED were still smaller than *dmax*^{1} salivary gland cell nuclei at 120 h AED.

The growth difference between *dm*^{4} *dmnt*^{1} and *dmax*^{1} larvae is also reflected in the total RNA content of the larvae: total RNA content of *dm*^{4} *dmnt*^{1} larvae is strongly decreased in comparison to *dmax*^{1} larvae, both in L1 (at 29-39 h AED, Figure 37d) and at 120 h AED (Figure 37e). At the later time point, the total RNA content roughly correlated to the differences in larval size. Surprisingly, the differences in total RNA content were already equally strong at the early time point, when not much visible growth had occurred.

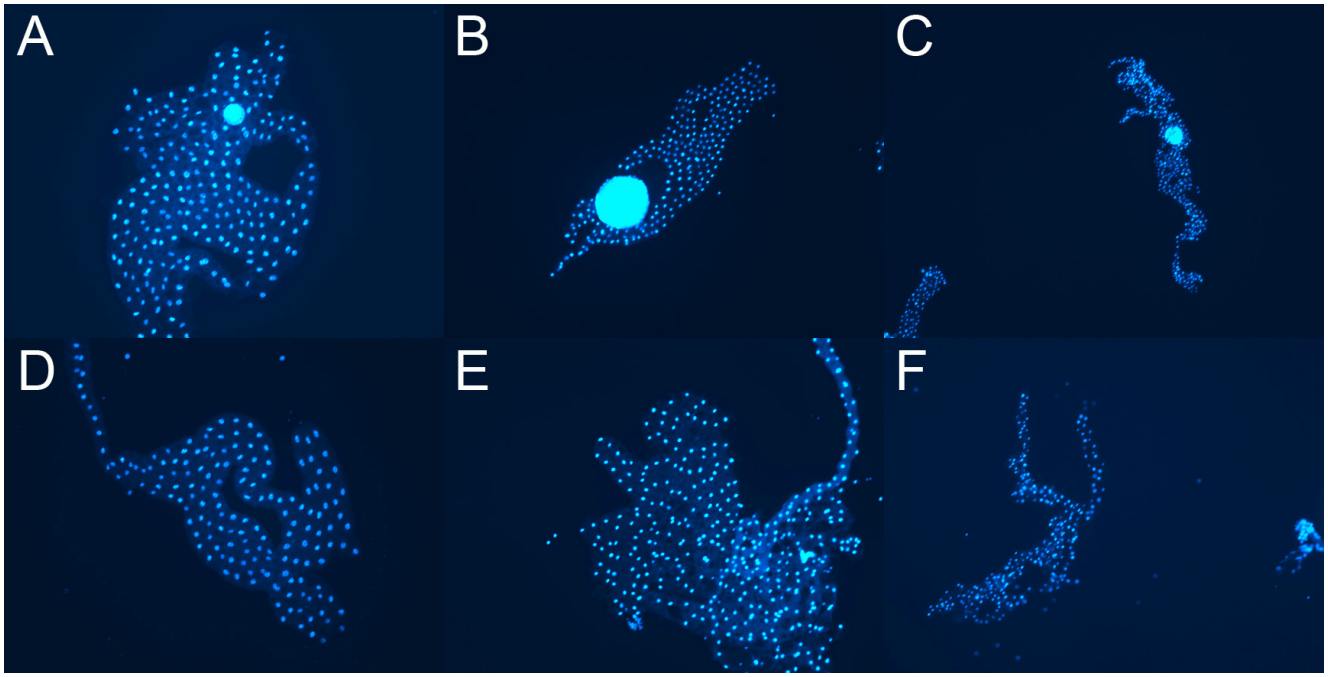

Figure 37a
Size comparison of fat bodies of *y w*, *dmax*^{1} and *dm*^{4} *dmnt*^{1} larvae (magnification: 5x). The fat bodies were stained with Hoechst dye. The circle-shaped organs embedded in the fat body tissue are the gonads (a female gonad in A, a male gonad in B and C).

Label:	Genotypes:	Age:
A	*y w*	120 h AED
B	*w; dmax*^{1}	120 h AED
C	*w dm*^{4} *dmnt*^{1}*/Y*	120 h AED
D	*y w*	120 h AED
E	*w; dmax*^{1}	192 h AED
F	*w dm*^{4} *dmnt*^{1}*/Y*	192 h AED

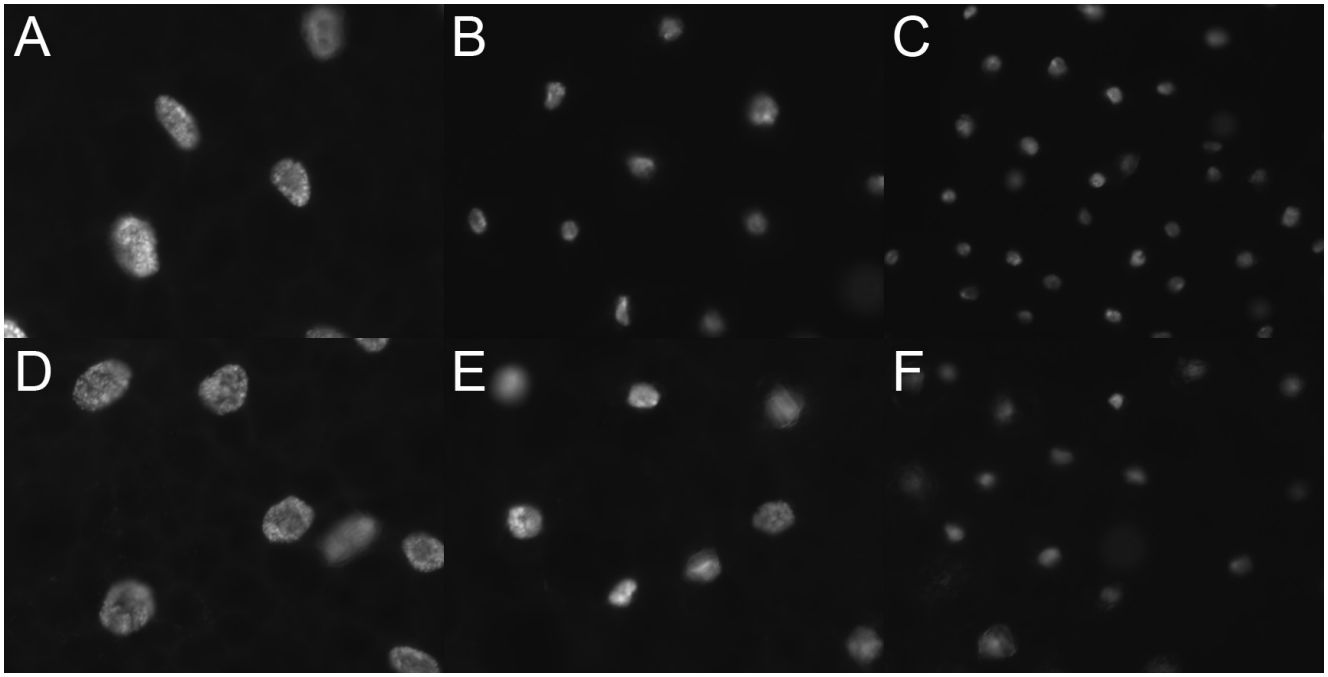

Figure 37b
Hoechst dye-stained fat body nuclei of *y w*, *dmax*^{1} and *dm*^{4} *dmnt*^{1} larvae (magnification: 63x).

Label:	Genotypes:	Age:
A	*y w*	120 h AED
B	*w; dmax*^{1}	120 h AED
C	*w dm*^{4} *dmnt*^{1}*/Y*	120 h AED
D	*y w*	120 h AED
E	*w; dmax*^{1}	192 h AED
F	*w dm*^{4} *dmnt*^{1}*/Y*	192 h AED

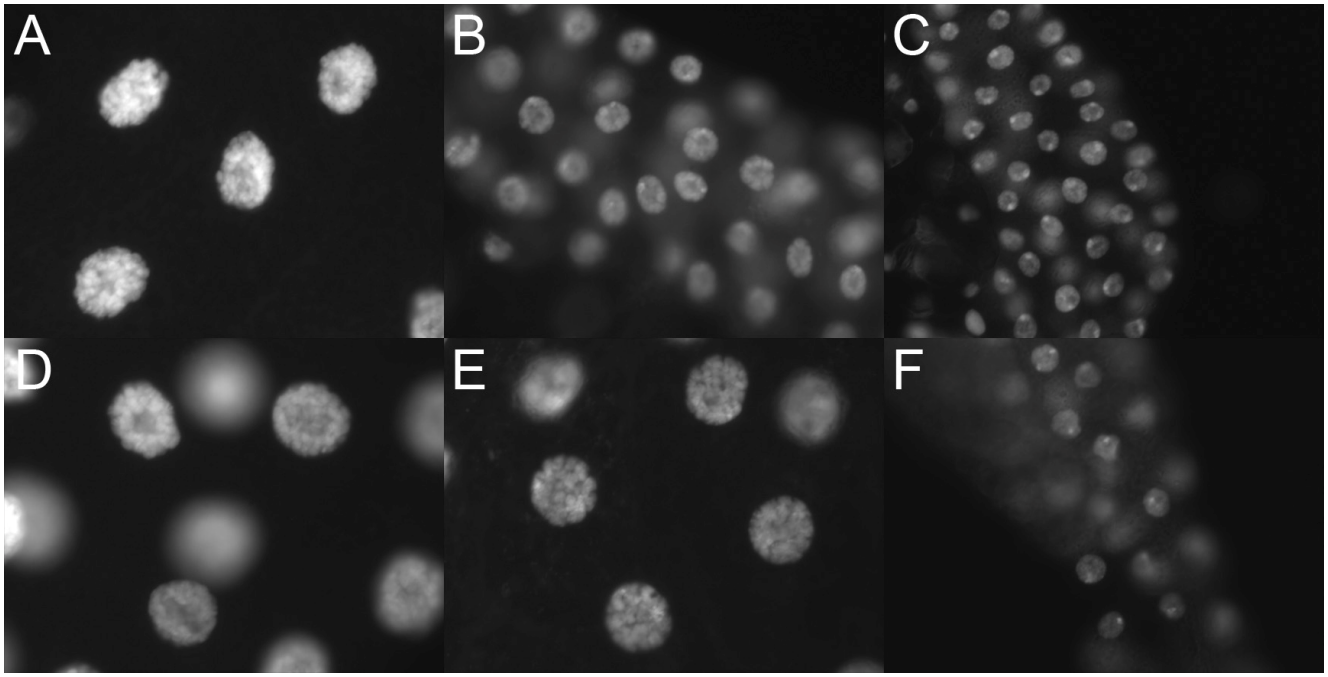

Figure 37c
Hoechst dye-stained salivary gland nuclei of *y w*, *dmax*^{1} and *dm*^{4} *dmnt*^{1} larvae (magnification: 63x).

Label:	Genotypes:	Age:
A	*y w*	120 h AED
B	*w; dmax*^{1}	120 h AED
C	*w dm*^{4} *dmnt*^{1}*/Y*	120 h AED
D	*y w*	120 h AED
E	*w; dmax*^{1}	192 h AED
F	*w dm*^{4} *dmnt*^{1}*/Y*	192 h AED

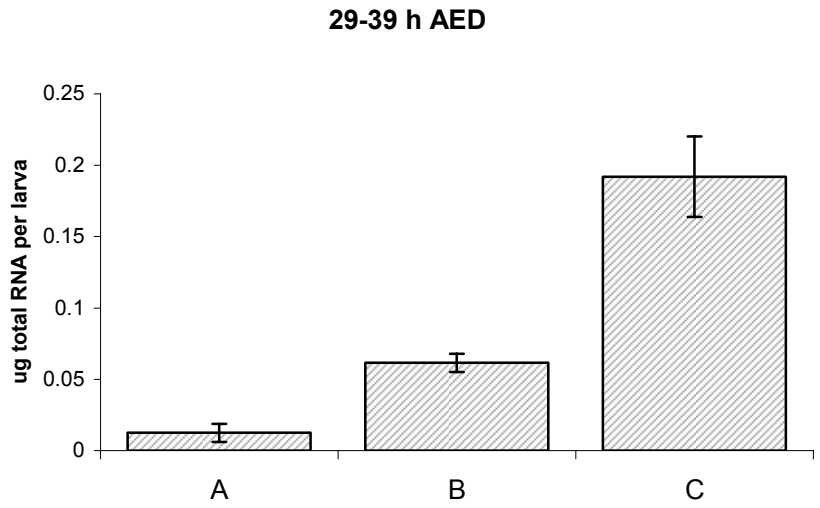

Figure 37d
Comparison of the total RNA levels of *dm*^{4} *dmnt*^{1} larvae, *dmax*^{1} larvae and *y w* larvae at 29-39 h AED. Two RNA extractions from 20 larvae were performed per genotype. The chart shows average total RNA amounts per larva and the standard deviation.

Label:	Genotypes:
A	*w dm*^{4} *dmnt*^{1}*/Y*
B	*w; dmax*^{1}
C	*y w*

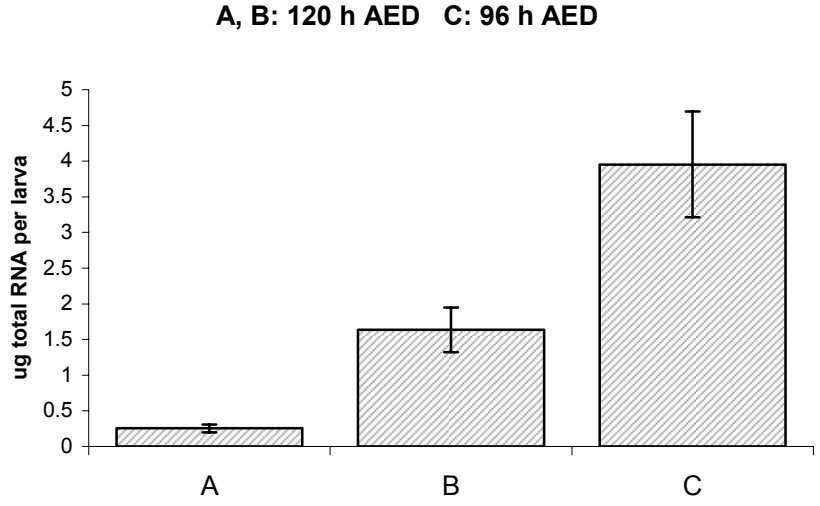

Figure 37e
Total RNA levels of *dm*^{4} *dmnt*^{1} larvae and *dmax*^{1} larvae at 120 h AED, compared to the total RNA levels of *y w* larvae at 96 h AED. A and B show the average total RNA amount per larva from 5 RNA extractions (20 larvae per extraction) each and the standard deviations. C shows the average total RNA amount per larva from 8 RNA extractions (12 larvae per extraction) and the standard deviation.

Label:	Genotypes:
A	*w dm*^{4} *dmnt*^{1}*/Y*
B	*y w/Y, y*$^{+}$*; dmax*^{1}
C	*y w*

2.5. Loss of *mlx* has no effect in *dmax*^{1} larvae

The comparison of the growth phenotypes and of the survival of different null mutant combinations of the Max network members has provided strong evidence that *dmyc* is still partly functional in the absence of *dmax*. We hypothesized that *dmyc* could retain part of its functions, if a protein with similarity to Max existed which would partially complement the loss of Max in *dmax*^{1} mutants. One candidate for such a factor was Mlx (Max-like factor X), a transcription factor with a bHLHzip domain similar to Max which had been shown to form repressive heterodimers with Mad proteins and activating heterodimers with the Myc-like transcription factor Mondo, thereby forming a transcriptional network that functions in parallel to the canonical Myc/Max/Mad transcriptional network (Billin et al., 1999; Billin et al., 2000). Since Mondo/Mlx and Mad/Mlx heterodimers also bind to E-Boxes, it was conceivable that hypothetical Myc/Mlx heterodimers might partially complement the loss of Max protein in *dmax*^{1} mutants. However, such a scenario was unlikely for several reasons: Mlx had been shown to bind poorly to Myc (Billin et al., 1999) and was found to locate primarily to the cytoplasm (Billin et al., 2000). Furthermore, our own finding that *dm*^{2} is still partially functional suggested that the *dmax*-independent functions of *dmyc* do not require binding to another bHLHzip transcription factor.

If Mlx would indeed complement the loss of Max, we could expect that *dmax*^{1} *mlx* double mutants should display a growth phenotype similar to the one of *dm*^{4} *dmnt*^{1} mutants. To generate *dmax*^{1} *mlx* double mutants, we recombined the *dmax*^{1} allele with the P element insertions *mlx*^{GE25479} (inserted 13 bp downstream of the transcription start site of *mlx* and 13 bp upstream of the *mlx* ORF) and *mlx*^{GE2850} (inserted 250 bp upstream of the start of the *mlx* transcript). Both these P element insertions are homozygous viable. *mlx*^{GE25479} is the only known P element that is located inside the *mlx* transcript. As Figure 38 shows, there was no size difference between the double mutants and the *dmax*^{1} single mutants. We therefore concluded, that *mlx* does not complement the loss of *dmax*.

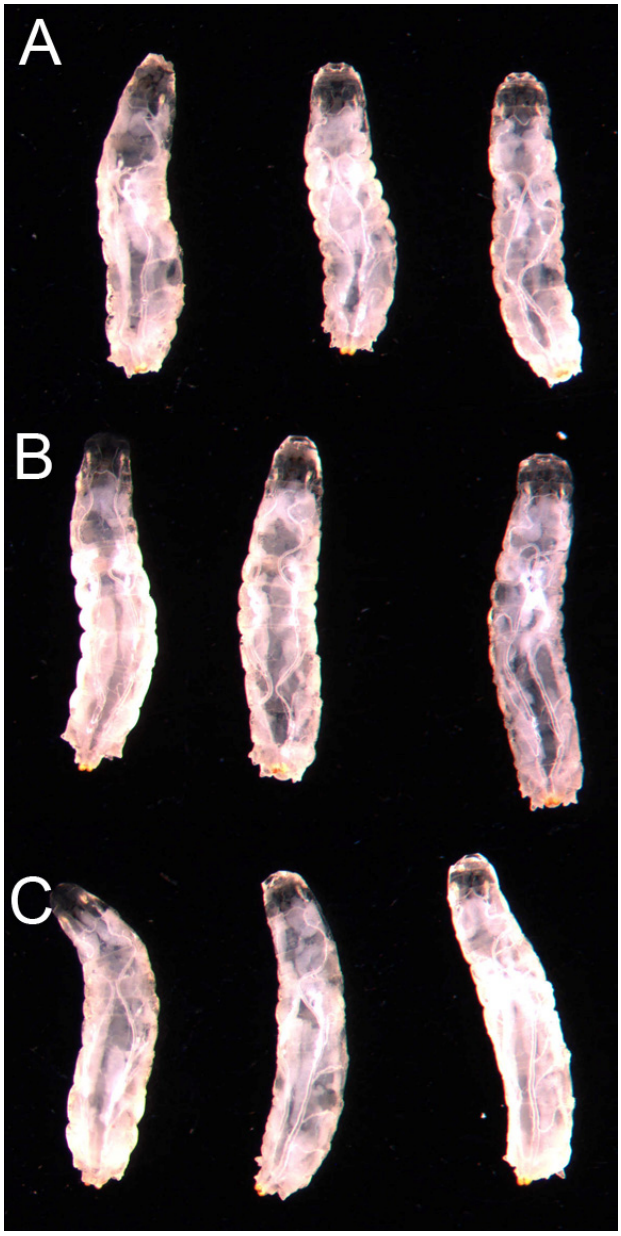

Figure 38
Loss of *mlx* does not alter the growth phenotype of *dmax*^{1} larvae. The larvae were photographed at 192 h AED.

Label:	Genotypes:
A	*w; dmax*^{1}
B	*w; dmax*^{1} *mlx*^{GE25479}
C	*w; dmax*^{1} *mlx*^{GE28050}

2.6. Clonal analysis

Since the effects of *dmyc* and *dmnt* on growth had shown to be cell-autonomous (Johnston et al., 1999; Pierce et al., 2004; Loo et al., 2005), we expected to see the observed growth differences between *dmyc* null, *dmyc dmnt* null and *dmax* null larvae also in mutant clones. We had shown that the differences in total larval size correlate with (and are probably caused by) different cell sizes of the polyploid organs (Figure 37abc). Using clonal analysis, we could also study the behavior of mutant diploid imaginal disc cells.

2.6.1. Clonal analysis in the eye: *ey-flp* clones

In order to generate flies that have *dmyc* null eyes, we used a *tub>dmyc>GAL4* transgene that rescues dm^{A51} null mutant flies to adulthood. Expression of this transgene in wild type flies does not induce lethality, but results in an increase in body weight, due to larger cell size (Bellosta et al., 2005). Flipase-mediated recombination at the FRT sites that flank the *dmyc* sequence in the transgene under control of the *eyeless-flipase* (*ey-flp*) transgene early in development results in a loss (flip-out) of *dmyc* in the eyes, in virtually all cells (D. Schwinkendorf, unpublished), producing *dmyc* null eyes (in a dm^{A51} background) or wild type eyes (in a *dmyc* wild type background). Figure 39 shows that the eye-specific loss of *dmyc* in dm^{A51} males resulted in small eyes with small ommatidia (Figure 39A, B). *dmyc* null eyes generated with this system often displayed a rough eye phenotype that was particularly pronounced in the ventral part of the eye.

We next generated $dmax^1$ mutant clones in the eye. To this end, we had recombined the $dmax^1$ allele with the FRT80B recombination site, which allowed us to generate $dmax^1$ somatic clones by flipase-mediated recombination (Xu and Rubin, 1993). In *y w ey-flp c-lacZ/w; FRT80B* P^{w+} *M(3)i55/FRT80B* $dmax^1$ flies, the action of *ey-flp* resulted in the generation of $dmax^1$ homozygous mutant clones (marked by the absence of *white* expression) in the eye. Since the sister chromosome arm carried a *Minute* allele (*M(3)i55*), only heterozygous tissue (marked w^+) and $dmax^1$ homozygous mutant tissue survived. Strikingly, $dmax^1$ mutant clones survived well and could cover large portions of the eye (Figure 39C, control: 39D). The size of $dmax^1$ mutant ommatidia was not visibly reduced compared to the wild type control and we never observed roughness in the eyes containing $dmax^1$ clones. It seemed that *dmax*, in contrast to *dmyc*, was not required to form a wild type eye. However, $dmax^1$ mutant macrochaetae of the head capsule were strongly reduced in size.

We next investigated whether the concomitant loss of *dmnt* in $dmax^1$ mutant clones was responsible for the milder phenotype of $dmax^1$ clones. We recombined the dm^4 and the dm^4 $dmnt^1$ chromosomes with the FRT19 recombination site and generated *ey-flp* clones of dm^4, dm^4 $dmnt^1$ and of $dmax^1$. In these experiments, recessive cell lethal alleles were used which allow for the elimination of homozygous wild type tissue, resulting in an eye that consists of heterozygous tissue (marked w^+) and homozygous mutant tissue (marked w^-). Figure 40 shows that the generation of dm^4 and of dm^4 $dmnt^1$

mutant clones resulted in eyes that consisted mainly of heterozygous tissue, with very few surviving *dm*^{4} or *dm*^{4} *dmnt*^{1} mutant clones (Figure 40 A, B). The size of surviving *dm*^{4} *dmnt*^{1} mutant clones was slightly larger than the one of *dm*^{4} mutant clones. In both cases, the heterozygous tissue very often was rough. *dmax*^{1} clones survived clearly better than *dm*^{4} *dmnt*^{1} clones and the resulting eyes never showed roughness, but the size of *dmax*^{1} clones was smaller than the size of wild type control clones (Figure 40 C, D) and smaller than the size of *dmax*^{1} clones produced in a *Minute* background (Figure 39 C). Since heterozygous *Minute* cells are viable, but suffer from cell competition, the larger size of *dmax*^{1} cells in a *Minute* background could be an indication for a competitive disadvantage of *dmax*^{1} cells. The observed roughness of the heterozygous tissue in eyes where *dm*^{4} or *dm*^{4} *dmnt*^{1} clones had been produced is an indication of cell competition: Roughness in the heterozygous tissue results when the homozygous mutant tissue does survive for a certain time and only then disappears. If two cell lethal mutations are juxtaposed on homologous chromosomes and *ey-flp* clones are generated, the only remaining unrecombined (heterozygous) tissue is never rough (H. Stocker, personal communication). If the homozygous mutant tissue first survives and only later dies (as it would occur due to cell competition), the remaining heterozygous tissue does not seem to be able to fully compensate for the loss of the homozygous tissue, resulting in roughness. *dm*^{4} and, to a lesser extent *dm*^{4} *dmnt*^{1}*,* mutant clones seem to be affected more strongly by cell competition than *dmax*^{1} mutant clones which can reach considerable - but not wild type - sizes and are not accompanied by roughness of the heterozygous tissue.

Cell competition seemed to play a lesser role in the experiments depicted in Figure 39. In the case of the *dm*^{A51} mutant eyes (Figure 39 A), flipase-mediated recombination occurs in cis at two FRT sites only separated by the *dmyc* transgene, making it occurring more frequently than between to FRT19 sites located in trans on homologous chromosomes. Therefore, most of the resulting tissue will be mutant for *dmyc* and almost no heterozygous tissue will remain, thus presumably eliminating cell competition. In the case of the *dmax*^{1} clones of Figure 39 C, cell competition is alleviated, because the *Minute*/+ heterozygous tissue has a competitive disadvantage compared to *dmax*^{1}/*dmax*^{1}.

Taken together, these data show that also in mutant clones in the eye, the *dmax*^{1} phenotype is less severe than the *dmyc* null phenotype and also less severe than the *dm*^{4} *dmnt*^{1} phenotype, consistent the existence of *dmax*- independent functions of *dmyc*.

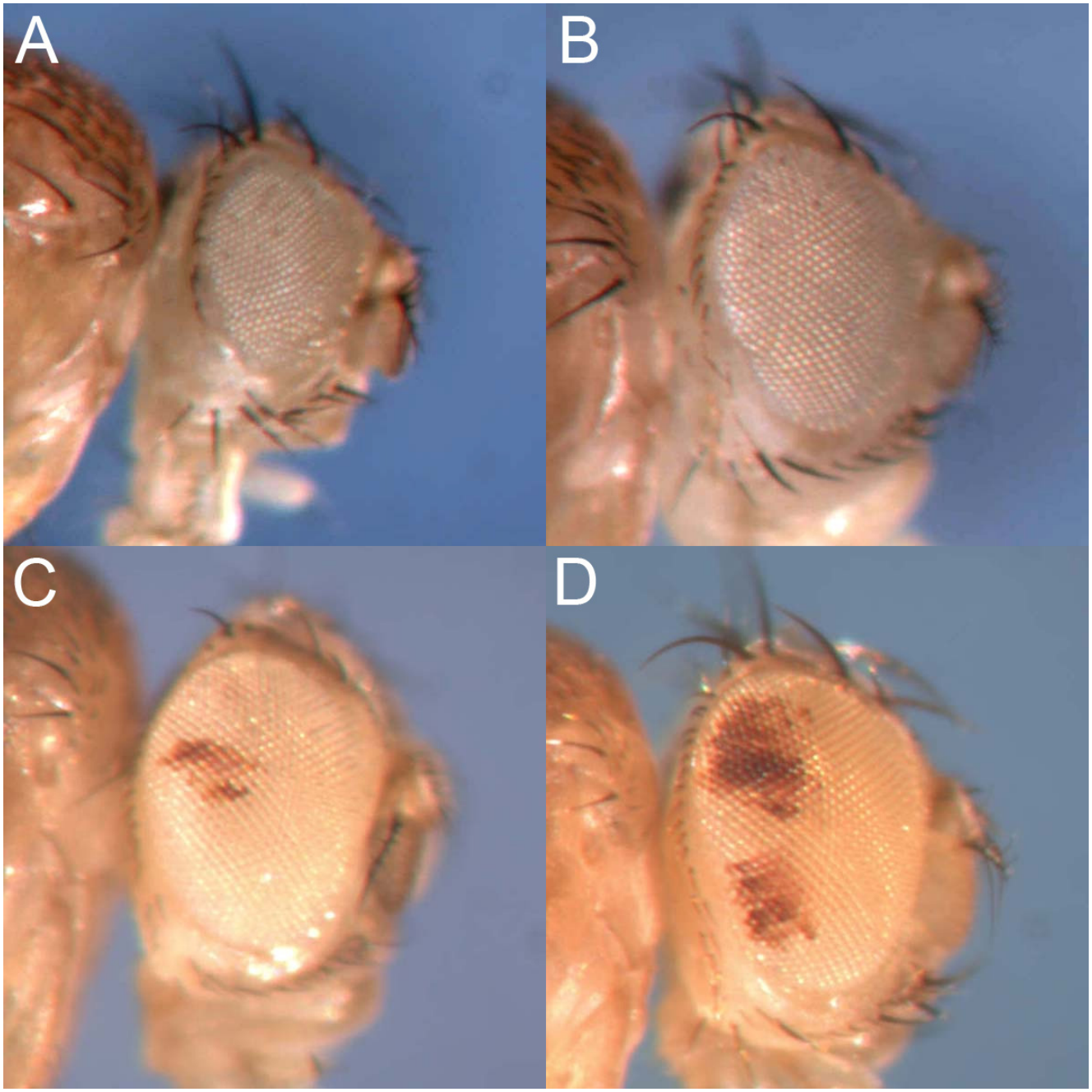

Figure 39
Whereas loss of *dmyc* in the eye results in a small and rough eye phenotype (A, control: B), *dmax*^{1} clones in the eye (*w*$^{-}$ tissue) survive well and form wild type ommatidia (C, control: D).

Label:	Genotypes:
A	*y w dm*^{A51} *tub>dmyc>GAL4 hs-flp/Y; CyO, ey-flp/+*
B	*y w dm*^{Rev} *tub>dmyc>GAL4 hs-flp/Y; CyO, ey-flp/+*
C	*y w ey-flp c-lacZ/w; FRT80B P*$^{w+}$ *(70C) M(3)i55/FRT80B dmax*^{1}
D	*y w ey-flp c-lacZ/w; FRT80B P*$^{w+}$ *(70C) M(3)i55/FRT80B*

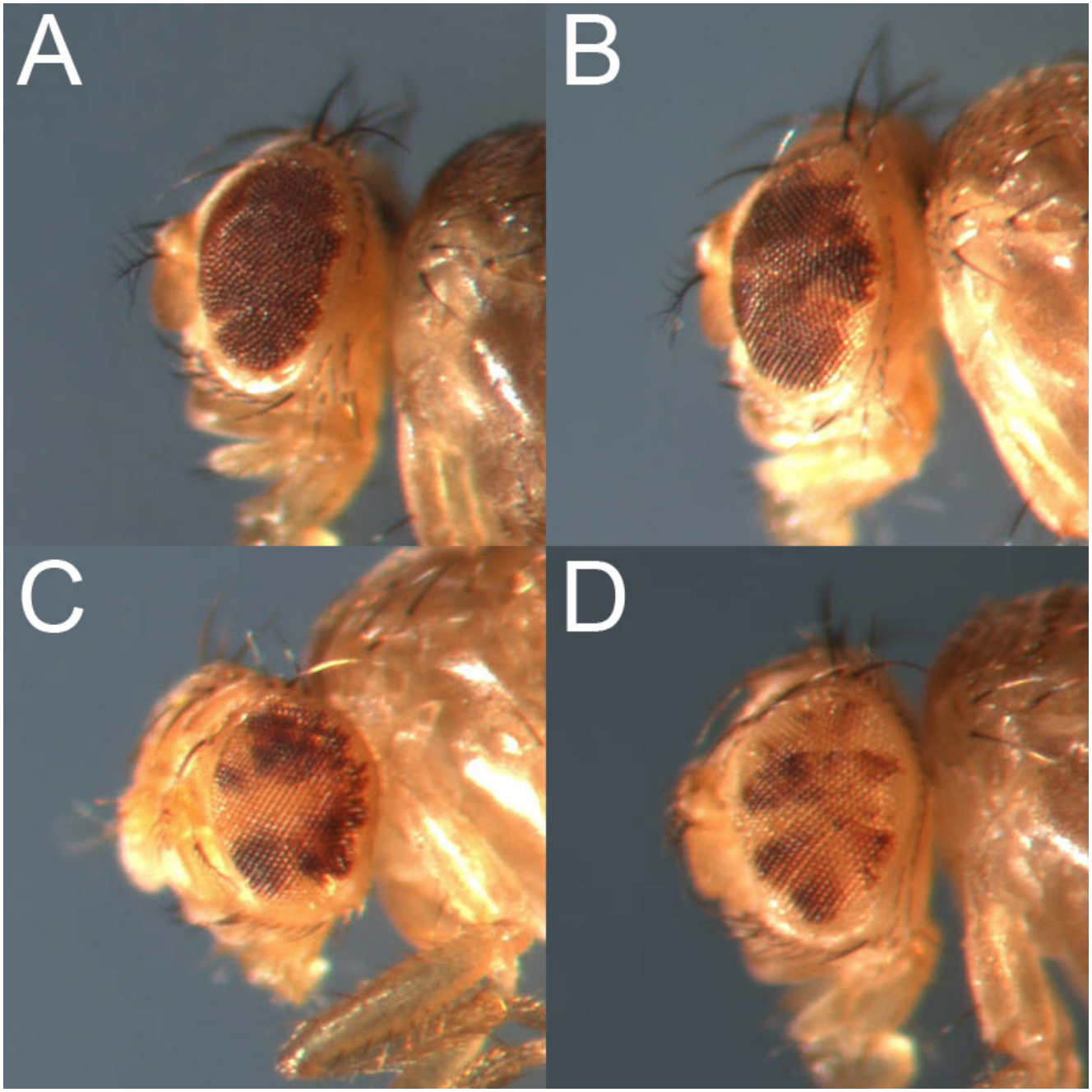

Figure 40
dm^{4} and *dm*^{4} *dmnt*^{1} clones in the eye (generated with the *ey-flp* system in a cell lethal background) survive poorly (A, B), resulting in rough eyes with almost no homozygous mutant *w*$^{-}$ ommatidia, in contrast to *dmax*^{1} clones (C). However, *dmax*^{1} clones occupy smaller areas compared to wild type control clones (D).

Label:	Genotypes:
A	*w dm*^{4} *FRT19/y cl(15b) FRT19; Sp/ey-flp*
B	*w dm*^{4} *dmnt*^{1} *FRT19/y cl(15b) FRT19; Sp/ey-flp*
C	*y w ey-flp/Y; +; FRT80 dmax*^{1}*/FRT80 cl*$^{w+}$
D	*y cl(15b) FRT19/y w FRT19; ey-flp/+*

2.6.2. Clonal analysis in the wing disc: twin spot clones

We next observed the growth and survival of *dm*^{4}, *dm*^{4} *dmnt*^{1} and *dmax*^{1} clones in the imaginal wing disc, using the hs-flp FRT system. This system allows for a timed generation of mutant clones in a heterozygous tissue. Every recombination event creates a homozygous mutant clone (marked by the lack of *GFP* expression) and a homozygous wild type twin spot (marked by two copies of *GFP*). Since mutant clone and wild type twin spot are created simultaneously, growth and survival of the mutant clone can be directly compared to the wild type twin spot, allowing an accurate analysis of growth, proliferation and cell competition. We examined *dm*^{4}, *dm*^{4} *dmnt*^{1} and *dmax*^{1} clones at an age of 72 h and *dmax*^{1} clones at an age of 96 h. All ages indicate the time that had elapsed since the generation of the clone. Figure 41 shows that *dm*^{4}, *dm*^{4} *dmnt*^{1} and *dmax*^{1} clones behaved very differently: Whereas *dm*^{4} and *dm*^{4} *dmnt*^{1} clones (Figure 41 A, B) at an age of 72 h were very small and often did not survive (as indicated by the presence of a twin spot clone un-accompanied by a mutant clone), *dmax*^{1} clones at the same age (Figure 41 C) showed sizes similar to the sizes of the twin spots, and most twin spots were accompanied by a *dmax*^{1} clone. At an age of 96 h, *dmax*^{1} clones showed a smaller size than the twin spot clones, and the number of twin spots without mutant clone was higher. Figure 42 shows a statistical analysis of the clone size distribution and the size of mutant cells compared to wild type cells. Both *dm*^{4} and *dm*^{4} *dmnt*^{1} clones were more than three times smaller than *dmax*^{1} clones at 72 h. For *dm*^{4}, 36% of the examined twin spots were not accompanied by a mutant clone (*dm*^{4} *dmnt*^{1}: 46%), whereas only 3% single twin spots were found for *dmax*^{1}. We concluded that both *dm*^{4} and *dm*^{4} *dmnt*^{1} clones showed strong signs of cell competition, whereas there was no clear indication for cell competition for *dmax*^{1} clones at 72 h (*dmax*^{1} clones were smaller than the wild type twin spots, but it is not possible to decide whether this was due to cell competition or due to slower proliferation of the *dmax*^{1} cells). However, at 96 h, 19% single twin spots were found in discs where *dmax*^{1} clones had been induced, and the *dmax*^{1} mutant clones showed a slightly smaller median size. We therefore find that also *dmax*^{1} clones suffered from cell competition, albeit at a smaller extent than *dm*^{4} or *dm*^{4} *dmnt*^{1} clones. The cell size in both *dm*^{4} and *dm*^{4} *dmnt*^{1} clones was clearly smaller than the cell size in the twin spot clones, whereas the cell size in *dmax*^{1} clones was similar to the cell size of the twin spot clones.

Taken together, these data indicate that *dmax*^{1} clones are clearly different from *dm*^{4} and *dm*^{4} *dmnt*^{1} clones, both in their susceptibility to cell competition and in cell size. Whereas *dm*^{4} *dmnt*^{1} clones survived better than *dm*^{4} clones in the eye (Figure 40), they did as poorly as *dm*^{4} clones in the imaginal wing disc. This finding might be explained by stronger cell competition in the wing disc.

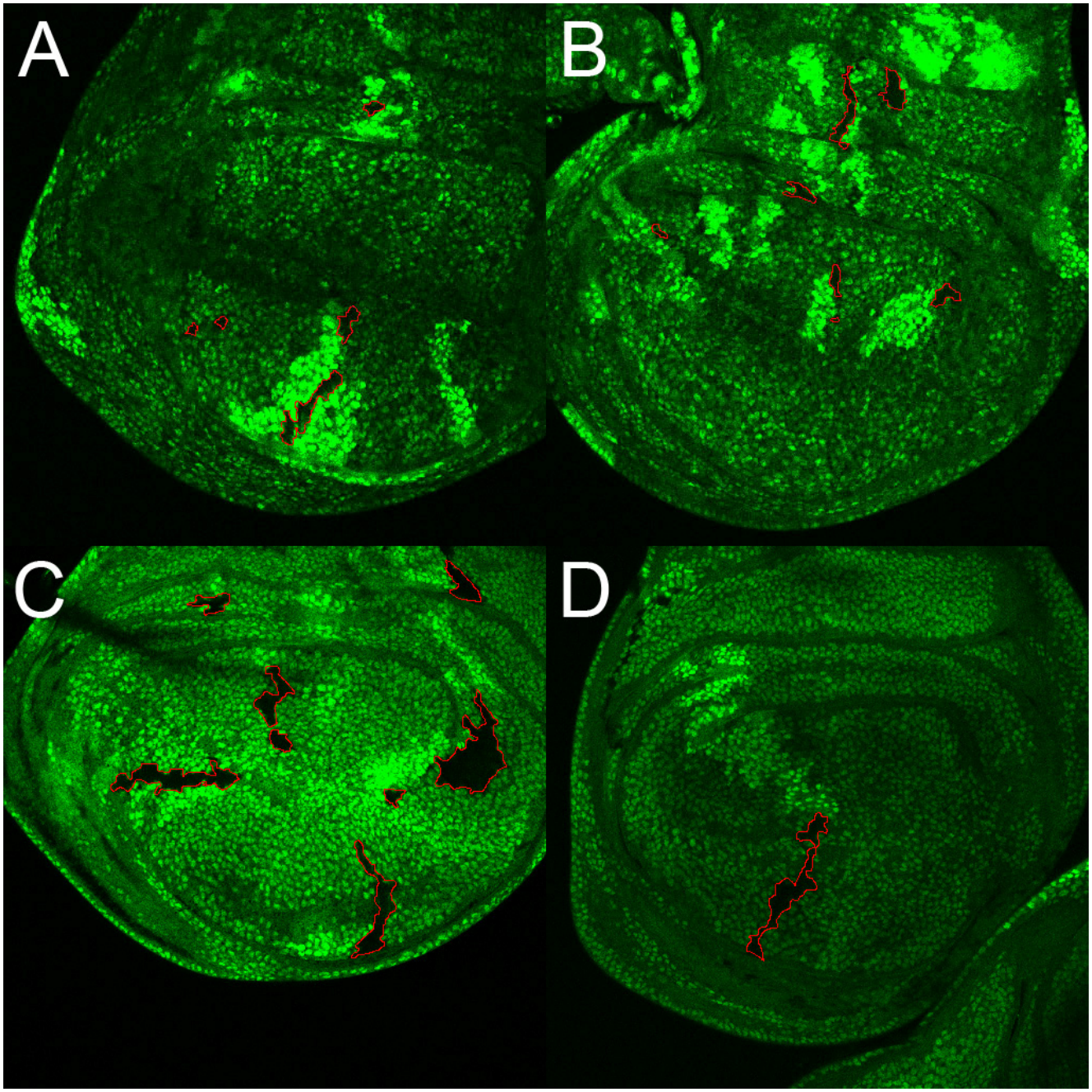

Figure 41
dm^{4} and *dm*^{4} *dmnt*^{1} mutant clones (*GFP*$^{-}$ cells) survive poorly and are smaller than wild type twin spot clones (harboring two copies of *GFP*) (A, B). At the same age (72 h), *dmax*^{1} clones are only slightly smaller than the wild type twin spot clones (C). 96 h old *dmax*^{1} clones are clearly smaller than the wild type twin spot clones (D). For better visibility of the *GFP*$^{-}$ clones are encircled with a red line.

Label:	Genotypes:	Age of the clones:
A	*w dm*^{4} *FRT19/y w hs-flp hs-GFP FRT19*	72 h
B	*w dm*^{4} *dmnt*^{1} *FRT19/y w hs-flp hs-GFP FRT19*	72 h
C	*y w hs-flp; dmax*^{1} *FRT80/FRT80 ubi-GFP*	72 h
D	*y w hs-flp; dmax*^{1} *FRT80/FRT80 ubi-GFP*	96 h

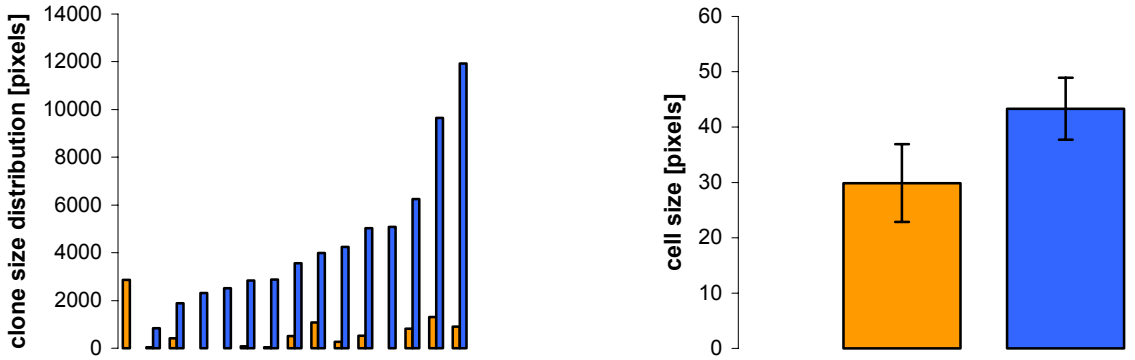

Figure 42a
Clone size distribution and average cell size of 72 h old *dm*^{4} clones (orange) and wild type twin spot clones (blue) in imaginal wing discs.

Median clone size:	*dm*^{4} clone	502 pixels
	wt twin spot	3556 pixels
Average cell size:	*dm*^{4} clone	31 pixels
	wt twin spot	43 pixels
Single twin spots:	36 %	

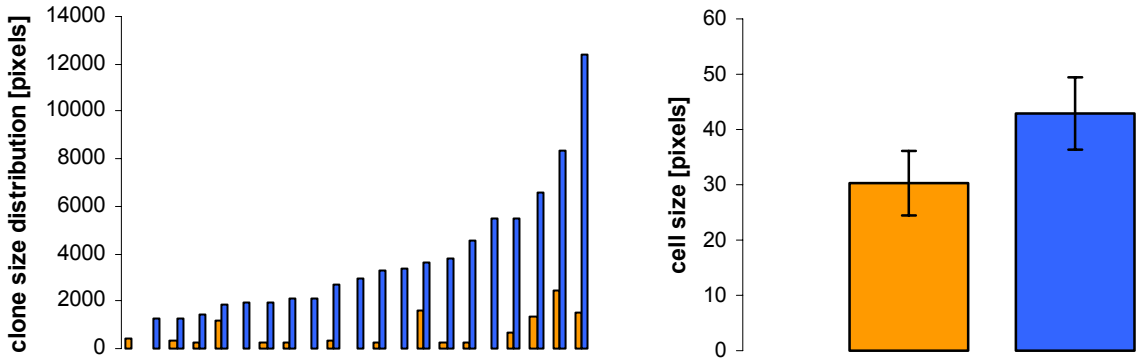

Figure 42b
Clone size distribution and average cell size of 72 h old *dm*^{4} *dmnt*^{1} clones (orange) and wild type twin spot clones (blue) in imaginal wing discs.

Median clone size:	*dm*^{4} *dmnt*^{1} clone	373 pixels
	wt twin spot	3137 pixels
Average cell size:	*dm*^{4} *dmnt*^{1} clone	29 pixels
	wt twin spot	41 pixels
Single twin spots:	46 %	

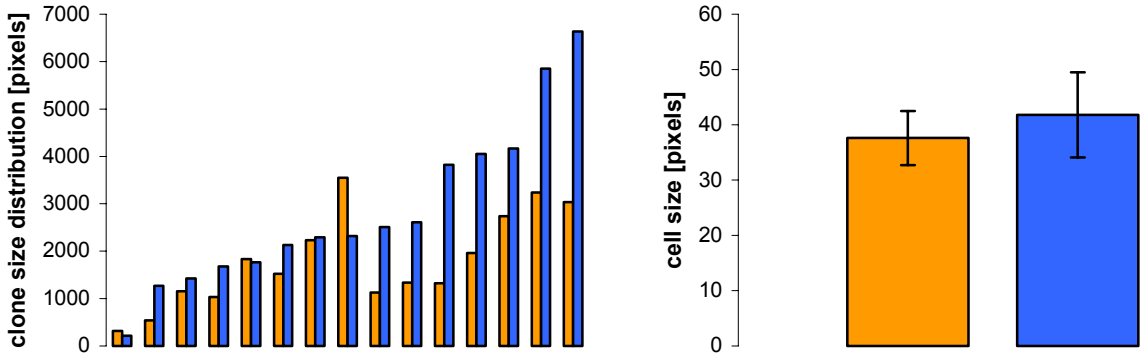

Figure 42c
Clone size distribution and average cell size of 72 h old *dmax*^{1} clones (orange) and wild type twin spot clones (blue) in imaginal wing discs.

Median clone size:	*dmax*^{1} clone	1525 pixels
	wt twin spot	2321 pixels
Average cell size:	*dmax*^{1} clone	35 pixels
	wt twin spot	39 pixels
Single twin spots:	3 %	

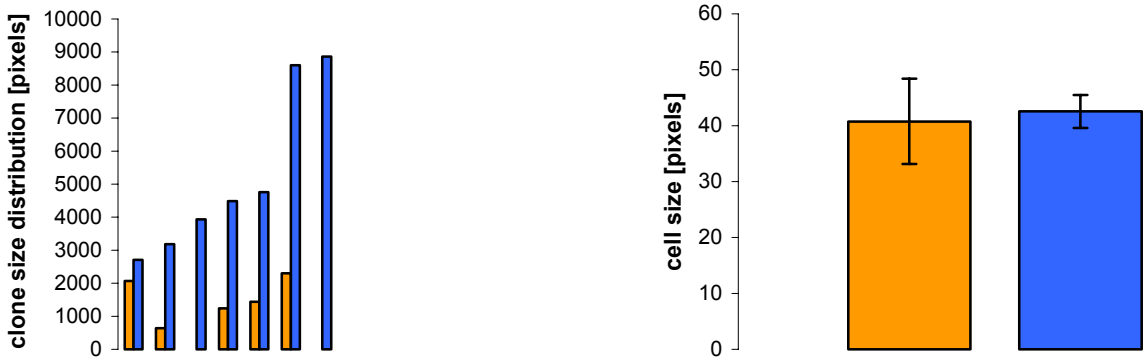

Figure 42d
Clone size distribution and average cell size of 96 h old *dmax*^{1} clones (orange) and wild type twin spot clones (blue) in imaginal wing discs.

Median clone size:	*dmax*^{1} clone	1441 pixels
	wt twin spot	4489 pixels
Average cell size:	*dmax*^{1} clone	40 pixels
	wt twin spot	41 pixels
Single twin spots:	19 %	

2.6.3. *dmyc* causes cell competition in *dmax*^{1} larvae

The clonal analysis of *ey-flp* clones in the eye (Figure 40) and of *hs-flp* twin spot clones in the wing disc (Figures 41, 42) had revealed that both *dm*^{4} and *dm*^{4} *dmnt*^{1} mutant clones suffered more strongly from cell competition than *dmax*^{1} clones. Apparently, the *dmax*-independent functions of *dmyc* that were still present in the *dmax*^{1} cells, but not in *dm*^{4} *dmnt*^{1} cells, had partially protected the *dmax*^{1} cells. We now asked whether differences in *dmyc* levels were still capable to induce cell competition in the absence of *dmax*. To study this question, we used a *tub>dmyc>GAL4* flip-out transgene (Bellosta et al., 2005). In flies which carry this transgene, clones can be induced in which the transgene has recombined to *tub>GAL4*. Therefore, the clones possess endogenous *dmyc* levels, whereas the surrounding unrecombined tissue has endogenous *dmyc* plus ectopically expressed *dmyc*. Since *dmyc* levels are higher in the surrounding tissue, the clones suffer from cell competition (Moreno and Basler, 2004). We generated *dmax*^{1} larvae which carried the *tub>dmyc>GAL4* transgene and asked whether *tub>GAL4* clones would still suffer from cell competition. As a control, neutral clones were generated in *dmax*^{1} larvae that carried the *actin>CD>GAL4* flip-out cassette. In both cases, clones were marked by the expression of *GFP*. We induced the clones at 5 d AED (a time when no detectable *dmax* mRNA was present anymore, see Figure 25), and examined the clones 4 d later, at 9 d AED. Figure 43 shows that the *act>CD2>GAL4* control clones were bigger (Figure 43 A) than the *tub>dmyc>GAL4* clones. The average clone size of the *act>CD2>GAL4* clones was 2213 pixels, the size of the *tub>dmyc>GAL4* clones was 1452 pixels. Since both types of clones contain the same endogenous levels of *dmyc*, the most likely explanation for the smaller size of the *tub>dmyc>GAL4* clones is that these clones suffer from cell competition caused by the surrounding tissue which has higher *dmyc* levels. Therefore, cell competition can also be induced by differing levels of *dmax*-independent functions of *dmyc*.

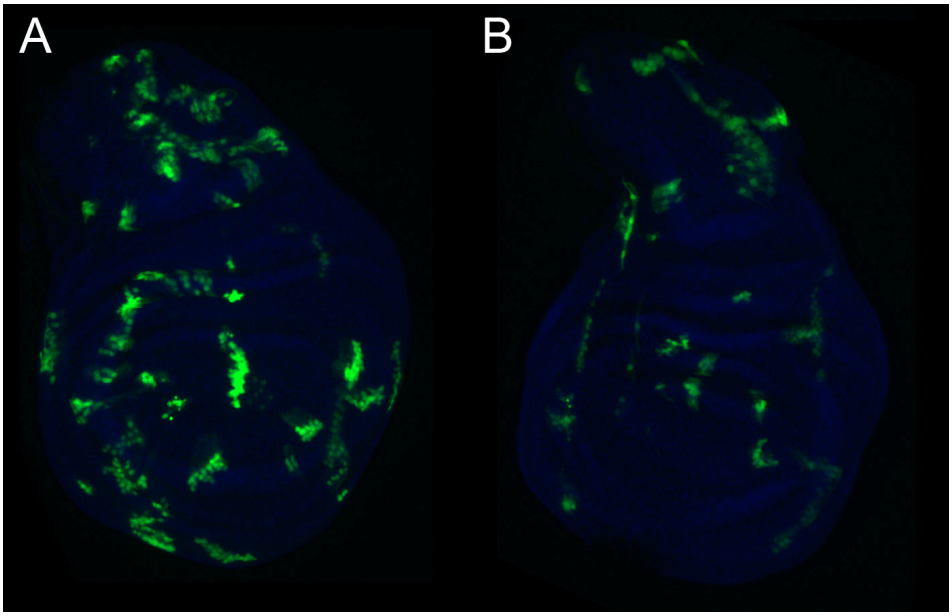

Figure 43a
dmyc causes cell competition in *dmax*^{1} larvae. Clones which had lower *dmyc* levels than the surrounding tissue (B) were smaller than control clones (A) whose *dmyc* levels were identical to the *dmyc* levels of the surrounding tissue. Clones were induced at 5 d AED and allowed 4 d to grow. The clones are marked by the expression of *UAS-GFP*.

Label:	Genotypes:
A	*y w hs-flp/[y w or Y]; actin>CD2>GAL4 UAS-GFP dmax*^{1}*/dmax*^{1}
B	*y w tub>dmyc>GAL4 hs-flp/[y w or Y]; UAS-GFP/+; dmax*^{1}

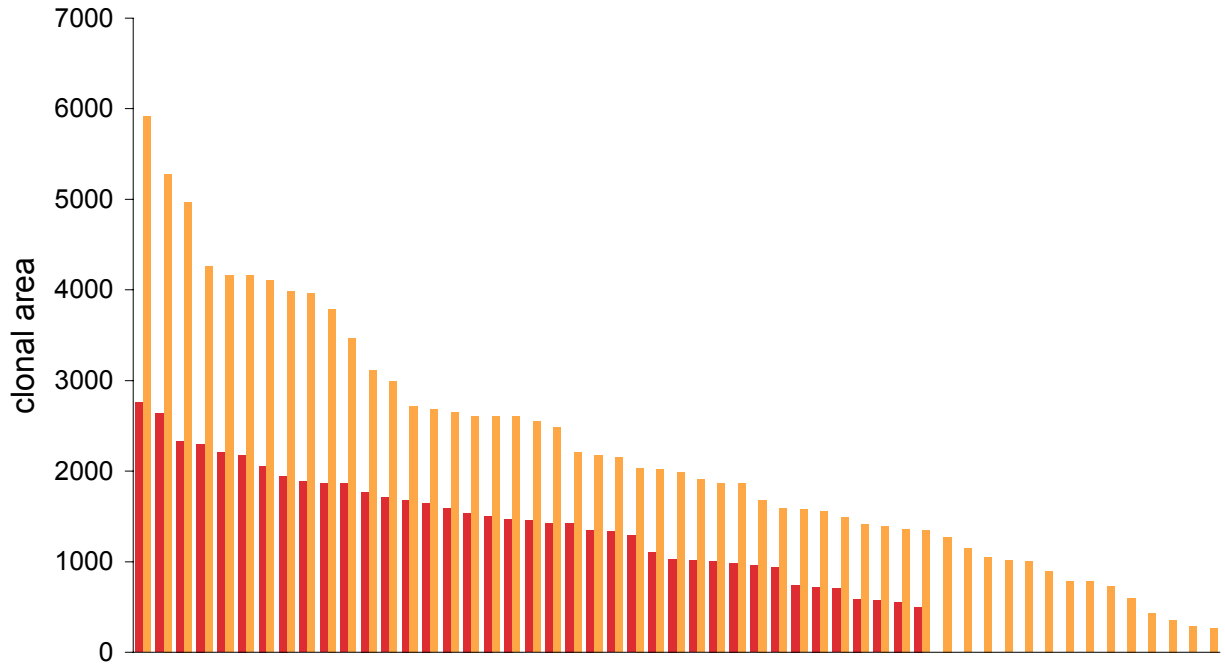

Figure 43b
Comparison of the clone sizes (orange: A genotype, red: B genotype). For A, the clone size of 53 clones from 14 wing discs, for B, the clone size of 39 clones from 6 wing discs was determined. A clones had an average clone size of 2213 pixels. B clones had an average clone size of 1452 pixels.

2.6.4. *dmax*^{1} bristles are small

Whereas *dmax*^{1} mutant cells in mutant clones in the wing disc did not show a reduced size (Figure 42c, 42d), we observed that the size of *dmax*^{1} prothoracic and thoracic macrochaetae was severely reduced (Figure 44). Bristles are very sensitive to the loss of *dmyc* or *dmax* function, since already weak hypomorphic alleles of *dmyc* and *dmax*-RNA*i* show a thin bristle phenotype, presumably due to a strong requirement for *dmyc* function in situations of high protein biosynthesis. A differential requirement for dMyc/dMax function might also explain why in *ey-flp* clones *dmax*^{1} ommatidia develop like wild type ommatidia, while *dmax*^{1} bristles of the head capsule are strongly affected.

2.6.5. *dm*^{4} *dmnt*^{1} and *dmax*^{1} clones in the fat body

We had shown that the cell size and the total organ size of *dm*^{4} *dmnt*^{1} fat bodies is smaller than the cell and total organ size of *dmax*^{1} fat bodies. In order to investigate whether this difference is cell-autonomous, we generated *dm*^{4} *dmnt*^{1} and *dmax*^{1} mutant fat body cells in a heterozygous background using the hs-flp FRT system. Figure 45 shows that *dm*^{4} *dmnt*^{1} mutant cells were clearly smaller than *dmax*^{1} mutant cells. Some *dmax*^{1} mutant cells were only slightly smaller than the cells of the surrounding heterozygous tissue In both cases, the size of the cell nuclei was proportional to the overall cell size. These results show that the different cell sizes found in the fat bodies of *dm*^{4} *dmnt*^{1} and *dmax*^{1} fat bodies are caused by cell-autonomous differences. It is therefore probable that an important part of the differences in the total larval sizes are a direct consequence of these cell-autonomous differences.

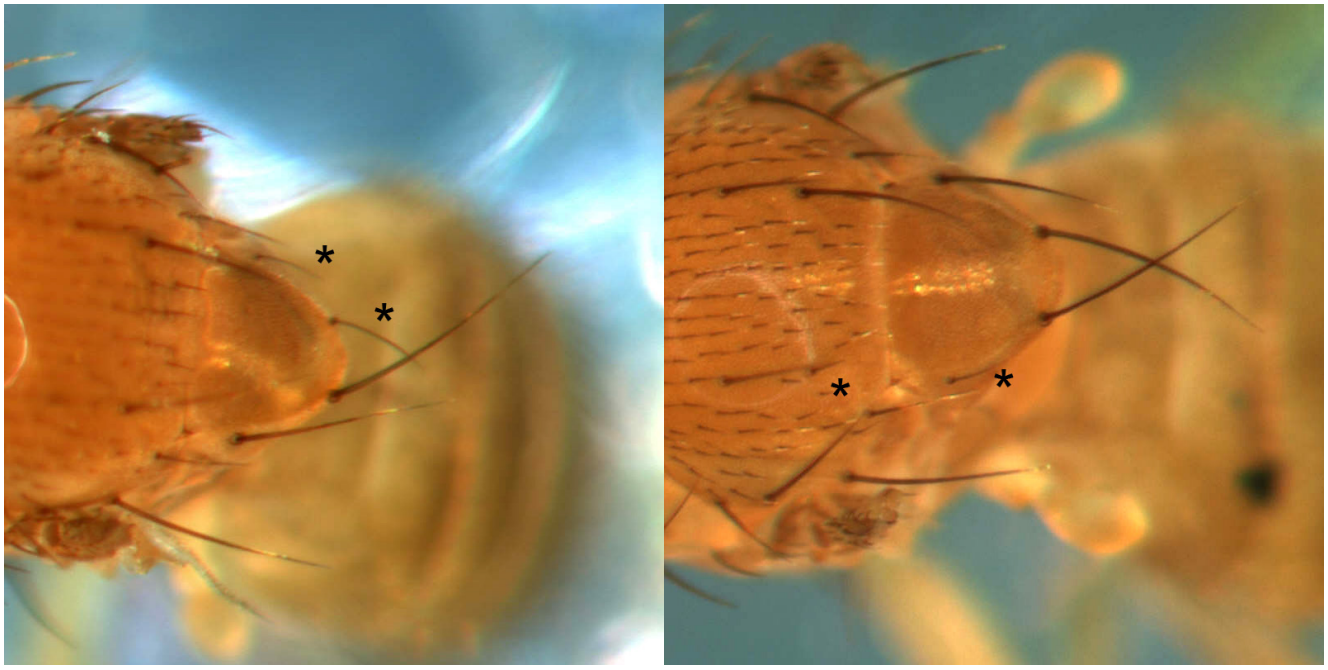

Figure 44
dmax^{1} macrochaetae (indicated with an asterisk) are very thin and short. *dmax*^{1} bristles were generated in *y w hs-flp; dmax*^{1} *FRT80/FRT80 ubi-GFP* animals which were subjected to a heat shock at 24 h AED.

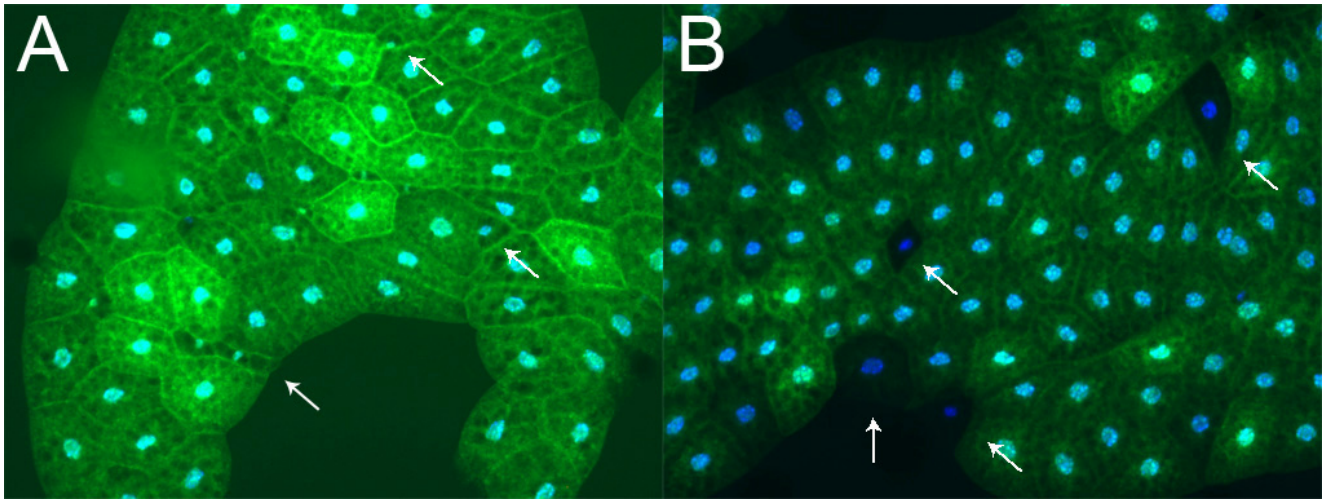

Figure 45
dm^{4} *dmnt*^{1} and *dmax*^{1} fat body cell clones, generated with the hs-flp FRT system. *dm*^{4} *dmnt*^{1} fat body cells and nuclei (A) are smaller than *dmax*^{1} fat body cell and nuclei (B). Mutant cells are marked by the lack of GFP expression and indicated by arrows. Nuclei were stained with Hoechst dye. Clones were induced at 6 h AED. Depicted are fat bodies of wandering larvae.

Label:	Genotypes:
A	*w dm*^{4} *dmnt*^{1} *FRT19/y w hs-flp hs-GFP FRT19*
B	*y w hs-flp; FRT80 dmax*^{1}*/FRT80 ubi-GFP*

2.7. *dmyc* overexpression in *dmax*^{1} larvae

The comparison of null mutant combinations of the Max network members had revealed that *dmyc* is still partly functional in the absence of *dmax*. Using RNA*i,* we had furthermore shown that the effects of overexpression of *dmyc* in the *Drosophila* eye were partly *dmax*-independent. We next examined the consequences of overexpression of *dmyc* in *dmax*^{1} mutants. Assuming that all functions of *dmyc* do require *dmax*, one would have to expect that a *dmyc* transgene is silent in a *dmax*^{1} background. However, if *dmyc* indeed had *dmax*-independent functions, then we could hope that overexpression of *dmyc* in *dmax*^{1} mutants should still produce observable effects.

In the following experiments, we used the *UAS-dmyc*^{132} transgene. Expression of *UAS-dmyc*^{132} under control of *GMR-GAL4* led to an increase in ommatidial size of more than 20% (Figure 14). Strong and ubiquitous expression of *UAS-dmyc*^{132} with *actin-GAL4* leads to partial larval lethality (Figure 47b), but most larvae reach the pupal stage and die as pupae. Expression of *UAS-dmyc*^{132} under control of *actin-GAL4* had a striking effect in *dmax*^{1} larvae: at a time point of 192 h AED, no *y w; actin-GAL4/UAS-dmyc*^{132}*; dmax*^{1} could be found (Figure 46). We repeated the experiment and collected the larvae at 120 h AED, a time point when wild type larvae which overexpress *UAS-dmyc*^{132} would still be alive. Figure 47 shows that at this time point, less than 20% of the *y w; actin-GAL4/UAS-dmyc*^{132}*; dmax*^{1} larvae were still alive. These surviving *dmax*^{1} larvae were smaller than the sister genotype (*y w; CyO, y+/UAS-dmyc*^{132}*; dmax*^{1}) which had reached L3, and they were all in L2. *dmax*^{1}*/TM6B* larvae were much less affected by the overexpression of *UAS-dmyc*^{132}: more than 60% were still alive, however some of them being smaller than the control sister genotype (*y w; CyO, y+/UAS-dmyc*^{132}*; dmax*^{1}*/TM6B*.

It was very surprising to find that the overexpression of *UAS-dmyc* not only did have an effect in *dmax*^{1} larvae, but that this effect was stronger in *dmax*^{1} homozygous mutants than in heterozygous *dmax*^{1}*/TM6B* animals. In order to examine the effect more closely, we switched to a system which allows for a conditional overexpression of *UAS-dmyc*. To this purpose, we generated *y w hs-flp; actin>CD2>GAL4 UAS-GFP dmax*^{1}*/TM6B* flies. Crossed to *y w; UAS-dmyc*^{132}*; dmax*^{1}*/TM6B* or *y w; UAS-dmyc*^{132}*; +* flies, the *actin>CD2>GAL4* flip-out cassette enabled the ubiquitous expression of *UAS-dmyc*^{132} upon a strong heat shock. The co-expressed *UAS-GFP* transgene was used to monitor the efficiency of heat-shock induced expression. The following experiments were all done with heat shocks of 2 hours at 37° C. With such a heat shock regimen, strong ubiquitous GFP expression resulted within few hours (data not shown).

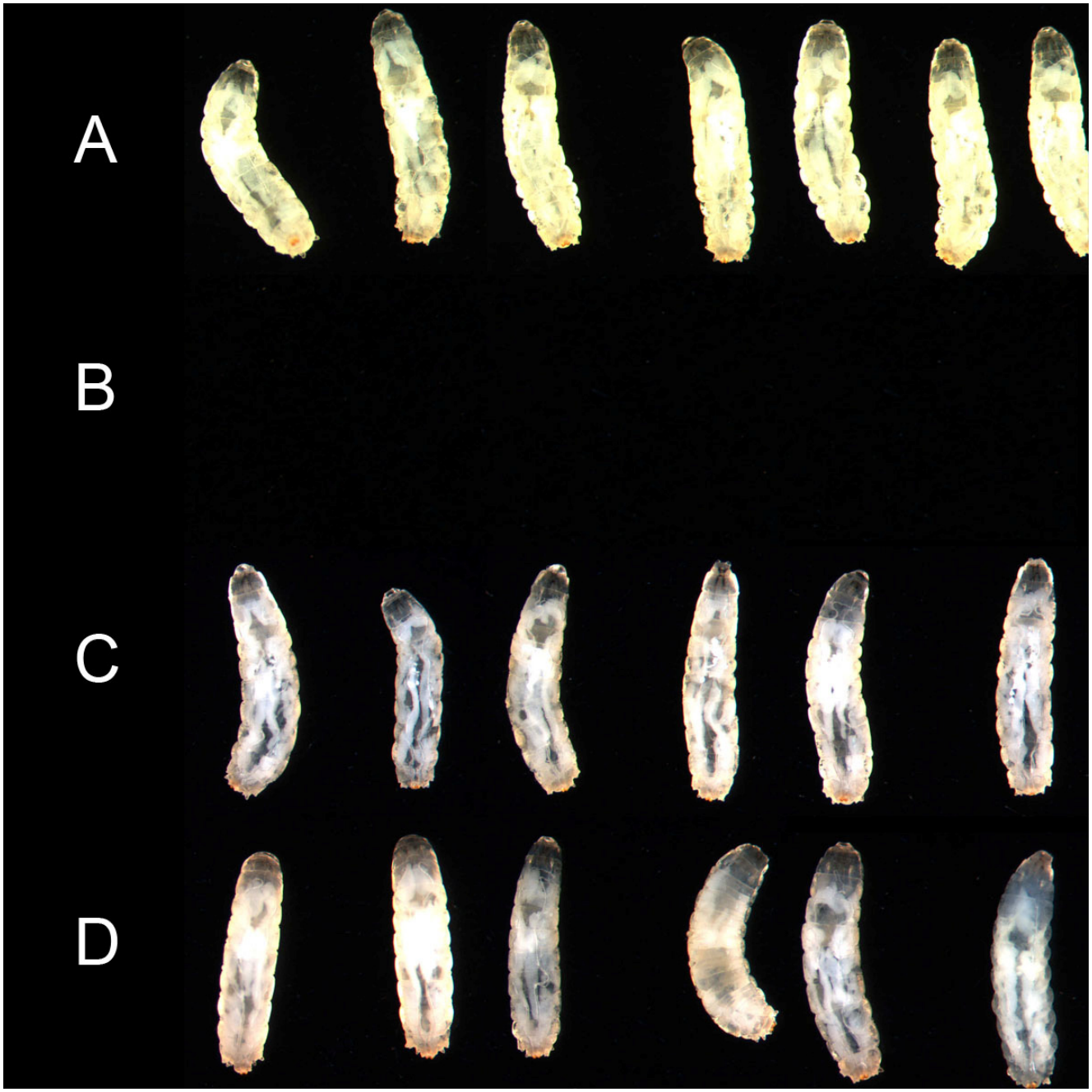

Figure 46
Constitutive expression of *UAS-dmyc*^{132} with the strong, ubiquitous GAL4 driver *actin-GAL4* is lethal in *dmax*^{1} larvae. At 192 h AED, no *y w; actin-GAL4/UAS-dmyc*^{132}*; dmax*^{1} could be found (B).

Label:	Genotypes:
A	*y w; CyO, y*$^{+}$*/UAS-dmyc; dmax*^{1}
B	*y w; actin-GAL4/UAS-dmyc*^{132}*; dmax*^{1}
C	*y w; CyO, y*$^{+}$*/+; dmax*^{1}
D	*y w; actin-GAL4/+; dmax*^{1}

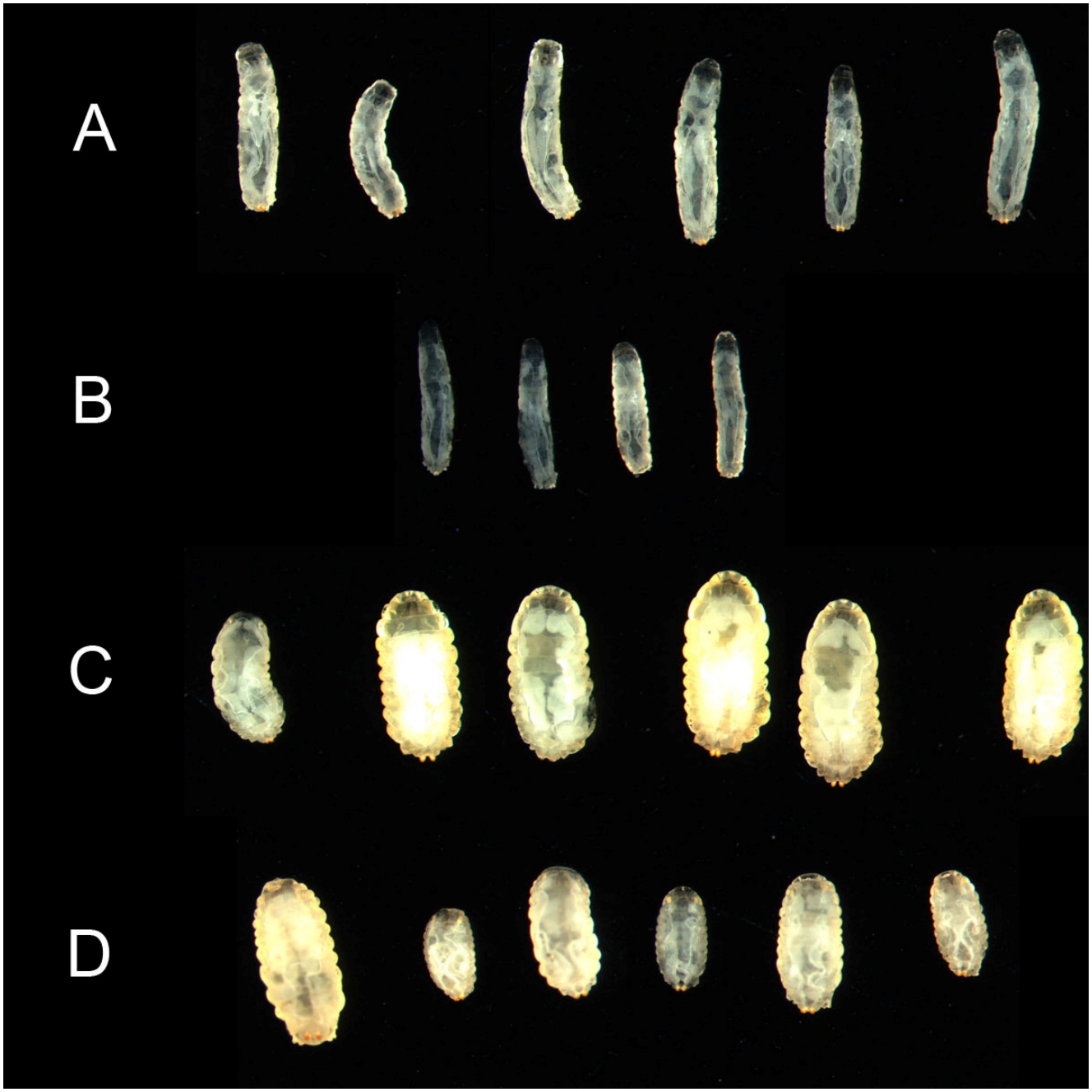

Figure 47a
At 120 h AED, *dmax*^{1} larvae in which *UAS-dmyc*^{132} is expressed by *actin-GAL4* were reduced in numbers, had not reached L3 and stayed small (B). *dmax*^{1}*/TM6B* larvae were much less affected by the overexpression of *UAS-dmyc*^{132}, showing a only a slight reduction in survival and all being in the L3 stage. Note: The rounded shape of the larvae in panel C and D is the *Tb* phenotype (one of the marker mutations of the *TM6B* balancer).

Label:	Genotypes:
A	*y w; CyO, y*$^{+}$*/UAS-dmyc*^{132}*; dmax*^{1}
B	*y w; actin-GAL4/UAS-dmyc*^{132}*; dmax*^{1}
C	*y w; CyO, y*$^{+/}$*UAS-dmyc*^{132}*;dmax*^{1}*/TM6B*
D	*y w; actin-GAL4/UAS-dmyc*^{132}*;dmax*^{1}*/TM6B*

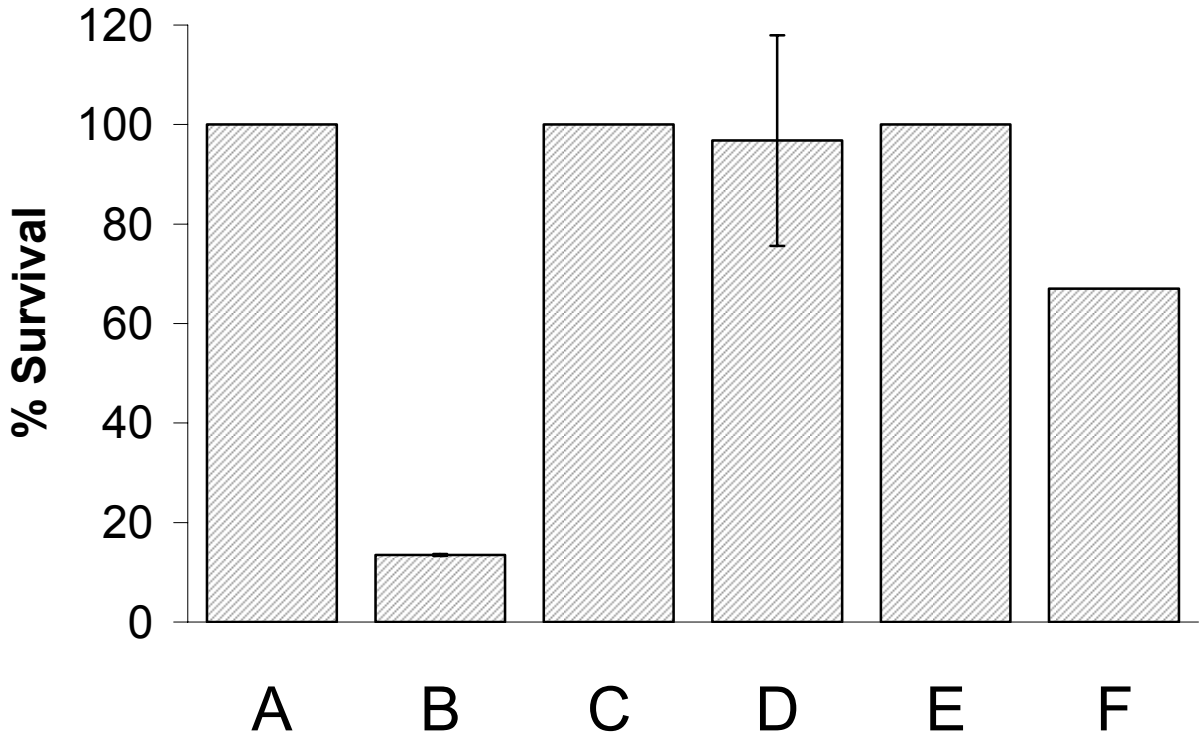

Figure 47b
Survival of *dmax*^{1} and *dmax*^{1}*/TM6B* larvae in the context of overexpressed *dmyc* at 120 h AED. The survival of the B, D and F genotypes is indicated relative to the control genotypes A, C and E. For A, B, C and D, two experiments were performed and the standard deviation is indicated. For E and F, one experiment was performed. Total number of offspring: A: 52, B: 7, C: 28, D: 28, E: 60, F: 40.

Label:	Genotypes:
A	*y w; UAS-dmyc*^{132}*/CyO, y*$^{+}$*; dmax*^{1}
B	*y w; UAS-dmyc*^{132}*/actin-GAL4; dmax*^{1}
C	*y w; +/CyO, y*$^{+}$*; dmax*^{1}
D	*y w; +/actin-GAL4; dmax*^{1}
E	*y w; UAS-dmyc*^{132}*/CyO, y*^{1}*; dmax*^{1}*/TM6B*
F	*y w; UAS-dmyc*^{132}*/actin-GAL4; dmax*^{1}*/TM6B*

Using the conditional expression system, we could show that the timing of the onset of *dmyc* overexpression is critical to induce lethality in *dmax*^{1} larvae. Figure 48 shows that induction of *dmyc* at an age of 3-4 d AED had no negative consequences on the survival of *dmax*^{1} larvae to an age of 8 d AED. However, when *dmyc* was induced at an age of 2-3 d AED, less than 10% of the *dmax*^{1} larvae survived until 8 d AED. The number of *dmax*^{1}/+ pupae was also reduced when the heat shock was given at the earlier time point, but to a much lesser degree.

In the above experiment, the survival of the *dmax*^{1} larvae was examined only at 8d AED. It was therefore not clear, how long *dmax*^{1} larvae would survive after induction of *dmyc* at the critical early time point. In the next experiment, a heat shock was given at 3 d AED, and the larvae were collected at 5 d AED. Figure 49 shows that less than 10% of the *dmax*^{1} larvae were alive at 5 d AED, if *dmyc* was expressed. In this experiment as well, *dmax*^{1}/+ larvae suffered much less from the overexpression of *dmyc*.

From these experiments, we concluded that at an age of 3 d AED, a critical event occurs in *dmax*^{1} larvae. If *dmyc* is induced prior to this time point, the *dmax*^{1} larvae die within a short time. Induction of *dmyc* after this time point has no visible consequences and the larvae survive normally. Since we had shown that the time window for the L2-L3 molt of *dmax*^{1} larvae is 70-80 h AED, we suspected that the critical event might be the L2-L3 molt.

In the next experiment, we induced *dmyc* expression at 2 d AED, well before the L2-L3 molt, both in *dmax*^{1}/+ and in *dmax*^{1} homozygous larvae. We then examined the larvae at 4 d AED, shortly after the L2-L3 molt should have occurred. Figure 50a shows that the *dmax*/+ larvae were all in L3 at 4 d AED, with and without expression of *dmyc*. *dmax*^{1} larvae in which *dmyc* was not expressed had also reached the L3 stage (Figure 50b A). However, of the 16 *dmax*^{1} larvae in which *dmyc* had been induced, 8 were dead. Two of these dead larvae displayed double sets of anterior spiracles, and in others, it became clear that they possessed two sets of cuticles, since the outer cuticle could be moved and detached easily (Figure 50b B). Of the surviving larvae, two displayed two sets of anterior spiracles, one was in L3, the rest were in L2.

From this experiment, it became clear that *dmax*^{1} larvae fail to properly undergo the L2-L3 molt or do not even initiate it, when *dmyc* is expressed prior to the molt. The molting phenotypes described (double sets of spiracles, double sets of cuticles) are reminiscent to the ones of *EcR-B* mutants (Schubiger et al., 1998). When *dmyc* was expressed ubiquitously under control of *actin-GAL4*, the few *dmax*^{1} larvae that were found at 5 d AED were all in L2. We therefore believe that also in this case, the rest of the *dmax*^{1} larvae had died due to problems with the L2-L3 molt. The experiments above show that it is sufficient to induce expression of *dmyc* shortly before the molt (as late as at 3 d AED) in order to provoke strong lethality in *dmax*^{1} larvae.

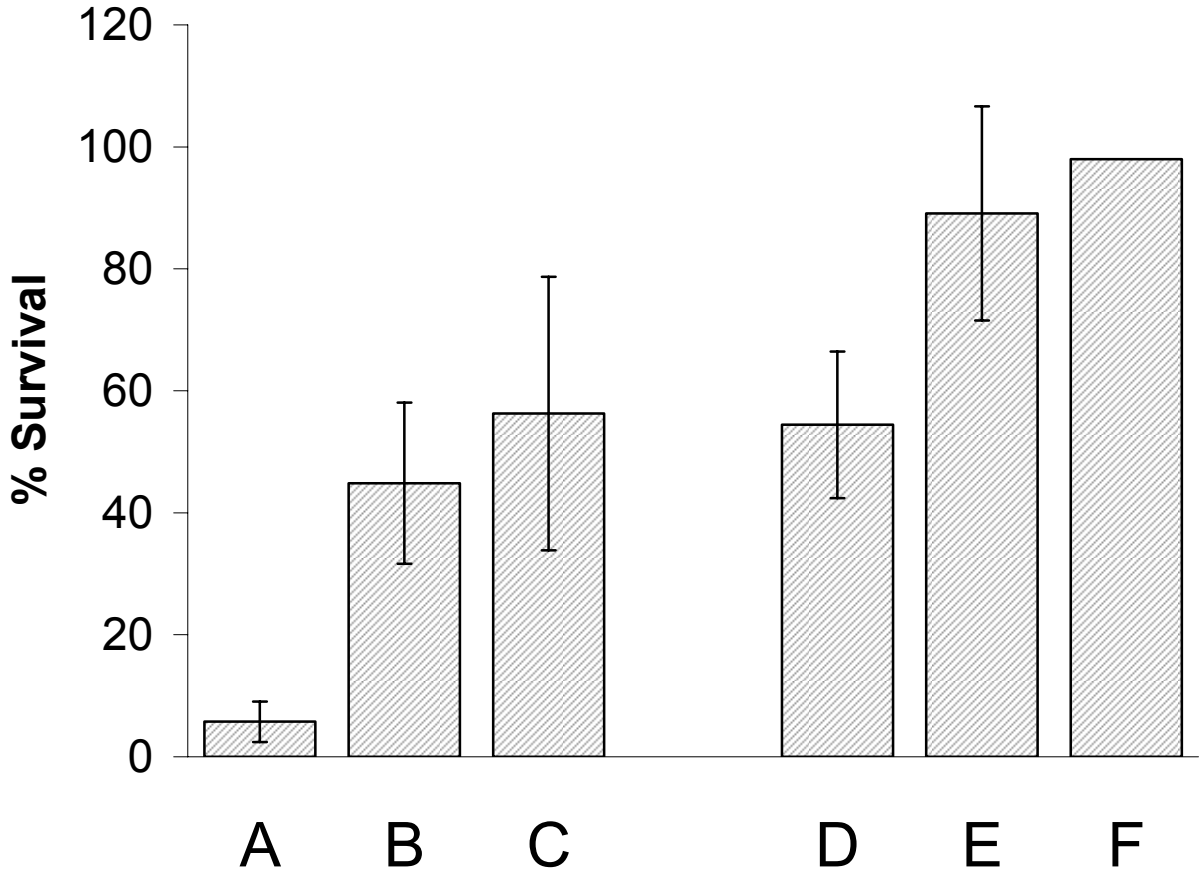

Figure 48
Survival of *dmax*^{1} and of *dmax*^{1}/+ larvae, measured at 8 d AED, upon heat shock induced overexpression of *UAS-dmyc*. Whereas a heat shock given at 2-3 d AED leads to strong lethality in *dmax*^{1} larvae, a heat shock given at 3-4 d AED does not. A heat shock at 2-3 d AED has not such a strong effect in *dmax*^{1}/+ larvae. For the genotypes A, B, D, E and F, two experiments were performed, for the genotype C, four experiments were performed, resulting in the indicated standard deviations. The survival rates were determined relative to control sister genotypes in the respective crosses. Total number of control genotype offspring: A: 137, B: 326, C: 247, D: 214, E: 309, F: 268.

Label:	Genotypes/Heat shock (HS) timing:
A	*y w hs-flp/[y w or Y]; UAS-dmyc*^{132}*/+; actin>CD2>GAL4 UAS-GFP dmax*^{1}*/dmax*^{1} HS 2-3 d AED
B	*y w hs-flp/[y w or Y]; UAS-dmyc*^{132}*/+; actin>CD2>GAL4 UAS-GFP dmax*^{1}*/dmax*^{1} HS 3-4 d AED
C	*y w hs-flp/[y w or Y]; UAS-dmyc*^{132}*/+; actin>CD2>GAL4 UAS-GFP dmax*^{1}*/dmax*^{1} no HS
D	*y w hs-flp/[y w or Y]; UAS-dmyc*^{132}*/+; actin>CD2>GAL4 UAS-GFP dmax*^{1}*/+* HS 2-3 d AED
E	*y w hs-flp/[y w or Y]; UAS-dmyc*^{132}*/+; actin>CD2>GAL4 UAS-GFP dmax*^{1}*/+* HS 3-4 d AED
F	*y w hs-flp/[y w or Y]; UAS-dmyc*^{132}*/+; actin>CD2>GAL4 UAS-GFP dmax*^{1}*/+* no HS

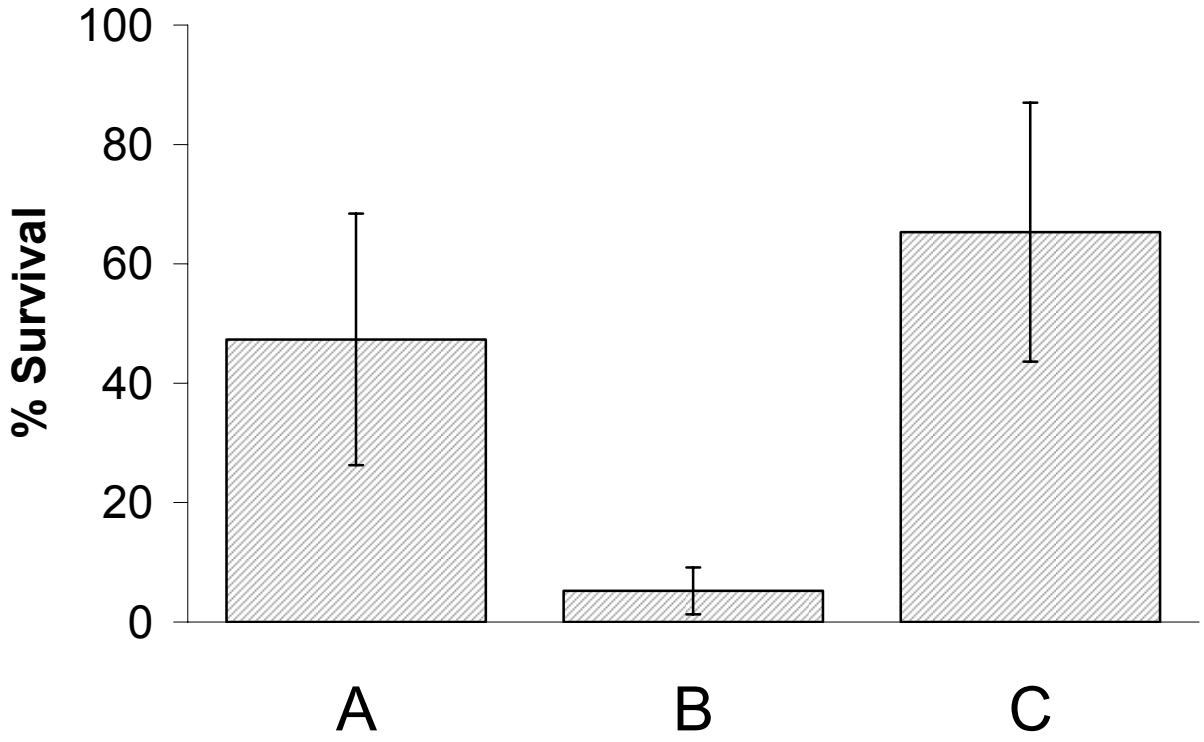

Figure 49
Overexpression of *UAS-dmyc* kills *dmax*^{1} larvae within 2 d after the heat shock. The chart depicts the survival of *dmax*^{1} and *dmax*^{1}/+ larvae at 5 d AED, after a heat shock was given at 3 d AED. For A and B, four experiments were performed, for C, three experiments were performed. The error bars indicate standard deviations. The survival rates were determined relative to control sister genotypes in the respective crosses. Total number of control genotype offspring: A: 325, B: 280, C: 205.

Label:	Genotypes/Heat shock (HS) timing:
A	*y w hs-flp/[y w or Y]; actin>CD2>GAL4 UAS-GFP dmax*^{1}*/dmax*^{1} HS 3 d AED
B	*y w hs-flp/[y w or Y]; UAS-dmyc*^{132}*/+; actin>CD2>GAL4 UAS-GFP dmax*^{1}*/dmax*^{1} HS 3 d AED
C	*y w hs-flp/[y w or Y]; UAS-dmyc*^{132}*/+; actin>CD2>GAL4 UAS-GFP dmax*^{1}*/+* HS 3 d AED

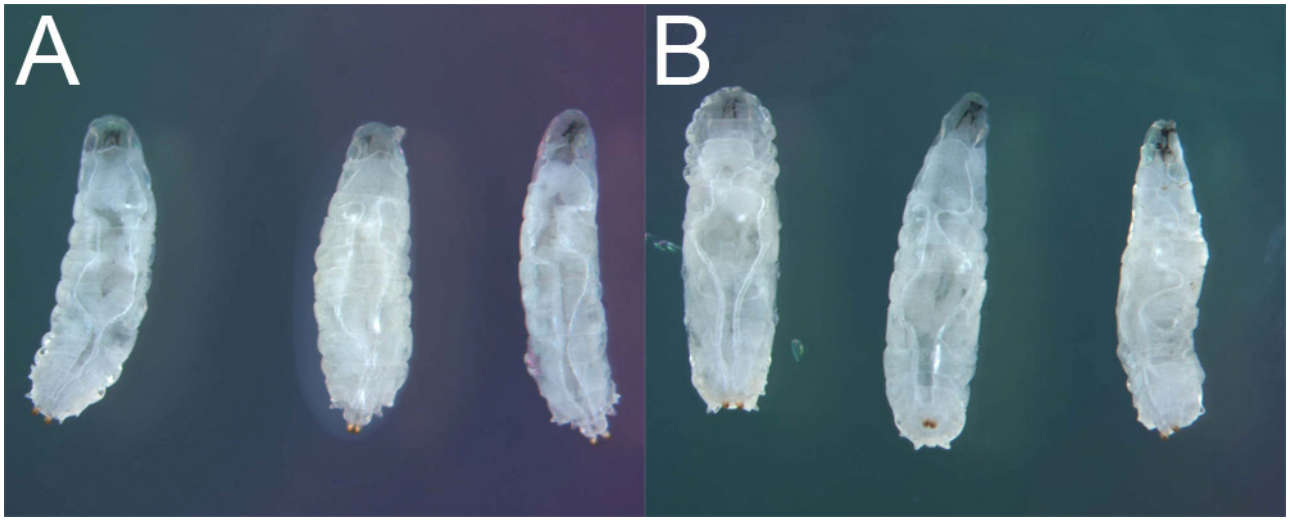

Figure 50a
dmax^{1}/+ larvae undergo the L2-L3 molt without problems also when *UAS-dmyc* is expressed (A). The picture shows L3 larvae that were collected at 4 d AED, after a heat shock was given at 2 d AED.

Label:	Genotypes/Heat shock (HS) timing:
A	*y w hs-flp/[y w or Y]; UAS-dmyc*^{132}*/+; actin>CD2>GAL4 UAS-GFP dmax*^{1}*/+* HS 2 d AED
B	*y w hs-flp/[y w or Y]; actin>CD2>GAL4 UAS-GFP dmax*^{1}*/+* HS 2 d AED

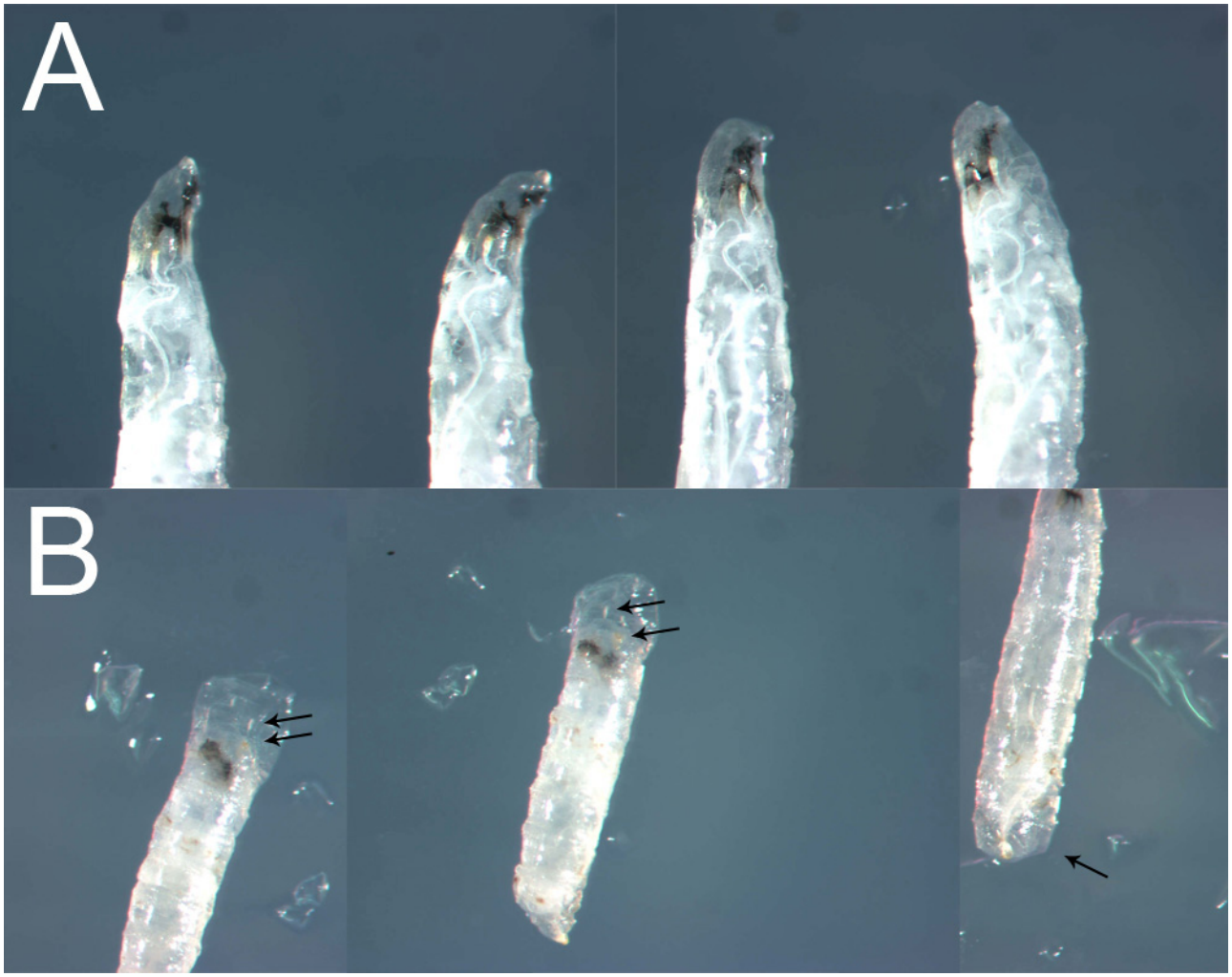

Figure 50b
dmax^{1} larvae die during the L2-L3 molt when *UAS-dmyc* is expressed. The picture shows larvae that were collected at 4 d AED, after a heat shock was given at 2 d AED. Whereas control *dmax*^{1} larvae have normally undergone the L2-L3 transition (A), *dmax*^{1} larvae in which *UAS-dmyc* was expressed have died with molting phenotypes (B). The larvae have an L2 and an L3 cuticle (visible where the L2 cuticle has detached from the L3 cuticle). In the left and the middle larva, two sets of anterior spiracles are visible (indicated with arrows). In the right larva, the L2 cuticle is detached from the L3 cuticle near the posterior spiracles (arrow).

Label:	Genotypes/Heat shock (HS) timing:
A	*y w hs-flp/[y w or Y]; actin>CD2>GAL4 UAS-GFP dmax*^{1}*/dmax*^{1} HS 2 d AED
B	*y w hs-flp/[y w or Y]; UAS-dmyc*^{132}*/+; actin>CD2>GAL4 UAS-GFP dmax*^{1}*/dmax*^{1} HS 2 d AED

In the experiments where we had overexpressed *dmyc* under control of *GMR-GAL4* in the eye, we had shown that the strong eye phenotype caused by *dmax*-RNA*i* could be partially suppressed by *UAS-p35* (Figure 16). Therefore, we had concluded that the *dmax*-independent functions of *dmyc* that caused the eye phenotype were associated with apoptosis. We now tested whether the lethality which we observed in $dmax^1$ larvae when *dmyc* was overexpressed prior to the L2-L3 molt could be rescued by blocking apoptosis. We induced the expression of *UAS-dmyc* and *UAS-p35* at 3 d AED. Figure 51a shows that coexpression of *UAS-p35* could not rescue the lethality associated with the L2-L3 molt. We also checked whether escapers which had survived the molt would develop differently, when *UAS-p35* was coexpressed, but we could not detect a difference (Figure 51b).

For control purposes, we had also collected *y w hs-flp; UAS-dmyc*^{132}*/+; actin>CD2>GAL4 UAS-GFP* $dmax^1$*/UAS-p35* $dmax^1$ larvae which had been subjected to a heat shock at 4 d AED. To our great surprise, we found that these larvae had not undergone pupariation. At an age of 31 d AED, 15 out of 80 collected larvae were still alive and in the L3 stage. The rest of the larvae had died as L3. Figure 52 shows one of the living L3 larvae and one that had recently died (Figure 52 B, C). These larvae were bigger than $dmax^1$ larvae at an age of 9 d AED (shortly before a $dmax^1$ larva would pupariate), but smaller than wandering *y w* larvae (Figure 52 A). The surviving larvae were found on top of the food, feeding only occasionally. They showed slow movements and intermittent phases in which no movement occurred and the larvae appeared stiff. The body of the larvae had a taut appearance and was almost translucent, no fat body tissue was visible. Dissection of the larva depicted in Figure 52 B revealed that the fat body was extremely reduced in size and that the fat body cells were translucent (Figure 52 D). The salivary glands were present and looked normal. Figure 52 E shows three leg discs that had undergone fusion. The surfaces of the two hemispheres of the brain and the imaginal wing discs had a wrinkled appearance. The failure of the larvae to initiate pupariation is reminiscent of the phenotype of common domain *EcR* mutants (embryonic lethal mutants in which all EcR protein isoforms (EcR-A, EcR-B1, and EcR-B2) are inactivated) that are rescued into the third larval stage by heat shock dependent expression of *EcR-B2* (Li and Bender, 2000). Taken together with the molting phenotypes that are produced when *dmyc* is expressed in $dmax^1$ larvae prior to the L2-L3 molt, the findings above provide strong evidence that the overexpression of *dmyc* in $dmax^1$ larvae interferes with the systems that govern molting and metamorphosis, possibly by interfering directly with the ecdysone system.

We next took a closer look at the pupariation behavior of $dmax^1$/+ heterozygous larvae and $dmax^1$ homozygous larvae, with and without overexpression of *UAS-dmyc* or *UAS-p35* alone, or with co-overexpression of *UAS-dmyc* and *UAS-p35*. We again used the conditional overexpression system, inducing the expression of the transgenes with a 2 h heat shock at 4 d AED. Figure 53a shows that the formation of $dmax^1$/+ pupae was normal (the pupae were photographed at 8 d AED), regardless of the overexpression of *dmyc* and/or *p35*. Whereas the formation of the pupae was normal, both transgenes

caused pupal lethality. Figure 53b shows the *dmax*^{1} animals, photographed at 28 d AED. Again, the co-overexpression of *dmyc* and *p35* had blocked pupariation and resulted in long-lived L3 larvae of which some were still alive at 28 d AED (Figure 53b D). Overexpression of *p35* alone resulted in the formation of pupae which looked similar to *dmax*^{1} pupae (Figure 53b C), displaying in most cases no eversion of the anterior spiracles. Interestingly, the overexpression of *dmyc* alone resulted in pupae that did differ from the shape of *dmax*^{1} pupae (Figure 53b B). Many of these pupae had not retracted the mouth hook and did not show a proper barrel-like shape, rather being bent and flattened in the head region. Even though pupariation seems to have been aberrant, these animals had clearly hardened larval cuticle and apolysis had taken place.

We also determined the timing of pupariation for the 4 genotypes (Figure 53c). Clearly, the overexpression of *dmyc* resulted in a delay in pupariation. Whereas most *dmax*^{1} larvae that did not express any of the transgenes had pupariated in the time between 8 d AED and 11 d AED, less than 30% of the *dmax*^{1} larvae that overexpressed *dmyc* had pupariated until day 11 AED and some even only pupariated in the time between 14 d AED and 20 d AED. This finding, taken together with aberrant morphology of the resulting pupae is reminiscent of certain classes of *EcR* mutants (Bender et al., 1997), providing further evidence that the overexpression of *dmyc* in *dmax*^{1} mutants interferes with the ecdysone system.

dmax^{1} larvae which overexpress *p35* were even more delayed than *dmax*^{1} larvae which overexpress *dmyc*, and 40% of the larvae did never appear as pupae. While most of these larvae had died, 5 of 118 larvae were found to be alive at 20 d AED, none at 28 d AED. This indicates that overexpression of *UAS-p35* alone is sufficient to delay the pupariation of *dmax*^{1} larvae or even block it to a certain extent.

Co-overexpression of *dmyc* and *p35* resulted in a strong block of pupariation: less than 20% of the larvae ever reached the pupal stage. At 20 d AED, only few dead larvae were found. In the time between 20 d AED and 28 d AED, most larvae died. At 28 d AED, 21 of 207 larvae were still alive.

These findings show that both *dmyc* and *p35* did modify the timing of pupariation if expressed alone. Expressed together, the two transgenes seemed to act synergistically, imposing a very strong block of pupariation. Interestingly, the strong block of pupariation did go along with longer survival of the non-pupariating larvae. Regarding *dmyc*, the data presented so far indicate strongly that in *dmax*^{1} mutants, overexpression of *dmyc* interferes with the systems that govern molting and metamorphosis. It is not clear why these effects were only seen in *dmax*^{1} homozygous larvae and not in heterozygous larvae, but of course this means that the described effects are *dmax*-independent. Regarding *p35*, it is conceivable that a block of apoptosis might interfere with metamorphosis, since apoptosis plays an important role in the process. However, the exact nature of the interaction between *dmyc* and *p35* remains unclear.

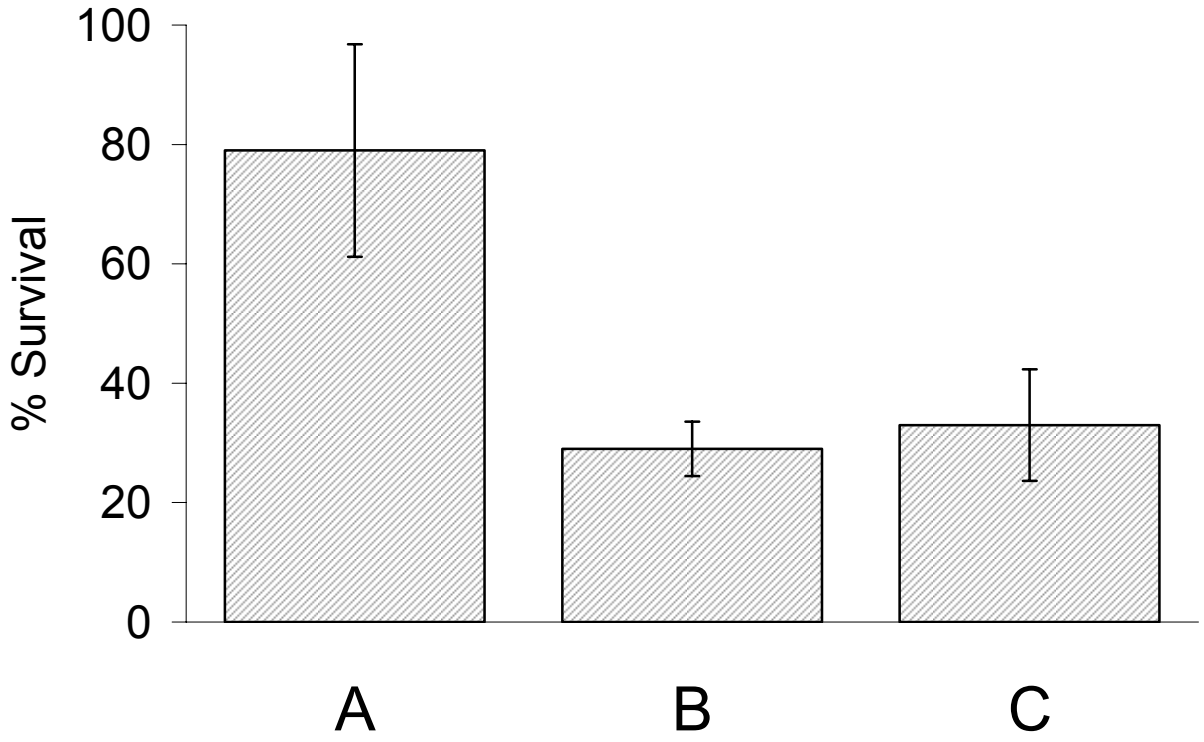

Figure 51a
Suppression of apoptosis by the expression of *UAS-p35* cannot rescue the lethality associated with the overexpression of *dmyc* in *dmax*^{1} larvae. The survival of the larvae was determined at 5 d AED, after administration of a heat shock at 3 d AED. Four experiments were performed per genotype. The error bars indicate standard deviations. The survival rates were determined relative to control sister genotypes in the respective crosses. Total number of control genotype offspring: A: 280, B: 274, C: 349.

Label:	Genotypes/Heat shock (HS) timing:
A	*y w hs-flp/[y w or Y]; actin>CD2>GAL4 UAS-GFP dmax*^{1}*/dmax*^{1} HS 3 d AED
B	*y w hs-flp/[y w or Y]; UAS-dmyc*^{132}*/+; actin>CD2>GAL4 UAS-GFP dmax*^{1}*/dmax*^{1} HS 3 d AED
C	*y w hs-flp/[y w or Y]; UAS-dmyc*^{132}*/+; actin>CD2>GAL4 UAS-GFP dmax*^{1}*/UAS-p35 dmax*^{1} HS 3 d AED

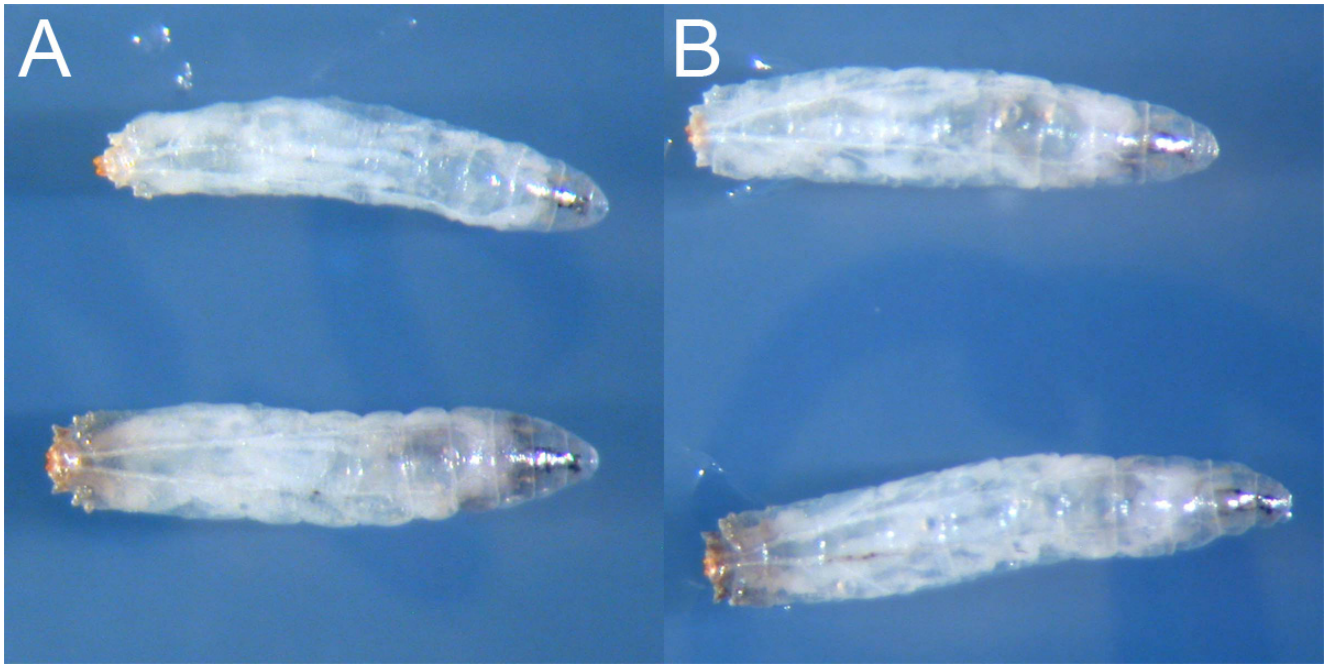

Figure 51b
At 7 d AED, *dmax*^{1} larvae that express *dmyc* (A) or *dmyc* and *p35* (B) since day 3 AED - i.e. escapers that survived the L2 L3 molt - have developed normally and do not differ in phenotype from regular *dmax*^{1} larvae.

Label:	Genotypes/Heat shock (HS) timing:
A	*y w hs-flp/[y w or Y]; UAS-dmyc*^{132}*/+; actin>CD2>GAL4 UAS-GFP dmax*^{1}*/dmax*^{1} HS 3 d AED
B	*y w hs-flp/[y w or Y]; UAS-dmyc*^{132}*/+; actin>CD2>GAL4 UAS-GFP dmax*^{1}*/UAS-p35 dmax*^{1} HS 3 d AED

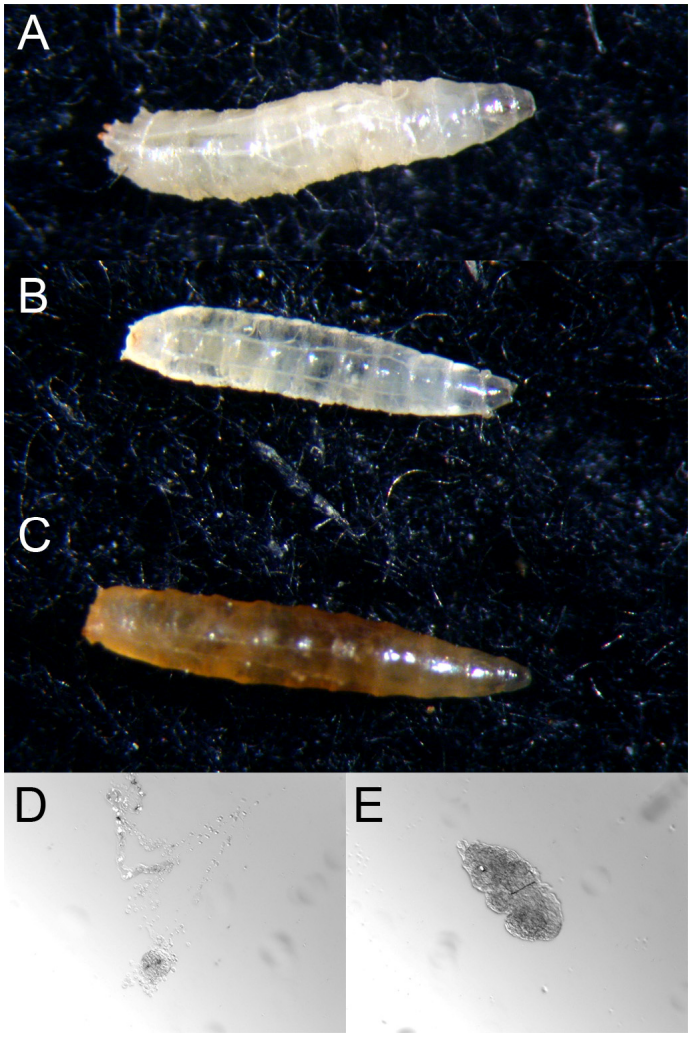

Figure 52
dmax^{1} larvae which coexpress *UAS-dmyc* and *UAS-p35* do not pupariate, but survive for extended periods as L3 larvae. The pictures show a *y w* larva at 5 d AED in the wandering stage (A) and two *y w hs-flp/[y w or Y]; UAS-dmyc*^{132}*/+; actin>CD2>GAL4 UAS-GFP UAS-p35 dmax*^{1}*/dmax*^{1} larvae at 33 d AED (B, C). The larva in C had died at 32 d AED, whereas the larva in B was still alive at the time the picture was taken. The transparent look of the larva in picture B is due to a largely dissolved fat body (D). Picture E shows leg discs of the larva in picture B which have fused, presumably due to ongoing metamorphosis.

Label:	Description:
A	*y w* larva, age: 5 d AED
B, C	*y w hs-flp/[y w or Y]; UAS-dmyc*^{132}*/+; actin>CD2>GAL4 UAS-GFP dmax*^{1}*/UAS-p35 dmax*^{1} larvae, HS 4 d AED, age: 33 d AED
D	fat body of larva B
E	fused leg discs of larva B

Figure 53a
dmax^{1}/+ larvae pupariated normally also when *UAS-dmyc*, *UAS-p35* or both are expressed. The presence of *p35* frequently led to aberrant metamorphosis. The expression of the indicated transgenes was initiated with a heat shock at 4 d AED. The pupae were photographed at 8 d AED.

Label:	Genotypes/Heat shock (HS) timing/age at collection:
A	*y w hs-flp/[y w or Y]; actin>CD2>GAL4 UAS-GFP dmax*^{1}*/+* HS 4 d AED, age: 8 d AED
B	*y w hs-flp/[y w or Y]; UAS-dmyc*^{132}*/+; actin>CD2>GAL4 UAS-GFP dmax*^{1}*/+* HS 4 d AED, age: 8 d AED
C	*y w hs-flp/[y w or Y]; actin>CD2>GAL4 UAS-GFP dmax*^{1}*/UAS-p35* HS 4 d AED, age: 8 d AED
D	*y w hs-flp/[y w or Y]; UAS-dmyc*^{132}*/+; actin>CD2>GAL4 UAS-GFP dmax*^{1}*/UAS-p35* HS 4 d AED, age: 8 d AED

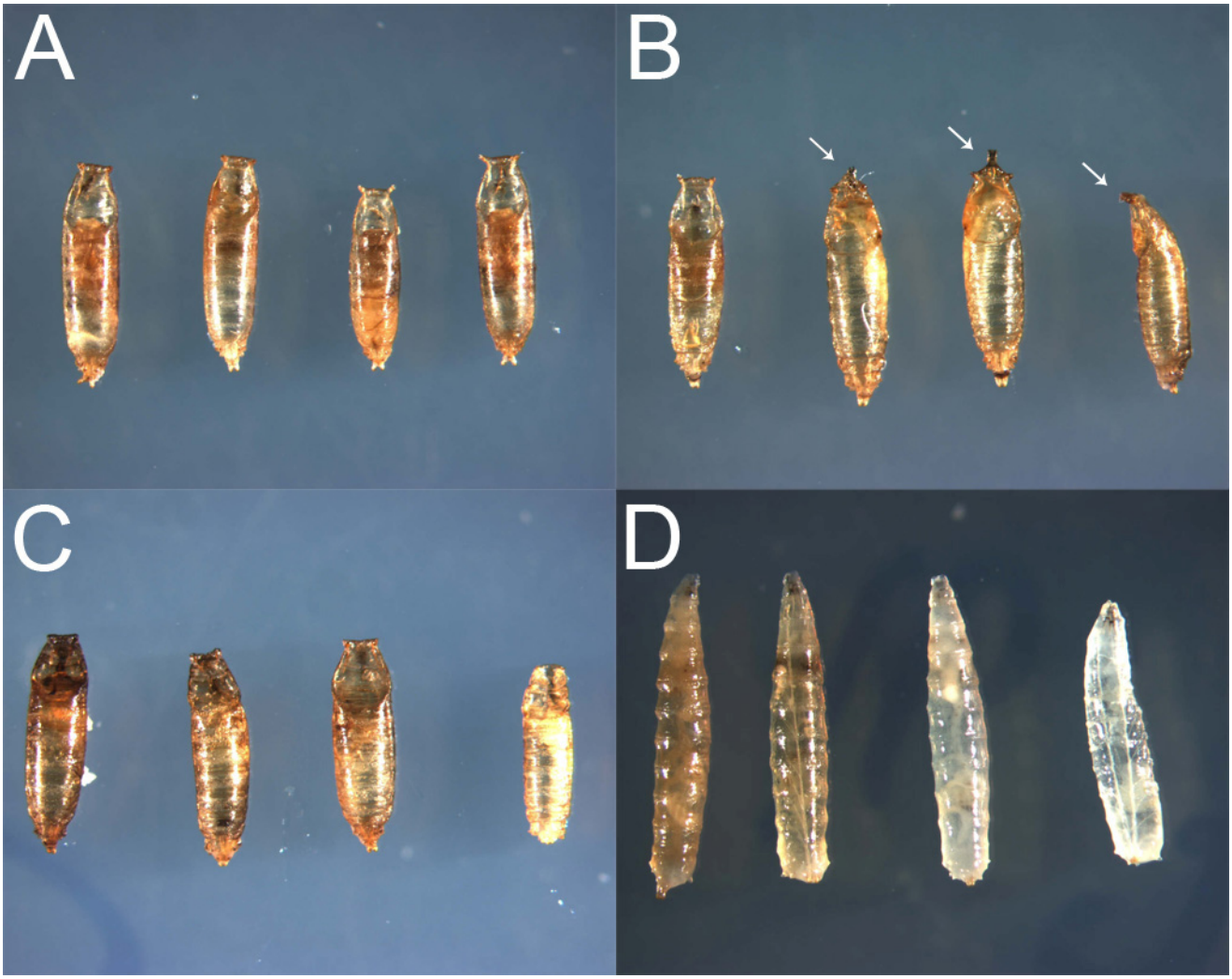

Figure 53b
Phenotype of *dmax*^{1} animals in which expression of *UAS-dmyc* (B), *UAS-p35* (C) or both (D) was initiated at 4 d AED, photographed at 28 d AED. Whereas expression of *UAS-p35* did not change the phenotype of *dmax*^{1} pupae, expression of *UAS-dmyc* led to malformed pupae in which frequently the mouth hook had not been properly retracted (B, see arrows). Coexpression of *UAS-dmyc* and *UAS-p35* inhibited the formation of pupae in most animals (D). Picture D shows 3 dead larvae and one larva that was still alive at 28 d AED.

Label:	Genotypes/Heat shock (HS) timing/age at collection:
A	*y w hs-flp/[y w or Y]; actin>CD2>GAL4 UAS-GFP dmax*^{1}*/ dmax*^{1} HS 4 d AED, age: 28 d AED
B	*y w hs-flp/[y w or Y]; UAS-dmyc*^{132}*/+; actin>CD2>GAL4 UAS-GFP dmax*^{1}*/dmax*^{1} HS 4 d AED, age: 28 d AED
C	*y w hs-flp/[y w or Y]; actin>CD2>GAL4 UAS-GFP dmax*^{1}*/UAS-p35 dmax*^{1} HS 4 d AED, age: 28 d AED
D	*y w hs-flp/[y w or Y]; UAS-dmyc*^{132}*/+; actin>CD2>GAL4 UAS-GFP dmax*^{1}*/UAS-p35 dmax*^{1} HS 4 d AED, age: 28 d AED

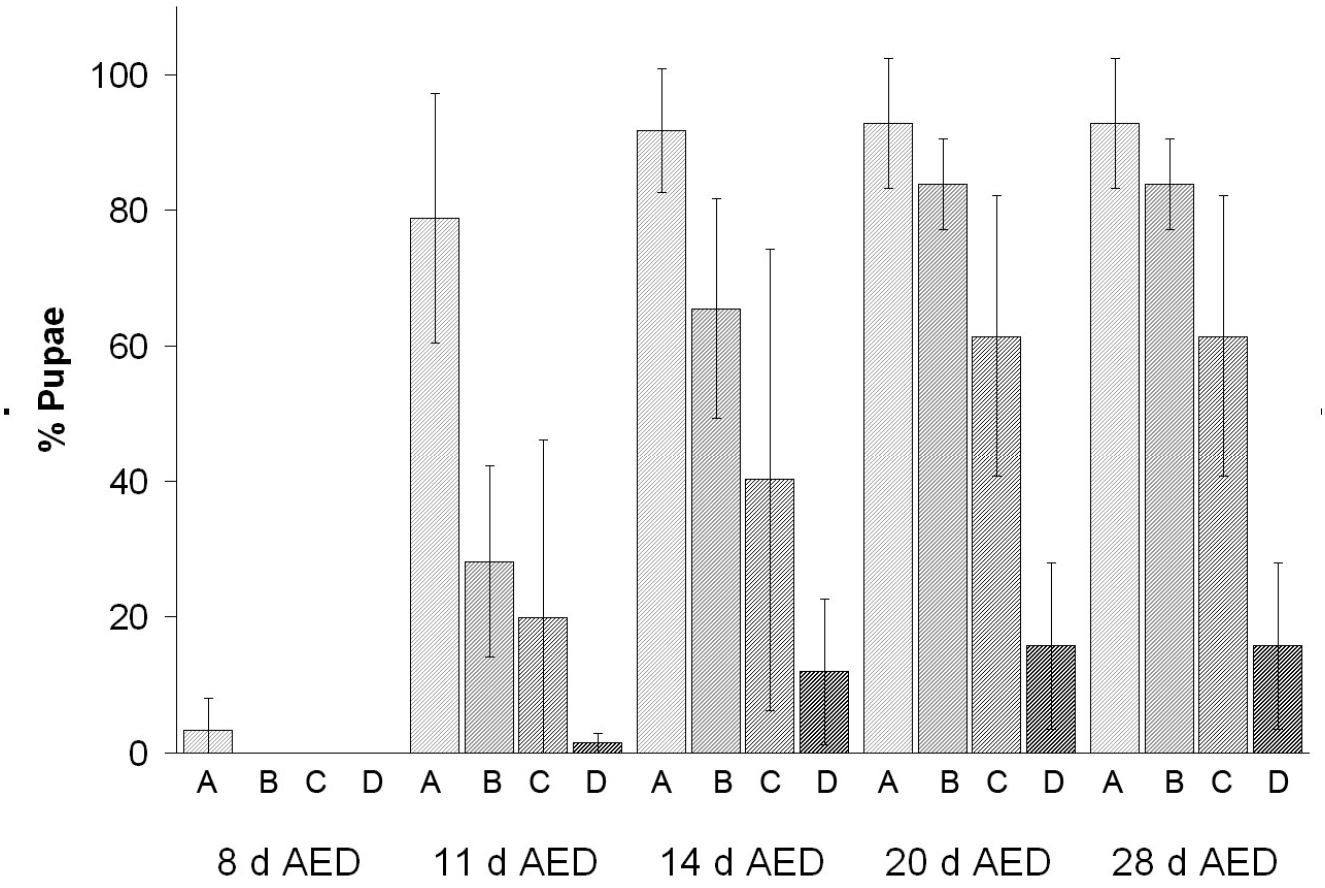

Figure 53c
Timing of pupariation of *dmax*^{1} larvae in which *UAS-dmyc*, *UAS-p35* or both were expressed. Both *UAS-dmyc* and *UAS-p35* caused a delay in pupariation (B, C), but a majority of the larvae did pupariate. When *UAS-p35* and *UAS-dmyc* were coexpressed (D), less than 20% of the larvae underwent pupariation. Total number of experiments/total number of animals: A: 3/110, B: 6/198, C: 3/118, D: 5/207.

Label:	Genotypes/Heat shock (HS) timing:
A	*y w hs-flp/[y w or Y]; actin>CD2>GAL4 UAS-GFP dmax*^{1}*/ dmax*^{1} HS 4 d AED
B	*y w hs-flp/[y w or Y]; UAS-dmyc*^{132}*/+; actin>CD2>GAL4 UAS-GFP dmax*^{1}*/dmax*^{1} HS 4 d AED
C	*y w hs-flp/[y w or Y]; actin>CD2>GAL4 UAS-GFP dmax*^{1}*/UAS-p35 dmax*^{1} HS 4 d AED
D	*y w hs-flp/[y w or Y]; UAS-dmyc*^{132}*/+; actin>CD2>GAL4 UAS-GFP dmax*^{1}*/UAS-p35 dmax*^{1} HS 4 d AED

Since the data presented so far suggested that the overexpression of *dmyc* in *dmax*^{1} larvae interferes with ecdysone signaling, we tested whether we could overcome the block of pupariation that occurred when *dmyc* and *p35* were coexpressed in *dmax*^{1} larvae by feeding them ecdysone. We again induced the overexpression of *dmyc* and *p35* at 4 d AED, knowing that this would block the formation of pupae in *dmax*^{1} larvae. At 6 d AED, we put the larvae on yeast paste that contained 1 mg/ml 20-hydroxyecdysone or on control yeast without ecdysone. Figure 54 shows that we could indeed induce pupariation in *dmax*^{1} larvae which co-overexpress *dmyc* and *p35* when they were kept on ecdysone-supplemented food (Figure 54 B). However, pupariation was aberrant and incomplete. Pupariation started at 10 d AED. The larvae clearly contracted and hardened their cuticle, and apolysis took place, but the process of the hardening and darkening of the cuticle was slower than in the controls. The resulting pupae were more elongated than normal pupae and did not retract the mouth hooks. Frequently, the cuticle around the tip of the larvae did not sclerotise at all. Feeding the larvae with 2 mg/ml ecdysone did not improve the rescue (data not shown). Ecdysone-feeding per se had no negative effects, since *dmax*^{1} control larvae that did not co-overexpress *dmyc* and *p35* did pupate normally in the presence of 20OH-ecdysone.

These findings provide strong evidence that overexpression of *dmyc* in *dmax*^{1} larvae interferes with ecdysone signaling. While it is possible that supplementation of ecdysone might rescue a partial defect in the signaling cascade downstream of the ecdysone receptors, it is more likely that an upstream defect can be rescued by ecdysone feeding. Therefore, all the data gathered so far would be compatible with a model in which overexpression of *dmyc* in *dmax*^{1} larvae blocks the production of ecdysone.

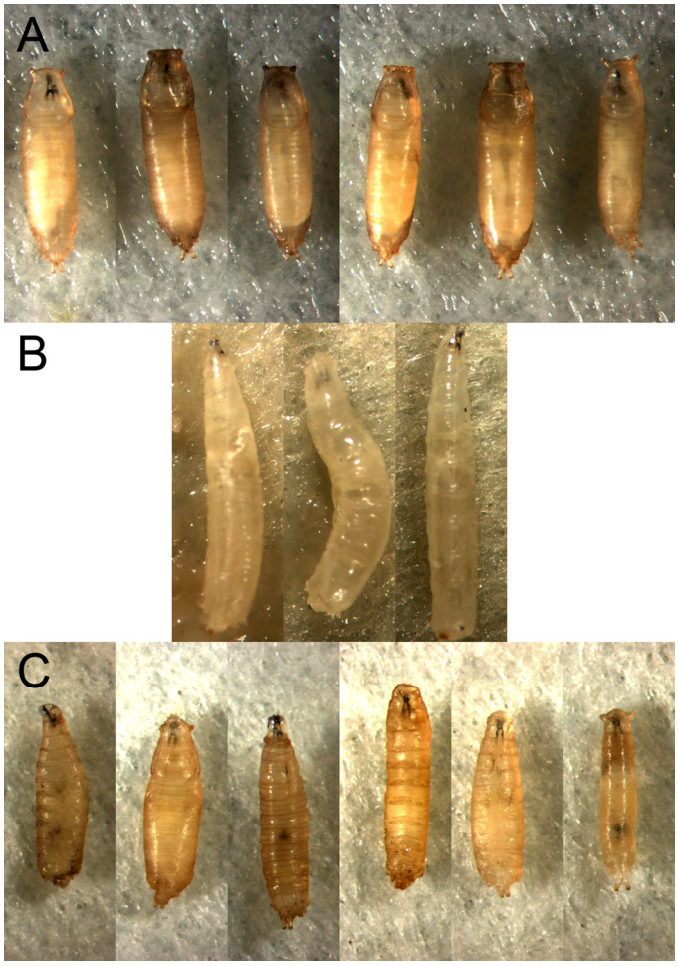

Figure 54
20-hydroxyecdysone rescues the pupariation block caused by the coexpression of *UAS-dmyc* and *UAS-p35* in *dmax*^{1} larvae. Expression of the indicated transgenes was initiated by a heat shock at 4 d AED. The larvae were transferred onto yeast paste containing 1 mg/ml 20-hydroxyecdysone (A, C) or 0 mg/ml 20-hydroxyecdysone (B) at 6 d AED. The presence of ecdysone induced the pupariation of *y w hs-flp/[y w or Y]; UAS-dmyc*^{132}*/+; actin>CD2>GAL4 UAS-GFP dmax*^{1}*/UAS-p35 dmax*^{1} larvae (C), which did not pupariate on unsupplemented medium (B). However, the rescue was partial: the emerging pupae were malformed, frequently displayed incomplete body contraction and rounding, failed to retract the mouth hooks and incompletely sclerotised the cuticular region around the mouth hook. A animals were photographed at 10 d AED, B and C animals were photographed at 13 d AED.

Label:	Genotypes/Ecdysone treatment:
A	*y w hs-flp/[y w or Y]; actin>CD2>GAL4 UAS-GFP dmax*^{1}*/dmax*^{1} 1 mg/ml 20-hydroxyecdysone at 6 d AED
B	*y w hs-flp/[y w or Y]; UAS-dmyc*^{132}*/+; actin>CD2>GAL4 UAS-GFP dmax*^{1}*/UAS-p35 dmax*^{1} 0 mg/ml 20-hydroxyecdysone at 6 d AED
C	*y w hs-flp/[y w or Y]; UAS-dmyc*^{132}*/+; actin>CD2>GAL4 UAS-GFP dmax*^{1}*/UAS-p35 dmax*^{1} 1 mg/ml 20-hydroxyecdysone at 6 d AED

2.8. Analysis of target gene expression in *dmax*^{1} larvae that overexpress *dmyc*

The genetic analysis presented so far provided strong evidence that *dmyc* is still partly functional in the absence of *dmax*, contradicting the current model. In order to gain more insight into the nature of these *dmax*-independent functions of *dmyc*, we decided to compare the expression levels of selected target genes in response to *dmyc* overexpression, both in *dmax*^{1} homozygous larvae and *dmax*^{1}/+ heterozygotes. As in the *dmyc* overexpression experiments shown before, we used the *act>CD2>GAL4* heat shock inducible expression system to initiate the overexpression of *UAS-dmyc*^{132}. We induced the expression of *dmyc* by a 2 h heat shock at 37° C in *dmax*^{1} larvae at 5 d AED and in *dmax*^{1}/+ larvae at 4 d AED. These induction times ensured that the larvae of both genotypes were in the third larval stage both at the time of *dmyc* induction and at the time when the larvae were collected (10 h later). *dmax*^{1} and *dmax*^{1}/+ larvae that did not carry the *UAS-dmyc*^{132} transgene, but were subjected to the same heat shock, served as controls. 10 h after the heat shock, we collected the larvae. We chose a relatively short interval between induction and collection because we were interested in the direct consequences of *dmyc* on target gene expression. As additional genotypes, we collected *dmax*^{1} male larvae (at 5 d AED) and *y w* larvae (at 4 d AED). Immediately after the collection, we extracted total RNA from the larvae. We confirmed the integrity of the extracted total RNA on bioanalyzer chips and generated cDNA. Subsequently, we analyzed the expression of selected genes with qRTPCR assays.

Based on microarray analysis, a set of direct *dmyc* targets had been established previously (Hulf et al., 2005). In this study, most of the genes found to be regulated by *dmyc* contained E-boxes, with a strong preference for a localization of the E-box downstream of the promoter. We included two of these *dmyc*-regulated genes: *nnp1* and *CG5033*. Both of these genes contain a downstream E-box, and for both of the genes it had been shown that their expression depends on the presence of the E-box (Hulf et al., 2005). The ability of these genes to be reliably upregulated by *dmyc* overexpression and downregulated by loss of *dmyc* had been confirmed by qRTPCR assays and luciferase reporter transgenes (Hulf et al., 2005, M. Furrer, personal communication). We deemed it unlikely that these E-box containing genes (or any of the E-box containing genes found in the microarray analysis) would still respond to overexpression of *dmyc* in the absence of *dmax*, since their expression most likely depends on dMyc/dMax heterodimers. Furthermore, we have shown that also the truncated form of *dmyc* which is expressed in *dm*^{2} mutants retains growth functions, making it unlikely that the *dmax*-independent functions of *dmyc* would require dimerization of Myc with an unknown protein and binding to E-boxes.

The microarrays used in the analysis mentioned above did only include RNA polymerase II-transcribed protein-coding genes, but not RNA polymerase I- and RNA polymerase III-transcribed RNA genes. Since it had been shown that Myc also controls the transcription of RNA polymerase III-dependent small RNA genes (Gomez-Roman et al., 2003; Grewal et al., 2005) in mammals and of

RNA polymerase I-dependent ribosomal RNA (Grandori et al., 2005; Grewal et al., 2005) in mammals and in *Drosophila*, we included *rRNA*, *5sRNA* and *tRNA(Leu)* in our analysis.

Two further small RNA genes were included in the analysis: *snoRNA U3* and *snoRNA 46*. We speculated that *dmyc* might be implicated in the biogenesis of snoRNAs, since first, many of the target genes found in Hulf et al. (2005) have a function in the nucleolus, second, *symplekin,* a gene found to interact with *dmyc* (C. Li, unpublished), was also shown to interact with snoRNAs (Kolev and Steitz, 2005), and third, *dmyc* was shown to interact with *reptin* and *pontin* (Bellosta et al., 2005). *snoRNA U3* had been shown to bind the human orthologs of *reptin* and *pontin* and its accumulation had been shown to be dependent on these proteins (Watkins et al., 2004). In yeast, the biogenesis of both *snoRNA U3* and *snoRNA 46* had been shown to depend on depend on the yeast orthologs of *reptin* and *pontin*.

Figure 55 shows the expression levels of *dmyc*, *dmax*, *nnp1*, *CG5033*, *rRNA*, *5sRNA*, *snoRNA U3* and *snoRNA 46*, in $dmax^1$ and $dmax^1$/+ larvae, with and without heat shock-induced ectopic expression of *dmyc*. For every genotype, two independent RNA extractions had been performed. The levels were normalized against the reference gene *actin5C* and charted relative to their expression levels in the *y w hs-flp; actin>CD2>GAL4 UAS-GFP* $dmax^1$/+ genotype (genotype C).

The induction of *dmyc* was efficient, since *dmyc* levels were more than ten-fold higher in the genotypes containing *UAS-*$dmyc^{132}$ than in the control genotypes. Interestingly, compared to $dmax^1$/+ larvae, *dmyc* levels were tripled in $dmax^1$ homozygous larvae even in the absence of *UAS-*$dmyc^{132}$. This suggests that the ability of dMyc to (auto)repress its own transcription, which has been documented for *Drosophila* and vertebrate *myc* genes (Penn et al., 1990; Goodliffe et al., 2005), depends on association with Max and hence cannot take place in $dmax^1$ larvae.

dmax was absent in $dmax^1$ larvae, the small remaining signals were shown to be a consequence of unspecific amplification products (see Figure 25).

The E-box dependent *dmyc* target genes *nnp1* and *CG5033* were strongly upregulated by overexpression of *dmyc* in $dmax^1$/+ larvae, but not so in $dmax^1$ homozygotes. In $dmax^1$ larvae, *nnp1* levels were lower upon overexpression of *dmyc* (a result that could not be confirmed in the second qRTPCR experiment, see Figure 56), whereas *CG5033* levels were slightly upregulated. However, these effects were small in comparison to the strong effect of *dmyc* in heterozygotes. We concluded that most likely, *dmyc* overexpression can no longer upregulate *nnp1* or *CG5033* in the absence of *dmax*.

We monitored *rRNA* with a primer pair specific to an internal transcribed spacer region (ITS1) which is excised from the maturing rRNA, thus measuring the production of rRNA, and not total accumulated levels. In $dmax^1$ larvae, transcription levels were lower than in $dmax^1$/+ larvae. In both genotypes, overexpression of *dmyc* had no effect.

However, we found strong upregulation of *5sRNA* and *snoRNA U3* levels in *dmax*^{1} larvae upon overexpression of *dmyc*. In heterozygous larvae, *dmyc* had no effect on these small RNAs. Also *snoRNA 46* levels were upregulated in *dmax*^{1} larvae, but only to the expression level shown by *snoRNA 46* in *dmax*^{1}/+ larvae. For *snoRNA 46* as well, overexpression of *dmyc* had no effect in *dmax*^{1}/+ larvae. These data provide evidence that *dmyc* is able to regulate the levels of the small RNA genes *5sRNA*, *snoRNA U3*, and *snoRNA 46* in a *dmax*-independent fashion.

To confirm these findings, we performed a second qRTPCR experiment, using a third independent RNA sample for the *y w hs-flp; actin>CD2>GAL4 UAS-GFP dmax*^{1}*/dmax*^{1} and the *y w hs-flp; UAS-dmyc*^{132}*/+; actin>CD2>GAL4 UAS-GFP dmax*^{1}*/dmax*^{1} genotypes. Additionally, we included two *y w* RNA samples and two RNA samples of *dmax*^{1} male larvae that had not been subjected to the heat shock. Figure 56 shows that for all tested genes, the heat shocked *y w hs-flp; actin>CD2>GAL4 UAS-GFP dmax*^{1}*/dmax*^{1} larvae showed the same expression levels as the *y w/Y, y+; dmax*^{1} control. Endogenous *dmyc* levels were 2.5-fold upregulated in these *dmax*^{1} genotypes, similar to the first experiment. Again, overexpression of *dmyc* in the *dmax*^{1} larvae had no effect on the expression of *nnp1, CG5033* and *rRNA*. In all four *dmax*^{1} samples, *rRNA* levels were lower than in the *y w* control samples, as they were lower in comparison to *dmax*^{1}/+ larvae in the first experiment. Strikingly, the levels of *5sRNA*, *snoRNA U3*, *snoRNA 46* and of *tRNA(Leu)* (a gene that was not included in the first qRTPCR experiment) were strongly upregulated in *dmax*^{1} larvae upon overexpression of *dmyc*, but not so in *y w* larvae. Without overexpression of *dmyc*, the levels of *snoRNA U3* and of *snoRNA 46* were lower in *dmax*^{1} larvae than in the *y w* control, as they were lower than in *dmax*^{1}/+ larvae in the first experiment. The levels for *5sRNA* and *tRNA(Leu)* were as high in the *dmax* larvae as in the *y w* controls.

Taken together, these data provide strong evidence that *dmyc* is capable of regulating the levels of small RNA genes in the absence of *dmax*. It is presently not clear why the overexpression of *dmyc* resulted in such a strong increase in the levels of these genes in *dmax*^{1} larvae, but not in *dmax*^{1}/+ larvae. One explanation for this finding might be that systems that regulate protein biosynthesis are affected by the loss of *dmax*-dependent functions in *dmax*^{1} larvae, resulting in a different outcome when *dmyc* is overexpressed. However, the finding that *dmyc* can regulate the levels of small RNA genes in the absence of *dmax* provides an intriguing explanation for the *dmax*-independent growth functions of *dmyc* described in this study, since the function of these genes is crucial for protein biosynthesis.

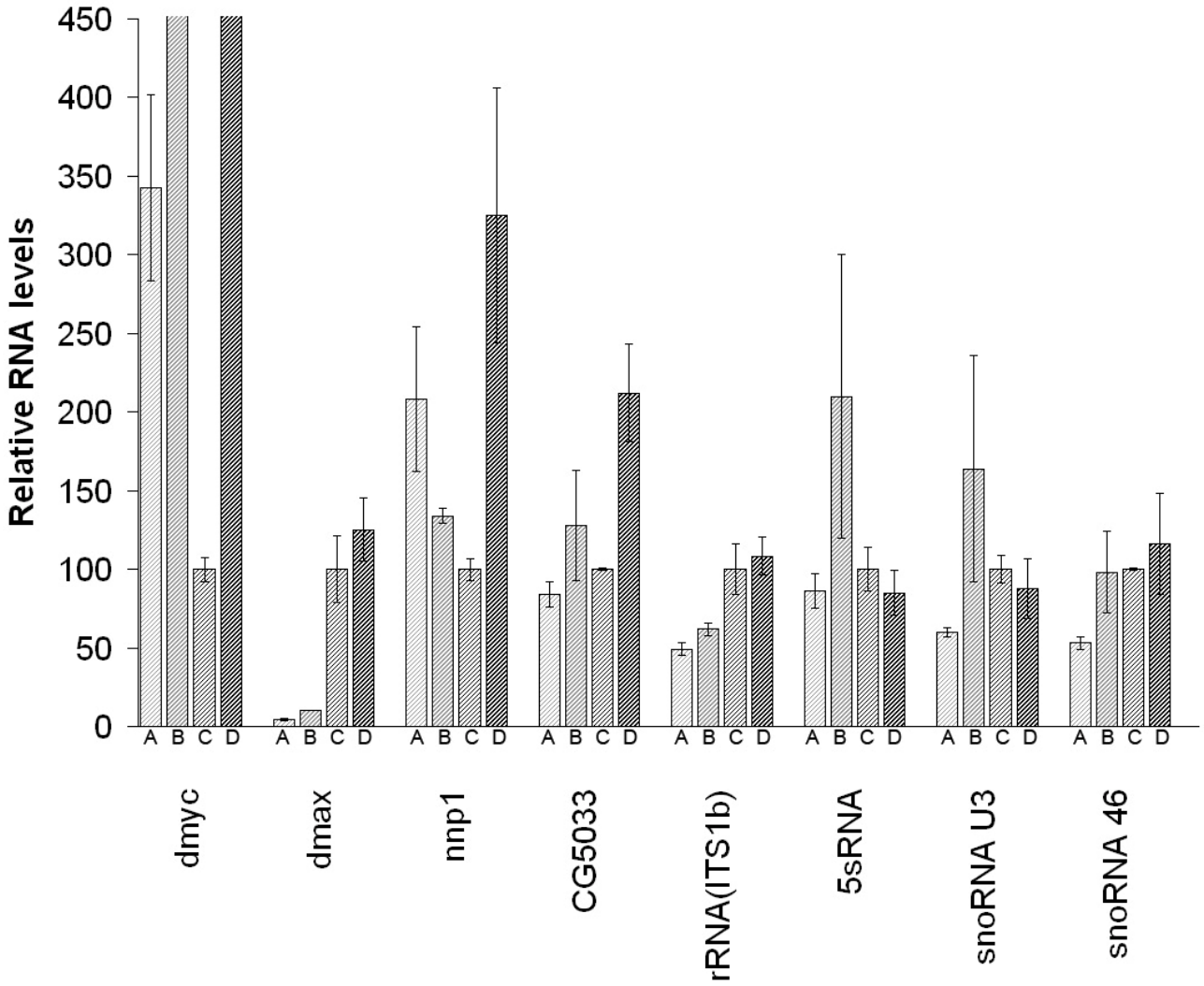

Figure 55
dmyc fails to upregulate *nnp1* and *CG5033* levels in *dmax*^{1} larvae, but surprisingly upregulates *5sRNA, snoRNA U3* and *snoRNA 46* levels. Transcript levels of *dmyc, dmax, nnp1, CG5033, rRNA, 5sRNA, snoRNA U3,* and *snoRNA46* were determined with qRTPCR in larvae of the indicated genotypes. The chart shows average values and the standard deviations for the indicated transcript levels, relative to the reference gene *actin5C*. The values are indicated normalized to the values of the C genotype. Two RNA samples were used per genotype, and 3 PCR reactions were performed per assayed transcript.

Label:	Genotypes/HS treatment/age at collection:
A	*y w hs-flp/[y w or Y]; actin>CD2>GAL4 UAS-GFP dmax*^{1}*/dmax*^{1} HS 5d AED, collection: 10 h post HS
B	*y w hs-flp/[y w or Y]; UAS-dmyc*^{132}*/+; actin>CD2>GAL4 UAS-GFP dmax*^{1}*/dmax*^{1} HS 5d AED, collection: 10 h post HS
C	*y w hs-flp/[y w or Y]; actin>CD2>GAL4 UAS-GFP dmax*^{1}*/+* HS 4d AED, collection: 10 h post HS
D	*y w hs-flp/[y w or Y]; UAS-dmyc*^{132}*/+; actin>CD2>GAL4 UAS-GFP dmax*^{1}*/+* HS 4d AED, collection: 10 h post HS

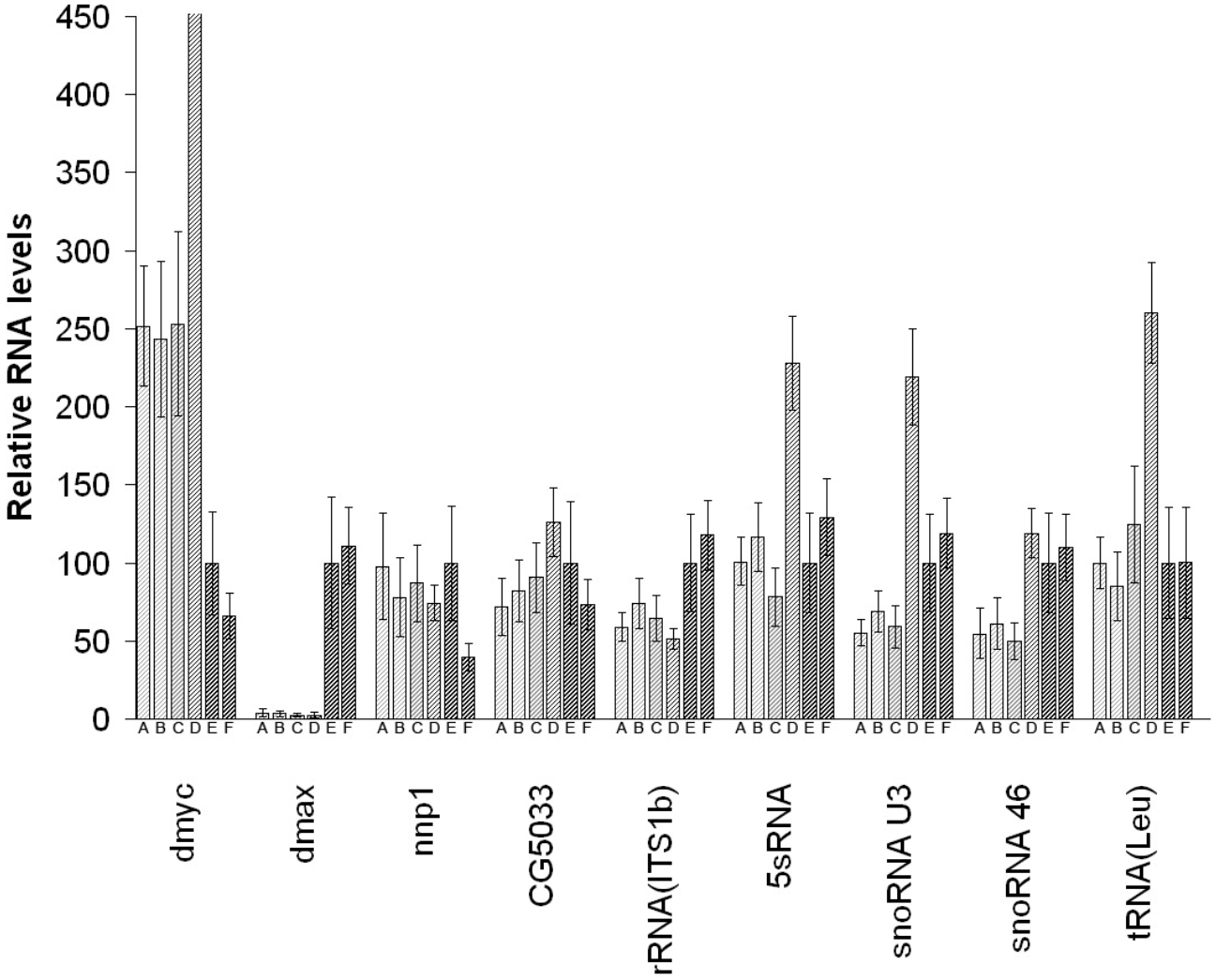

Figure 56
qRTPCR experiment, confirming the data presented in Figure 55. Transcript levels of *dmyc, dmax, nnp1, CG5033, rRNA, 5sRNA, snoRNA U3, snoRNA46* and *tRNA(Leu)* were determined with qRTPCR in larvae of the indicated genotypes. The chart shows average values and the standard deviations for the indicated transcript levels, relative to the reference gene *actin5C*. The indicated values are normalized against the values of the C genotype. One RNA samples was used per genotype, and 3 PCR reactions were performed per assayed transcript.

Label:	Genotypes/HS treatment/age at collection:
A, B	*y w/Y, y^{+}; dmax^{1}* no HS, collection: 5 d AED
C	*y w hs-flp/[y w or Y]; actin>CD2>GAL4 UAS-GFP dmax^{1}/dmax^{1}* HS 5d AED, collection: 10 h post HS
D	*y w hs-flp/[y w or Y]; UAS-dmyc^{132}/+; actin>CD2>GAL4 UAS-GFP dmax^{1}/dmax^{1}* HS 5d AED, collection: 10 h post HS
E, F	*y w* no HS, collection: 4 d AED

Discussion

In this study, we present an RNA*i* system that allows to create situations of low *dmax* levels (as they would be found in hypomorphic *dmax* mutants) and we report the generation of *dmax* null mutants. With both these tools, we conducted a detailed functional analysis of *dmax*. Together with already published null mutants of the other Max network members, *dmyc* and *dmnt* (Pierce et al., 2004; Loo et al., 2005), the *dmax* null mutants were a prerequisite for a rigorous functional analysis of the *Drosophila* Max network. The analysis proved fruitful and yielded a highly surprising result: We could show that an important part of the functions of *dmyc* do not require the presence of *dmax*. For these *dmax*-independent functions of *dmyc*, we present several lines of evidence, analyzing the consequences of both *dmyc* loss of function and *dmyc* overexpression in a variety of situations.
In the first part of this discussion, the phenotypes of *dmax*-RNA*i* and of the $dmax^{1}$ mutants and their similarity to known *dmyc* loss of function phenotypes will be discussed. In a second and third part, we will recapitulate and discuss the evidence for *dmax*-independent functions of *dmyc*.

1. Functional analysis of *dmax*

Based on the demonstrated physical interaction between dMax and dMyc, on dMax's ability to stimulate dMyc-dependent transcription (Gallant et al., 1996) and on the wealth of data from mammalian systems (see Introduction), we expected that a loss of *dmax* function should result in phenotypes similar to the ones seen with a loss of *dmyc* function. However, since we could also expect that a loss of *dmax* function would abrogate *dmnt* function, it was possible that the consequences of a loss of *dmax* would differ from the ones of a loss of *dmyc* function.
Using the dmax-*RNAi* system, we could indeed show that the loss of *dmax* phenocopies the loss of *dmyc*. Animals in which *dmax* levels were lowered by *dmax*-RNA*i* showed phenotypes that were similar to the phenotypes of dm^{P0} animals (flies that carry a hypomorphic mutation of *dmyc*). Like dm^{P0} flies, *dmax*-RNA*i* flies showed a reduced body weight (Figures 6, 31c). When *dmax* levels were ubiquitously reduced, or specifically reduced in bristle precursor cells, a marked decrease in bristle size resulted (Figures 7, 8), similar to the small bristle size observed in weak *dmyc* hypomorphic mutants (Johnston et al., 1999). A stronger reduction in *dmyc* levels, like in dm^{PG45} or dm^{PL35} animals, results in pupal lethality (Benassayag et al., 2005). Similarly, ubiquitous expression of three *dmax* dsRNA transgenes in wild type animals or ubiquitous expression of one *dmax* dsRNA transgene in *Df(3L)fz2*/+ or $dmax^{1}$/+ animals led to strong pupal lethality (Figure 3).
Consistent with the assumption that dMax is a cofactor of dMyc, we could show positive genetic interactions between *dmyc* and *dmax*: In dm^{P0} animals, which did not show reduced viability (Figure 31b), a reduction of *dmax* levels by *dmax*-RNA*i* caused strong pupal lethality (Figure 11). Conversely,

the increase in ommatidial size that was caused by overexpression of *dmyc* by the eye-specific driver *GMR-GAL4* could be shown to be partially dependent on *dmax* (Figures 13-18). Close examination of this interaction yielded also strong evidence for *dmax*-independent functions of *dmyc* which will be discussed separately. *dmax* was also shown to positively interact genetically with *reptin* and *pontin* (Figure 12), two genes that had been previously shown to be required for *dmyc* function (Bellosta et al., 2005).

Complete removal of *dmax* in the $dmax^1$ mutants resulted in strong growth phenotypes. Like it had been reported for *dmyc* null mutants (Pierce et al., 2004), $dmax^1$ mutants hatched at approximately the same rate and size as control larvae. However, larval growth was reduced throughout the development of $dmax^1$ larvae (Figures 20ab). While the clearly reduced size of $dmax^1$ L2 larvae was not accompanied by a delay in the L2-L3 molt, $dmax^1$ L3 larvae showed a strong developmental delay, initiating the L3-P molt only at 9 d AED (Figure 23c), without having reached the final size of control larvae (Figure 23a). The size of fat body and salivary gland cells and cell nuclei was reduced in $dmax^1$ larvae (Figure 20c) and correlated to the reduced total larval size. It is therefore likely that the growth phenotype of $dmax^1$ larvae is due to reduced growth of the larval polyploid tissues. The smaller sizes of the nuclei of the polyploid cells points to reduced levels of endoreplication in $dmax^1$ larvae. Since loss of *dmyc* function strongly reduces endoreplication (Maines et al., 2004; Pierce et al., 2004), it is likely that the underlying cause for the reduced growth of $dmax^1$ larvae is the loss of *dmax*-dependent growth functions of *dmyc*.

Loss of $dmax^1$ function was associated with strongly reduced total RNA content (Figure 24). At 120 h AED, the reduction in RNA content roughly correlated to the size difference between $dmax^1$ and control larvae (Figure 20a). Strikingly, already L1 larvae showed equally strongly reduced total RNA levels compared to controls, even though not much visible growth had occurred at this time point. Since the accumulation of total RNA (consisting mainly of rRNA) precedes protein accumulation in young larvae (Church and Robertson, 1966), it is likely that loss of $dmax^1$ has a direct impact on rRNA synthesis. It has been shown that *dmyc* controls rRNA synthesis and ribosome biosynthesis during larval development by regulating the levels of the Pol I transcriptional machinery (Grewal et al., 2005). Therefore, the reduced RNA levels in young $dmax^1$ larvae can be explained by a reduction of *dmyc*-driven rRNA synthesis. A reduced rate of rRNA synthesis is presumably one the reasons for the reduced growth rates of $dmax^1$ larvae. Consistent with such an explanation, a qRTPCR assay specific for the internal transcribed spacer 1b (ITS1b) region of the primary rRNA transcript - therefore reflecting transcription rates, not total rRNA levels - showed reduced levels in $dmax^1$ larvae (Figures 55, 56).

Surprisingly, loss of *dmax* did not forestall imaginal development. More than 40% of the $dmax^1$ mutant larvae developed into pharate imagines with a delay of not more than one day (compared to the duration from pupariation to the pharate stage in wild type animals) (Figure 23b). The resulting

pharate animals were smaller in size than controls (Figure 23c), proportional to the smaller size of *dmax*^{1} pupal cases, and had thin bristles, but showed an otherwise completely wild type morphology. Some *dmax*^{1} pharate imagines showed the typical limb movements that occur prior to eclosion, but none never eclosed. The reason for the failure to eclose is not clear - it is probably not to be found in the size of the imagines, since *chico* mutant flies (Bohni et al., 1999) or strongly starved flies do eclose at even smaller sizes.

In order to investigate the role of *dmax* in imaginal growth more closely, we generated *dmax*^{1} clones in different imaginal tissues. While *dmax*^{1} mutant bristles were very small and thin (Figure 44), *dmax*^{1} mutant ommatidia did not show a reduced size, nor was the ommatidial pattern disrupted in *dmax*^{1} mutant clones (Figures 39 C, 40 C). Clearly, different requirements for *dmax* functions exist in different cell types. Since the formation of bristles requires high rates of protein biosynthesis, and thin bristle phenotypes emerge when protein synthesis is impaired, like in *Minute* or *dmyc* mutant situations (Lambertsson, 1998; Johnston et al., 1999), it is likely that the thin bristle phenotype in *dmax*^{1} mutants arises because *dmax*-dependent *dmyc* functions in protein biosynthesis are rate-limiting in bristle precursor cells. In the eye, wild type ommatidia can develop in the absence of *dmax*, possibly because *dmax*-dependent functions of *dmyc* in protein biosynthesis are not rate-limiting in this situation. However, *dmax*^{1} mutant clones showed impaired growth. While *dmax*^{1} mutant clones could reach large sizes when surrounded by *Minute*/+ tissue (Figure 39), the clones were much smaller compared to control when surrounded by *cl*/+ tissue (Figure 40 C) - unlike the dominant *Minute* allele, the *cl* allele is fully recessive and only serves to eliminate *cl/cl* tissue. This finding indicates that in the imaginal eye disc, *dmax*^{1} mutant cells grow more slowly than wild type cells and/or suffer from cell competition. Growth phenotypes were also found when *dmax*^{1} clones were generated in the imaginal wing disc. While the loss of *dmax*^{1} did not result in smaller cells (Figures 42c, 42d), it strongly affected clonal size. Clearly, *dmax*^{1} mutant clones suffered from cell competition: The median clone size was smaller at 96 h than at 72 h, and the frequency of single wild type twinspots was higher at the later time point (Figures 42c, 42d). Possibly, slower proliferation does also contribute to the smaller size of *dmax*^{1} mutant clones, but solely based on clone size, it was not possible to discriminate between the effect of cell competition and cell proliferation.

In the experiments discussed so far, reduction of *dmax* levels resulted in phenotypes that had also been described for *dmyc* loss of function situations. Taken together with the positive genetic interactions with *dmyc*, *reptin* and *pontin* and the demonstrated physical interaction between dMyc and dMax (Gallant et al., 1996), these data show (not surprisingly, given the wealth of evidence from vertebrate systems) that dMax is an essential cofactor of dMyc. However, a comparison of the null mutant phenotypes of the Max network members (and of combinations thereof) revealed - next to an important contribution of *dmnt* - that *dmyc* also has functions that do not require *dmax*.

2. Functional analysis of the Max network

Even though a loss of *dmax* functions recapitulates the consequences of a loss of *dmyc*, we found striking differences in the severity of the resulting phenotypes. While *dmyc* null larvae showed an almost complete failure to grow and very poor viability, *dmax* null larvae had much less pronounced growth defects and high survival rates (Figures 32 - 36). In order to explain the comparatively mild phenotype of the $dmax^1$ mutants, we considered three hypotheses: Firstly, the loss of *dmyc* might have more severe consequences because *dmyc* has *dmax*-independent functions. Secondly, $dmax^1$ mutants might show a milder phenotype than *dmyc* null mutants due to the concomitant loss of *dmnt* mediated repression. Thirdly, and along the lines of the second hypothesis, the loss of repression by as yet unknown negative *dmax*-dependent growth factors besides *dmnt* might contribute to the mildness of the $dmax^1$ phenotype. We could discriminate between these hypotheses by comparing the growth and survival of different null mutant combinations of *dmyc*, *dmax* and *dmnt*.

We could indeed show that removal *dmnt* in *dmyc* null larvae rescued part of the poor growth and survival of *dmyc* null mutants (Figure 35). However, dm^4 $dmnt^1$ larvae grew more slowly and showed lower survival rates than $dmax^1$ larvae (Figures 35, 36). Therefore, two factors contribute to the mildness of the $dmax^1$ phenotype: the loss of *dmnt* function in $dmax^1$ mutants and *dmax*-independent functions of *dmyc*. Consistent with this interpretation, removal of *dmax* in *dmyc* null mutants led to similarly improved growth and survival as the removal of *dmnt* (Figures 34, 35), while removal of *dmnt* in $dmax^1$ mutants did not alter the $dmax^1$ phenotype (Figure 36). These results show that *dmnt* has fully *dmax*-dependent functions which antagonize *dmyc* function in larval growth, probably via repression of *dmyc*-dependent E-box promoters. In its direct antagonistic effect, *dmnt* hence behaves similar to vertebrate *mnt* (see Introduction).

Since both dm^4; $dmax^1$ or dm^{A51}; $dmax^1$ double mutants and dm^4 $dmnt^1$; $dmax^1$ triple mutants did not show better growth or viability compared to dm^4 $dmnt^1$ mutants (Figures 34, 35), we could exclude that an unknown *dmax*-dependent negative growth factor is responsible for the difference in growth and survival between $dmax^1$ and dm^4 $dmnt^1$ mutants. These findings also rule out the possibility that the milder phenotype of $dmax^1$ larvae (compared to dm^4 $dmnt^1$ larvae) is due the loss of hypothetical repressive dMax homodimers. However, both dm^4; $dmax^1$ double mutants and dm^4 $dmnt^1$; $dmax^1$ triple mutants were slightly smaller and showed slightly reduced survival compared to the dm^4 $dmnt^1$ double mutants (Figure 35). Therefore, it is possible that *dmax* has *dmyc*- and *dmnt*-independent positive growth functions.

Consistent with the assumption that *dmyc* has *dmax*-independent growth functions, we found that dm^2 mutants, expressing a form of dMyc that lacks the leucine zipper and therefore cannot bind to dMax, grow und survive better than *dmyc* null mutants, both in the presence and the absence of *dmax* (Figures 33, 34). However, dm^2; $dmax^1$ mutants did not reach the growth and survival rates of $dmax^1$ animals, indicating that either part of *dmyc's dmax*-independent functions do require the leucine zipper

or that the form of dMyc that is expressed in the *dm*^{2} mutants is less stable than wild type dMyc. The observation that *dm*^{2} retains a part of *dmyc's* growth functions suggests that these functions do not require heterodimerization and subsequent E-box binding with a dMax-like partner molecule (i.e. a hypothetical bHLHzip protein with similarities to dMax, to which dMyc could bind) . Consistent with this assumption, we could show that the two E-box-regulated genes *nnp1* and *CG5033* failed to respond to *dmyc* overexpression in *dmax*^{1} larvae (Figures 55). In addition to these findings, we could exclude that Mlx, an obvious candidate "dMax surrogate" (see Results, 2.5.), complements the dMax function in *dmax*^{1} mutants (Figure 38).

We found that the size difference between *dm*^{4} *dmnt*^{1}, *dmax*^{1} and control larvae correlated with the size differences of the polyploid larval organs (e.g. the fat body, see Figure 37a). Both in the fat body and in the salivary glands, we found strong differences in nuclear and overall cell sizes between the three genotypes (Figures 37b, 37c). Strikingly, *dm*^{4} *dmnt*^{1} mutant fat body and salivary gland cells did only show a minor increase in cells size between 5 d AED and 8 d AED, while *dmax*^{1} cells showed robust growth, reaching a final size that was only slightly smaller compared to the cell size in 5 d old *y w* larvae. These findings suggest that *dmyc* can support growth and endoreplication in the absence of *dmax*. Moreover, the sustained growth of the polyploid tissues at late time points rules out the trivial explanation that the differences between *dm*^{4} *dmnt*^{1} and *dmax*^{1} mutants would merely arise from the presence of maternally contributed Max protein. The different sizes of *dm*^{4} *dmnt*^{1} and *dmax*^{1} mutant polyploid cells is due to a cell-autonomous growth difference, since *dm*^{4} *dmnt*^{1} mutant clones in the fat body showed a clearly smaller cell size (and smaller cell nuclei) than *dmax*^{1} mutant clones (Figure 45).

Total RNA content correlated to the differing larval sizes of *dm*^{4} *dmnt*^{1}, *dmax*^{1} and control larvae at 5 d AED (Figure 37e). Strikingly, there were already as big differences in total RNA content in L1 larvae at 29-39 h AED, when almost no visible growth had occurred (Figure 37d). Since ribosomal RNA makes up most of the total RNA, we concluded that *dmyc* can contribute to the accumulation of rRNA in the absence of *dmax*. A *dmax*-independent role of *dmyc* in ribosome biosynthesis (and protein synthesis as a consequence) might be one of the underlying causes for the observed growth difference between *dm*^{4} *dmnt*^{1} and *dmax*^{1} mutants. Consistent with such a scenario, we could show that overexpression of *dmyc* in *dmax*^{1} larvae resulted in the upregulation of *5sRNA*, *tRNA(Leu)* and two snoRNAs (Figure 55, 56).

Examining *dm*^{4}, *dm*^{4} *dmnt*^{1} and *dmax*^{1} mutant clones in adult eyes and L3 wing discs, we could show that *dmax*-independent growth functions of *dmyc* do also play an important role in imaginal tissues. In the eye, both *dm*^{4} and *dm*^{4} *dmnt*^{1} mutant clones occupied smaller areas than *dmax*^{1} clones, and the surrounding heterozygous tissue was rough, suggesting that *dm*^{4} and *dm*^{4} *dmnt*^{1} mutant tissue was lost during development, likely due to cell competition (Figure 40). In the imaginal wing disc, we analyzed mutant and twin spot clones that had an age of 72 h. At this time point, *dm*^{4} and *dm*^{4} *dmnt*^{1} mutant clones showed reduced cell sizes, were extremely small compared to the twinspots (less than 15% twin

spot size), and more than 30% of the twinspots were not accompanied by a *dm*^{4} or *dm*^{4} *dmnt*^{1} mutant clone (Figures 42a, 42b). In contrast to this, *dmax*^{1} clones of the same age did not show a reduced cell size. *dmax*^{1} clonal area was only reduced by 35%, and only 3% of the twin spots were not accompanied by a *dmax*^{1} mutant clone (Figure 42c). The difference in cell size between *dm*^{4} *dmnt*^{1} and *dmax*^{1} mutant cells shows that *dmax*-independent functions of *dmyc* contribute to the cell growth of wing disc cells, while the difference in the frequency of single twin spots, together with the strongly reduced clonal size, shows that *dm*^{4} *dmnt*^{1} mutant clones suffer more strongly from cell competition than *dmax*^{1} clones. It is likely that *dm*^{4} and *dm*^{4} *dmnt*^{1} mutant cells are also more defective in proliferation than *dmax*^{1} cells, but based on clonal area, it is not possible to discriminate between the effects of reduced proliferation and of cell competition. Consistent with the finding that cell competition is induced more severely in cells that lack *dmax*-independent functions of *dmyc*, we could show that *dmyc* is still able to induce cell competition in *dmax*^{1} mutant wing discs (Figure 43).

It is tempting to speculate that the observed differences between *dm*^{4} *dmnt*^{1} and *dmax*^{1} mutant situations (growth and endoreplication in polyploid cells, cell growth and cell competition in diploid imaginal cells) might have a common basis: namely, that *dmyc* can still partially drive protein biosynthesis in the absence of *dmax*, potentially because of a *dmax*-independent function of *dmyc* in ribosome biosynthesis (as the differing rRNA levels in L1 larvae (Figure 37d) and the dmyc-dependent upregulation of *5sRNA*, *tRNA(Leu), snoRNA U3* and *snoRNA 46* in *dmax*^{1} larvae suggest). The hypothesis that the same process (protein biosynthesis) is already affected in *dmax*^{1} mutant situations (due to downregulation of E-box regulated target genes involved in protein biosynthesis - like *nnp1* and *CG5033*), but even more strongly in *dm*^{4} *dmnt*^{1} mutant situations (due to additional loss of *dmax*-independent functions of *dmyc*), would fit well with the observed phenotypes.

A combination of observations suggests that *reptin* and *pontin* are required in the *dmax*-independent functions of *dmyc*. In *dm*^{P0} flies, loss of one copy of *pontin* frequently results in small, irregularly shaped, and slightly rough eyes (Bellosta et al., 2005). Eye-specific, complete removal of *dmyc* in *y w dm*^{A51} *tub>dmyc>GAL4/Y; +/CyO, ey-flp* flies produces similar eye phenotypes (Figure 39), suggesting that *dmyc* function falls below a critical threshold for normal development in *dm*^{P0}*/Y; pontin/+* flies. A similar interaction was demonstrated between *reptin* and the stronger *dmyc* hypomorphic allele *dm*^{PL35} (Bellosta et al., 2005). In stark contrast to these findings, complete removal of *dmax* in the eye does not produce a rough eye phenotype and seems not to reduce ommatidial size (Figure 39). This finding indicates that *dmax* is not required for normal eye development, in contrast to *dmyc*. From this it follows that *reptin* and *pontin* are required for *dmyc* functions that do not require *dmax*. Consistent with this conclusion, *dm*^{P0}*/Y; dmax*^{1}*/+* flies never showed a rough eye phenotype, were not reduced in viability or weight and showed only an extremely small developmental delay compared to *dm*^{P0}*/Y* flies (Figure 31), in contrast to *dm*^{P0}*/Y; pontin/+* flies that frequently show a rough eye phenotype, reduced viability and weight and a strong developmental delay (Bellosta et al.,

2005). While these findings suggest that *reptin* and *pontin* are required in the *dmax*-independent functions of *dmyc*, the data leave open the question whether these proteins are also involved in the *dmax*-dependent functions of *dmyc*. Several reports have pointed to connections between *reptin*, *pontin* and certain snoRNAs (see Results, 2.9.), which was the reason for us to examine the effect of *dmyc* overexpression on *snoRNA U3* and *snoRNA 46*. Indeed we could show that the levels of *snoRNA U3* and *snoRNA 46* are elevated in $dmax^1$ larvae upon overexpression of *dmyc*. The upregulation of these snoRNAs might be mediated by *reptin* and *pontin*. Given the importance of snoRNAs in ribosome biosynthesis and hence protein biosynthesis, such a function of *reptin* and *pontin* could at least partially account for the *dmyc*-dependent growth in the absence of *dmax*.

3. *dmax*-independent effects of *dmyc* overexpression

Besides the broad evidence for *dmax*-independent growth functions in polyploid and imaginal tissues discussed above, we have observed specific consequences of *dmax*-independent functions when *dmyc* is overexpressed. We have studied two situations: overexpression of *dmyc* with the eye-specific GAL4 driver *GMR-GAL4* in wild type animals, and ubiquitous overexpression of *dmyc* with *actin-GAL4* (for constitutive overexpression) or with the *hs-flp actin>CD2>GAL4* system (for conditional overexpression) in $dmax^1$/+ and $dmax^1$ larvae. We could show that the eye phenotype that is caused by strong overexpression of *dmyc* in the eye with *GMR-GAL4* is a result of both *dmax*-dependent and *dmax*-independent functions, and that the *dmax*-independent functions in this situation are associated with apoptosis. Using the constitutive or conditional ubiquitous overexpression system, we made the surprising discovery that overexpression of *dmyc* in $dmax^1$ larvae interferes with the ecdysone system. The findings in both overexpression situations will be discussed below.

3.1. *dmax*-independent functions of overexpressed *dmyc* in the eye

We have overexpressed *dmyc* with *GMR-GAL4*, a GAL4 driver that causes high-level expression in the eye imaginal discs in cells posterior to the morphogenetic furrow (Freeman, 1996; Hay et al., 1997). The morphogenetic furrow - wandering from the posterior margin of the eye imaginal disc to the anterior margin - marks the onset of cell fate specification and the end of asynchronous proliferation of the unspecified imaginal eye disc cells. The cell cycle arrests in the morphogenetic furrow, and cell fate specification begins with the formation of 5-cell preclusters that define the future ommatidia. The remaining cells reenter the cell cycle in a second mitotic wave posterior to the morphogenetic furrow and later give rise to further cell types (reviewed in Neufeld and Hariharan, 2002).

Overexpression of *dmyc* posterior to the morphogenetic furrow therefore cannot not have an influence on the total number of ommatidia (which is already determined by the amount of 5-cell preclusters that in turn depends on the total number of unspecified cells), but can be expected to influence the growth

of the developing ommatidia. We could indeed show that the expression of one copy of *dmyc* with *GMR-GAL4* increases the ommatidial size by 28%, without causing a rough eye phenotype. Strikingly, expression of three copies of *dmyc* did not further increase ommatidial size (ommatidia were 24% bigger than control), but resulted in rough eyes with a pigmentation defect (Figure 14), suggesting that additional growth by the increased *dmyc* dosis is cancelled out by *dmyc*-induced apoptosis. Consistent with this assumption, blockage of apoptosis by coexpression of the pan-caspase inhibitor *p35* resulted in an additional 10% increase of ommatidial size (i.e. it increased the overgrowth by almost one third). At the same time, block of apoptosis resulted in smoother eyes, partially rescued the internal structure of the ommatidia and fully rescued the pigmentation defect (Figure 16). Taken together with direct measurements of apoptosis levels (L. Montero and P. Gallant, unpublished), these findings clearly show that strong overexpression of *dmyc* by *GMR-GAL4* is associated with apoptosis.

Downregulation of *dmax* by expression of *dmax* dsRNA with *GMR-GAL4* did not change ommatidial size (Figure 14), suggesting that either *dmax* levels have not been sufficiently reduced, or that normal ommatidial growth and development does not require *dmax*, a conclusion that is supported by the finding that in $dmax^{1}$ mutant clones, normal ommatidia are formed (Figures 39, 40). When one copy of *dmyc* was overexpressed, *dmax*-RNA*i* did only partially rescue the *dmyc*-induced increase in ommatidial size. Strikingly, *dmax*-RNA*i* in the context of overexpression of three copies of *dmyc* led to a strong decrease in ommatidial size, resulting in ommatidia that were smaller than wild type ommatidia, but removal of *dmax* could not rescue the rough eye phenotype nor the pigmentation defect (Figure 14). From this we concluded that removal of *dmax* could only partially suppress the effects of strongly overexpressed *dmyc*: While it reduced *dmax*-dependent growth functions, *dmyc*-induced apoptosis levels stayed high, the combination of both resulting in smaller-than-wild type ommatidia. Consistent with this interpretation, coexpression of *p35* in these eyes increased ommatidial size, partially rescued the rough eye phenotype and restored wild type pigmentation, completely analogous to the effect *p35* had in the absence of *dmax*-RNA*i* (Figure 16).

A direct comparison of the measured ommatidial sizes in the different genotypes in Figure 16 (overexpression of three copies of *dmyc* ("*3xdmyc*") with or without *dmax*-RNA*i* and with or without *p35*) strongly supports the assumption that *dmyc*-induced apoptosis is *dmax*-independent: *3xdmyc* ommatidia with normal *dmax* levels are ~30% bigger than *3xdmyc* ommatidia in which *dmax* has been removed, regardless of whether apoptosis is blocked. At the same time, *3xdmyc* ommatidia in which apoptosis is blocked are ~10% bigger, regardless of whether *dmax* has been removed. Based on ommatidial size, apoptosis is therefore completely uncoupled from *dmax* levels.

With a simple model, the final ommatidial sizes in all *3xdmyc* genotypes of Figure 16 can be explained as a combination of *dmax*-dependent growth, *dmax*-independent growth, *dmax*-dependent and *dmax*-independent apoptosis. Assuming that *dmax*-RNA*i* completely removes dMax and that expression of *p35* completely blocks apoptosis, and taking into account that the expression of *p35* with *GMR-GAL4*

increases ommatidial size by 10% on its own, we set up and solved a system of equations with 4 variables (*dmax*-dependent and -independent growth and apoptosis). The following contributions to final ommatidial size resulted: *dmax*-dependent growth: +29%, *dmax*-independent growth: +6%, *dmax*-dependent apoptosis: -0.2%, *dmax*-independent apoptosis: -9%. These calculated contributions coincide remarkably well with the values derived with the comparative approach, where no assumptions about the efficiency of *dmax*-RNA*i* and *p35* had been made (see preceding paragraph), indicating that the assumptions in the model are not unreasonable. Also in this model, apoptosis turns out to be almost completely *dmax*-independent.

From the phenotypes and calculations above, we concluded that strong overexpression of *dmyc* with *GMR-GAL4* results in both *dmax*-dependent and *dmax*-independent growth, but also in *dmax*-independent apoptosis. Presumably, the *dmax*-dependent growth is a function of dMyc/dMax heterodimers, while the *dmax*-independent growth and apoptosis are functions of free dMyc. Based on the changes in ommatidial size, one further has to assume that *dmax*-independent growth and apoptosis are not increased when dMax levels are lowered and more free dMyc would be available, suggesting that upon wild type dMax levels, the presence of bound dMax does not interfere with these *dmax*-independent functions.

An alternative model in which the loss of dMnt function through titration of dMax from dMnt by high levels of dMyc is the cause for the observed apoptosis could be ruled out, since the same *dmyc* overexpression phenotype (and the same interaction with *dmax*) could be observed in *dmnt* null flies (Figure 17). With the same argument, we can exclude that the observed *dmax*-independent apoptosis would be the result of *dmax*-independent functions of *dmnt*.

Overexpression of *myc* has been shown to induce apoptosis both in vertebrate systems and in *Drosophila*. Intriguingly, *c-myc* has been shown to induce apoptosis in PC12 cell, in the absence of functional *dmax* (Wert et al., 2001), reminiscent of our findings. However, it is not clear whether the *dmax*-independent apoptosis we describe is representative for situations in which *dmyc* induces apoptosis in exponentially growing cells, or whether the apoptosis in the eye is caused by a specific function of *dmyc* in the differentiation of the ommatidia. We have shown that loss of *dmyc*, but not loss of *dmax* results in a rough eye phenotype (Figure 39), and it might well be that this phenotype is not just a consequence of the lack of *dmax*-independent growth, but also results from the loss of specific, *dmax*-independent functions in the development of the ommatidia. In such a scenario, strong overexpression of *dmyc* might interfere with these functions and cause apoptosis.

Even though the nature of these functions, and the connection to apoptosis remains unclear, we could provide unequivocal evidence that the effects of *dmyc* overexpression with *GMR-GAL4* are partly caused by *dmax*-independent functions of *dmyc.*

3.2. *dmyc* overexpression in *dmax*^{1} larvae interferes with molting and pupariation

Given the broad evidence for *dmax*-independent functions of *dmyc* derived from the comparison of *dmax* and *dmyc dmnt* loss of function situations, we did expect that ubiquitous *dmyc* overexpression in *dmax*^{1} larvae would have observable consequences. However, it was greatly surprising to discover that *dmyc* overexpression in *dmax*^{1} larvae resulted in very specific phenotypes: Induction of *dmyc* expression prior to the L2-L3 molt killed most of the *dmax*^{1} larvae during the molt (Figures 48-50), while *dmyc* induction after the molt did not increase lethality. Even more astounding, coexpression of *dmyc* and *p35* after the L2-L3 molt almost completely blocked the pupariation of *dmax*^{1} larvae, letting these animals survive as larvae for up to one month (Figure 52). Similar phenotypes have been described for mutants defective in ecdysone synthesis, like *ecdysoneless (ecd)* mutants (Garen et al., 1977), and for mutants defective in ecdysone signaling, like *Ecdysone Receptor B (EcR-B)* mutants (Schubiger et al., 1998; Li and Bender, 2000). We could rescue the pupariation block imposed by coexpression of *dmyc* and *p35* in *dmax*^{1} larvae by ecdysone feeding, proving that overexpression of *dmyc* interferes with the ecdysone system (Figure 54). The finding that exogenous ecdysone can rescue the pupariation block might indicate that *dmyc* overexpression in *dmax*^{1} larvae results in defects in ecdysone signaling upstream of the receptors. However, we cannot rule out the possibility that a defect at the level of the ecdysone receptors or downstream of the receptors might be overcome by higher than wild type levels of exogenous ecdysone.

While we could convincingly show that the overexpression of *dmyc* in *dmax*^{1} larvae interferes with ecdysone signaling, the nature of this interaction remains mysterious in many aspects. Evidently, the observed effects are *dmax*-independent. However, it is not clear why *dmax*^{1}/+ larvae are much less affected. A significant decrease in viability could also be observed in heterozygotes (Figure 48), but no pupariation block. It is possible that the loss of *dmax* creates a sensitized situation in which an interaction between *dmyc* and the ecdysone system is uncovered. It has indeed been shown that *dmyc* overexpression in the ring gland of starved animals, but not in normal animals, leads to a developmental delay (P. Léopold, personal communication). One might speculate that *dmax*^{1} mutants share characteristics with starved animals, which would explain why the interaction between *dmyc* and ecdysone signaling creates stronger phenotypes in *dmax*^{1} animals, even though it is not clear why starvation increases the response to *dmyc* overexpression. Whatever is the reason for the different response to *dmyc* overexpression in *dmax*^{1} and *dmax*^{1}/+ larvae, it is not restricted to the observed molting and pupariation phenotypes: similarly, *dmyc* overexpression has resulted in strong upregulation of *5sRNA*, *tRNA(Leu)* and two snoRNAs only in *dmax*^{1} larvae, but not in the heterozygotes. A common cause might exist for both observations. Another mysterious aspect of the observed interaction between *dmyc* and ecdysone signaling is the connection to apoptosis. *dmyc* overexpression in *dmax*^{1} also interferes with pupariation when apoptosis is not blocked, resulting in a strong delay and misshapen pupal cases, but upon coexpression of *p35*, pupariation is almost

completely blocked (Figure 53). While it is possible that this is an additive effect, one could also imagine that *p35* prevents *dmyc*-induced apoptosis of tissues in which *dmyc* exerts its pupariation-inhibiting role, e.g. the in the ring gland, thereby intensifying *dmyc's* effects.

Our findings might point to a role of *dmyc* in the control of developmental timing. Recently, several studies have shown connections between insulin signaling and the control of developmental timing by ecdysone signaling (Caldwell et al., 2005; Colombani et al., 2005; Mirth et al., 2005). Given *dmyc's* importance in the control of cell growth, it is conceivable that links between *dmyc* and ecdysone signaling exist. The exact nature of the interaction between *dmyc* and ecdysone signaling remains to be elucidated.

4. Conclusion

In this work, we present unequivocal evidence for *dmax*-independent functions of *dmyc*. This finding is of great importance, since it shows that the standard model of *myc* function (heterodimerization with *max* and subsequent E-box-dependent regulation of target gene transcription) does not sufficiently describe the scope of *myc's* functions. We found that a substantial part of the growth-promoting effect of *dmyc* does not require *dmax* and we could draw the same conclusion for other known aspects of *dmyc* activity, like cell competition and *dmyc*-induced apoptosis. Furthermore, we describe a previously unknown aspect of *dmyc* function: We discovered that *dmyc* interferes with the ecdysone system in a *dmax*-independent way.

The elucidation of the molecular mechanisms underlying these *dmax*-independent functions of *dmyc* will be crucial for a better understanding of the biological functions of *dmyc* in growth control. Given the high degree of functional conservation of *dmyc* between *Drosophila* and vertebrates, it is likely that our findings are also of importance for the understanding of vertebrate *myc.*

Materials and Methods

1. *dmax*- and *lacZ*-RNA*i* constructs

For a detailed description of the cloning strategy, see Steiger (2002). The *dmax* and *lacZ* inverted repeats were cloned into the KpnI and BglII sites of pUAST. The repeats are separated by a single SfiI restriction site. The following table shows the end coordinates of the single repeat cDNAs relative to the indicated Genbank and Flybase entries as well as the 5'-most (respectively 3'-most) sequences of the repeats. These end sequences are given in 5'-3' orientation relative to the primer sequences.

1.1. *dmax*-RNA*i*

Repeat length: 784 bp

Sequence:	AE003517.3 (Genbank entry)	
End	Coordinate	Sequence in primer
5'	64690	5' TTTGCGCGCAATCCGTGCAAAAC 3'
3'	63243	5' TAAGGTCGATTGGGTGGGTTAC 3'

Sequence:	Max-RA (Flybase entry FBtr0075018)
Length:	1011 bp
End	Coordinate
5'	132
3'	915

1.2. *lacZ*-RNA*i*

Repeat length: 769 bp

Sequence:	J01636.1 (Genbank entry)	
End	Coordinate	Sequence in primer
5'	3092	5' TATGAACGGTCTGGTCTTTGCCG 3'
3'	3860	5' AATCCGGTAGGTTTTCCGGCT 3'

Sequence:	*lacZ* cDNA
Length:	3113 bp
End	Coordinate
5'	1847
3'	2615

2. Generation and characterization of *dmax* mutants

2.1. Imprecise excision screen to generate *dmax* mutants

To generate *dmax* mutants, flies of the genotype *y w; P{y$^+$ w$^+$}CG9666^{EY02775}* were used. These flies harbor a *P{EPgy2}* insertion at the 3' end of the second exon of *CG9666* (insertion positions: 19257703..19257704 on chromosome 3L, 65233..65234 on AE003517.3), 412 bp upstream of the start

of the *dmax* transcript. This P element was mobilized using the *Δ2-3* P element transposase. Based on the assumption that strong hypomorphic *dmax* alleles and *dmax* null alleles should lead to pupal or earlier lethality if put over *Df(3L)fz2*, we isolated putative *dmax* mutants with the following screening scheme:

P0 *y w; P{y$^+$ w$^+$}CG9666^{EY02775}* x *y w; Δ2-3 Sb/TM6B*

F1 3 ♂ *y w; P{y$^+$ w$^+$}CG9666^{EY02775} / Δ2-3 Sb* x 3 ♀ *y w; D gl/TM3, Ser y$^+$*

402 F1 crosses were set up. The offspring of these crosses were screened for *Sb$^+$* males that had lost the *w$^+$* marker, indicating successful mobilization of *P{y$^+$ w$^+$}CG9666^{EY02775}*. 270 *Sb$^+$ w$^-$* males from individual crosses were collected. Note: *w/[y w or Y]; P{y$^+$ w$^+$}CG9666^{EY02775}/Df(3L)fz2* flies were fully viable.

F2 single ♂ *y w; P$^{mut[y- w-]}$/[TM3, Ser y$^+$ or D gl]* x 3 ♀ *w; Df(3L)fz2/TM6C, Tb Hu Sb*

180 F2 crosses were set up, of which all had offspring. In 5 crosses, no *w/[y w or Y]; P$^{mut[y- w-]}$/Df(3L)fz2* flies eclosed. In further 2 crosses, the viability of *w/[y w or Y]; P$^{mut[y- w-]}$/Df(3L)fz2* flies was reduced. Subsequently, lines carrying these *P$^{mut[y- w-]}$* chromosomes were established. Additionally, lines containing *P$^{mut[y- w-]}$* chromosomes that did not result in lethality in heterozygosity with *Df(3L)fz2* were established, since these chromosomes were expected to be derived from precise excision events.

Established lines (named after the F1 cross they originated from):

50, 70, 85, 100, 283	lethal over *Df(3L)fz2*
9, 54	semilethal over *Df(3L)fz2*
25, 188, 296, 301, 377	viable over *Df(3L)fz2*

2.2. Molecular characterization of the alleles isolated in the imprecise excision screen

We used PCR to characterize the *P$^{mut[y- w-]}$* chromosomes isolated in the imprecise excision screen. To this end, genomic DNA from adult *P$^{mut[y- w-]}$/Balancer* flies was isolated. The following PCR primers were used (the positions indicated correspond to the 3' most base of the primer sequence and are relative to AE003517.3. The P* primer is specific for P element ends. The indicated position corresponds to the *EY02775* insertion. It allows for generation of PCR products if used with primers in the flanking genomic sequence):

dmax3B.SfiI
5' GCGGCGGCCATCTAGGCCTAAGGTCGATTGGGTGGGTTAC 3'
63264

CG9666rev1
5' GTCGGCTGTCCCAGCAACTGGGG 3'
65320

CG9666forw1
5' GCCGAGACGAACCGCAAGATAC 3'
65157

P*
CGACGGGACCACCTTATGTTATTTCATCATG
65233

Analysis of the lines 9 and 54 revealed that both ends of the P element were still present, even though the w^+ and y^+ markers were lost. In line 283, none of the P element ends was detectable anymore. In the lines 50, 70, 85 and 100, the 3' P element end (the one closer to *CG9666*) was still present, but not the P element end close to *dmax*. In the lines 85 and 100, PCR with the primers dmax3B.SfiI, situated near the 3' end of the *dmax* transcript, and CG9666.5prime.rev, situated 3' of the $P\{y^+ w^+\}CG9666^{EY02775}$ insertion site (relative to the genome annotation) yielded bands that were shorter than the bands generated on wild type genomic DNA, indicating deletions caused by imprecise excision events. DNA from these bands were isolated and sequenced to reveal the molecular nature of the lesions. Based on the results of the sequencing, the allele from line 100 was termed $dmax^1$, the allele from line 85 was termed $dmax^2$. With the lines, 50, 70 and 283, no bands other than the one derived from the wild type sequence on the balancer was derived. Together with the early lethal phenotype of the larvae, it is probable that in these cases large deletions had been produced that do also affect neighboring essential genes. A PCR with the primers CG9666forw1 and CG9666rev1 which are situated directly next to the P element insertion site revealed that in line 25, a precise excision event had occurred.

2.3. Sequence of the $dmax^1$ (line 100) and $dmax^2$ (line 85) mutant alleles

The direction of the sequences in the following description is corresponding to the scaffold sequence AE003517.3 and to the sequence of the *Drosophila* chromosome 3L: AE014296.4, i.e. opposite to the sequence of the *dmax* transcript. Position indications are referring to the positions of the breakpoint nucleotides (underlined and marked in bold) on AE003517.3 and AE014296.4.

2.3.1. $dmax^1$ sequence

In line 100, a deletion has been created that stretches from the *EY02775* insertion position (at the 3' end of the second exon of *CG9666*) until the last exon of *dmax* (position 729 on the *dmax* transcript), spanning 1804 bp. The deletion uncovers the whole of the *dmax* ORF.

Sequence until breakpoint (63428 (AE003517) / 19255898 (AE014296):
5' TGGAACCGTTTCCTTCACAACTTTTCGAGGGCTATT
GCTTTCGTATAACACAACTCAAAGTTGAACTAAAT**C** 3'
Sequence after breakpoint (65233 (AE003517) / 19257703 (AE014296):
5' **G**TCTGAGTCCGCCGAACCAGGTGAGTTCGTTGGGAAC 3'

Between these breakpoints, the sequence GATAAATGTTATTTCATCATG was found, of which ATGTTATTTCATCATG is identical to the P element end, whereas the GATAA sequence is of unknown origin.

2.3.2. *dmax*^{2} sequence

In line 85, a 550 bp deletion has been created that stretches from the *EY02775* insertion position until the first exon of *dmax* (position 139 on the *dmax* transcript), 27 bp upstream of the start of the *dmax* ORF.

Sequence until breakpoint (64682 (AE003517) / 19257152 (AE014296):
5' ACTCATGTTGCTTCACTTGTTTTGCACGGATT**G** 3'
Sequence after breakpoint (65233 (AE003517) / 19257703 (AE014296):
5' **G**TCTGAGTCCGCCGAACCAGGTGAGTTCGTTGGGAAC 3'

Between these breakpoints, the sequence TTATTTCATCATG was found, originating from the P element end.

3. Cloning of the *dmax* genomic construct

The following primers were used to generate the *dmax* genomic construct (indicated is the whole primer sequence in 5'-3' direction. The position indications are relative to the AE003517.3 scaffold sequence and to the sequence of the *Drosophila* chromosome 3L: AE014296.4. They denote the 5' most annealing nucleotide of the respective primer (underlined):

rescue2 primer: CGG **GGTACC** GCGGCCGC GGTTGTATTTGGTTCGGAATG
62792 (AE003517) / 19255262 (AE014296)

rescue3 primer: CGG **GGTACC** TCCGGCTATTTGCTGATACTG
65579 (AE003517) / 19258049 (AE014296)

These primers amplify a 2788 bp sequence that extends from the end of the transcript of *CG14084*, the gene 3' of the end of the *dmax* transcript, to the start of the ORF of *CG9666*. The bold sequences in the primer sequences denote Asp718 restriction sites. The amplicon was cut with Asp718 and ligated into the Asp718 site of pCaSpeR 4. With the resulting generated plasmid, pDS29, transgenic fly lines were established.

4. Fly culture

Flies were kept on standard *Drosophila* medium. If not indicated otherwise, test crosses were performed in climate chambers at 25° C.

5. Weight measurements

The wet weight of adult flies was measured with a Mettler Toledo MX5 micro balance. Before the weighing, the flies were killed by freezing. The flies had an age of 1-7 d (Figure 6), 1-5 d (Figure 30b), and 1-4 d (Figure 31c).

6. Determination of bristle size

Scutella were removed, cleaned from attaching muscle tissue and mounted on glass slides, in glycerol. Pictures were taken with a Zeiss Axiophot microscope / Progres scanner camera system (objective magnification: 5x). Bristle size was determined as the total pixel count a bristle covers in a picture. Pixel counts were determined with Adobe Photoshop.

7. Determination of wing area and wing cell size

Wings were mounted on glass slides with the dorsal side up, in glycerol. Pictures were taken with a Zeiss Axiophot microscope / Progres scanner camera system (objective magnification: 2.5x (total wings), 20x (determination of cell density)). The total wing surface area (pixel count) was directly determined in Adobe Photoshop. For the determination of wing cell size, the number of dorsal microchaetae (which occur once per cell) was counted in a defined rectangle of 300 x 300 pixels. Cell size was calculated as the reciprocal value of the determined bristle density.

8. Determination of ommatidial size

Pictures of fly eyes were acquired with a JEOL JSM-6360 LV scanning electron microscope at a magnification of 180x. The depicted eyes were gold-coated (except for the following cases, where uncoated eyes of flies that had been killed by freezing were photographed: Figure 14, panels BE, Figure 17, panels A'B'C'D'). The area of 20 central ommatidia was determined using Adobe Photoshop. For each genotype, at least 5 eyes were scored. Fusions of two ommatidia were counted as two individual ommatidia.

9. Autofluorescence microscopy of fly eyes

The pictures of Figure 16d were taken with a Leica DMRA compound microscope, using a 10x objective. Whole flies (killed by freezing) were positioned on a glass slide (dry, without coverslip). Excitatory light that is suitable to induce fluorescence of GFP causes autofluorescence in the ommatidial tissue, allowing the acquisition of the pictures of Figure 16d.

10. Determination of survival rates (viability rates) and larval growth

Figure 3: The genotypes A, B, C originated from a cross of ♀ *y w; actin-GAL4/CyO, y*$^{+}$ x ♂ *y w; UAS-dmax-IR(2-7)/CyO*. The viability of B (or C) was determined as the ratio of B (or C) offspring number (eclosed flies) compared to A offspring number (eclosed flies), in %. The genotypes D, E, F originated from a cross of ♀ *y w; actin-GAL4/CyO, y*$^{+}$*; dmax*^{1}*/TM6B* x ♂ *y w; UAS-dmax-IR(2-7)/CyO*. The viability of E and F was indicated relative to D. The genotypes G and I originated from a cross of ♀ *y w; [actin-GAL4; Df(3L)fz2]/SM5-TM6B* x ♂ *y w; UAS-dmax; UAS-dmax-IR(6-1)*, the genotypes H and K originated from a cross of ♀ *y w; [actin-GAL4; Df(3L)fz2]/SM5-TM6B* x ♂ *y w; +; UAS-dmax-IR(6-*

1). The viability of G and H were compared by normalizing with I and K. Since G showed higher viability than the genotypes I and K, the viability of G was set to 100%.

Figure 11: The genotypes A and D originated from the cross ♀ *y w; da-GAL4/MKRS* x ♂ *y w; UAS-dmax-IR(2-7)/CyO*, B and E from ♀ *w* dm^{P0} *tub>dmyc>GAL4/FM7; da-GAL4/MKRS* x ♂ *y w; UAS-dmax-IR(2-7)/CyO*, C and F from ♀ *w* dm^{P0}*/FM7; da-GAL4/MKRS* x ♂ *y w; UAS-dmax-IR(2-7)/CyO*. The viabilities of A-F was determined as the ratio of (A-F) offspring number (eclosed flies) compared to the offspring numbers (eclosed flies) of the sister genotypes indicated below, the ratio of [genotype/reference (sister offspring) genotype] is indicated in brackets: A: *y w/y w; CyO/+; da-GAL4/+* (38/48), B: dm^{P0} *tub>dmyc>GAL4/y w; CyO/+; da-GAL4/+* (18/22), C: dm^{P0}*/y w; CyO/+; da-GAL4/+* (28/29), D: *y w/Y; CyO/+; da-GAL4/+* (17/50), E: dm^{P0} *tub>dmyc>GAL4/Y; CyO/+; da-GAL4/+* (14/17), F: dm^{P0}*/Y; CyO/+; da-GAL4/+* (1/18).

Figure 12: Crosses from which the genotypes A-E originated: A: ♀ *y w; actin-GAL4/CyO,* y^+ x ♂ *y w; UAS-dmax-IR(2-7)/CyO*, B: ♀ *y w; actin-GAL4/CyO,* y^+ x ♂ *y w; UAS-dmax-IR(2-7)/CyO,* y^+*; UAS-dmax-IR(5-2)UAS-dmax-IR(6-1)/TM6B*, C: ♀ *y w; actin-GAL4/CyO,* y^+ x ♂ *y w; UAS-dmax-IR(2-7)/CyO,* y^+*; Df(3L)fz2/TM6B*, D: ♀ *y w; actin-GAL4/CyO,* y^+ x ♂ *y w; UAS-dmax-IR(2-7)/CyO,* y^+*; reptin/TM6B*, E: ♀ *y w; actin-GAL4/CyO,* y^+ x ♂ *y w; UAS-dmax-IR(2-7)/CyO,* y^+*; pontin/TM6B*. The viability of the genotypes A-E (% eclosed flies) was determined relative to the offspring numbers (eclosed flies) of the following reference (sister offspring) genotypes (numbers in brackets indicate the total number of eclosed reference genotype animals).: A: *y w; actin-GAL4/CyO* (82), B: *y w; CyO,* y^+*/UAS-dmax-IR(2-7); UAS-dmax-IR(5-2) UAS-dmax-IR(6-1)/+*, *y w; actin-GAL4/CyO,* y^+*; TM6B/+*, *y w; CyO,* y^+*/UAS-dmax-IR(2-7); TM6B/+* (98), C: *y w; actin-GAL4/CyO,* y^+*; Df(3L)fz2/+*, *y w; actin-GAL4/CyO,* y^+*; TM6B/+*, *y w; CyO,* y^+*/UAS-dmax-IR(2-7); Df(3L)fz2/+*, *y w; CyO,* y^+*/UAS-dmax-IR(2-7); TM6B/+* (119), D: *y w; actin-GAL4/CyO,* y^+*; reptin/+*, *y w; CyO,* y^+*/UAS-dmax-IR(2-7); reptin/+* (85), E: *y w; actin-GAL4/CyO,* y^+*; pontin/+*, *y w; CyO,* y^+*/UAS-dmax-IR(2-7); pontin/+* (74). In the cases where more than one reference genotype is listed, the viability ratios were calculated using the combined total offspring numbers of the indicated genotypes.

Figures 20ab, 21, 23a, 28a, 32, 33, 34abc, 35ab, 36ab, 38: Egg lays (duration: 6-10 h) were performed on apple agar plates supplemented with yeast paste. At 48 h AED (Figures 33, 34: 24 h AED), hatched larvae were flushed from the plates using tap water and collected in a sieve (indications for the time AED usually refer to the midpoints of the egg lays). Subsequently, the larvae were genotyped and put into tubes containing standard fly food (numbers of collected larvae: see Figures). At the time points indicated in the figures (e.g. 120 h AED) the larvae (or pupae) were collected by floatation with 30% glycerol. The survival rates of the larvae were determined as the ratio of larvae (or pupae) that were

found alive at the time of collection compared to the number of larvae that were initially put into the tubes (at 48 or 24 h AED). To compare larval size, the larvae were frozen and later photographed, using a Zeiss AxioCam HRc camera attached to a Zeiss Stemi SV 11 microscope.

Figure 48: The following crosses were set up: ♀ *y w hs-flp; actin>CD2>GAL4 UAS-GFP dmax^{1}/TM6B* x ♂ *y w; UAS-dmyc^{132}* (offspring D, E, F) and ♀ *y w hs-flp; actin>CD2>GAL4 UAS-GFP dmax^{1}/TM6B* x ♂ *y w; UAS-dmyc^{132}; dmax^{1}/TM6B* (offspring A, B, C). Egg lays (duration: 24 h) were performed on standard food and a heat shock (2 h 37° C in a water bath) was given at the time points indicated in the Figure. At 8 d AED, the offspring was collected by floatation with 30% glycerol. To calculate survival rates, the number of surviving A-F larvae was compared to the total number of sister genotype offspring in the respective crosses. Sister genotypes used in the calculation: D-F: *y w hs-flp/[y w or Y]; UAS-dmyc^{132}/+; TM6B/+*, A-C: *y w hs-flp/[y w or Y]; UAS-dmyc^{132}/+; TM6B/dmax^{1}*, *y w hs-flp/[y w or Y]; UAS-dmyc^{132}/+; TM6B/actin>CD2>GAL4 UAS-GFP dmax^{1}*.

Figure 49: The following crosses were set up: ♀ *y w hs-flp; actin>CD2>GAL4 UAS-GFP dmax^{1}/TM6B* x ♂ *y w; dmax^{1}/TM6B* (offspring A), ♀ *y w hs-flp; actin>CD2>GAL4 UAS-GFP dmax^{1}/TM6B* x ♂ *y w; UAS-dmyc^{132}; dmax^{1}/TM6B* (offspring B), ♀ *y w hs-flp; actin>CD2>GAL4 UAS-GFP dmax^{1}/TM6B* x ♂ *y w; UAS-dmyc^{132}* (offspring C). Egg lays (duration: 5 h) were performed on standard food. At 3 d AED, a heat shock (2 h 37° C in a water bath) was given. At 5 d AED, the offspring was collected by floatation with 30% glycerol. To calculate survival rates, the number of surviving A-C larvae was compared to the total number of sister genotype offspring in the respective crosses. Sister genotypes used in the calculation: A: *y w hs-flp/[y w or Y]; TM6B/dmax^{1}*, *y w hs-flp/[y w or Y]; TM6B/actin>CD2>GAL4 UAS-GFP dmax^{1}*, B: *y w hs-flp/[y w or Y]; UAS-dmyc^{132}/+; TM6B/dmax^{1}*, *y w hs-flp/[y w or Y]; UAS-dmyc^{132}/+; TM6B/actin>CD2>GAL4 UAS-GFP dmax^{1}*, C: *y w hs-flp/[y w or Y]; UAS-dmyc^{132}/+; TM6B/+*.

Figure 50: The following crosses were set up: ♀ *y w hs-flp; actin>CD2>GAL4 UAS-GFP dmax^{1}/TM6B* x ♂ *y w; UAS-dmyc^{132}* (offspring 50a A), ♀ *y w hs-flp; actin>CD2>GAL4 UAS-GFP dmax^{1}/TM6B* x ♂ *y w* (offspring 50a B), ♀ *y w hs-flp; actin>CD2>GAL4 UAS-GFP dmax^{1}/TM6B* x ♂ *y w; dmax^{1}/TM6B* (offspring 50b A), ♀ *y w hs-flp; actin>CD2>GAL4 UAS-GFP dmax^{1}/TM6B* x ♂ *y w; UAS-dmyc^{132}; dmax^{1}/TM6B* (offspring 50b B). Egg lays (duration: 12 h) were performed on standard food. At 2 d AED, a heat shock (2 h 37° C in a water bath) was given. At 3 d AED, larvae of the genotypes indicated in Figure 50ab were collected, staged and put on apple agar plates (supplemented with yeast paste). 24 h later (at 4 d AED), the larvae were inspected and staged again.

Figure 51a: The following crosses were set up: ♀ *y w hs-flp; actin>CD2>GAL4 UAS-GFP dmax^{1}/TM6B* x ♂ *y w; dmax^{1}/TM6B* (offspring A), ♀ *y w hs-flp; actin>CD2>GAL4 UAS-GFP dmax^{1}/TM6B* x ♂ *y w; UAS-dmyc^{132}; dmax^{1}/TM6B* (offspring B), ♀ *y w hs-flp; actin>CD2>GAL4 UAS-GFP dmax^{1}/TM6B* x ♂ *y w; UAS-dmyc^{132}; UAS-p35 dmax^{1}/TM6B* (offspring C). Egg lays (duration: 8 h) were performed on standard food. At 3 d AED, a heat shock (2 h 37° in a water bath) was given. At 5 d AED, At 5 d AED, the offspring was collected by floatation with 30% glycerol. To calculate survival rates, the number of surviving A-C larvae was compared to the total number of sister genotype offspring in the respective crosses. Sister genotypes used in the calculation: A: *y w hs-flp/[y w or Y]; TM6B/dmax^{1}*, *y w hs-flp/[y w or Y]; TM6B/actin>CD2>GAL4 UAS-GFP dmax^{1}*, B: *y w hs-flp/[y w or Y]; UAS-dmyc^{132}/+; TM6B/dmax^{1}*, *y w hs-flp/[y w or Y]; UAS-dmyc^{132}/+; TM6B/actin>CD2>GAL4 UAS-GFP dmax^{1}*, C: *y w hs-flp/[y w or Y]; UAS-dmyc^{132}/+; TM6B/UAS-p35 dmax^{1}*, *y w hs-flp/[y w or Y]; UAS-dmyc^{132}/+; TM6B/actin>CD2>GAL4 UAS-GFP dmax^{1}*.

Figures 52, 53: Egg lays (duration: maximally 12 h) were performed on standard food. Heat shocks (2 h 37° in water baths) were given as described in the figures. At an age of 6-9 d AED (Figure 53) or 4 d (Figure 52), larvae of the genotypes indicated in the figures were collected by floatation with 30% glycerol and put into fresh tubes. At 8, 11, 14, 20 and 28 d AED, the number of pupae was counted. The larvae (or pupae) were collected and photographed at the time points indicated in the figures.

11. Comparison of the sizes of larval fat bodies and salivary glands

Egg lays (duration: 10 h) were performed on standard fly food. At 5 d AED, *w dm^{4} dmnt^{1}*, *w; dmax^{1}* and *y w* larvae were collected, at 8 d AED, *w dm^{4} dmnt^{1}* and *w; dmax^{1}* were collected. The larvae were dissected in Ringer's solution, fat bodies and salivary glands were collected. The fat bodies and salivary glands were fixed in 4% paraformaldehyde in PBS for 20 min and washed in PBS three times for 10 min (each step). To stain the nuclei, 0.5 ug/ml Hoechst dye (33342) was included in the second washing step. Subsequently, the fat bodies and salivary glands were mounted in Vectashield mounting solution. Pictures (objective magnification: 5x and 63x) were taken using a Leica DMRA compound microscope.

12. Determination of larval total RNA content

Larvae of the genotypes and ages indicated in the Figures 24a, 24b, 37d and 37e were collected on ice. Subsequently, the larvae were homogenized in 1 ml of TRIZOL reagent (Invitrogen) using a Polytron tissue homogenizer (duration: 60 s). Immediately after homogenization, the homogenate was frozen at -80° C for at least 1 d. The total RNA was extracted and purified according to the protocol supplied with the TRIZOL reagent. The precipitated purified total RNA was redissolved in 20 ul ddH_2O. The concentration of the purified total RNA was measured with a Nanodrop ND-1000 spectrophotometer.

Based on the numbers of larvae that were homogenized, the total RNA content per larva was calculated.

13. Clonal analysis

13.1. *ey-flp* clones

The genotypes depicted in the Figures 39 and 40 originate from the following crosses:

y w dm^{A51} tub>dmyc>GAL4 hs-flp/Y; CyO, ey-flp (Figure 39, panel A):
♀ *y w dm^{A51} tub>dmyc>GAL4 hs-flp/FM7* x ♂ *y w; CyO, ey-flp/Bc Gla bw*

y w dm^{Rev} tub>dmyc>GAL4 hs-flp/Y; CyO, ey-flp (Figure 39, panel B):
♀ *y w dm^{Rev} tub>dmyc>GAL4 hs-flp* x ♂ *y w; CyO, ey-flp/Bc Gla bw*

y w ey-flp c-lacZ/w; FRT80B P^{w+}(70C) M(3)i55/FRT80B dmax^{1} (Figure 39, panel C):
♀ *y w ey-flp c-lacZ/FM6; FRT80B P^{w+}(70C) M(3)i55/TM6B* x ♂ *w; FRT80B dmax^{1}/TM6B*

y w ey-flp c-lacZ/w; FRT80B P^{w+}(70C) M(3)i55/FRT80B (Figure 39, panel D):
♀ *y w ey-flp c-lacZ/FM6; FRT80B P^{w+}(70C) M(3)i55/TM6B* x ♂ *w; FRT80B*

w dm^{4} FRT19/y cl(15B) FRT19; Sp/ey-flp (Figure 40, panel A):
♀ *y cl(15B) FRT19/FM6; ey-flp* x ♂ *w dm^{4} FRT19/Y; tub>dmyc>GAL4/Sp*

w dm^{4} dmnt^{1} FRT19/y cl(15B) FRT19; Sp/ey-flp (Figure 40, panel B):
♀ *y cl(15B) FRT19/FM6; ey-flp* x ♂ *w dm^{4} dmnt^{1} FRT19/Y; tub>dmyc>GAL4/Sp*

y w ey-flp/Y; FRT80 dmax^{1}/FRT80 cl^{w+} (Figure 40, panel C):
♀ *y w ey-flp; FRT80 cl^{w+}/TM6B, y^{+}* x ♂ *w; FRT80 dmax^{1}/TM6B*

y w FRT19/y cl(15B) FRT19; ey-flp/+ (Figure 40, panel D):
♀ *y cl(15B) FRT19/FM6; ey-flp* x ♂ *y w FRT19*

The fly lines *y w ey-flp c-lacZ/FM6; FRT80B P^{w+}(70C) M(3)i55/TM6B*, *y w ey-flp; FRT80 cl^{w+}/TM6B, y^{+}* and *y cl(15B) FRT19/FM6; ey-flp* were kindly provided by H. Stocker.

13.2. *hs-flp* clones

13.2.1. Crosses

To generate *dmax^{1}* clones, *y w hs-flp; FRT80 dmax^{1}/TM6B* males were crossed to *y w hs-flp; FRT80 ubi-GFP* virgins. To generate *dm^{4}* clones, *w dm^{4} FRT19/FM7* virgins were crossed to *y w hs-flp hs-GFP FRT19* males. To generate *dm^{4} dmnt^{1}* clones, *w dm^{4} dmnt^{1} FRT19/FM7* virgins were crossed to *y w hs-flp hs-GFP FRT19* males. The *y w hs-flp hs-GFP FRT19* line was kindly provided by K. Basler.

13.2.2. Generation and analysis of wing disc clones

Egg lays (duration: 6 h) were performed on standard food. *dm*^{4} and *dm*^{4} *dmnt*^{1} clones with a final age of 72 h were induced at 48 h AED (Heat shock: 15 min 37°C in a water bath). *dmax*^{1} clones with a final age of 72 h were induced at 48 h AED (Heat shock: 30 min 37°C in a water bath). *dmax*^{1} clones with a final age of 96 h were induced at 24 h AED (Heat shock: 30 min 37°C in a water bath). At 120 h AED, the larvae were dissected in Ringer's solution and the wing discs were collected. In the *dm*^{4} and *dm*^{4} *dmnt*^{1} genotypes, the expression of *hs-GFP* was induced by a heat shock (1 h 37° in a water bath) at 3 h prior to dissection. The wing discs were fixed in 4% paraformaldehyde in PBS for 15 min and washed in PBS three times for 10 min. To stain the nuclei, 0.5 ug/ml Hoechst dye (33342) was included in the second washing step. Subsequently, wing discs were mounted in Vectashield mounting solution. Pictures of the wing discs were taken with a Leica SP2 confocal microscope (objective magnification: 40x). Clone (and twin spot) size was determined as the total pixel count a clone (and a twinspot) covers in a picture. Pixel counts were determined with Adobe Photoshop. Counting the number of cell nuclei in a clone, the cell sizes were calculated. Number of analyzed clones/twinspots: *dm*^{4} 72 h: 12/15, *dm*^{4} *dmnt*^{1} 72 h: 15/19, *dmax*^{1} 72 h: 16/16, *dmax*^{1} 96 h: 5/7. In order to determine the frequency of single twin spots, the following number of twin spots was checked for the presence of a mutant clone: *dm*^{4} 72 h: 28, *dm*^{4} *dmnt*^{1} 72 h: 24, *dmax*^{1} 72 h: 106, *dmax*^{1} 96 h: 16.

13.2.3. Generation of clones in the fat body

The clones had to be induced prior to polyploidization (after which FRT-mediated recombination would only shuffle chromosome arms, but not create homozygous mutant cells). An egg lay of 3 h was performed. 6 h later, clones were induced by a heat shock of 1 h (37° in a water bath). At 120 h AED, the larvae were dissected in Ringer's solution and the fat bodies were collected. In the *dm*^{4} *dmnt*^{1} genotype, the expression of *hs-GFP* was induced by a heat shock (1 h 37° in a water bath) at 3 h prior to dissection. The fat bodies were fixed in 4% paraformaldehyde in PBS for 15 min and washed in PBS three times for 10 min. To stain the nuclei, 0.5 ug/ml Hoechst dye (33342) was included in the second washing step. Subsequently, fat bodies were mounted in Vectashield mounting solution. Pictures (objective magnification: 10x) were taken using a Leica DMRA compound microscope.

13.2.4. Generation of *dmax*^{1} mutant bristles

A heat shock of 1 h at 37° C in a water bath was given at 24 h AED.

13.3. Analysis of competition in *dmax*^{1} larvae

To generate *tub>dmyc>GAL4* flp-out clones, the following cross was set up: ♀ *y w tub>dmyc>GAL4 hs-flp; dmax*^{1}*/TM6B, ubi-GFP* x ♂ *y w; UAS-GFP; dmax*^{1}*/TM6B, ubi-GFP*. To generate *actin>CD2>GAL4* flp-out clones, the following cross was set up: ♀ *y w hs-flp; actin>CD2>GAL4*

UAS-GFP dmax^{1}*/TM6B* x ♂ *y w; dmax*^{1}*/TM6B*. Egg lays (duration: 12 h) were performed on standard food. Flp-out clones with a final age of 96 h were induced at 120 h AED (Heat shock: for the *act>CD2>GAL4* clones: 5 min 37°C in a water bath, for the *tub>dmyc>GAL4* clones: 12 min 37°C in a water bath). At 216 h AED, *dmax*^{1} larvae were dissected in Ringer's solution and the wing discs were collected. The wing discs were fixed in 4% paraformaldehyde in PBS for 15 min and washed in PBS three times for 10 min. To stain the nuclei, 0.5 ug/ml Hoechst dye (33342) was included in the second washing step. Subsequently, wing discs were mounted in Vectashield mounting solution. Pictures (objective magnification: 10x) were taken using a Leica DMRA compound microscope. Clone size was determined as the total pixel count a clone covers in a picture. Pixel counts were determined with Adobe Photoshop. The sizes of 53 *act>CD2>GAL4* clones from 14 discs and 39 *tub>CD2>GAL4* from 6 discs were determined.

14. Ecdysone feeding assay

The protocol used in the feeding assay is a modified version of Gates et al. (2004). Larvae of the genotypes indicated in Figure 54 were grown on standard food. At 6 d AED (in a second experiment that gave similar results: at 7 d AED), the larvae were collected by floatation with 30% glycerol and placed on plates with yeast paste containing 1 mg/ml ecdysone or control plates with yeast paste without ecdysone. Subsequently, the development of the larvae was observed.

Preparation of the yeast plates: To make yeast paste for 1 feeding plate containing 1 mg/ml 20-hydroxyecdysone (H5142, Sigma-Aldrich), 16.8 ul of a 12 mg/ml stock solution (in EtOH abs.) was diluted in 183.2 ul water and added to 0.1 g of dry yeast. For control plates, 16.8 ul of EtOH abs. was diluted in 183.2 ul water and added to 0.1 g of dry yeast. The yeast paste was placed as a blob on damp filter paper (Schleicher & Schuell filter papers circles, diameter: 55 mm, Ref. No. 10336207) in plastic petri dishes (Greiner Bio-One, diameter 60 mm). Small holes were burnt into the petri dish covers to allow circulation of air. The covered petri dishes had to be sealed tightly to prevent escape of the larvae. To prevent drying of the yeast, the filter paper was moistened with water every 24 h.

15. qRTPCR

Figure 5: Wandering third instar larvae of the genotypes *y w; +/actin-GAL4* (10 larvae), *y w; UAS-dmax-IR(2-7)/actin-GAL4; TM6B/+* (9 larvae), *y w; UAS-dmax-IR(2-7)/actin-GAL4; UAS-dmax-IR(5-2) UAS-dmax-IR(6-1)/+* (8 larvae) and *y w; P{y*$^{+}$ *w*$^{+}$*}CG9666*^{EY02775} (10 larvae) were collected. The larvae were homogenized in 800 µl TRIZOL reagent (Invitrogen) using a Polytron tissue homogenizer (duration: 30 s). RNA was extracted and purified according to the protocol supplied with the TRIZOL reagent. The RNA was further purified with the RNeasy Mini Kit (Qiagen) and subjected to an on-column DNase digestion (RNase-Free DNase Set (Qiagen)). The resulting RNA (elution volume: 30 ul) had concentrations between 0.2 ug/ul and 0.9 ug/ul. The quality of the extracted RNA was assessed

with agarose gel electrophoresis. cDNA was synthesized with the Omniscript Reverse Transcription Kit (Qiagen) using an oligo dT primer (AffyT7 2450969-F, sequence 5' GGCCAGTGAATTGTAATACGACTCACTATAGGGAGGCGG $(dT)_{24}$ 3'). 2 ul of template RNA was used in the reverse transcription step. Control reactions lacking the RT enzyme were set up to control for genomic DNA contamination. qRTPCR reactions were performed on an ABI 7900 Real Time PCR Instrument (Applied Biosystems) using the SYBR GREEN PCR Master Mix (Applied Biosystems). PCR conditions: volume (total): 20 ul, volume (primer pairs at 10 uM): 2 ul, volume (template): 1 ul, cycling parameters: 2 min 50° C, 10 min 95° C, 40 x [15 s 95° C, 1 min 60° C]. Dissociation curve measurements were included in the PCR run to document the specificity of the amplification reaction. Data collection and primary analysis were conducted using SDS 2.0 software (Applied Biosystems), subsequent analyses and relative target gene quantitation was performed using Microsoft Excel. The amount of target, normalized to *act42A*, and relative to the calibrator (target gene levels in the *y w; +/actin-GAL4* genotype), is given by $2^{-\Delta\Delta Ct}$, where $\Delta\Delta Ct = \Delta Ct(\text{sample}) - \Delta Ct(\text{calibrator})$, and ΔCt is the Ct of the target gene subtracted from the Ct of the *act42A* reaction. The following primer pairs were used in the qRTPCR reactions:

Gene	Primer name	Sequence (5'-3')
dmax	dmaxF.3UTR	AACCCACCCAATCGACCTTAAT
	dmaxR.3UTR	TTCTTTGCGCACAGAGTGACA
CG9666	CG9666.3prime.forw	GTTTACTCCCTACACAAGACGTCAAC
	CG9666.3prime.rev	CCCCATTCCAGTGCCTTTT
Act42A	Act42A.F	GAGCGCGGTTACAGCTTCA
	Act42A.R	TCCTTGATGTCGCGCACA
RpL32	RpL32_fwd	GCAAGCCCAAGGGTATCG
	RpL32_rev	TTGGGCATCAGATACTGTCCC

Figures 25a, 55, 56: Larvae of the genotypes and ages indicated in the Figures 25a, 55 and 56 were collected on ice (*y w* and $dmax^1$/+ larvae: 12 larvae per RNA sample, $dmax^1$ larvae: 20 larvae per RNA sample). Subsequently, the larvae were homogenized in 1 ml of TRIZOL reagent (Invitrogen) using a Polytron tissue homogenizer (duration: 60 s). Immediately after homogenization, the homogenate was frozen at -80° C for at least 1 d. The total RNA was extracted and purified according to the protocol supplied with the TRIZOL reagent. The precipitated purified total RNA was redissolved in 20 ul ddH_2O. The concentration of the purified total RNA was measured with a Nanodrop ND-1000 spectrophotometer. To remove traces of genomic DNA, 10 ug of RNA were subjected to a DNase digestion, using the Ambion TURBO DNA-free kit. Subsequently, the quality of the purified RNA was confirmed using Bioanalyzer chips (Agilent). The Bioanalyzer electropherograms also served to confirm the Nanodrop concentration measurements. cDNA was synthesized with the Omniscript Reverse Transcription Kit (Qiagen) using random hexamer primers. 1 ug of template RNA was used in the reverse transcription step. Mock RT reactions (containing 1 ug of

template RNA and H_2O) were performed in order to control for remaining traces of genomic DNA. qRTPCR reactions were performed on an ABI 7900 Real Time PCR Instrument (Applied Biosystems) using the SYBR GREEN PCR Master Mix (Applied Biosystems). PCR conditions: volume (total): 10 ul, volume (primer pairs at 10 uM): 0.3 ul, volume (template): 2 ul, cycling parameters: 2 min 50° C, 10 min 95° C, 40 x [15 s 95° C, 1 min 60° C]. Dissociation curve measurements were included in the PCR run to document the specificity of the amplification reaction. Data collection and primary analysis were conducted using SDS 2.0 software (Applied Biosystems), subsequent analyses and relative target gene quantitation was performed using Microsoft Excel. The amount of target, normalized to *actin5C*, and relative to the calibrator (target gene levels in *y w hs-flp/[y w or Y]; actin>CD2>GAL4 UAS-GFP dmax*^{1}/+ larvae for Figure 55, in *y w* larvae for Figure 56), is given by $2^{-\Delta\Delta Ct}$, where $\Delta\Delta Ct = \Delta Ct(sample) - \Delta Ct(calibrator)$, and ΔCt is the Ct of the target gene subtracted from the Ct of the *actin5C* reaction. The following primer pairs were used in the qRTPCR reactions:

Assay/Gene	Primer name	Sequence (5'-3')
actin5C	PG_act5C_F1	GCCCATCTACGAGGGTTATGC
	PG_act5C_R1	AATCGCGACCAGCCAGATC
dmyc	dmyc_RTPCR_f	GAATCGCGCTCGGTTAGTG
	dmyc_RTPCR_r	CTACGCCGCCGCTTTAAG
dmax	dmax_qRTPCR_ex2ex3_forw	CACAAACACCGCCAATTTCA
	dmax_qRTPCR_ex2ex3_rev	CGCCTTCGCTCCAAAGC
nnp1	PG_nnp1_F1	CTATACACACGAAAGTTTCC ATGCTATA
	PG_nnp1_R1	CAACACGGAACTATCGTAAATTTCA
CG5033	PG_CG5033_F1	TAACCGCTCGGCTTTAATTCAT
	PG_CG5033_R1	CCCTTGCTCTTGGAGAATGG
*rRNA(ITS1b)**	rDNA_ITS1_2fw	GCTTGGCAACCTCATAAAAAGATTT
	rDNA_ITS1_rev	AGGAAACGCCGTTGTTGTAAGT
5sRNA	5sRNA_fw	CGTCCGATCACCGAAATTAAG
	5sRNA_rev	CCAAGCGGTCCCTCATCTAA
snoRNA U3	PG_U3_f	TTTCACACTAGCTGAAAGCCAAGT
	PG_U3_r	CCTCACGCTGCCGAATAGAA
snoRNA 46	PG_snR46_f	CTTTGTCGAAGACCGTTTTGC
	PG_snR46_r	TGCTTTGGGCTTCGTTTTG
tRNA(Leu)	tRNALeu.L	TAAGGCGCCAGACTCAAGAT
	tRNALeu.R	CCTCAAAGAGGACCAGAACG

* The primers in the *rRNA(ITS1b)* assay bind to the internal transcribed spacer 1 (ITS1) of the polycistronic gene cassette encoding the 18sRNA, 5.8sRNA, 2sRNA and 28sRNA. Tandem arrays of this gene cassette form the X-chromosomal *bobbed* and the Y-chromosomal *Y-bobbed* locus.

16. Data represented in multiple figures

For the sake of clarity, the data listed below were shown in multiple figures. The data are listed in the order of their appearance.

14ab A	15ab A	16ab A	18ab A
14ab C	15ab A'	16ab A'	18ab A'
14ab D	15ab C	16ab C	18ab B
14ab F	15ab C'	16ab C'	18ab B'
14b A	17b R		
14b C	17b R'		
14c A	16c A		
14c C	16c A'		
14c D	16c C		
14c F	16c C'		
20a A	34a A		
20a B	34a B		
20b B	36a A		
20c A	37b B		
20c A'	37c B		
20c B	37b E		
20c B'	37c E		
20c C	37b D		
20c C'	37c D		
21 A (120 h AED)	35b A		
21 A (192 h AED)	36b A		
21 B (192 h AED)	36b B		
24a A	37d B		
24a B	32 A	37d C	
24b A	37e B		
24b B	37e C		
25a A1	56 A (*dmax* assay)		
25a A2	56 B (*dmax* assay)		
25a B1	56 E (*dmax* assay)		
25a B2	56 F (*dmax* assay)		
32 B	34a C		

References

Amati, B., Dalton, S., Brooks, M. W., Littlewood, T. D., Evan, G. I., and Land, H. (1992). Transcriptional activation by the human c-Myc oncoprotein in yeast requires interaction with Max. Nature *359*, 423-426.

Amati, B., Brooks, M. W., Levy, N., Littlewood, T. D., Evan, G. I., and Land, H. (1993a). Oncogenic activity of the c-Myc protein requires dimerization with Max. Cell *72*, 233-245.

Amati, B., Littlewood, T. D., Evan, G. I., and Land, H. (1993b). The c-Myc protein induces cell cycle progression and apoptosis through dimerization with Max. EMBO Journal *12*, 5083-5087.

Arsura, M., Deshpande, A., Hann, S. R., and Sonenshein, G. E. (1995). Variant Max protein, derived by alternative splicing, associates with c-Myc in vivo and inhibits transactivation. Mol Cell Biol *15*, 6702-6709.

Ashburner, M., Golic, K. G., and Hawley, R. S. (2005). Drosophila: a laboratory handbook, Vol 1, 2nd edn (Cold Spring Harbor, New York, Cold Spring Harbor Laboratory Press).

Askew, D. S., Ashmun, R. A., Simmons, B. C., and Cleveland, J. L. (1991). Constitutive c-myc expression in an IL-3-dependent myeloid cell line suppresses cell cycle arrest and accelerates apoptosis. Oncogene *6*, 1915-1922.

Ayer, D. E., and Eisenman, R. N. (1993). A switch from Myc:Max to Mad:Max heterocomplexes accompanies monocyte/macrophage differentiation. Genes & Development *7*, 2110-2119.

Ayer, D. E., Kretzner, L., and Eisenman, R. N. (1993). Mad: a heterodimeric partner for Max that antagonizes Myc transcriptional activity. Cell *72*, 211-222.

Barone, M. V., and Courtneidge, S. (1995). Myc but not fos rescue of pdgf signalling block caused by kinase inactive src. Nature *378*, 509-512.

Bellosta, P., Hulf, T., Diop, S. B., Usseglio, F., Pradel, J., Aragnol, D., and Gallant, P. (2005). Myc interacts genetically with Tip48/Reptin and Tip49/Pontin to control growth and proliferation during Drosophila development. Proc Natl Acad Sci U S A *102*, 11799-11804.

Benassayag, C., Montero, L., Colombie, N., Gallant, P., Cribbs, D., and Morello, D. (2005). Human c-Myc isoforms differentially regulate cell growth and apoptosis in Drosophila melanogaster. Mol Cell Biol *25*, 9897-9909.

Bender, M., Imam, F. B., Talbot, W. S., Ganetzky, B., and Hogness, D. S. (1997). Drosophila ecdysone receptor mutations reveal functional differences among receptor isoforms. Cell *91*, 777-788.

Berberich, S. J., and Cole, M. D. (1992). Casein kinase II inhibits the DNA-binding activity of Max homodimers but not Myc/Max heterodimers. Genes Dev *6*, 166-176.

Billin, A. N., Eilers, A. L., Queva, C., and Ayer, D. E. (1999). Mlx, a novel Max-like BHLHZip protein that interacts with the Max network of transcription factors. J Biol Chem *274*, 36344-36350.

Billin, A. N., Eilers, A. L., Coulter, K. L., Logan, J. S., and Ayer, D. E. (2000). MondoA, a novel basic helix-loop-helix-leucine zipper transcriptional activator that constitutes a positive branch of a max-like network. Mol Cell Biol *20*, 8845-8854.

Blackwell, T. K., Huang, J., Ma, A., Kretzner, L., Alt, F. W., Eisenman, R. N., and Weintraub, H. (1993). Binding of myc proteins to canonical and noncanonical DNA sequences. Molecular & Cellular Biology *13*, 5216-5224.

Blackwood, E. M., and Eisenman, R. N. (1991). Max: a helix-loop-helix zipper protein that forms a sequence-specific DNA-binding complex with Myc. Science *251*, 1211-1217.

Blackwood, E. M., Kretzner, L., and Eisenman, R. N. (1992). Myc and Max function as a nucleoprotein complex. Current Opinion in Genetics & Development *2*, 227-235.

Bohni, R., Riesgo-Escovar, J., Oldham, S., Brogiolo, W., Stocker, H., Andruss, B. F., Beckingham, K., and Hafen, E. (1999). Autonomous control of cell and organ size by CHICO, a Drosophila homolog of vertebrate IRS1-4. Cell *97*, 865-875.

Boon, K., Caron, H. N., van Asperen, R., Valentijn, L., Hermus, M. C., van Sluis, P., Roobeek, I., Weis, I., Voute, P. A., Schwab, M., and Versteeg, R. (2001). N-myc enhances the expression of a large set of genes functioning in ribosome biogenesis and protein synthesis. EMBO Journal *20*, 1383-1393.

Bourbon, H. M., Gonzy-Treboul, G., Peronnet, F., Alin, M. F., Ardourel, C., Benassayag, C., Cribbs, D., Deutsch, J., Ferrer, P., Haenlin, M.*, et al.* (2002). A P-insertion screen identifying novel X-linked essential genes in Drosophila. Mech Dev *110*, 71-83.

Bridges, C. B. (1935). Drosophila melanogaster: Legend for symbols, mutants, valuations. Drosophila Information Service *3*, 5-19.

Caldwell, P. E., Walkiewicz, M., and Stern, M. (2005). Ras activity in the Drosophila prothoracic gland regulates body size and developmental rate via ecdysone release. Curr Biol *15*, 1785-1795.

Cheng, S. W., Davies, K. P., Yung, E., Beltran, R. J., Yu, J., and Kalpana, G. V. (1999). c-MYC interacts with INI1/hSNF5 and requires the SWI/SNF complex for transactivation function. Nature Genetics *22*, 102-105.

Chin, L., Schreiber-Agus, N., Pellicer, I., Chen, K., Lee, H. W., Dudast, M., Cordon-Cardo, C., and DePinho, R. A. (1995). Contrasting roles for Myc and Mad proteins in cellular growth and differentiation. Proc Natl Acad Sci U S A *92*, 8488-8492.

Church, R. B., and Robertson, F. W. (1966). Biochemical analysis of genetic differences in the growth of Drosophila. Genet Res *7*, 383-407.

Colombani, J., Bianchini, L., Layalle, S., Pondeville, E., Dauphin-Villemant, C., Antoniewski, C., Carre, C., Noselli, S., and Leopold, P. (2005). Antagonistic actions of ecdysone and insulins determine final size in Drosophila. Science *310*, 667-670.

Cowling, V. H., and Cole, M. D. (2006). Mechanism of transcriptional activation by the Myc oncoproteins. Seminars in Cancer Biology *16*, 242.

Crouch, D. H., Fisher, F., Clark, W., Jayaraman, P. S., Goding, C. R., and Gillespie, D. A. (1993). Gene-regulatory properties of Myc helix-loop-helix/leucine zipper mutants: Max-dependent DNA binding and transcriptional activation in yeast correlates with transforming capacity. Oncogene *8*, 1849-1855.

Davis, A. C., Wims, M., Spotts, G. D., Hann, S. R., and Bradley, A. (1993). A null c-myc mutation causes lethality before 10.5 days of gestation in homozygotes and reduced fertility in heterozygous female mice. Genes & Development *7*, 671-682.

De La Cova, C., Abril, M., Bellosta, P., Gallant, P., and Johnston, L. A. (2004). Drosophila myc regulates organ size by inducing cell competition. Cell *117*, 107-116.

Dezfouli, S., Bakke, A., Huang, J., Wynshaw-Boris, A., and Hurlin, P. J. (2006). Inflammatory disease and lymphomagenesis caused by deletion of the Myc antagonist Mnt in T cells. Mol Cell Biol *26*, 2080-2092.

Etard, C., Gradl, D., Kunz, M., Eilers, M., and Wedlich, D. (2005). Pontin and Reptin regulate cell proliferation in early Xenopus embryos in collaboration with c-Myc and Miz-1. Mech Dev *122*, 545-556.

Evan, G. I., Wyllie, A. H., Gilbert, C. S., Littlewood, T. D., Land, H., Brooks, M., Waters, C. M., Penn, L. Z., and Hancock, D. C. (1992). Induction of apoptosis in fibroblasts by c-myc protein. Cell *69*, 119-128.

Foley, K. P., McArthur, G. A., Queva, C., Hurlin, P. J., Soriano, P., and Eisenman, R. N. (1998). Targeted disruption of the MYC antagonist MAD1 inhibits cell cycle exit during granulocyte differentiation. EMBO Journal *17*, 774-785.

Freeman, M. (1996). Reiterative use of the EGF receptor triggers differentiation of all cell types in the Drosophila eye. Cell *87*, 651-660.

Gallant, P., Shiio, Y., Cheng, P. F., Parkhurst, S. M., and Eisenman, R. N. (1996). Myc and Max homologs in Drosophila. Science *274*, 1523-1527.

Gallant, P. (2006). Myc / Max / Mad in invertebrates - the evolution of the Max network CTMI *302*, 237-254.

Garen, A., Kauvar, L., and Lepesant, J. A. (1977). Roles of ecdysone in Drosophila development. Proc Natl Acad Sci U S A *74*, 5099-5103.

Gates, J., Lam, G., Ortiz, J. A., Losson, R., and Thummel, C. S. (2004). rigor mortis encodes a novel nuclear receptor interacting protein required for ecdysone signaling during Drosophila larval development. Development *131*, 25-36.

Gomez-Roman, N., Grandori, C., Eisenman, R. N., and White, R. J. (2003). Direct activation of RNA polymerase III transcription by c-Myc. Nature *421*, 290-294.

Goodliffe, J. M., Wieschaus, E., and Cole, M. D. (2005). Polycomb mediates Myc autorepression and its transcriptional control of many loci in Drosophila. Genes Dev *19*, 2941-2946.

Grandori, C., Mac, J., Siebelt, F., Ayer, D. E., and Eisenman, R. N. (1996). Myc-Max heterodimers activate a DEAD box gene and interact with multiple E box-related sites in vivo. Embo J *15*, 4344-4357.

Grandori, C., Gomez-Roman, N., Felton-Edkins, Z. A., Ngouenet, C., Galloway, D. A., Eisenman, R. N., and White, R. J. (2005). c-Myc binds to human ribosomal DNA and stimulates transcription of rRNA genes by RNA polymerase I. Nat Cell Biol *7*, 311-318.

Grewal, S. S., Li, L., Orian, A., Eisenman, R. N., and Edgar, B. A. (2005). Myc-dependent regulation of ribosomal RNA synthesis during Drosophila development. Nat Cell Biol *7*, 295-302.

Hatton, K. S., Mahon, K., Chin, L., Chiu, F. C., Lee, H. W., Peng, D. M., Morgenbesser, S. D., Horner, J., and Depinho, R. A. (1996). Expression and activity of l-myc in normal mouse development. Molecular & Cellular Biology *16*, 1794-1804.

Hay, B. A., Maile, R., and Rubin, G. M. (1997). P element insertion-dependent gene activation in the drosophila eye. Proceedings of the National Academy of Sciences of the United States of America *94*, 5195-5200.

Henriksson, M., and Luscher, B. (1996). Proteins of the Myc network: essential regulators of cell growth and differentiation. [Review] [267 refs]. Adv Cancer Res *68*, 109-182.

Hollis, G. F., Mitchell, K. F., Battey, J., Potter, H., Taub, R., Lenoir, G. M., and Leder, P. (1984). A variant translocation places the lambda immunoglobulin genes 3' to the c-myc oncogene in Burkitt's lymphoma. Nature *307*, 752-755.

Hopewell, R., and Ziff, E. B. (1995). The nerve growth factor-responsive PC12 cell line does not express the Myc dimerization partner Max. Mol Cell Biol *15*, 3470-3478.

Hulf, T., Bellosta, P., Furrer, M., Steiger, D., Svensson, D., Barbour, A., and Gallant, P. (2005). Whole-genome analysis reveals a strong positional bias of conserved dMyc-dependent E-boxes. Mol Cell Biol *25*, 3401-3410.

Hurlin, P. J., Queva, C., Koskinen, P. J., Steingrimsson, E., Ayer, D. E., Copeland, N. G., Jenkins, N. A., and Eisenman, R. N. (1995). Mad3 and Mad4: novel Max-interacting transcriptional repressors that suppress c-myc dependent transformation and are expressed during neural and epidermal differentiation. EMBO Journal *14*, 5646-5659.

Hurlin, P. J., Queva, C., and Eisenman, R. N. (1997a). Mnt, a novel Max-interacting protein is coexpressed with Myc in proliferating cells and mediates repression at Myc binding sites. Genes & Development *11*, 44-58.

Hurlin, P. J., Queva, C., and Eisenman, R. N. (1997b). Mnt: a novel Max-interacting protein and Myc antagonist. Current Topics in Microbiology & Immunology *224*, 115-121.

Hurlin, P. J., Steingrimsson, E., Copeland, N. G., Jenkins, N. A., and Eisenman, R. N. (1999). Mga, a dual-specificity transcription factor that interacts with Max and contains a T-domain DNA-binding motif. Embo J *18*, 7019-7028.

Hurlin, P. J., Zhou, Z. Q., Toyo-oka, K., Ota, S., Walker, W. L., Hirotsune, S., and Wynshaw-Boris, A. (2003). Deletion of Mnt leads to disrupted cell cycle control and tumorigenesis. Embo J *22*, 4584-4596.

Hurlin, P. J., and Huang, J. (2006). The MAX-interacting transcription factor network. Seminars in Cancer Biology *16*, 265.

Iritani, B. M., and Eisenman, R. N. (1999). c-Myc enhances protein synthesis and cell size during B lymphocyte development. Proceedings of the National Academy of Sciences of the United States of America *96*, 13180-13185.

Johnston, L. A., Prober, D. A., Edgar, B. A., Eisenman, R. N., and Gallant, P. (1999). Drosophila myc regulates cellular growth during development. Cell *98*, 779-790.

Karn, J., Watson, J. V., Lowe, A. D., Green, S. M., and Vedeckis, W. (1989). Regulation of cell cycle duration by c-myc levels. Oncogene *4*, 773-787.

Kato, G. J., Barrett, J., Villa, G. M., and Dang, C. V. (1990). An amino-terminal c-myc domain required for neoplastic transformation activates transcription. Molecular & Cellular Biology *10*, 5914-5920.

Kato, G. J., Lee, W. M., Chen, L. L., and Dang, C. V. (1992). Max: functional domains and interaction with c-Myc. Genes Dev *6*, 81-92.

Kelly, K., Cochran, B. H., Stiles, C. D., and Leder, P. (1983). Cell-specific regulation of the c-myc gene by lymphocyte mitogens and platelet-derived growth factor. Cell *35*, 603-610.

Kohl, N. E., Kanda, N., Schreck, R. R., Bruns, G., Latt, S. A., Gilbert, F., and Alt, F. W. (1983). Transposition and amplification of oncogene-related sequences in human neuroblastomas. Cell *35*, 359-367.

Kolev, N. G., and Steitz, J. A. (2005). Symplekin and multiple other polyadenylation factors participate in 3'-end maturation of histone mRNAs. Genes Dev *19*, 2583-2592.

Koskinen, P. J., Ayer, D. E., and Eisenman, R. N. (1995). Repression of Myc-Ras cotransformation by Mad is mediated by multiple protein-protein interactions. Cell Growth & Differentiation *6*, 623-629.

Kretzner, L., Blackwood, E. M., and Eisenman, R. N. (1992). Myc and Max proteins possess distinct transcriptional activities. Nature *359*, 426-429.

Krippner-Heidenreich, A., Talanian, R. V., Sekul, R., Kraft, R., Thole, H., Ottleben, H., and Luscher, B. (2001). Targeting of the transcription factor Max during apoptosis: phosphorylation-regulated cleavage by caspase-5 at an unusual glutamic acid residue in position P1. Biochem J *358*, 705-715.

Lambertsson, A. (1998). The minute genes in Drosophila and their molecular functions. Advances in Genetics *38*, 69-134.

Leone, G., Degregori, J., Sears, R., Jakoi, L., and Nevins, J. R. (1997). Myc and ras collaborate in inducing accumulation of active cyclin e/cdk2 and e2f. Nature *387*, 422-426.

Li, T., and Bender, M. (2000). A conditional rescue system reveals essential functions for the ecdysone receptor (EcR) gene during molting and metamorphosis in Drosophila. Development *127*, 2897-2905.

Loo, L. W., Secombe, J., Little, J. T., Carlos, L. S., Yost, C., Cheng, P. F., Flynn, E. M., Edgar, B. A., and Eisenman, R. N. (2005). The transcriptional repressor dMnt is a regulator of growth in Drosophila melanogaster. Mol Cell Biol *25*, 7078-7091.

Maines, J. Z., Stevens, L. M., Tong, X., and Stein, D. (2004). Drosophila dMyc is required for ovary cell growth and endoreplication. Development *131*, 775-786.

Makela, T. P., Koskinen, P. J., Vastrik, I., and Alitalo, K. (1992). Alternative forms of Max as enhancers or suppressors of Myc-ras cotransformation. Science *256*, 373-377.

Mao, D. Y., Watson, J. D., Yan, P. S., Barsyte-Lovejoy, D., Khosravi, F., Wong, W. W., Farnham, P. J., Huang, T. H., and Penn, L. Z. (2003). Analysis of Myc bound loci identified by CpG island arrays shows that Max is essential for Myc-dependent repression. Curr Biol *13*, 882-886.

McMahon, S. B., Van, B. H., Dugan, K. A., Copeland, T. D., and Cole, M. D. (1998). The novel ATM-related protein TRRAP is an essential cofactor for the c-Myc and E2F oncoproteins. Cell *94*, 363-374.

Min, S., and Taparowsky, E. J. (1992). v-Myc, but not Max, possesses domains that function in both transcription activation and cellular transformation. Oncogene *7*, 1531-1540.

Mirth, C., Truman, J. W., and Riddiford, L. M. (2005). The role of the prothoracic gland in determining critical weight for metamorphosis in Drosophila melanogaster. Curr Biol *15*, 1796-1807.

Montagne, J., Stewart, M. J., Stocker, H., Hafen, E., Kozma, S. C., and Thomas, G. (1999). Drosophila S6 kinase: A regulator of cell size. Science *285*, 2126-2129.

Moreno, E., and Basler, K. (2004). dMyc transforms cells into super-competitors. Cell *117*, 117-129.

Nau, M. M., Brooks, B. J., Battey, J., Sausville, E., Gazdar, A. F., Kirsch, I. R., McBride, O. W., Bertness, V., Hollis, G. F., and Minna, J. D. (1985). L-myc, a new myc-related gene amplified and expressed in human small cell lung cancer. Nature *318*, 69-73.

Nesbit, C. E., Tersak, J. M., and Prochownik, E. V. (1999). MYC oncogenes and human neoplastic disease [Review]. Oncogene *18*, 3004-3016.

Neufeld, T. P., and Hariharan, I. K. (2002). Regulation of growth and cell proliferation in eye development. In Drosophila Eye Development, K. Moses, ed. (New York, Springer Verlag), pp. 107-133.

Nilsson, J. A., Maclean, K. H., Keller, U. B., Pendeville, H., Baudino, T. A., and Cleveland, J. L. (2004). Mnt loss triggers Myc transcription targets, proliferation, apoptosis, and transformation. Mol Cell Biol *24*, 1560-1569.

Ogawa, H., Ishiguro, K., Gaubatz, S., Livingston, D. M., and Nakatani, Y. (2002). A complex with chromatin modifiers that occupies E2F- and Myc-responsive genes in G0 cells. Science *296*, 1132-1136.

Orian, A., van Steensel, B., Delrow, J., Bussemaker, H. J., Li, L., Sawado, T., Williams, E., Loo, L. W., Cowley, S. M., Yost, C*., et al.* (2003). Genomic binding by the Drosophila Myc, Max, Mad/Mnt transcription factor network. Genes Dev *17*, 1101-1114.

Penn, L. J., Brooks, M. W., Laufer, E. M., and Land, H. (1990). Negative autoregulation of c-myc transcription. Embo J *9*, 1113-1121.

Pierce, S. B., Yost, C., Britton, J. S., Loo, L. W., Flynn, E. M., Edgar, B. A., and Eisenman, R. N. (2004). dMyc is required for larval growth and endoreplication in Drosophila. Development *131*, 2317-2327.

Prendergast, G. C., Lawe, D., and Ziff, E. B. (1991). Association of Myn, the murine homolog of max, with c-Myc stimulates methylation-sensitive DNA binding and ras cotransformation. Cell *65*, 395-407.

Queva, C., McArthur, G. A., Iritani, B. M., and Eisenman, R. N. (2001). Targeted deletion of the S-phase-specific Myc antagonist Mad3 sensitizes neuronal and lymphoid cells to radiation-induced apoptosis. Mol Cell Biol *21*, 703-712.

Roussel, M. F., Cleveland, J. L., Shurtleff, S. A., and Sherr, C. J. (1991). Myc rescue of a mutant CSF-1 receptor impaired in mitogenic signalling. Nature *353*, 361-363.

Sawai, S., Shimono, A., Hanaoka, K., and Kondoh, H. (1991). Embryonic lethality resulting from disruption of both N-myc alleles in mouse zygotes. New Biologist *3*, 861-869.

Sawai, S., Shimono, A., Wakamatsu, Y., Palmes, C., Hanaoka, K., and Kondoh, H. (1993). Defects of embryonic organogenesis resulting from targeted disruption of the N-myc gene in the mouse. Development *117*, 1445-1455.

Schreiber-Agus, N., Chin, L., Chen, K., Torres, R., Rao, G., Guida, P., Skoultchi, A. I., and DePinho, R. A. (1995). An amino-terminal domain of Mxi1 mediates anti-Myc oncogenic activity and interacts with a homolog of the yeast transcriptional repressor SIN3. Cell *80*, 777-786.

Schreiber-Agus, N., Stein, D., Chen, K., Goltz, J. S., Stevens, L., and DePinho, R. A. (1997). Drosophila Myc is oncogenic in mammalian cells and plays a role in the diminutive phenotype. Proc Natl Acad Sci U S A *94*, 1235-1240.

Schreiber-Agus, N., Meng, Y., Hoang, T., Hou, H. J., Chen, K., Greenberg, R., Cordon, C. C., Lee, H. W., and DePinho, R. A. (1998). Role of Mxi1 in ageing organ systems and the regulation of normal and neoplastic growth. Nature *393*, 483-487.

Schubiger, M., Wade, A. A., Carney, G. E., Truman, J. W., and Bender, M. (1998). Drosophila EcR-B ecdysone receptor isoforms are required for larval molting and for neuron remodeling during metamorphosis. Development *125*, 2053-2062.

Schuhmacher, M., Staege, M. S., Pajic, A., Polack, A., Weidle, U. H., Bornkamm, G. W., Eick, D., and Kohlhuber, F. (1999). Control of cell growth by c-Myc in the absence of cell division. Current Biology *9*, 1255-1258.

Sheiness, D., Fanshier, L., and Bishop, J. M. (1978). Identification of nucleotide sequences which may encode the oncogenic capacity of avian retrovirus MC29. J Virol *28*, 600-610.

Shen, X., Mizuguchi, G., Hamiche, A., and Wu, C. (2000). A chromatin remodelling complex involved in transcription and DNA processing. Nature *406*, 541-544.

Shen-Li, H., O'Hagan, R. C., Hou, H., Jr., Horner, J. W., 2nd, Lee, H. W., and DePinho, R. A. (2000). Essential role for Max in early embryonic growth and development. Genes Dev *14*, 17-22.

Shibuya, H., Yoneyama, M., Ninomiya, T. J., Matsumoto, K., and Taniguchi, T. (1992). IL-2 and EGF receptors stimulate the hematopoietic cell cycle via different signaling pathways: demonstration of a novel role for c-myc. Cell *70*, 57-67.

Simpson, P., and Morata, G. (1981). Differential mitotic rates and patterns of growth in compartments in the Drosophila wing. Dev Biol *85*, 299-308.

Staller, P., Peukert, K., Kiermaier, A., Seoane, J., Lukas, J., Karsunky, H., Moroy, T., Bartek, J., Massague, J., Hanel, F., and Eilers, M. (2001). Repression of p15INK4b expression by Myc through association with Miz-1. Nat Cell Biol *3*, 392-399.

Steiger, D. (2002). RNAi against lacZ and dmax in transgenic Drosophila. Diploma Thesis.

Toyo-oka, K., Bowen, T. J., Hirotsune, S., Li, Z., Jain, S., Ota, S., Escoubet-Lozach, L., Garcia-Bassets, I., Lozach, J., Rosenfeld, M. G.*, et al.* (2006). Mnt-deficient mammary glands exhibit impaired involution and tumors with characteristics of myc overexpression. Cancer Res *66*, 5565-5573.

Trumpp, A., Refaeli, Y., Oskarsson, T., Gasser, S., Murphy, M., Martin, G. R., and Bishop, J. M. (2001). c-Myc regulates mammalian body size by controlling cell number but not cell size. Nature *414*, 768-773.

Vastrik, I., Koskinen, P. J., Alitalo, R., and Makela, T. P. (1993). Alternative mRNA forms and open reading frames of the max gene. Oncogene *8*, 503-507.

Vennstrom, B., Sheiness, D., Zabielski, J., and Bishop, J. M. (1982). Isolation and characterization of c-myc, a cellular homolog of the oncogene (v-myc) of avian myelocytomatosis virus strain 29. J Virol *42*, 773-779.

Wanzel, M., Herold, S., and Eilers, M. (2003). Transcriptional repression by Myc. Trends Cell Biol *13*, 146-150.

Watkins, N. J., Lemm, I., Ingelfinger, D., Schneider, C., Hobach, M., Urlaub, H., and Luhrmann, R. (2004). Assembly and Maturation of the U3 snoRNP in the Nucleoplasm in a Large Dynamic Multiprotein Complex. Molecular Cell *16*, 789.

Wert, M., Kennedy, S., Palfrey, H. C., and Hay, N. (2001). Myc drives apoptosis in PC12 cells in the absence of Max. Oncogene *20*, 3746-3750.

Wood, M. A., McMahon, S. B., and Cole, M. D. (2000). An ATPase/helicase complex is an essential cofactor for oncogenic transformation by c-Myc. Mol Cell *5*, 321-330.

Xu, T., and Rubin, G. M. (1993). Analysis of genetic mosaics in developing and adult Drosophila tissues. Development *117*, 1223-1237.

Yin, X. Y., Grove, L., and Prochownik, E. V. (1998). Lack of transcriptional repression by max homodimers. Oncogene *16*, 2629-2637.

Zeller, K. I., Jegga, A. G., Aronow, B. J., O'Donnell, K. A., and Dang, C. V. (2003). An integrated database of genes responsive to the Myc oncogenic transcription factor: identification of direct genomic targets. Genome Biol *4*, R69.

Zervos, A. S., Gyuris, J., and Brent, R. (1993). Mxi1, a protein that specifically interacts with Max to bind Myc-Max recognition sites [published erratum appears in Cell 1994 Oct 21;79(2):following 388]. Cell *72*, 223-232.

Zindy, F., Eischen, C. M., Randle, D. H., Kamijo, T., Cleveland, J. L., Sherr, C. J., and Roussel, M. F. (1998). Myc signaling via the ARF tumor suppressor regulates p53-dependent apoptosis and immortalization. Genes & Development *12*, 2424-2433.

Curriculum vitae

Name	STEIGER
Vorname	Dominik
Geburtsdatum	15.2.1976
Heimatort	Waldkirch-Bernhardzell SG

Bildungsgang

Mittelschule	Kantonsschule Baden
Matura	Typus B (Literargymnasium)
Abschlussjahr	1996
ETH Zürich, Physik	1997
Universitaet Zürich, Biologie	1997 - 2002
Grundstudium Biologie	1997 - 1999
Fachstudium Molekularbiologie	1999 - 2002
Nebenfachstudium	Immunologie biochemischer Richtung
weiteres Nebenfach	Physikalische Chemie
Diplomarbeit	RNA*i* against *lacZ* and *dmax* in transgenic *Drosophila*
Diplom in Molekularbiologie	7. November 2002
Angestellt als Doktorand seit	11. November 2002